

IAEA-TECDOC-1460

Elements of power plant design for inertial fusion energy

*Final report of a coordinated research project
2000–2004*



IAEA

International Atomic Energy Agency

June 2005

IAEA-TECDOC-1460

Elements of power plant design for inertial fusion energy

*Final report of a coordinated research project
2000–2004*



IAEA

International Atomic Energy Agency

June 2005

The originating Section of this publication in the IAEA was:

Physics Section
International Atomic Energy Agency
Wagramer Strasse 5
P.O. Box 100
A-1400 Vienna, Austria

ELEMENTS OF POWER PLANT DESIGN FOR INERTIAL FUSION ENERGY

IAEA, VIENNA, 2005
IAEA-TECDOC-1460
ISBN 92-0-107005-5
ISSN 1011-4289

© IAEA, 2005

Printed by the IAEA in Austria
June 2005

FOREWORD

There are two major approaches in fusion energy research: magnetic fusion energy (MFE) and inertial fusion energy (IFE). The basic physics of IFE (compression and ignition of small fuel pellets containing deuterium and tritium) is being increasingly understood. Based on recent advances by individual countries, IFE has reached a stage at which benefits could be obtained from a coordinated approach in the form of an IAEA Coordinated Research Project (CRP) on Elements of Power Plant Design for Inertial Fusion Energy. This CRP helped Member States to promote the development of plasma/fusion technology transfer and to emphasize safety and environmental advantages of fusion energy. The CRP was focused on interface issues including those related to,

- the driver/target interface (e.g. focusing and beam uniformity required by the target),
- the driver/chamber interface (e.g. final optics and magnets protection and shielding),
- and the target/chamber interface (e.g. target survival during injection, target positioning and tracking in the chamber).

The final report includes an assessment of the state of the art of the technologies required for an IFE power plant (drivers, chambers, targets) and systems integration as presented and evaluated by members of the CRP. Additional contributions by cost free invited experts to the final RCM are included.

The overall objective of this CRP was to foster the inertial fusion energy development by improving international cooperation. The variety of contributions compiled in this TECDOC reflects, that the goal of stimulating the exchange of knowledge was well achieved. Further the CRP led to the creation of a network, which not only exchanged their scientific results, but also developed healthy professional relations and strong mutual interest in the work of the group members.

The IAEA would like to express its gratitude to S. Nakai for chairing the final research coordination meeting, 14–15 October 2004, held in Daejon, supported and hosted by the Republic of Korea.

The IAEA officer responsible for this publication was G. Mank of the Division of Physical and Chemical Sciences.

EDITORIAL NOTE

The papers in these proceedings are reproduced as submitted by the authors and have not undergone rigorous editorial review by the IAEA.

The views expressed do not necessarily reflect those of the IAEA, the governments of the nominating Member States or the nominating organizations.

The use of particular designations of countries or territories does not imply any judgement by the publisher, the IAEA, as to the legal status of such countries or territories, of their authorities and institutions or of the delimitation of their boundaries.

The mention of names of specific companies or products (whether or not indicated as registered) does not imply any intention to infringe proprietary rights, nor should it be construed as an endorsement or recommendation on the part of the IAEA.

The authors are responsible for having obtained the necessary permission for the IAEA to reproduce, translate or use material from sources already protected by copyrights.

CONTENTS

SUMMARY	1
DRIVER STUDIES	
Feasibility study of a high power laser system with beam combination method using phase conjugation mirrors of a stimulated Brillouin scattering for generating an ultra high power output with a high repetition rate over 10Hz	15
<i>H.J. Kong, S.K. Lee, D.W. Lee</i>	
Investigation of beam plasma interaction as specific problem of the heavy ion driver target interface.....	21
<i>B.Y. Sharkov</i>	
Beam plasma interaction experiments with intense laser and particle beams at GSI	29
<i>D.H.H. Hoffmann</i>	
CHAMBER STUDIES	
Peripheral elements and technology associated with pulsed power inertial fusion; IFE chamber wall ablations with high-flux pulsed beams including ions and UV laser lights.....	39
<i>K. Kasuya, T. Norimatsu, S. Nakai, A. Prokopiuk, W. Mroz</i>	
Chamber dynamic response, laser driver-chamber interface and system integration for inertial fusion energy.....	47
<i>M.S. Tillack, F. Najmabadi, A.R. Raffray</i>	
Vapor cleaning rate and condensation study for IFE liquid chambers	53
<i>A. Ying</i>	
Investigation of secondary processes by interaction of plasma streams with various materials	63
<i>R.T. Khaydarov, G.R. Berdiyev, U. Kunishev, M. Khalmuratov, E. Tojikhonov</i>	
TARGET PHYSICS	
Investigation of the high-z laser produced plasma with the use of ion-diagnostics for optimization of the laser interaction with Hohlraumtype targets	73
<i>J. Wolowski</i>	
Fast electrons for the fast ignitor scheme of inertial confinement fusion	97
<i>I.B. Földes, J. Bohus, K. Gál, B. Hopp, G. Kocsis, N.R. Kresz, E. Rácz, T. Suta, T. Smausz, S. Szatmári, Zs. Tóth, G. Veres</i>	
Thermal smoothing of laser imprint using low-intensity prepulse or low-density porous matter	105
<i>M. Kálal, N.N. Demchenko, S.Yu. Gus'kov, A.I. Gromov, A. Kasperczuk, V.N. Kondrashov, E. Krouský, J. Limpouch, K. Mašek, M. Pfeifer, P. Pisarczyk, T. Pisarczyk, K. Rohlena, V.B. Rozanov, J. Ullschmied</i>	
Laser driven ablative surface in IFE	121
<i>N. Rudraiah</i>	
TARGET TECHNOLOGY	
Extension of free-standing target technology on IFE requirements.....	133
<i>E.R. Koresheva, I.V. Aleksandrova, G.D. Baranov, S.V. Bazdenkov, V.I. Chtcherbakov, E.L. Koshelev, B.V. Kuteev, A.I. Nikitenko, S.M. Tolokonnikov, I.E. Osipov, I.D. Timofeev, T.P. Timasheva, L.S. Yaguzinskiy</i>	

Next steps for target technology and power plant design	153
<i>T. Norimatsu</i>	
IFE SYSTEM DEVELOPMENTS	
IFE research at LLNL	157
<i>W.R. Meier</i>	
Design study and technology assessment on inertial fusion energy power plant design	159
<i>S. Nakai</i>	
Elements of power plant design for inertial fusion energy at DENIM	167
<i>G. Velarde, O. Cabellos, M.J. Caturla, R. Florido, J.M. Gil, P.T. León,</i>	
<i>R. Mancini, J. Marian, P. Martel, J.M. Martínez-Val, E. Mínguez, F. Mota,</i>	
<i>F. Ogando, J.M. Perlado, M. Piera, R. Rodríguez, J.G. Rubiano,</i>	
<i>M. Salvador, J. Sanz, P. Sauvan, M. Velarde, P. Velarde</i>	
LIST OF PARTICIPANTS	173

SUMMARY

1. Drivers

Introduction

Reports on three driver related CRP activities are included in this section. The first report (Section 1.1, Kong) covers research on laser beam combination techniques using stimulated Brillouin scattering that is being conducted at KAIST. The second report (Section 1.2, Sharkov) covers work at ITEP on beam plasma interactions relevant to heavy ion driver beam coupling to the target. The third report (Section 1.3, Hoffman) reviews activities at GSI on heavy ion beam interactions with plasma.

Laser research at KAIST

Scientists at KAIST are conducting research on laser beam combination laser with stimulated Brillouin scattering (SBS) phase conjugate mirrors (SBSPCMs) as a candidate for a future laser fusion driver. In order to develop the beam combination laser with the SBS-PCMs, it is necessary to control the phase of each SBS wave whose phases are known as inherently random. Researchers have proposed a new phase control technique by a self-generated density modulation in order to control the phase of the SBS waves. Theoretical analysis shows that the phase fluctuation is inversely proportional to the pump energy and is proportional to the pump energy fluctuation. By means of the amplitude dividing, they have shown that the relative phase difference between two SBS waves can be made smaller than $4/\lambda$. Their work suggests that this phase control technique will very useful in developing a practical laser fusion driver using the beam combination with SBS-PCMs. KAIST scientists conclude that this system will be very easy to install and maintain because of the compensation of the optical distortions by the phase conjugated mirrors and the alignment insensitiveness by the cross type amplifier system with the symmetrical SBS-PCMs.

Ion beam/plasma interaction research at ITEP

Scientists at ITEP are investigating ion beam interactions with plasma, which is relevant to beam/target interactions for heavy ion driven IFE. The work supported by this CRP and reported here consisted of two parts: 1) Experiments on energy loss and charge state distribution measurements of Cu^{2+} ions in gas discharge plasma targets, and 2) Experimental measurements of the stopping power of explosively driven Ar plasma for Carbon and Xe. The 27 MHz RFQ linac at ITEP has been upgraded and now is capable of providing an output beam of 110 keV/nucleon and the beam transport line for multi-charged heavy ions from the accelerator to plasma target has been designed and assembled. The ITEP facility was used for the Cu ion experiments. Results of the Cu/plasma interaction experiments are given and compared to SRIM code output. Interaction of heavy ions with strongly coupled plasmas and possible non-ideality effects in the density regime up to $10^{22} \text{ e}^-/\text{cm}^3$ and temperatures between 1–10 eV is of interest for basic research in the warm dense matter physics. Results of experimental investigation of the stopping power of explosively driven plasma (Xe or Ar), performed at GSI in close collaboration of the ITEP, GSI and ICP Chernogolovka groups, are summarized in this report.

Ion beam/plasma interaction research at GSI

Scientists at GSI are using their experimental and theoretical expertise in beam plasma interaction physics as well as in accelerator physics to address key physics issues associated with intense beams. The focus of their CPR project is high current experiments with heavy ion beams and diagnostic methods. The goal of this project concerns machine developments towards the production and diagnostics of conditions of high power density in matter generated by heavy ion beams. Various experimental capabilities at GSI are discussed in the context of much broader research activities on beam/plasma interactions and other high-energy physics research at GSI. A typical experimental set-up for ion irradiation of a tamped cylindrical target is described including the diagnostic capabilities such as interferometer, pyrometer and X ray backlighter. A robotic target mounting system that allows many experiments (up to 50) without breaking chamber vacuum has been developed and tested. The report also discusses work on alternative focusing scheme for high current beams based on a plasma lens.

2. Chambers

Introduction

Reports on four chamber related CRP activities are included in this section. The first report (Section 2.1, Kasuya) covers research on pulsed ion and laser irradiations of candidate IFE chamber walls. This is a collaborative programme between Tokyo Institute of Technology, ILE Osaka and the Institute of Optoelectronics in Warsaw Poland. The second report (Section 2.2, Tillack) covers work performed at the University of California in San Diego. Three topics are included: IFE chamber physics, final optic development and testing, and IFE chamber assessment studies in the ARIES program. The third report (Section 2.3, Ying) reviews activities at UCLA, which focused on investigations of the condensation of excited vapors generated from molten Flibe in an electrothermal discharge experiment. The fourth report (Section 2.4, Khaydarov) reviews activities at the National University of Uzbekistan in Tashkent. There, a Nd:YAG laser was used to explore the interactions of a laser ablation plume with a secondary target of Al or Mo.

IFE chamber wall ablation with high-flux pulsed ion and laser beams

Experiments were performed using pulsed intense proton beams and a UV laser beam in order to study IFE first wall ablation. Interest in the use of these beams arises from the simulation of first wall ablation of candidate inertial fusion materials. To know the precise relation between the thickness of the ablated surface layers of various materials and the proton beams used to ablate the targets, precise in-situ measurements of the characteristic of the focused proton beams were made. Sample materials were brought to Warsaw, where an ArF laser in the Polish authors' laboratory was used to irradiate the samples. After the irradiation, the sample surfaces were observed with various diagnostic tools including a laser microscope (Olympus-LS1200) in the Analysis Center of the second Japanese authors (ILE-Osaka University). The most important data were the first wall ablation rates under different experimental conditions of different beams, while the surface specie changes under the successive beam irradiations were also interesting in some cases. All of the experimental results were gathered and compared with former results for the compilation of future database of IFE reactor designs.

Chamber dynamic response, laser driver-chamber interface and system integration for inertial fusion energy

In the area of IFE chamber physics, progress was made in both modeling and experimental studies. The SPARTAN 2D gasdynamic code was developed, validated and used to study the dynamic response of dry-wall IFE chambers following target explosions. In the area of Final Optics, grazing-incidence metal mirrors were developed for laser-IFE. Scaled prototype testing demonstrated the survival of these mirrors up to 18 J/cm^2 of laser fluence over 10^5 shots. In the area of IFE design studies, UCSD led a national conceptual design study entitled ARIES-IFE. This study focused on an assessment of IFE chambers and chamber interfaces for the three main chamber types: dry walls, wetted walls and liquid walls.

Vapor clearing rate and condensation study for IFE liquid chambers

This work investigates the condensation of excited vapors generated from the molten salt Flibe. The high repetition rates necessary to keep an IFE power plant economically competitive makes the issue of chamber clearing a key feasibility factor. The motivation behind this work stems from the need for an experimental assessment of the achievable condensation rates of flibe vapors under IFE relevant conditions. Experiments were performed using a high-current electrical arc to generate the excited vapors from a pool of molten salt. The vapor expands inside a scaled chamber and condenses in contact with the walls, which are maintained at a controlled temperature. The experiments showed that vapor clearing is characterized by an exponential decay with a time constant of 6.58 milliseconds in the density range between $5 \times 10^{17} \text{ cm}^{-3}$ and $2 \times 10^{15} \text{ cm}^{-3}$. The low limit of the range is determined by the impurities dissolved in the salt. Extending the result to the expected low limit of HYLIFE-II ($3 \times 10^{13} \text{ cm}^{-3}$), the period for vapor clearing is 68 milliseconds, which is compatible with the required 6 Hz repetition rate.

Investigation of secondary processes by interaction of plasma streams with various materials

Charge and energy spectra of laser-produced W, Mo, V, Al plasma ions were investigated after their interaction with secondary targets (Mo, Al), located at the distance 2–10 mm from the surface of the first target. It was found experimentally that the presence of the secondary target changes mass-charge and energy spectra of plasma ions; singly charged ions of the secondary target were detected in a narrow low energy range (100–300 eV). The emission of ions from the secondary target depends on plasma parameters, material of secondary target and on the distance between primary and secondary targets.

3. Target physics

Reports on four CRP activities related to target physics are included in this section. The first report (Section 3.1, Wolowski) covers studies of high-Z plasma produced with high-power lasers either with picosecond (IPPLM) or subnanosecond (PALS) pulse duration employing various ion diagnostic methods for determination of physical processes taking place in such plasmas (similar to plasmas produced inside the Hohlraum target). The second report (Section 3.2, Földes) describes experiments carried out with ultrashort laser pulses to investigate nonlinear phenomena as high-harmonics generation (HILL), participation in the high-intensity experiments aimed to generate fast electrons and protons for fusion applications (MPQ), and initiation of material damage studies for UV radiation concerning prospective chamber-wall

materials. The third report (Section 3.3, Kalal) is dedicated to thermal smoothing of laser imprint using either low-intensity prepulse or low-density porous materials. Results of extensive experimental research (PALS) are complemented by analytical and numerical approach. The fourth report (Section 3.4, N. Rudraiah) is a purely theoretical work in which significant results were obtained on the reduction of the growth rate of the Rayleigh-Taylor instability at the ablative surface of IFE targets using nanostructured smart porous lining together with external constraints of magnetic or electric fields.

High-Z laser produced plasma

Scientists from IPPLM in Warsaw together with their colleagues from PALS Research Centre in Prague are conducting extensive studies of high-Z plasma produced with high-power lasers. These studies are oriented towards the determination of physical processes in such plasma (in particular the ion generation and acceleration) as well as towards important applications (optimisation of indirect laser fusion, X ray laser-plasma source, and intense sources of multi-charged ions). The main objective of this CRP was application of ion diagnostic methods to investigate the physical properties of this high-Z plasma similar to the plasma produced inside the Hohlraum target. The characteristics of such plasma were investigated in dependence on laser pulse parameters (intensity, wavelengths, energy, prepulse), irradiation geometry (focus position, target tilt angle) and target material. Ion collectors (IC), a cylindrical electrostatic ion energy analyzer (IEA) based on the time-of-flight method (TOF), and solid-state track detectors were employed in these experiments. For Ta ions $Z_{\max} = 57$ and $E_i > 20$ MeV were obtained. The ion collector signals recorded at higher laser pulse energies clearly show the existence of three separate ion groups: fast, thermal and slow. At high laser pulse energies, $E_L > 200$ J, fast ion current density attained $j_{\max} \sim 20$ mA/cm² at the distance of 1 m from the target. An efficient production of highly charged high-energy ions by an intense short-wavelength laser pulse suggests that the mechanisms of the fast ion generation with the use of such laser pulses need to be further clarified.

Fast electrons for the fast ignitor scheme

The ultrashort pulse KrF laser at the HILL laboratory of the University of Szeged serves as a basis for the experimental work in Hungary. The laser system delivers presently 15 mJ energy of 600 fs duration on the 248 nm wavelength. The following work performed within the CRP is described: upgrading the KrF laser system and increasing the focused intensity up to 5×10^{17} W/cm²; laser plasma experiments on high harmonics generation as an interesting nonlinear phenomenon giving insight to the intrinsic nature of surface rippling, thus being relevant even for the physics of fast ignition; preparation for spectroscopic studies of isochoric heating; damage threshold studies for possible wall materials; participation in the high intensity experiments in the MPQ Garching on self-focusing and fast electron generation in a preformed plasma and on fast electron propagation in high-density matter.

Thermal smoothing of laser imprint

In the framework of this CRP an international group of scientists from the Czech Republic, Poland and the Russian Federation has gradually formed — centred around a new acquisition — Prague Asterix Laser System (PALS). Their initial intention was to further extent the laser imprint treatment studies using the low-intensity prepulse (initially performed with the iodine laser PERUN — presently dismantled). Much more powerful PALS represented a crucial improvement of available experimental arrangements. However, a need for several rather

expensive components (mainly large diameter mirrors) temporarily prevented this idea from its realization (preliminary experiments — quite promising — were performed only very recently and are reported in the paper). Due to this fact, an alternative approach towards the laser imprint treatment was adopted — application of layers from low-density porous matter. An extensive research in this field was carried out: numerous experiments were realized complemented by computer simulations and development of analytical model. The experimental results are in a good agreement with the two-dimensional hydrodynamic calculations that do not take fine structure of the porous material into account. Results provided by the analytical model are also in a reasonably good agreement. Somewhat outside of the CRP scope a considerable amount of work was also devoted to laser produced craters and double-target experiments (presented only as a list of publications).

Laser driven ablative surface instability

The main goal put forward by scientists from NRIAM (Bangalore) in their CRP was the reduction of the growth rate of Rayleigh-Taylor instability (RTI) at the ablative surface of IFE target. They proposed using nanostructured smart porous lining at the ablative surface together with the external constraints of magnetic or electric fields. For this particular arrangement they derived analytical expression for the dispersion relation which incorporates the constraints of a) nanostructured porous lining with incompressible viscous fluid in the presence of surface tension, b) the effect of magnetic field in conducting plasma of finite electrical conductivity, c) the effect of electric field in poorly conducting plasma of infinitesimal electrical conductivity. They found that these constraints reduce the growth rate of RTI significantly. This dispersion relation involves all the relevant physical parameters required for a suitable design of IFE target. They also derived an analytical expression for the growth rate considering laser radiation effect. This was done by solving the energy equations for shell and porous regions. The growth rate obtained, incorporating the laser radiation effect, also involves all the relevant physical parameters required for the design of efficient IFE target. Recently they just started investigating the Kelvin-Helmholtz instabilities at the ablative surface. The preliminary work with nanostructure porous lining has been completed and an analytical expression for the dispersion relation as in the case of RTI was obtained.

4. IFE target technology and delivery

Inertial fusion energy (IFE) research indicates that the energy generation by means of fuel target compression requires that targets must be delivered to the target chamber center, namely, at a rate of ~ 6 Hz (laser or heavy ion drivers) or 0.1 Hz (Z-pinch). This condition dictates how many targets have to be fabricated and delivered per day: about 500,000 for laser or heavy ion power plant and about 8,600 for Z-pinch power plant.

The first power plants will work with radioactive DT-mixture, which is a major limitation to IFE. Therefore, each production step of the target supply process must be completed for minimal time and space scales, aiming at the tritium inventory minimization. Besides, there is a strict requirement to supply IFE power plant with fuel targets on the very economic basis, meaning that all the production steps have to be optimized.

Over the period of 2000–2005, specific research objectives of the IAEA Coordinated Research Project (CRP) on Elements of Power Plant Design for Inertial Fusion Energy fall into six main categories:

1. free-standing targets mass-production,
2. target acceleration and rep-rate injection,
3. fast target characterization,
4. survivability of a fuel core,
5. target tracking and shooting,
6. elements assembly.

The research in different countries has been carried out in line with their own R&D IFE programmes. The target development programme in the USA considers the target supply issues for direct-drive (laser driver) and indirect drive (heavy-ion driver and Z-pinch) targets, whereas the fast-ignition and direct-drive target concepts for laser driver is under consideration in Japan. The target technology programme in the Russian Federation is centered on the fuel core fabrication inside the moving free-standing shells, the target delivery and survivability.

The main results have been presented and discussed during four CRP meetings held in May 2001 (Vienna, Austria), June 2002 (San Diego, USA), November 2003 (Vienna, Austria) and October 2004 (Daejeon, Rep.Korea), which makes it possible to coordinate efforts and to avoid the overlapping of investigations. The present status of this research is as following.

1. TARGETS MASS PRODUCTION

Direct drive target production includes the following main steps: capsule fabrication, capsule overcoating (gas barrier), fuel load, and fuel layering. For the indirect drive/fast ignition target we must add two more steps: hohlraum cylinder/reentrant cone production and target assembly. The conceptual plants for mass production of the direct-drive, indirect-drive and fast ignition targets were proposed in the USA, Japan and the Russian Federation.

The important feature of an IFE target is the foam capsule. The materials under consideration were divinyl benzene (DVB), polymethyl metacrilat (PMMA) and resorcinol formaldehyde (RF) foams as well as polyvinyl phenol (PVP) and polyvinyl alcohol (PVA) gas barriers. In the USA, the current product rate of 4 mm-diam 200 μm -thick overcoated foam shells is 3 Hz. The key matter that must be understood is how to overcome shrinkage of the foam capsules arising as a result of overcoating with a gas barrier layer.

The original method of frozen foam shells drilling to make a hole for the reentrant cone followed by the cone-and-shell assembly has been demonstrated in Japan for an individual target. The egg plate method for handling the shell batch during the drilling and assembly with cones is proposed. The mass production of the reentrant cones with necessary precision seems to be the most critical issue. Further proof-of-principle (POP) batch experiments are urgent.

One of the topical problems of target fueling is rapid loading of the shell batch with a fuel. In this frame, D_2 permeation process through a thin PVP barrier has been experimentally studied (USA). It was found that the ability to withstand buckling during filling is the key feature.

Fuel loading by the thermal cavitations technique is the alternative approach for target batch processing (proposed in Japan), the principle of which has been demonstrated with hemi foam sphere. The next step is the technique demonstration for the foam shell batch.

The fluidized bed concept is under consideration in the USA for mass-production layering. At present, the system design is completed and custom cryo-circulator is being fabricated. Cryogenic experiments for demonstration of this concept are planned to the next (2005) year. An alternative concept for cryogenic target mass production is based on the FST-technologies (Russian Federation). The fuel-layering is realized inside moving free-standing targets owing to the following two principles: (1) fuel freezing due to heat removal through the contact area between the shell and the cold substrate, and (2) layer symmetrization due to target random rotation. Basing on this concept, a prototypical system for mass-producing the cryogenic targets has been created, which operates with 5-to-25 free-standing targets at each production step. The transport process involves the target injection between fundamental system elements: shell container — layering module — test chamber. The main steps of IFE targets supply have been demonstrated with 1.0-to-1.8 mm-diam polystyrene shells using this system: shells permeation filling with D₂-fuel (300-to-1000 atm at 300 K), fuel layering inside moving free-standing shells (50-to-100 μm- thick layer), and injecting the created cryogenic targets into the test chamber with a rep-rate of 0.1 Hz. The modeling results have shown that the developed technologies (i.e. FST-technologies) are promising for fabrication of reactor-scaled targets. The next step is the experimental demonstration of the FST-technologies with reactor-scaled targets of different design.

2. ACCELERATION AND INJECTION

To ensure the continuous supply of the born area with fuel the cryogenic gun capable of ~6 Hz operation for ~500,000 shots per a day must be developed. Hereby, the injection velocity of a target must be as high as 200–400 m/sec (with reproducibility of about 3–5%). In addition, such an injection gun must operate at a minimal risk of reactor chamber contamination with foreign gases.

Note, that target assembly with a special sabot shall precede the target acceleration and injection. The main function of the sabot is to transmit effectively the acceleration impulse to the target. The sabot also protects the target during handling and acceleration. Therefore, the task of target and sabot assembly and separation is under careful consideration.

In the USA, the key issues of the injection process have been demonstrated using the gas gun system (at room temperature), namely: the rep-rated operation (6 Hz), sabot separation and deflection (at 400 m/sec), membrane support of target in sabot, injection velocity of ≥ 400 m/s, target in-flight tracking, 2.5 μm position reproducibility (in stationary tests). The next step is the demonstration of gas gun operation at the cryogenic temperature.

A certain attention was paid to an alternative approach, which considers the application of a coil gun or hybrid injector for target acceleration (USA, Japan, Russian Federation). One of the key issues is the choice of sabot material, which makes it possible to drive a target most effectively.

Soft ferromagnetic materials are in common use for acceleration in electro-magnetic injector (i.e. coil gun) at 300 K. The experiments carried out in the Russian Federation with a single coil have confirmed the possibility of the ferromagnetic sabot electro-magnetic acceleration at cryogenic temperature. In optimal conditions a 1 cm-length, 2.6 mm-diam sabot was accelerated in a single coil up to 8 m/s at 77 K and up to 4.5 m/s at 4.2 K ($Jw \approx 1280$ A*turns and 1000 A*turns correspondingly).

The computer simulation experiments have shown that a sabot made of magneto-insulator material (consisting of ferromagnetic particles uniformly distributed over the polystyrene matrix) can be accelerated in the coil gun more effectively than that from pure ferromagnetic. In addition, the application of magneto-insulator materials makes it possible to reduce the sabot weight in 3-to-4 times with retention of its magneto active properties, which allows such a sabot to be used both in the coil and gas guns as well as in the hybrid injector. The experimental demonstration is urgent.

Another promising material for sabot is a superconductor. The multi-pulse acceleration concept for a superconductor Pb sabot has been proposed in Japan and the numerical model of sabot acceleration-deceleration (due to Meissner effect) and rotation (due to pinning effect) was developed. POP experiments with the sabot made from high temperature superconductor have been conducted at 77 K, which confirmed the modeling results. Further study with Pb sabot at $T < 7.2$ K (critical temperature for Pb) is planned.

The electrostatic concept of target injector was also considered (USA). Such kind of injector requires no sabot but insulator performance is a concern (especially in radiation environments).

3. FAST CHARACTERIZATION

Fueling the commercial power plant requires fast characterization of a target just before injection. Possible approaches to this issue and results of computer experiments are presented in the research work of the Russian Federation. The optical scheme based on the Fourier holography has been proposed for target on-line diagnostic — the actuating unit and photo-detector only determine the operation rate of such a scheme (several μ sec). The computer experiments have demonstrated that such scheme is promising for simultaneous measuring target quality, velocity and trajectory as well as for experimental study of target survival.

4. FUEL CORE SURVIVABILITY

The critical issues of target survival during the injection process (both inside injector and reactor chamber) are to withstand overload during target acceleration, and to withstand overheat during target flight inside reactor chamber. To protect fuel core from destruction it is necessary to meet the alternative requirements, namely: (1) to reduce the injection velocity with the aim of overloads reduction, and (2) to increase the injection velocity with the aim of target flight shortening. The resolution lies in the optimization of target supply scenario as well as in the reduction of fuel core sensitivity to the heat- and g- loads. Several approaches to resolve the last feature have been considered including target shielding, profiling of target support in sabot, optimal choice of fuel layer microstructure.

As was shown in modeling results, the direct-drive targets can withstand the injection into a high temperature chamber if they are overcoated with a very thin insulating layer of hydrocarbon foam (USA) or with an ablative layer of solid hydrogen, deuterium or xenon (Russian Federation). The computer optimization of target support geometry showed that spherical or conical supports could considerably increase the permissible level of overloads (Russian Federation). In this view, the membrane support proposed and demonstrated at 300 K (USA) looks as the most promising technique allowing the overloads to be reduced and the point loading of target to be avoided. Note, that almost all the materials lose their elasticity and become fragile at cryogenic temperatures, which may be obstacle to realize the

idea of the membrane support for cryogenic targets. The choice of special material for such membrane and the demonstration of this technique at cryogenic temperature are urgent.

Fuel layer microstructure can control the layer ability to withstand the negative action of environment. The modeling results have shown (Russian Federation) that the surface finish spoiling of a crystalline fuel layer goes quicker than that of finely dispersed layer, as a result of anisotropy in the sound wave propagation through a crystal. Thus, the development of finely dispersed layer technology is in urgent need. Note, that the dispersity (grain size) level of 0.1 μm allows forming such a layer with the required smoothness. There is further reasoning to use fine dispersed fuel layer, namely: such a microstructure can withstand higher overloads than its crystalline analogue.

Recent cryogenic experiments (Russian Federation) have demonstrated (for shell diam 1.8 mm and layer thickness up to 50 μm) that the effect of vibrations with a certain frequency on fuel during its crystallization allows forming a fine-dispersed layer, while adding a small doping to a fuel allows to sufficiently reduce the layer sensitivity to thermal loads.

Note, that the foam layering (USA, Japan) can be considered as the alternative approach to form finely dispersed fuel layer. Here, the dispersity level is controlled by the pore size in foam material. Recent experiments show that improved DT ice inner smoothness can be achieved by using an underlying layer of low-density foam. The ability of such a layer to withstand overheating is still unknown and must be investigated. Unfortunately, low-density foam capsules (like DVB or PMMA) are not transparent for visual light, which is the obstacle to characterize the fuel layer inside a capsule. To investigate the fundamentals underlying the foam layering method the transparent RF foams can be used.

5. TARGET TRACKING AND SHOOTING

The precision of target and beam meeting at the chamber center must be as accurate as $\pm 20 \mu\text{m}$ (for direct drive target) and 200 μm (for indirect drive target). Target drive tracking and/or beam steering can allow achieving these requirements.

Chamber gas modeling indicates that the target in-chamber tracking is inevitable (USA, Japan). The potential target steering concept based on laser light ablation has been proposed aiming to compensate the action of winds in the chamber (USA). In this scenario, driver beams would only be adjusted for “long term” drift. Note, that according to this concept the ablative cryogenic layer (Russian Federation) can be also useful for target steering.

6. ELEMENTS ASSEMBLY

The concepts for the target plants including different elements for mass production and repeated delivery of IFE targets into reactor burn area have been proposed for each kind of target designs. A further detailed study of the elements assembly is highly needed with emphasis on the problems of tritium inventory minimization and radioactive safety and hazard. Since the processes of target formation and delivery takes place at cryogenic temperature, the protection of interior operating units from the influence of the room environment is one of the key features guaranteeing the operation of all the system. This issue should be taken care of due to application of special separating vacuum jackets and cryogenic shields.

In the case of a gas gun/chamber assembly a special measures should be applied to protect the reactor chamber from the contamination with a propellant gas. These measures (e.g. a set of

sluices with independent pump system, fast electro-magnetic valves etc.) may reduce the reliability of the delivery process and increase the cost of the system. In this regard, the application of the electromagnetic, electrostatic or hybrid injectors appears to be more promising.

7. CONCLUSIONS

The key issues of IFE target technology and delivery have been considered over the period of 2000–2005 with special attention to the technology assessment, interface issues and elements assembly problems. The scenarios for IFE target supply have been proposed for each kind of target concepts (direct-drive, indirect-drive and fast ignition) basing on the earlier developed and the advanced technologies. Target scenarios have many common elements, which are derived from ICF experience. At the moment, almost all steps of target supply, shells mass production, fuel loading, cryogenic layering, target assembly, fast characterization, acceleration and injection, have been demonstrated, but at a reduced scale. The fabrication of 4 mm-diam 200 μm -thick overcoated foam shells with the rates of 3 Hz has been demonstrated. A full scaled scenario for free standing target batch fuel load (up to 1000 atm D_2 at 300 K), fuel layering (up to 100 μm cryogenic layer thickness), and injection into the test chamber with a rate of 0.1 Hz has been demonstrated for millimeter-size targets.

As a result of this activity, the fundamentals underlying the processes of target mass production and rep-rated delivery become more comprehensible. This allows outlining new promising research directions and urgent additional investigations, namely:

1. The key features that must be understood in the area of foam shells production are the following: (1) how to overcome the shrinkage of capsules arising as a result of gas barrier deposition, and (2) the ability of PVP gas barrier to withstand buckling during the permeation process.
2. Rapid fuel loading in a fast ignition target batch is the key problem. In this frame, the proof-of-principle experiments on the thermal cavitations technique are urgently needed.
3. Fuel layering inside a foam capsule is one of the key issues of target technology. The ability of such a layer to withstand overheat is still unknown and must be investigated.
4. The experimental demonstration of the FST-technologies with reactor-scaled targets of different design (including fine-dispersed layer fabrication and reduction of its sensitivity to overheat using small doping) is highly desirable. It will allow to proof theoretical results and to make final decision concerning the applicability of this alternative approach to IFE requirements.
5. Proof-of-principle experiments in the area of target fast characterization using the Fourier holography approach are strongly required. This allows carrying out investigations into fuel core survivability as well as characterizing target parameters just before injection (fuel layer quality, target velocity and trajectory).
6. Pneumatic injector operability at cryogenic temperature and additional research work in the area of injector/chamber safe assembly is urgently needed.
7. Electro-magnetic injector looks promising with respect to the solution of the problem of chamber contaminations with foreign gases. Demonstration of target acceleration and injection using this kind of injector is highly important.
8. The choice of the optimal material for a sabot will allow carrying out the delivery process more effectively. In this regard, experimental investigation with sabots made from magneto-insulators and superconductors is urgently needed.
9. Further detailed study of elements assembly is very important with special attention to the problems of tritium inventory minimization, radioactive safety and hazard, chamber

contamination with foreign gases, protection of the interior operating units from the room environment, etc.

10. There are some other issues, which require more attention in the next period. Target design simplification, tritium content minimization in the fuel core, optimal choice of the fuel layer microstructure, etc. can lead to additional cost reduction as well as to safety increase of IFE target supply system.

The above listed research activities will allow making the next step in the world IFE programme, i.e. demonstrating experimentally the reactor-scaled targets mass production and delivery at the conditions close to operational.

In conclusion, we would like to emphasize that the research work in the frame of the IFE target technology and delivery has been carried out just according to the overall objective of the IAEA Coordinated Research Project of Elements of Power Plant Design for Inertial Fusion Energy, namely: to stimulate and promote the Inertial Fusion Energy development by improving international cooperation. This made it possible to avoid duplication of efforts, to accelerate progress in resolving many IFE issues and to define the necessary directions for further research.

5. Inertial fusion energy systems development

In spite of ending some previous long-standing conceptual reactors such as ARIES IFE (USA) or Japanese concept KOYO Upgrade, this IAEA programme has been able to identify and develop real theory-EXPERIMENTAL work in some selected areas, components of the advanced systems necessary in future technology linked to IFE reactors. We could classify advances in the following fields:

- New IFE reactor concepts to generate Energy *accommodating* new driver-target implosion schemes:
 - Fast ignition (use of femtosecond lasers as second beam to contribute exclusively to ignition phase through intense charge particle illumination of the core of the imploded target)
 - Jet and impact fusion (use of one simple common laser beam for implosion and ignition of the core of the target)
 - Z-pinch concepts (X rays intense illumination, generated by Z-pinch machine, obtaining very high gain/energy per pulse and low repetition rate)
 - It also appears the use of heavy ions in a new upgraded reactor that incorporates the advance knowledge in materials and systems.
- Development of conceptual and **experimental (and this is the most important aspect)** proof of principles of **jet formation and fluid-dynamics physics of protection blanket** (thick walls)/heat recovery and tritium extraction from engineering systems.
- Progressing in the comparison between solid wall chambers, and thick and thin wall protected schemes.
- New **experimental** results and simulation results in **optics** resistant to irradiation by **X rays** and debris.
- Identification of some key future research and parameters in **safety of systems** component of a future power plant. That includes simulation of realistic conditions of systems (in conceptual manner) corresponding to heat extraction with a full analysis of fluid-dynamics and conditions of routinely and accidental incidents in their work, concluding with public consequences.

- Identification of effects of **tritium releases** including new mechanisms and chemical forms such as HT and organically bound tritium (OBT) in routinely and accidental potential releases.
- A large and cooperative work in small scale experiments and ignition devoted manufacturing processes of **tritium fabrication** (well described in other part of this IAEA CRP summary).
- Identification of lines of **efficient drivers** for reactor applications to obtain commercial viability: higher efficiency and repetition rate as possible. That includes:
 - Diode pumped solid state lasers (DPSSL)
 - Excimer gas lasers (KrF)
 - X rays from Z-pinch machines
 - Much upgrade line of research in heavy ions accelerator lines for illumination and Plasma interaction.
- Incorporate work done in fusion area, such as **materials** resistant to **radiation damage** (charged particles, X rays and neutrons) and **activation**, to the design of inertial fusion reactors. That includes not only structural materials (expected long-lifetime in the reactor) but also optical, blanket and other low-lifetime components in the reactor. New results on modification of macroscopic properties of materials by irradiation, using simulation multiscale modelling and experiments in a consistent and tested procedure through microscopic and macroscopic results, using medium size experimental facilities.
- Start of consistent programme of **irradiation facilities in medium-size scale** for significant **experiments in charge particles and X rays** on materials in chamber design, target emissions, structural components, laser optics and heavy ion focusing through US, Europe, Japan and the Russian Federation programmes.

To summarize the importance of the IAEA CRP on Elements of IFE Power Plants in the Systems Area, a common international interchange of knowledge has been (for the first time) produced which includes not only conceptual “*papers*” but experiments in key technological fields in order to adjust some of the engineering largely proposed for IFE reactors.

DRIVER STUDIES

Feasibility study of a high power laser system with beam combination method using phase conjugation mirrors of a stimulated Brillouin scattering for generating an ultra high power output with a high repetition rate over 10Hz

H.J. Kong, S.K. Lee, D.W. Lee

Dept. of Physics, Korea Advanced Institute of Science and Technology,
Daejeon, Republic of Korea

Abstract. A beam combination laser with stimulated Brillouin scattering phase conjugate mirrors (SBS-PCMs), which is expected to produce a high output energy and power with a repetition rate over 10 Hz, is a candidate for a practically useful laser fusion driver in future. In order to develop the beam combination laser with the SBS-PCMs, it is necessary to control the phase of each SBS wave whose phases are known as inherently random. We have proposed a new phase control technique and demonstrated experimentally that the relative phase difference between two SBS waves can be controlled to a certain value and locked to it with an accuracy less than $\lambda/4$. Additionally we have proposed and demonstrated a new technique to preserve the pulse shape of the SBS wave. Based on these experimental results, we have proposed 2 schemes of the new schemes for the high repetition and high energy/power beam combination laser system (laser fusion driver) using the SBS-PCMs of amplitude division and wave-front division techniques, which can operate with repetition rate over 10Hz, in this paper.

1. INTRODUCTION

For achieving a high power laser with a repetition rate over 10 Hz, which is required for a laser fusion driver, several methods have been widely investigated by many researchers such as a beam combination technique, a diode pumped laser system with gas cooling, an electron beam pumped gas laser, and a large sized ceramic Nd:YAG [1–5]. Especially, the beam combination method seems to be one of the most practical techniques for this application [2–4]. The laser system using a beam combination technique, in which a laser beam is divided into several beams and recombined after separate amplification does not need a large gain medium. Hence, it can operate at a repetition rate exceeding 10 Hz regardless of the output energy and is easily adaptable to the modern laser technology. H.J.Kong et al. proposed a promising beam combination laser system using the stimulated Brillouin scattering-phase conjugate mirrors (SBS-PCMs), whose output energy can be unlimitedly scaled up by increasing the number of separate amplifiers [2]. In addition, the SBS-PCMs produces a phase conjugated wave to compensate many kinds of the optical distortions in the system, induced during the amplification [6]. In the beam combination laser using the SBS-PCMs, however, it is necessary to control the phase of each beam reflected by the SBS-PCM to get the good beam recombination. It has been known that the phase of the beam reflected by the SBS-PCM is inherently random [4, 7] because the SBS starts from a noise in the SBS medium. There have been several works to control or lock the phases of SBS wave, and some of them are very successful [3, 4]. By overlapping the laser beams at one focal point, the phases are almost locked [3]. However, since all the beams must be focused at one point, the energy scaling is limited and also the beams are not symmetrically focused at the focal spot. The back seeding of the Stokes beam overcomes the above drawbacks [4], but the phase conjugation becomes to be incomplete if the injected Stokes beam is not completely correlated. In this paper, we have proposed and demonstrated a new phase control technique, wherein each

beam is focused at the separate focal points without using any backward Stokes seed beams and hence, the energy scaling is not limited and the phase conjugation is not disturbed at all. For getting a given output energy, we may simply install the proper number of amplifier lines in parallel for beam combination, because the whole system is alignment insensitive in this new laser systems.

2. PHASE CONTROL OF SBS WAVE BY SELF-GENERATED DENSITY MODULATION

The acoustic wave, Brillouin grating, is simply represented as

$$\tilde{\rho}(z,t) = \rho(z,t) \cos[q(z-z_0) - \Omega(t-t_0)] \quad (1)$$

propagating in the positive z direction, where $\rho(z,t)$, q , and Ω are the amplitude, the wave vector, and the frequency of the acoustic wave, respectively. The initial phase is given by $\phi_a = qz_0 - \Omega t_0$, where z_0 and t_0 are known to vary randomly because the acoustic wave begins from a random acoustic noise [7]. However, we have found it is possible to decide z_0 and t_0 by putting a mirror in the back of the SBS-PCM to make a standing wave at the focus [8]. One of the standing wave is the candidate of the ignition position z_0 , and t_0 is determined by the pumping energy E_c from the equation, $E_c = \int_0^{t_c} P(t) dt$, where E_c and $P(t)$ are the threshold energy for SBS if the medium and pumping pulse form, respectively, and $t_0 = t_c$ as described in [8].

Figures 1, 2, and 3 shows the theoretical values of the ignition time (t_c), phase uncertainty ($\Delta\phi$), and the relative phase difference uncertainty ($\Delta\phi$) depending on the pumping energy, respectively. It should be noted that $\Delta\phi$ is inversely proportional to the pumping energy E_t .

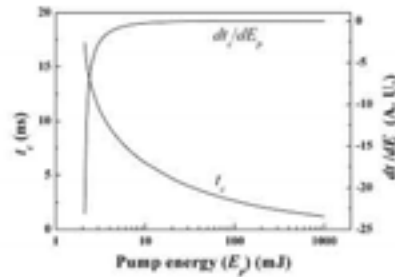


Figure 1. t_c & dt_c/dE_p as a function of the pump energy.

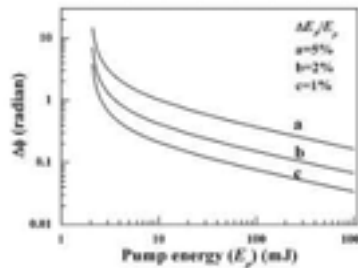


Figure 2. Phase change of the SBS wave as a function of the pump energy ($\Delta E_p / E_p = 1, 2$ and 5%).

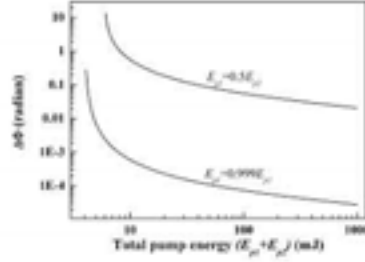


Figure 3. Change of the relative phase difference as a function of pump energy for the cases of $E_{p1} = 0.5E_{p2}$ and $E_{p1} = 0.999E_{p2}$.

3. EXPERIMENTS ON THE PHASE CONTROLLING AND LOCKING

We have measured the relative phase difference $\Phi = \phi_1 - \phi_2$ between two Stokes beams for the case of the amplitude dividing. The experimental setup is shown schematically in Fig 4. A Q-switched 1064 nm Nd:YAG oscillator with a bandwidth of ~ 120 MHz and $\sim 2\%$ energy stability was used for the pump. The pulse width was 7-8 ns and the repetition rate was 10 Hz. The output from an oscillator is divided into two sub-beams by a beam splitter (BS). Both beams then pass through the separate wedges (W1&W2) and are backward focused into each SBS-PCM. The wedge reflects a part of the backward Stokes beam, which is overlapped with that of the other Stokes beam onto a CCD camera to get an interference pattern of them. For stabilizing the phase by the self-generated density modulation, the pump pulse is backward focused by a concave mirror with $R=50$ cm and reflectivity $>99\%$. The density modulation is induced by the electrostriction in the SBS material, especially at the focal area by the standing wave interference pattern at the focal region. We used Fluorinert FC-75 as a SBS medium. The length of a SBS cell of 50 cm is used in this experiment [9].

The diagnostics for the phase control of the Stokes beams is straightforward. The interference pattern acquired by the CCD camera yields the relative phase difference $\Phi = \phi_1 - \phi_2$ between the Stokes beams incident on the CCD, where ϕ_1 and ϕ_2 denote the phases of two Stokes beams, respectively. Therefore, we can quantitatively analyze the degree of the phase stabilization by measuring the movement of the peaks.

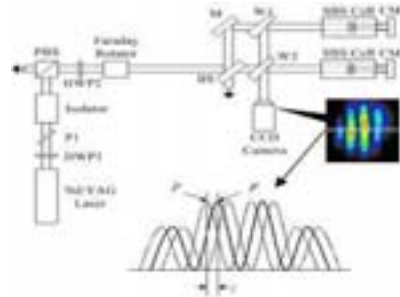


Figure 4. Experimental setup for measuring the relative phase difference; HWP1&HWP2; half wave plate; BS; beam splitter; M; mirror; W1&W2; wedges; P1; polarizer; PBS; polarization beam splitter; CM1&CM2; concave mirrors.

From the interference pattern of every shot, the intensity profile of its horizontal line is selected and stacked as shown in Fig. 4. A peak position P is then determined from the selected line. Since the relative phase difference Φ between two beams fluctuates, the peak position P also moves to the left or right with respect to a fixed point F . The relative phase

difference ϕ can be expressed as $2\pi\ell/T$, where ℓ is the distance between F and P and T is a spatial period of the interference pattern.

4. RESULTS AND DISCUSSION

We have measured ϕ for two specific cases of $E_{p1} \cong E_{p2}$ and $E_{p1} \cong 0.5E_{p2}$. Fig 5 shows the experimental results for the case of $E_{p1} = 9.4$ mJ and $E_{p2} = 4.66$ mJ. Each point in Fig. 5 (a) represents one of 256 laser pulses. Figure 5 (b) shows the intensity profile of the 256 horizontal lines selected from each interference pattern. It show that there some missing of phase locking.

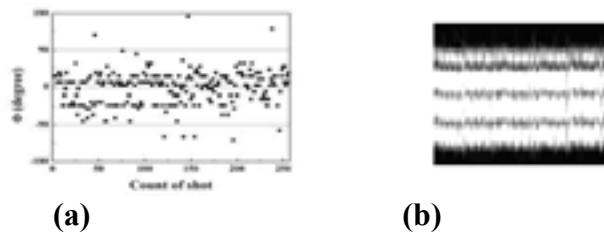


Figure 5. (a) Relative phase difference for 256 laser pulses and (b) Intensity profile of horizontal lines selected from 256 interference patterns for the case of $E_{p1} = 9.4$ mJ and $E_{p2} = 4.66$ mJ.

Figure 6 shows the experimental results for the case of $E_{p1} = 10.56$ mJ and $E_{p2} = 10.55$ mJ. The relative phase difference between two SBS waves is smaller than $\lambda/4$ for every shot. Compared to the previous results, the fluctuation of relative phase difference is considerably reduced. The profile also represents that the relative phase difference is stabilized quite a lot. The experimental results qualitatively agree with the theoretical results in Figure 3. Consequently, we have shown that it is possible to control and lock the relative phase difference by a self-density modulation, provided that the energies of the two beams are made similar.

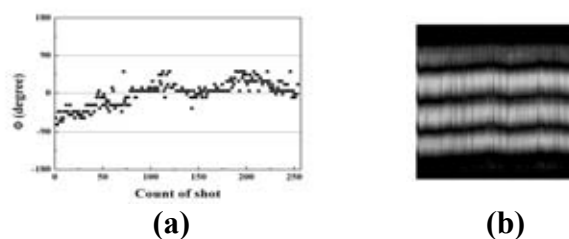


Figure 6. (a) Relative phase difference for 254 laser pulses and (b) Intensity profile of horizontal lines selected from 254 interference patterns for the case of $E_{p1} = 10.56$ mJ and $E_{p2} = 10.55$ mJ.

5. PRE-PULSE TECHNIQUE FOR THE SBS WAVE FORM

The wave form is deformed by the SBS reflection, due to the consumption of the front part of the wave energy for the formation of the acoustic grating formation and the extension of the interaction zone during the pulse propagation. We have found it is possible to keep the wave form by using the pre-pulse technique [10]. In Fig.7, (a) is the input pulse, (b) is the SBS

wave without pre-pulse, (c) is the SBS wave with pre-pulse, and (d) is the comparison of the input pulse and (c) shows the pulse shapes with or without pre-pulse. From these experimental results, it is clear that the pre-pulse technique is quite useful to preserve the pulse shape.

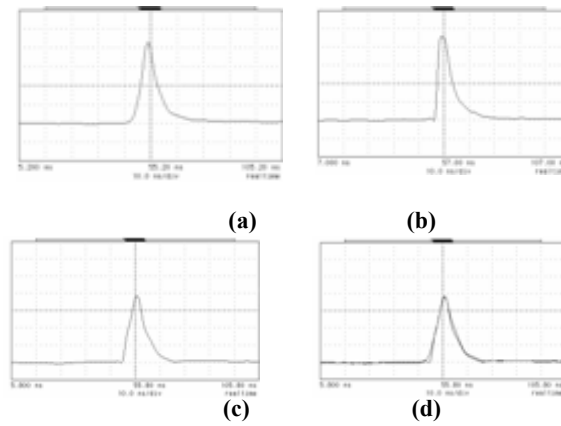


Figure 7. The pulse shapes, (a); input wave, (b);SBS wave without pre-pulse, (c): SBS wave with pre-pulse, and (d); comparison of the input pulse and SBS wave with the pre-pulse.

6. A NEWLY PROPOSED LASER FUSION DRIVER

We have proposed 2 laser fusion drivers of amplitude dividing and wave-front dividing schemes as shown in Fig.8 (a) and (b). With the phase controlling technique and the pre-pulse technique described upper, we can produce huge output energy as we want by scaling-up.

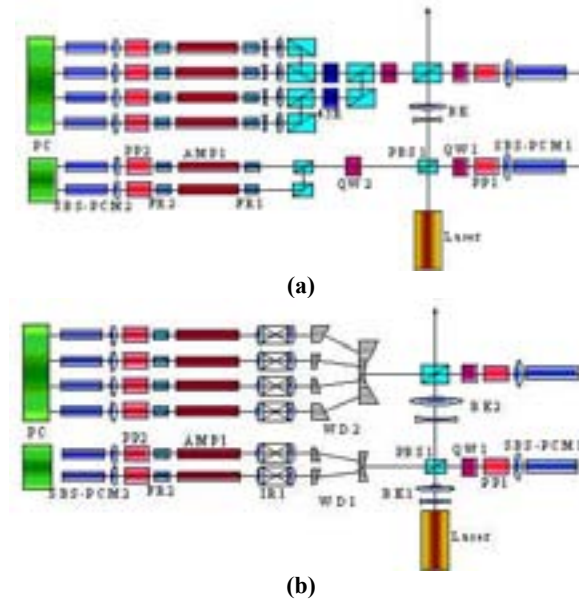


Figure 8. Schematic diagrams of the proposed laser fusion driver with SBS-PCM beam combination; (a) amplitude dividing scheme and (b) wave-front dividing scheme: PC;phase controller, PP1 and PP2; prepulsors, AMP1 and AMP2; amplifiers, FR1 and FR2; faraday rotators, IR1 and IR2; image relays, WD1 and WD2; wave-front dividers, BE1 and BE2; beam expanders, PBS1; polarizing beam expanders, QW1 and QW2; quarter wave plates, 45R; 45 degree rotator.

The wave-front dividing scheme was proposed already by one of the authors in 1997 [2]. Also these proposed laser systems are alignment insensitive so that it is very easy to install or maintain the system for we may just put the components in their position with the mechanical accuracy not optical accuracy. Also this system requires low quality of the optical components but the polarizing components, because the optical distortions caused by the low quality optical components and during the amplifications in the gain media can be compensated by this system automatically.

7. CONCLUSION

We have proposed a new phase control technique by a self-generated density modulation in order to control the phase of the SBS waves, which is required for the beam combination laser with the SBS-PCMs. Theoretical analysis shows that the phase fluctuation is inversely proportional to the pump energy and is proportional to the pump energy fluctuation. By means of the amplitude dividing, we have achieved that the relative phase difference between two SBS waves can be made smaller than $\lambda/4$. We expect that this phase control technique is very useful to develop a practically useful laser fusion driver using the beam combination with SBS-PCMs. Even if a large number of amplifiers should be installed in parallel for huge energy/power output, it will be very easy to install or maintain them because of their special characteristics such as the compensation of the optical distortions by the phase conjugated mirrors and the alignment insensitiveness by the cross type amplifier system with the symmetrical SBS-PCMs.

ACKNOWLEDGEMENTS

This work was supported by the KISTEP, the RRC at Dankook University and the IAEA, Austria, contract no. 11636/R2.

REFERENCES

- [1] HOGAN, W.J., et al., Energy from Inertial Fusion (International Atomic Energy Agency, Vienna, 1995), Chap. 3.
- [2] KONG, H.J., et al., Opt. Rev. 4, 277 (1997). Kong, H.J., et al., Fusion Engineering and Design, Vol. 44, P. 407–417, 1999.
- [3] ROCKWELL, D.A., GIULIANO, C.R., Opt. Lett. 11, 147 (1986).
- [4] LOREE, et al., Opt. Lett. 12, 178 (1987).
- [5] JUNHUA. LU, JIANREN. LU, MURAI, T., TAKAICHI, K., UEMATSU, T., XU, J., UEDA, K., YAGI, H., YANAGITANI, T., KAMINSKII, A.A., Opt. Lett. 27, 1120 (2002).
- [6] ROCKWELL, D.A., IEEE J. Quantum Electron. QE-24, 1124 (1988).
- [7] BOYD, R.W., RZAŻEWSKI, K., NARUM, P., Phys. Rev. A 42, 5514 (1990).
- [8] KONG, K., LEE, S.K., LEE, D.W., GUO, H., “Phase control of stimulated Brillouin scattering phase conjugate mirrors by a self-generated density modulation“, submitted in Appl. Phys. LETT. IN MAY OF 2004.
- [9] YOSHIDA, H., et al., Appl. Opt. 36, 3739 (1997).
- [10] KONG, H.J., BEAK, D.H., LEE, S.K., “Pre-pulse technique for preserving the wave form of the stimulated Brillouin scattering”, papers in preparation.

Investigation of beam plasma interaction as specific problem of the heavy ion driver target interface

B.Y. Sharkov

ITEP Moscow, Russian Federation

Abstract. The activities of the ITEP experimental group in 2004 are reported. The work consisted of two parts: 1. Experiments on energy loss and charge state distribution measurements of 100.8 keV/u Cu^{2+} ions in gas discharge plasma target and 2. Experimental measurements of the stopping power of explosively driven Ar plasma for 6 MeV/u Carbon and 11.5 MeV/u Xe ions.

1. ENERGY LOSS AND CHARGE STATE DISTRIBUTION MEASUREMENTS

The 27 MHz RFQ linac has been upgraded in ITEP [1]. The output energy of accelerated beam was increased from 36 keV/nucleon up to 110 keV/nucleon. The accelerator assembly consists of the 150 kV terminal with MEVVA ion source, low energy beam transport (LEBT) line with two electrostatic lenses, 12 m long 27 MHz RFQ section and diagnostic station at the output of the accelerator. The linac provides acceleration of ion current ~ 12 mA with specific mass A/Z up to 60. The MEVVA ion source with Copper cathode is currently used. During last year the beam transport line for multicharged heavy ions from 27 MHz ITEP RFQ accelerator to plasma target have been designed and assembled. The new pumping system has been commissioned. A principle layout of the experimental set-up is shown in. The optimisation of the beam transport for the maximum beam current behind the plasma target were carried out [2] by using the Trace-3D code.

The plasma was generated by igniting of 3 kA electric discharge in two 78 mm long collinear quartz tubes of 6 mm in diameter.

The measurements of free electron density and ionization degree are being performed using the method of time-resolved two-wavelength interferometry. As the first step the diagnostic of the plasma areal density $n_e dx$ was realized with Mach-Zehnder interferometer on one wavelength $\lambda=0.63\mu\text{m}$. For the initial pressure of the hydrogen gas ranging from 40 to 120 Pa (0.4 – 1.2 mbar), the linear plasma electron density from $(1.4 \pm 0.2) \cdot 10^{17} \text{ cm}^{-3}$ to $(2 \pm 0.2) \cdot 10^{17} \text{ cm}^{-3}$ was experimentally determined. The Stark broadening of the H_β line of 484.8 nm was complimentary measured for determination of the free electron density in the discharge plasma. The maximum free electron density $(1.4 \pm 0.2) \cdot 10^{16} \text{ cm}^{-3}$ for the initial hydrogen pressure 1.2 mbar correlates, within the experimental errors, with interferometric measurements.

The first measurements of the energy loss for two pressure levels inside the discharge target have been performed for Cu^{2+} ions. The resulting plasma stopping power has been estimated:

$$S_{\text{exp}}^{pl.\text{min}}(r_o = 0.95\text{Mbar}) = 158.1\text{MeV} / \text{mg} / \text{cm}^2);$$

$$S_{\text{exp}}^{pl.\text{min}}(r_o = 1.45\text{mbar}) = 124.6\text{MeV}(\text{mg} / \text{cm}^2).$$

The comparison with the stopping power obtained experimentally for cold Hydrogen (10.7 ± 0.7 i $30.6 \pm 5.3 \text{ MeV}/(\text{mg}/\text{cm}^2)$) gives the enhancement factor 4.5–6.

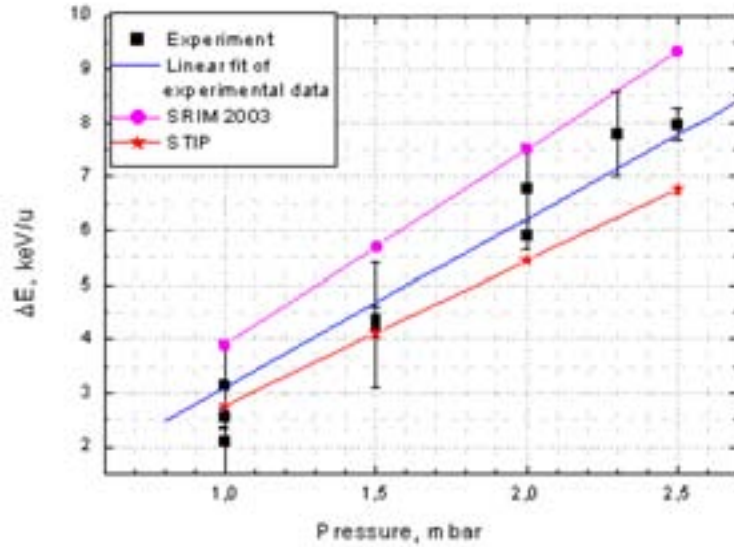


Figure 1. Energy losses of 100.8 keV/u copper ion in Nitrogen.

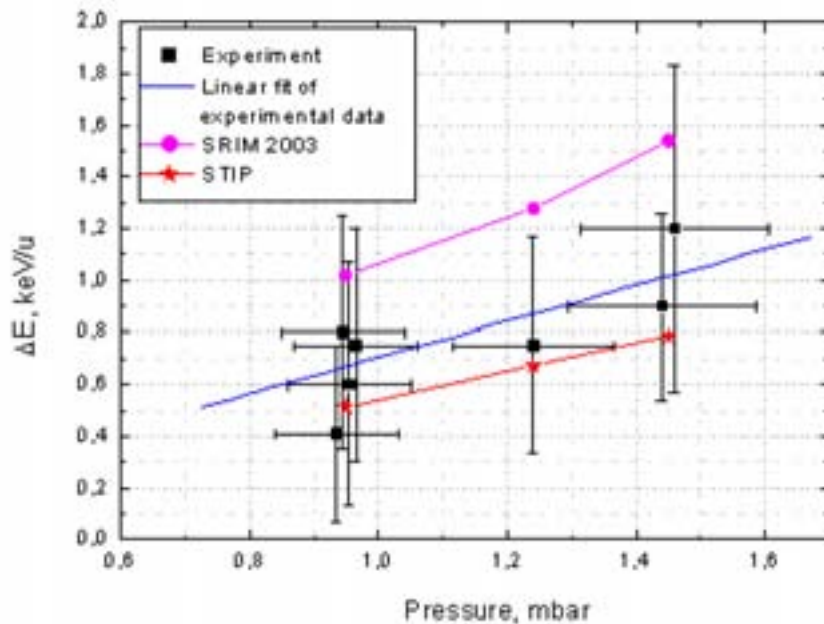


Figure 2. Energy losses of 100.8 keV/u C ion in hydrogen.

New experimental data on the stopping power of fast ions are traditionally compared with the values predicted by the publicly available SRIM code [1]. We also present such a comparison in Figs 1–3. Figure 3 shows that the ion energy $E = 100$ keV/u is well below the Bragg peak on the $S(E)$ curve for Cu ions, i.e. in a region which is most difficult for theoretical modelling. A significant (by about 30%) discrepancy between the 2000 and 2003 SRIM versions indicates that the SRIM predictions are not very reliable in this region - which, in particular, keeps motivation high for conducting new stopping experiments with high- Z projectiles at low energies. As it is seen in Figs. 1 and 2, our experimental values of S for both H_2 and N_2 targets are about 20% below the SRIM 2003 values (and about a factor 1.5 below the SRIM 2000 values). The same tendency was noted in Ref. [2] for the Ne, Na, and Mg ions in a H_2

target. Besides the semi-empirical SRIM model, based essentially on the concept of effective charge for heavy ions, a comparison with a clearly defined theoretical model would be of significant interest. As such, Figs 1–3 show the values calculated with a new beam transport code STIP, which is currently under development at ITEP. The beam transport part of the STIP code is based on solving numerically the system of equations,

$$\frac{\partial f_m}{\partial x} - \frac{\partial}{\partial E}(S_m f_m) - \frac{\partial^2}{\partial E^2}(D_m f_m) = k_{m-1,m} f_{m-1} (k_{m,m-1} + k_{m,m+1}) f_m + k_{m+1,m} f_{m+1}, \quad (4)$$

for the distribution function $f_m(x,E)$ of the beam ions over the ion energy E and charge states $m = 0, 1, 2, \dots, Z_p$ along the beam trajectory x . In doing so, we abandon the notion of the effective charge and calculate explicitly the evolution of the projectile charge q due to single-electron charge transfer events $m \rightarrow m \pm 1$; in Eq. (4) $k_{m, m \pm 1} = n_e \sigma_{m, m \pm 1}$ [cm^{-1}] are the corresponding rate coefficients. Energy loss accompanying in the charge transfer events is ignored. Also, Eq. (4) accounts for the collisional energy straggling of the ion beam in the fokker-Planck approximation by means of the diffusion coefficients $D_m = D_m(E)$, for which the classical Bohr value [3] is used.

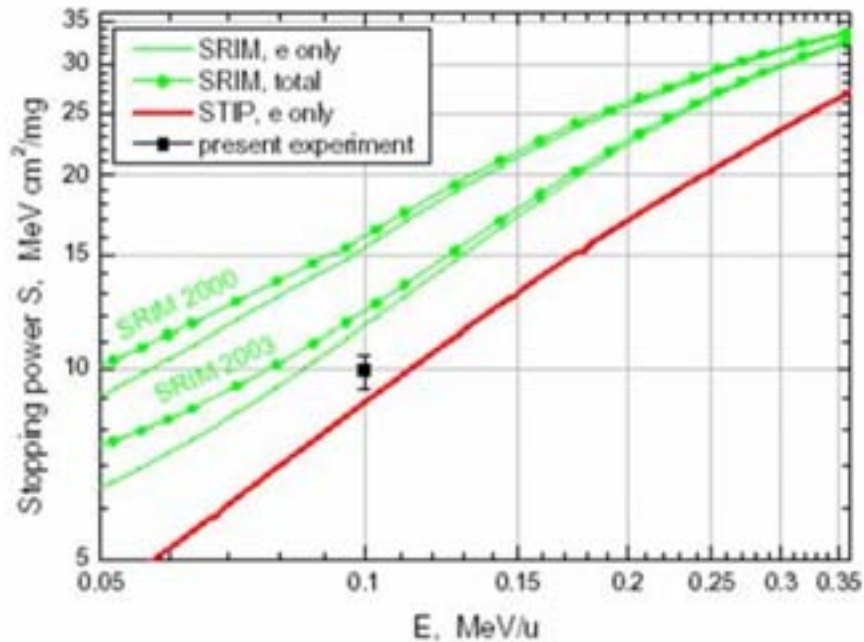


Figure 3. Stopping power for Cu ions in nitrogen as a function of the projectile energy around 100 keV/u. Curves show the values calculated by the SRIM 2000, SRIM 2003, and STIP codes for a Cu beam with equilibrium distribution over projectile charge states. For the SRIM code both the total (nuclear + electronic) and electronic (e only) stopping powers are given; the STIP values take no into account of the nuclear stopping.

In addition to the beam transport model, the key ingredients in the STIP code are a theoretical model for the stopping force $S_m = S_m(E)$ acting on a projectile ion $+q$ with an energy E , and the charge transfer cross-sections $\sigma_{m, m \pm 1}$, for which usually either a semi-empirical model or experimental data are used. The stopping force $S_m(E)$ is calculated by applying the Bloch [4] formula for a point-like charge $+m$ to each nl shell of the target atom, and then summing up the contributions from all shells. Where no atomic calculations are available, the mean excitation energies $h\omega_{nl}$ of individual shells, needed in the Bohr-Bethe-Bloch formulae, are

evaluated by an approximate semi-empirical procedure proposed in Ref. [5]. Extension of the Bloch formula into the low-velocity region, where the stopping number (Coulomb logarithm) for a given atomic shell $L_{nl} < 1$, is done by using the formula (4) from Ref. [6], which represents the rigorous low-velocity solution for the classical Bohr model of harmonically bound target electrons. In this way we effectively account for the shell corrections — also in the region where they are large, i.e. where the Bloch formula formally leads to $L_{nl} < 0$. So far, contribution to the stopping power due to the collisions with target nuclei (nuclear stopping) has been ignored.

Under the conditions of the present experiment, charge changing events for the Cu^{m+} projectiles are dominated by ionization in collisions with neutral atoms of the target gas, and recombination via capture of bound electrons from the target atoms. For the ionization cross-section we used a generalization of the scaling law from Ref. [7], which takes into account a Thomas-Fermi-like screening of the nuclear potential by the bound electrons in target atoms. For the recombination cross-section, a semi-empirical formula from Ref. [8] was used. Simulations with the STIP code have shown that the equilibrium charge distribution of Cu projectiles, shown in Fig. 4, is established very rapidly, over a fraction of 1 cm of the target length even for the lowest pressure of 1 mbar in both the N_2 and H_2 targets. In particular, this implies that precise knowledge of the entrance charge (Cu^{2+} or Cu^{3+}) is absolutely irrelevant for our stopping power measurements.

In Figures 1–3 one sees that the STIP values of the beam stopping power agree fairly well (within 15%) with the present experimental results but, in contrast to the SRIM values, lie systematically below the experimental points. The agreement becomes even better after one takes into account that the STIP results correspond to the electronic stopping only. As one can infer from the SRIM data in Figs 1 and 2, nuclear stopping should add some 5–6% to the pure electronic stopping force from the STIP calculations.

It should be noted however that a good agreement between the STIP simulations and the experimental values may, to a certain extent, be spurious. The fact is that the present STIP model for $S_m(E)$ does not account for two important effects, namely, that partially ionized projectile ions are not point charges, and the low-energy extension of the Bloch formula would be more appropriate to do on the basis of the quantum rather than classical oscillator model [6]. These two effects should, however, partially cancel one another, and their relative contribution remains to be investigated. It is worth noting here that an adequate description of the low-velocity regime of the Coulomb stopping is very important for the conditions of the present experiment: if we write the original Bloch value of L_{nl} as $L = \ln \Lambda_{nl}$, we find that $\Lambda_{nl} \sim 0.17 / (h\nu)_{eV} < 0.01$ for 100 keV/u Cu^{3+} ions in H_2 and N_2 targets.

The stated distinctions between the received experimental data of energy loss of copper ions with initial energy of 100 keV/u in cold gases with SRIM code and STIP theoretical model have evidently shown that the modern understanding of the stopping processes of heavy ions with low energy even in cold gases is not full, and new experiments in this area is extremely useful for verification of reliability of various theories.

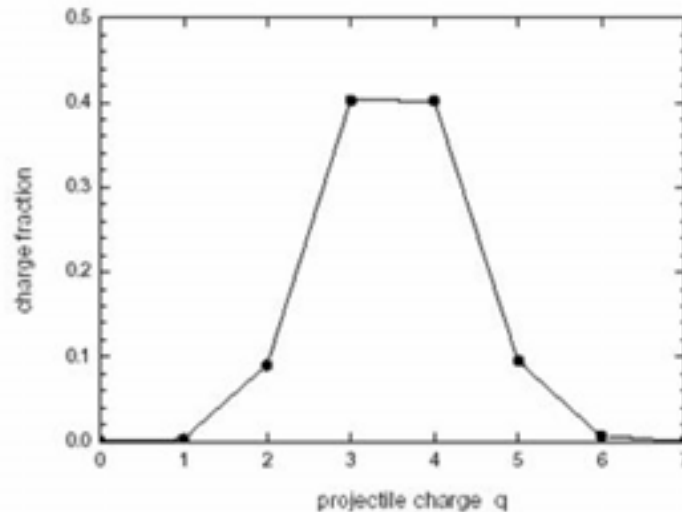


Figure 4. Distribution of Cu ions over the charge states q , as calculated by the STIP code, after they traverse 1 cm of N_2 gas at a pressure of 1 mbar.

2. MEASUREMENTS OF THE STOPPING POWER OF EXPLOSIVELY DRIVEN AR PLASMA

Interaction of heavy ions with strongly-coupled plasmas and possible non-ideality effects in the density regime up to 10^{22} e-/cm³ and temperatures between 1-10 eV is of interest for basic research in the warm dense matter physics. The shockwave that creates the plasma is driven by the detonation of a high explosive. Shock compresses gas (Xe or Ar) in a glass-tube. Experimental investigation of the stopping power of explosively driven plasma has been performed at GSI in close collaboration of the ITEP, GSI and ICP Chernogolovka groups.

Besides the ideal plasmas, which are normally associated with the research field of 'hot dense matter' and where the energy loss of charged particles in the plasma exhibits a Z_{eff}^2 -proportionality, the field of 'warm dense matter' has come under closer scientific interest in the last years. These are non-ideal, strongly-coupled plasmas, where in the area of comparable particle density the electron temperature is much lower as in the case of ideal plasma. Thus, non-ideal plasmas are characterized by a Γ -parameter ≥ 1 . For these plasmas a proportionality of the energy loss of charged particles of $< Z_{\text{eff}}^2$ is predicted [1]. A possibility to create non-ideal, strongly coupled plasmas are shockwave-driven plasmas, where gas is compressed and becomes ionized in front of a shock front and a plasma sheath of a thickness of several millimeters is created. The homogeneity of the plasma parameters depend on the planeness of the shock-wave and interactions between the region of the plasma edges with the vessel enclosing the gas volume. The shock-wave is created by a small amount of a high explosive and reaches velocities of several km/s. Flyer-plates (metal- or mylar-foils) between high explosive and gas volume improve the planeness of the shock-wave [2]. Since 2001 at the UNILAC accelerator at GSI an experimental set-up exists for measuring the interaction of heavy ions with non-ideal plasmas, as they have been characterized in the section above. The center is a compact vacuum pumped steel chamber, located at the Z6 experimental area, designed for explosions up to 200 g RDX (a high explosive on hexogen base). Actually 55 g of RDX are used in each explosive target per detonation. Differential pumping and fast valves [4] guarantee the protection of the high vacuum beam-line from the pressure increase and detonation products. The energy loss measurements are performed by using well-established time-of-flight (TOF) methods with a micro-spherical plate (MSP) used in the stop detector, also phase probes are an alternative for TOF-measurements at sufficient intensity of the ion

beam. The charge state distribution of the ions after passing the plasma can be analyzed by a 10° magnetic-spectrometer.

In the last 2 years several successful beam-times were carried out with:

Xe-plasmas (initial gas pressures between 0.2 – 0.8 bar) and 5.9 MeV/u C^{2+} -ions as projectiles

Argon plasmas (initial gas pressures between 0.2 – 3 bar) with 5.9 MeV/u and 11.4 MeV/u C^{2+} -, Ar^{10+} and Xe^{22+} -ions as projectiles

Between these beam-times the development of an optimized target with respect to free electron density, straggling and inhomogenities from interaction between plasma sheath and target walls was one main aspect. The target development reached from targets, where the detonator, which usually ignites the high explosive, was the sole source of the shock-wave, back to cumulative generators, with two stages, where in a conical section the shockwave is accelerated, to the finally successful design, the development of the ‚gap target‘ (see Fig. 5). In the head section of this target two small metal tubes, through which the ion beam enters, face each other 180° opposite, between them a gap of 3.6–6 mm exists. This is now the interaction zone with the plasma. Like in the earlier targets the shock-wave travels through the target, but the outer areas with possible inhomogenities due to plasma-wall-interaction are shaded by the tubes. Because of the short interaction distance with the compressed gas in the plasma phase the problem of low transmission due to straggling is minimized. The reflection of the shock-wave on the surfaces of glass rods of different length in the target head and observation of the distance in time between the peaks in the light emission created by the reflections result in the shock-wave velocity (see also Fig. 5) which beside the initial gas pressure is the only parameter needed to determine free electron density and plasma temperature.

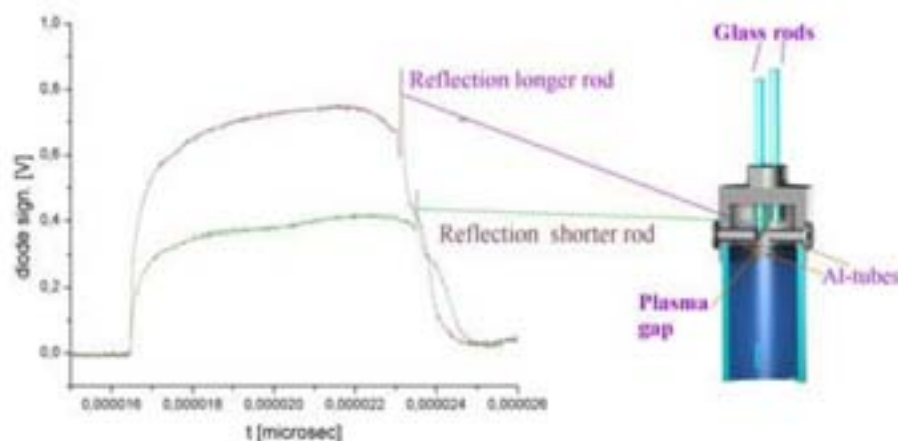


Figure 5. The gap-target design and the principle of shock-wave velocity measurement.

With the so-called gap-targets the following parameters could be obtained in three beam-times with Ar-plasmas:

- Free electron densities between $3 \cdot 10^{19}$ – $1.5 \cdot 10^{20}$ cm^{-3}
- Free electron temperatures 1.8–2.0 eV
- Compression factor between original gas pressure and pressure in the plasma phase ~ 10
- G-Parameters between 0.55–1.5
- Ionization degree in the plasma 30–50 %

Figure 6 shows the energy loss of 5.9 MeV/u C²⁺-ions in the Argon plasma [5], where the original gas pressure varied between 0.2 bar and 0.8 bar, and of 5.9 MeV/u Xe-ions also in an Ar-plasma, with initial gas pressures in the target between 0.3–1 bar. The energy loss is shown as a function of the line density of the uncompressed gas and the shock-compressed gas during the plasma phase. (The energy loss in the uncompressed cold gas in the tubes has been subtracted before.) In the plasma phase there exists a mixture of the non-ionized, compressed gas and a free electron gas. The line densities for one plasma shot in the cold gas and during the plasma-phase are comparable due to the different geometry of the interaction zones, the length of the whole gas column at the initial pressure and the short plasma gap in the case of the compressed gas in front of the shock-front.

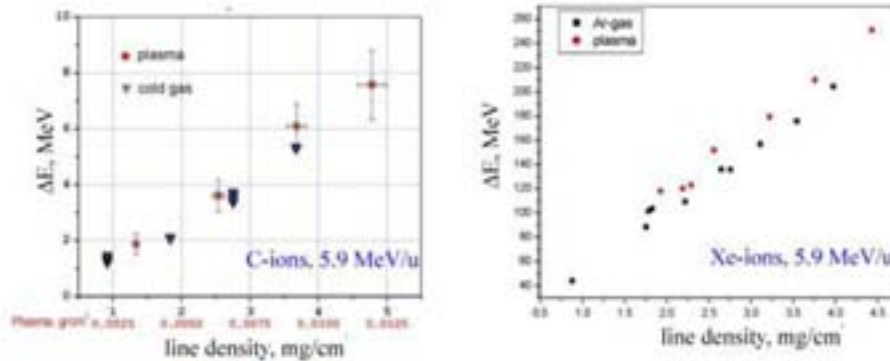


Figure 6. Energy loss of 5.9 MeV/u C- and Xe-ions in cold Ar-gas and in the plasma phase.

For these two examples the energy loss is enhanced in the plasma-phase compared to the energy loss in the cold gas at the same line density. This observation could be made also for Ar-ions interacting with the Ar-plasma, and for the higher ion energy at 11.4 MeV/u, where the initial gas pressures reached up to 3 bar, for all three ion species. An increased energy loss of about 10% in the plasma phase at the same line density as the cold gas could be systematically identified in all measurements. We conclude that this enhancement is due to the energy loss in the free electron gas during the plasma phase, and we are able to observe here the influence of the free electrons on the energy loss of the ions, even if the major number of electrons is still bound at these plasma temperatures.

ACKNOWLEDGEMENT

The work was supported by IAEA Research Contract No 11637/RBF.

REFERENCES

- [1] J.F. ZIEGLER, SRIM 2000, SRIM 2003, www.srim.org.
- [2] U. GREIFE, et al., Nucl. Instr. and Meth. B 217 (2004) 1.
- [3] N. BOHR, Philos. Mag. 30 (1915) 581.
- [4] F. BLOCH, Ann. Physik 16 (1933) 285.
- [5] M.M. BASKO, Fiz. Plazmy 10 (1984) 1195 (English translation: Sov. J. Plasma Phys. 10 (1984) 689).
- [6] M.M. BASKO, Eur. Phys. J. D 00 (2004) 0000.
- [7] I.D. KAGANOVICH, E.A. STARTSEV, R.C. DAVIDSON, Phys. Plasmas 11 (2004) 1229.
- [8] R.A. PHANEUF, R.K. JANEV, H.T. HUNTER, Nucl. Fusion (Special Suppl. 1987) (1987).
- [9] P. SIGMUND, Phys. Rev. A 56 (1997) 3781.

Beam plasma interaction experiments with intense laser and particle beams at GSI

D.H.H. Hoffmann

Plasma Physics Department, GSI-Darmstadt,
Darmstadt, Germany

Abstract. Following the recommendations of the panel of experts, GSI should not engage in a full scale inertial fusion energy research program, but use the experimental and theoretical expertise in beam plasma interaction physics as well as in accelerator physics to address key physics issues associated with intense beams. In the context of the CRP-project the experimental work concentrates mainly on the following topics:

1. High current experiments with heavy ion beams and diagnostic methods
2. Xray spectroscopy of projectile and target radiation to investigate heavy ion energy loss processes in solid, gaseous and ionized matter
3. Interaction experiments of heavy ion beams with laser generated plasma

In this report we concentrate on the first topic, since this is at the center of our CRP project.

HIGH CURRENT EXPERIMENTS WITH HEAVY ION BEAMS AND DIAGNOSTIC METHODS

The goal of the suggested subproject concerns machine developments towards the production and diagnostics of conditions of high power density in matter generated by heavy ion beams [1–3]. These research activities are an important component of the current concept of the proposed GSI-FAIR (Facility for Antiproton and Ion Research) facility and are also directed to prepare the conditions for the effective future use of the new accelerator scenario at GSI. In this context also perspectives result for the development of improved key components for the GSI research program in nuclear structure research, i.e. the development of a high performance production target at the fragment separator FRS [4].

Figure 1 shows the principle outline of the experiment as well as diagnostics procedures. An intense ion beam of the SIS 18 at GSI heats a macroscopic target volume in a very homogeneous way. Depending on the ion beam parameters thereby matter conditions of high power density are reached. The surface temperature is measured by radiation detection with a fast pyrometer that covers different wavelength regimes from the near infrared to the visible and beyond. The surface expansion speed is measured by interferometer methods. Back lighter experiments with the kJ beam of the PHELIX (Pet watt High Energy Laser for Ion Experiments) high power laser of laser supply information about the density change inside the target heated target material. These measurements are complimented by Thomson scattering experiments, which supply independent information on the density and temperature of the target plasma.

During the period covered by this report a new pyrometer with time resolution in the nanosecond range was built. It is represented in Figure 2. The target surface radiation of the target measured with fast photomultipliers. Interfilters, these are mirrors with a high transmission in a small fraction of the radiation spectrum, and a high reflectivity in the remaining part of the spectrum, are used to make optimum use of the radiation intensity in a broad wavelength regime. Combining the result of at least 6 wavelength regimes a surface brightness temperature is determined. Moreover, if a homogenous heating of the target

material is assumed, then this measurement also gives first insight into the temperature of the target volume, which is difficult to measure with other methods.

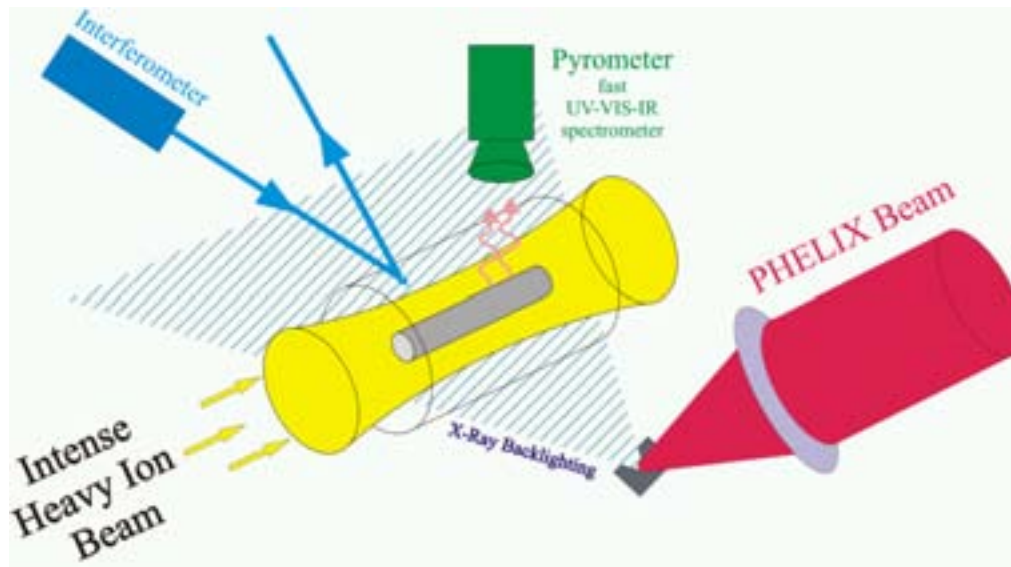


Figure 1. Schematic outline of the experimental set up with the diagnostics methods. At present measurements with a fast pyrometer are performed. Interferometry, laser backlighting and Thomson scattering are developed for a later part of the program. The experiments using the PHELIX laser beam can of course only be developed after the laser beam is available at this experimental area, which is currently under construction.

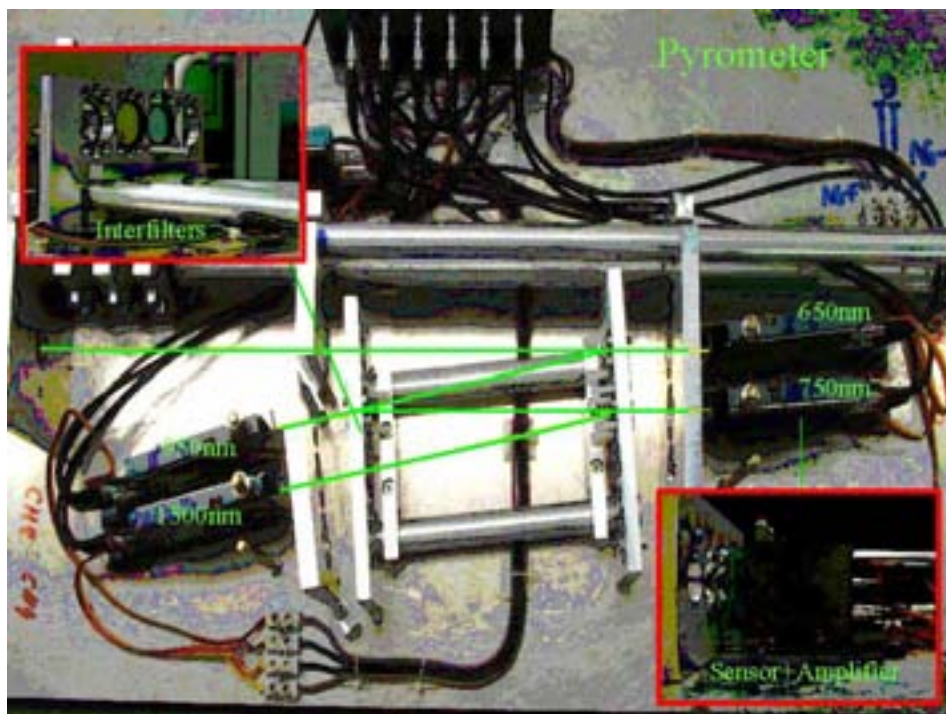


Figure 2. Pyrometer with ns time resolution. At present 4 wave bands are accessible.

For the preparation of the high current experiment towards end of 2003, new target mounting plates were designed and a new target robot was built. Thus we were able to investigate up to 50 targets in one experimental period without breaking the chamber vacuum. The targets are placed in a screw head with thread to accommodate (Figure 3 left above) the target material Pb between optically transparent sapphire discs (Figure 3 at the bottom left hand corner). The screw head shows an opening at the front for the ion beam and lateral diagnostics entrances, which are sealed off by sapphire disks. The remaining part of Figure 3 (right), shows the target shelf the inside one the target chamber. It holds 28 targets.

In December 2003 the structure was tested for the first time. In this experimental campaign the highest intensity of the ion beam with 4×10^9 particles (uranium) was measured. At the same time the capability for ion bunch compression at the heavy ion synchrotron was tested. This also resulted in a new record bunch compression parameter at GSI. In Figure 4 the bunch length with 124 ns is to be seen. This is an important result also for the future experiments at the fragment separator as well as for inertial fusion applications, where a bunch compression down to 10 ns is required.

Photos of targets and target chamber

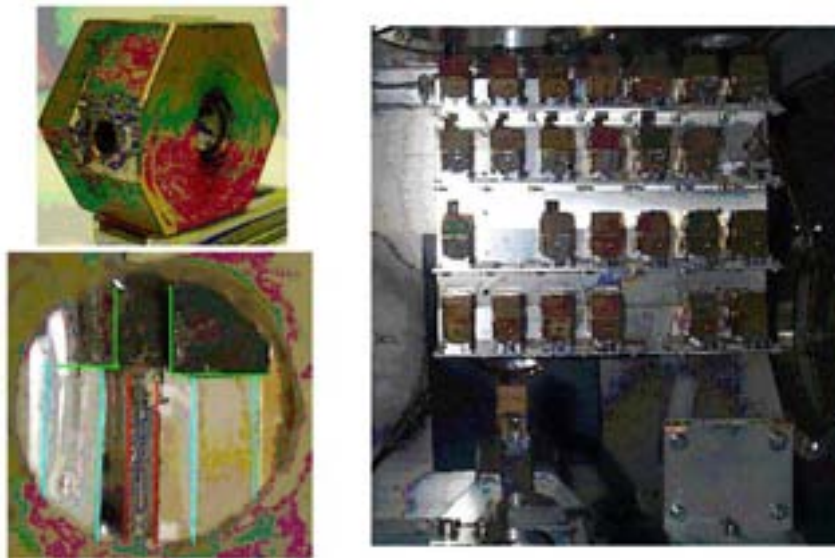
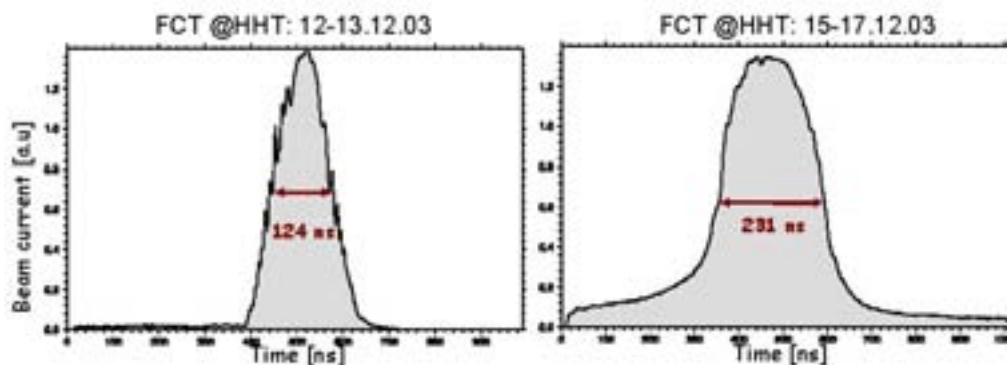


Figure 3. Target mounting plate and target shelf inside the target chamber.

At the beginning of 2004 the existing beam line at the High Energy Density experimental site of GSI was upgraded. The 6 Tm dipole magnets were replaced by 18Tm dipoles. Set-up and commissioning of the experimental area kept the team busy during a large part of 2004. The diagnostics procedures for the beam parameter optimization were improved and extended in the meantime. Together with the partners in Russia the theoretical bases was extended to understand high-energy density matter conditions. This is documented by numerous publications named in the publications list.

The best bunch compression at SIS-18: full intensity U beam - 125 ns bunch



bunch compression optimized by P.Spiller (GSI Acc. Dep.)

Figure 4. Bunch compression of a full intensity Uranium beam to 124 ns.

DIAGNOSTICS METHOD

The diagnostics methods described here, refer to methods that make specific use of high energy and high power and/or short pulse lasers. A typical example is the Thomson scattering method. The target configuration shown in Fig. 5 has an outer tamper layer that is made of an element with higher Z - atomic number than the inner target. In this case it is a compressed hydrogen target confined dynamically by a carbon tamper. In order to penetrate this outer layer it requires intense high energy x rays in the energy region of 8keV or more. This can be made available by laser plasma (see Fig. 5).

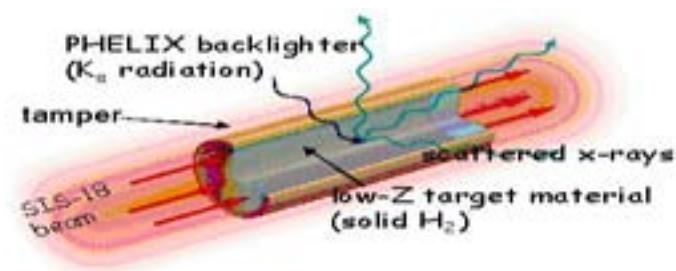


Figure 5. Typical set-up for a Thomson scattering experiment. The PHELIX Lasersystem provides the necessary intensity.

Before the PHELIX laser is available for such experiments, we started to investigate laser plasmas and tried to optimize the emission to narrow-band line radiation in the context of a thesis (diploma). The PHELIX laser of the GSI was used for these experiments. Chlorine

plasmas were produced by irradiation of NaCl and PVC samples. For the investigation of the emitted line radiation a spectrometer with a flat, highly reflecting mosaic crystal was designed and characterized. The special characteristics of high-oriented, pyrolytic graphite for the mosaic focusing were considered. The measured spectra were interpreted with the help of a particularly developed spectral line simulation with approximate temperature diagnostics. The analysis of the spectra resulted in temperatures of for instance 5×10^6 K. as result of these measurements is to be noted that with sufficient laser intensity sufficient in principle intensity in a narrow-band wavelength coverage for Thomson scattering experiments can be made available. The thesis (diploma) was begun and locked in the first year of the course of the project.

TRANSPORT AND FOCUSING

Plasma based transport and focusing systems have become an interesting alternative to traditional focusing devices [10], since they combine the property of high focusing strength with the fact of current- and space charge neutralized beam transport.

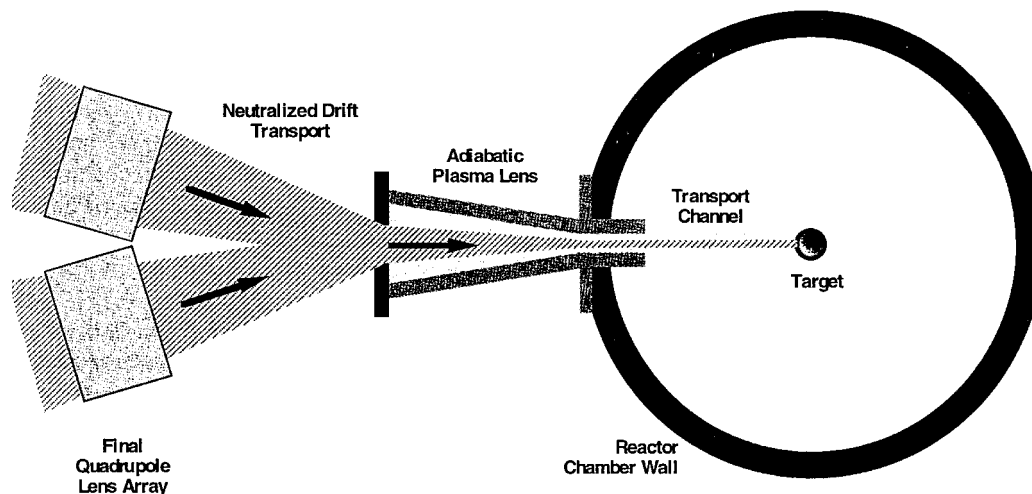


Figure 6. Schematic of plasma channel based reactor and final transport system.

The scheme shown in Figure 6 makes use of conventional beam transport and focusing schemes based on magnetic quadrupoles up to the final quadrupole lens array. An adiabatic plasma lens then combines several beams. In this region space charge effects of the intense beam become important, but the plasma of the plasma lens reduces or even eliminates this effect on a time scale given by the plasma frequency ω_p . The final transport to the pellet inside the reactor chamber is achieved inside a plasma channel.

Plasma lens focusing has been investigated over a number of years in experiments with intense heavy ion beams. Such systems have achieved quite remarkable results with respect to focusing power and focal spot shape. Moreover they have proved to be a reliable tool in the environment of accelerator laboratories.

The transport of the heavy ion beam over the distance of several meters through the target chamber of a heavy ion beam driven fusion reactor requires a different concept. For this purpose plasma channels of considerable length are required and the particles will undergo a large number of betatron oscillations inside the transport channel. Moreover the discharge

channel has to be established without any guiding structures. One way to achieve this is to initiate a discharge channel with a laser beam. Recent experiments at Berkeley and GSI Darmstadt show that such a laser initiated plasma transport channel can be generated with sufficient stability. Figure 7 shows the experimental set-up to study beam transport in a laser initiated discharge plasma channel. The laser channel is generated in a NH_3 atmosphere. A pepper pot mask splits the incoming beam into a large number of beamlets. Analysis of the beam at the exit of the channel shows that the quality of the beam may be maintained in plasma channel transport.

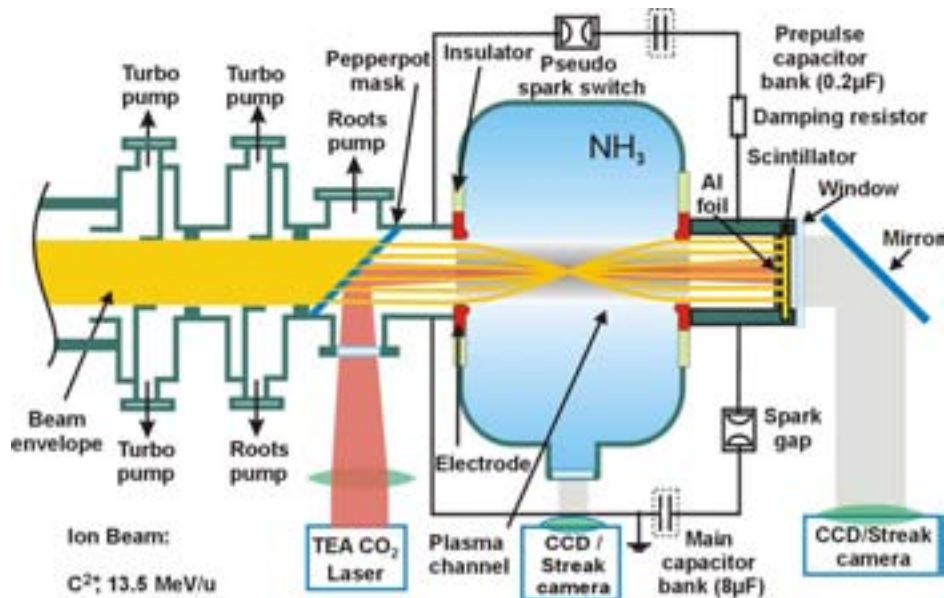


Figure 7. Set-up of a beam transport experiment in a laser initiated discharge channel.

BIBLIOGRAPHY

- A. Kozyreva, M.M. Basko, T. Schlegel, A. Tauschwitz, and D.H.H. Hoffmann, Dynamic confinement of quasi-isochorically heated targets, *Physical Review E* 68, 05406, (2003)
- D. Varentsov, N.A. Tahir, I.V. Lomonosov, D.H.H. Hoffmann, J. Wieser, and V.E. Fortov Energy loss dynamics of an intense uranium beam interacting with solid neon for equation of state studies. *Europhys. Lett.* 64, 57 (2003)
- E. Dewald, C. Constantin, C. Niemann, S. Udrea, J. Jacoby, J. Wieser, D. Varentsov, N.A. Tahir, A. Kozyreva, A. Shutov, T. Schlegel, A. Tauschwitz, D.H.H. Hoffmann, and R. Bock, Fundamental studies of heavy-ion beam interaction with solid targets, *IEEE Trans. Plasma Sci.* 31, 221 (2003)
- N.A. Tahir, FRS Group GSI, and D.H.H. Hoffmann, High power production targets for the Super-FRS using a fast extraction scheme. *Nucl. Instr. Meth. B.* 204 282–285 (2003)
- N.A. Tahir, A. Shutov, D. Varentsov, P. Spiller, S. Udrea, D.H.H. Hoffmann, I.V. Lomonosov, J. Wieser, M. Kirk, R. Piriz, V.E. Fortov, and R. Bock. *Phys. Rev. Spec. Topic Acc. and Beams* 6, 020101, (2003)
- N.A. Tahir, H. Juranek, A. Shutov, R. Redmer, A.R. Piriz, M. Temporal, D. Varentsov, S. Udrea, D.H.H. Hoffmann, C. Deutsch, I. Lomonosov, and V.E. Fortov. Influence of the equation of state on the compression and heating of hydrogen. *Physical Review B* 67, 184101 (2003)
- N.A. Tahir, C. Deutsch, V.E. Fortov, D.H.H. Hoffmann, H. Juranek, I. Lomonosov, A.R. Piriz, R. Redmer, A. Shutov, P. Spiller, M. Temporal, S. Udrea, D. Varentsov. Intense heavy ion beams as a tool to induce high energy density states in matter. *Contr. Plasma Phys.* 43, 1733 (2003)
- N.A. Tahir, A.R. Piriz, A. Shutov, D. Varentsov, S. Udrea, D.H.H. Hoffmann, H. Juranek, R. Redmer, R.F. Protugues, I.V. Lomonosov, and V.E. Fortov. The creation of strongly coupled plasmas using an intense heavy ion beam: low entropy compression of hydrogen and the problem of hydrogen metallization. *J. Phys. A* 36, 6129 (2003)
- C. Constantin, E. Dewald, C. Niemann, D.H.H. Hoffmann, S. Udrea, D. Varentsov, J. Jacoby, U.N. Funk, U. Neuner, and A. Tauschwitz., Cold compression of solid matter by intense heavy ion beam generated pressure waves. *Laser and Particle Beams* 22, 59015–63 (2004)
- C. Constantin, C. Niemann, E. Dewald, S. Udrea, J. Jacoby, D. Varentsov, P. Schwab, J. Wieser, and D.H.H. Hoffmann. Density measurements of heavy-ion-beam-induced stress waves in solid matter by a sensitive laser deflection technique. *Review Sci. Instr.* 75, 1268–1273 (2004)

PhD-Thesis and Diploma Thesis work

Marius Schollmeier: Untersuchung schmalbandiger Linienstrahlung lasererzeugter dichter Plasmen für Röntgenstreudiagnostik an Materie.
Diplomarbeit, TU-Darmstadt, Juni 2004

Serban Udrea: Elektrische Leitfähigkeit schwerioneninduzierter Plasmen.
Dissertation, TU-Darmstadt, 2004

A. Kozyreva: Creation of High Energy Density in Matter with Heavy Ion Beams for Equation of State Studies.
Dissertation, TU-Darmstadt, 2003.

Collaboration

In two years during the CRP project we had a research visit of Professor Dr. R. Khaydarov from Uzbekistan, and all the research is done in close collaboration with the group headed by Professor Dr. B. Yu. Sharkov, from ITEP Moscow.

This collaboration is extremely valuable. Professor Sharkov does not only provide the expertise that is available from him or his group, but he also does establish the necessary contact to other research institutions within the Russian Federation.

CHAMBER STUDIES

Peripheral elements and technology associated with pulsed power inertial fusion; IFE chamber wall ablations with high-flux pulsed beams including ions and UV laser lights

K. Kasuya¹, T. Norimatsu, S. Nakai², A. Prokopiuk³, W. Mroz³

¹Department of Energy Sciences, Tokyo Institute of Technology, 4259 Nagatsuta, Midori-ku, Yokohama, Japan

²Institute of Laser Engineering, Osaka University, Osaka, Japan

³Institute of Optoelectronics, Warsaw, Poland

Abstract. Two kinds of experiments were performed to observe the characteristics of a pulsed intense ion beam and a UV laser beam. The former particle beam specie was proton and the latter laser was ArF laser. These beams were used for the IFE first wall ablation. Our interests for the uses of these beams arise from the modeling of the first wall ablation of the candidate inertial fusion materials [1]. To know the precise relation between the thickness of the ablated surface layers of various materials and the used proton beams to ablate the targets, it is necessary to know (in-situ) the precise characteristic of the focused proton beams just under the irradiation. We produced such proton beams with one of our pulsed power machines in Japan, and measured the current and voltage characteristics at the focal point. The half part of the focused proton beam was used for this kind of measurement, while the rest half of the same beam was used to ablate the sample targets. With this kind of method, we could investigate the precise relation between the exact beam condition and the ablated thickness without much ambiguity. The first author brought various sample materials to Warsaw, and an ArF laser in the Polish authors' laboratory [2] was used to irradiate the samples. After the irradiation, the sample surfaces were observed with various diagnostic tools including a laser microscope (Olympus-LS1200) in the Analysis Center of the second Japanese authors (ILE-Osaka University). Most important data were the first wall ablation rates under different experimental conditions of different beams, while the surface specie changes under the successive beam irradiations were also interesting in some cases. All of the experimental results were gathered and compared with our former results [3–6], for the compilation of future database of IFE reactor designs. The details shall be presented during the Technical Meeting.

1. INTRODUCTION

Many issues must be clarified before we can design more advanced versions of IFE reactor chambers in the near future. These issues change some times as the results of new concepts for the target implosion schemes. Most recently, the fast ignition scheme brought a little bit different productions of neutrons, X ray and ion beams as the results of target implosions.

Although the neutrons share the highest rate of fusion burn energy, they are not caught with the first walls, which face the targets, and almost all part of the energy must be transformed into heat within the thick blankets behind the first walls. On the contrary, the peak power of the X rays is highest among the energy sharers, although the shared energy itself is lowest. The second energy transporters are the ion beams accompanied with co-moving electrons, almost all energy of which is transformed into heat within the very thin layers of the first walls facing the targets. The rate of the wall ablation thickness with these ion beams is highest among the three components. So, we tried to contribute to the database of ion beams at first, in this article. On the contrary, the ablation with laser light is also important because the laser

light hits the tail cone of the fast ignition laser driven target, and the reactor chamber wall in the case of accident.

2. INTENSE FLUX BOMBARDMENT OF CHAMBER WALL WITH IFE TARGET IMPLOSION

A few examples of the direct irradiation targets are shown in the reference [1–6]. In the case of 400MJ fusion energy output per shot [4], the energy partitions among the neutron, ion beams, alpha particles and X ray are 82.0%, 14.5%, 2.5% and 1.0%. As for the energy partitions among the ion species, the carbon ions seem to be most dominant, while the deuterium and proton ions follow. If these results are true, it is necessary for us to investigate the carbon beam ablation of the wall materials, as the first priority in this field. The second is the deuterium ablation, and then comes the proton ablation.

3. SIMULTANEOUS MEASUREMENTS OF BEAM AND ABLATION CHARACTERISTICS

There were shot-to-shot characteristic changes of the produced proton beams, which were used to irradiate the targets. To derive from this ambiguity we tried to make simultaneous measurements of the beam and the ablation characteristics. Figure 1 shows the schematic diagram of the experiment. Two parts were extracted from the converging ring-shaped proton beam with two beam apertures. One part was used to measure the beam current density with a biased ion collector, while the other part was used to irradiate the target, simultaneously. The beam apertures were placed at a distance from the focal point (ahead of the focal point).

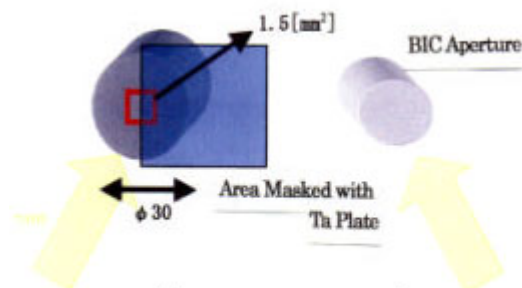


FIG. 1 Schematic Diagram of Proton Beam Irradiation

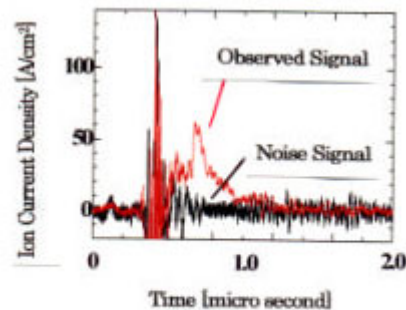


FIG. 2 Ion Current Density vs. Time

The diameter and the thickness of the graphite target were 30 mm and 5 mm. After the beam irradiation, the surface of the target with the area of 1.5 mm^2 was observed with a laser microscope (Keyence VK-8550 in our diagnostic center at our TI Tech main campus). The spatial resolution of the microscope was 1.46 micron along the 3D axes. The half part of the irradiated surface was covered with a Ta masking plate.

The current density profile vs. time of the proton beam is shown in Figure 2. Although the noise level was high, we could distinguish the beam current signal from the noise. Table I summarize the observed beam characteristics in our experiment.

TABLE I: OBSERVED PROTON BEAM CHARACTERISTICS

Peak Ion Current	2.00 kA
Peak Ion Current Flux	$\sim 200 \text{ A/cm}^2$
Pulse Width	$\sim 400 \text{ ns}$
Total Ion Flux	$2.75 \times 10^{19} / \text{cm}^2$
Energy Flux	11.0 J/cm^2

With the laser microscope, we could obtain a 3D image of the graphite surface, which is shown in Fig. 3. The left- lower half is the beam- irradiated place, while the right-upper half is the original surface without the beam irradiation. With the software of the microscope, we could estimate the ablated thickness of the surface with the proton beam. The over-all ablated thickness in this case was 13.3 micron. The more details about the ion beam ablation results are described in our other paper [1], because we have not enough space here.

A Thomson parabola ion spectrum analyzer was used to record the ion tracks on a small plastic plate similar to CR-39. After the surface etching of the plastic with a 6N-NaOH water solution for 2 hours under 70°C, it was found that the beam specie, the beam charge state and the mean beam energy were H⁺, 1 and 241keV. We assumed that the beam had a Gaussian shape of energy spectrum with the half- width of 29.8keV. The energy spectrum distribution of the beam is shown in Figure 4.

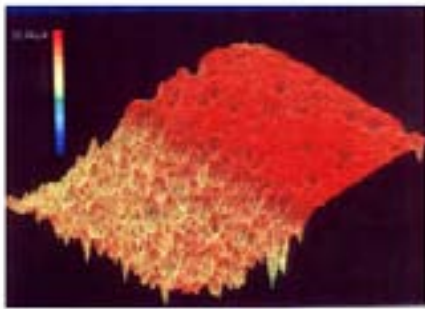


FIG. 3 3D Image of Graphite Surface

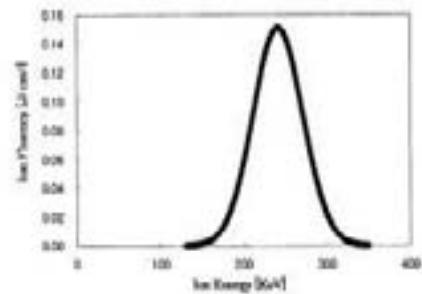


FIG. 4 Beam Energy Spectrum

4. OBSERVATION OF VARIOUS MATERIAL SURFACES IRRADIATED AND CRATERED WITH FOCUSED ARF LASER LIGHTS

It is necessary to know the ablation rates of various material surfaces under the irradiation of intense UV laser lights, as one of the ablating beams, when we design the future inertial fusion reactors driven by big lasers. So, we irradiated various materials with a UV laser light. The laser wavelength, the pulse width and the maximum repetition rate were 193 nm, 20 ns and 50 Hz. Irradiated materials were LiPb, Pb as the wet wall candidates of the inertial fusion reactors, while W, C, Al₂O₃, SiC and SiC-Si composite material were also irradiated as the dry wall candidates. The changes of the irradiated surface conditions under different irradiation conditions were observed with three different kinds of optical diagnostic tools. The structures of the produced craters were investigated precisely. We could show how strong the tungsten was against such laser ablations, compared with LiPb or Pb etc.

4.1 Purpose of ArF laser experiments

Without the knowledge of the ablation rates of the wall and target candidate materials, it is not possible to design reactor chambers for the inertial fusion energy (IFE) power plants. An example of a fast ignition laser IFE target design contains a tail cone to guide the intense fs laser light into the central ignition region. The cone material is (or materials are) supposed to be one or two of the LiPb, Pb and gold which matching is better with the reactor wall. We must also take into an account of the various cases in which intense short wavelength laser lights impinge upon such candidate material surfaces under consecutive normal and abnormal (accidental) situations.

The UV lasers with short wave lengths, such as KrF (248 nm), ArF (193 nm) and F₂ (157 nm) lasers, give the new possibility of using such laser radiation for different application to pulsed laser deposition, laser micro-fabrication, and also give the new experimental possibility for the investigation of the interaction between the intense UV laser radiation and material surfaces [2, 7].

In the case of the KrF laser with the photon energy of 4,99eV, we can observe (dependent on laser fluency (laser power density) on the target) the effects of the classical (“inverse bremsstrahlung”) absorption, as well as the effects of multi-photon absorption and absorption through the excited levels.

Effects of different absorption mechanisms are visible for example, during the laser deposition of thin films. With low laser fluencies, the deposited layers are smooth, without any droplets of debris, while (starting from the laser fluency of about 8 J/cm²) some droplets appear in the deposited layers. In the case of film deposition with the ArFlaser, the thermal effects caused by classical absorption are not visible with moderate laser fluencies. The photon energy of the ArF laser radiation (6,42eV) is enough high to increase the probability of the multi-photon absorption and the absorption through the excited levels, which causes these two processes to become the dominant absorption mechanisms. A comparison of the quality of thin films from hydroxylapatites, deposited with KrF and ArF lasers is made in other paper by the authors of this article.

In the case of the F₂ lasers, the photon energy is higher than the case of ArF laser, and the efficiency of non-classical absorption mechanism is more effective than the case of ArF laser radiation. However, as the today’s F₂ laser output energy per pulse is much smaller than the other UV laser energy, the F₂ laser is not often used in the laboratory investigations.

In our article, we present results of the interaction of the ArF laser radiation under high laser fluencies. The depth of the laser-produced craters was observed precisely with three different kinds of diagnostic methods. The first one was a laser microscope. The highest spatial resolution was obtained under the high spatial multiplication, although only the average value over a rather large area of the craters could be distinguished among different materials and different irradiation conditions. If the average was taken within a smaller area, the background noise level was too much to observe the real value. The second method was a digital microscope with a conventional light source, with which three dimensional crater photographs with the highest reality were easily taken. The third method was a laser displacement counter with a precision motor-drive locater, with which the depth and height of the crater and wall were recorded along a rather narrow traverse line on the surface. The obtained images of various material surfaces with these different methods were compared in detail.

4.2 Experimental procedure

An ArF laser was used to shoot the targets at the angle from 10° to 45° with respect to the normal to the target surface. The sample targets were placed on a movable X-Y-Z holder, which was driven with precision step motors in a vacuum chamber. The vacuum pressure inside the target chamber was about 2×10^{-5} Pa. The maximum output energy of the laser was about 650 mJ, while the size at the laser focus was $0.07 \times 0.17 \text{ cm}^2$. The laser radiation was focused onto the investigated materials by a spherical CaF_2 lens with $f = 350$ mm, with anti-reflection layers. The distance between the laser light source and the focal point was ~ 270 cm. Although the laser beam was guided through the vacuum of $p \sim 3 \times 10^{-5}$ torr, high energy-losses with (at least 50%) were observed. The energy losses were caused mainly by the three optical elements: (1) the entrance CaF_2 vacuum window, which cut off the vacuum tube near the laser source, (2) the focusing lens and (3) the second CaF_2 window, which prevented the lens from material surface deposition. A part of the laser energy was absorbed also in the residual gas in the guide tube between the laser and the target chamber. The laser fluency was changed between 15 J/cm^2 and 25 J/cm^2 , and the repetition rate of laser was changed from 1 Hz to 50 Hz. The maximum number of laser shots per one place on the irradiated samples was 2×10^5 . Irradiated materials were LiPb, Pb as the wet wall candidates of the inertial fusion reactors, while W, C, Al_2O_3 , SiC and SiC-Si composite material as the dry wall candidates were also irradiated.

The first author brought various sample materials to the fourth and fifth authors, and an ArF laser (Lamdaphysik- LPX305i) in their laboratory was used to irradiate the samples. After the irradiation, the sample surfaces were observed with a laser microscope (Olympus-LS1200) in the Analysis Center of the second and fourth authors, and a few depth-meters of different kinds (TI Tech) and so on.

With a simple-minded consideration, the normal incidence of the laser light on the target surface is preferable to utilize the laser energy as effective as possible for the maximum ablation of the surface. On the contrary, the absorption of the laser light with the ablated plumes becomes more intense if the incident angle becomes smaller. This effect becomes larger if the repetition rate of the laser light becomes higher. The more quantitative comparison with the experimental results must be made.

4.3 Experimental results

Obtained experimental results can be divided into two groups, as follows. The first group is composed of the materials with the low melting temperature (LiPb, Pb), and the second group is composed of the materials with the high melting temperature.

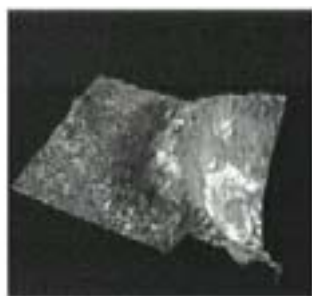


Fig. 5. 3D-image of LiPb crater.

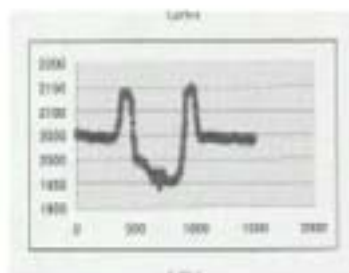


Fig. 6. 1D-plot of LiPb crater.



Fig. 7. 2D-image of LiPb crater.

The materials with the low melting temperature were irradiated by the laser radiation with the high fluency of 25 J/cm^2 , at the angle of 10° with respect to the normal to the target surface, with the repetition rate of 10 Hz. Figure 5 shows a part of the three dimensional crater with visible droplet of re-melted LiPb target after the 10^3 laser shots. The visualization of the partial crater was done with a digital microscope (Keyence, VHX-100 Model). Under the successive laser irradiations, the surface was heated over the temperature higher than the melting temperature. The flow formed such a typical crater with the wall higher than the original surface of the irradiated samples (Figure 6). To obtain these pictures, we used a combined diagnostic tool with two elements, (1) a laser displacement counter (Keyence, LE-4010 Model) and (2) a motor-driven precision locator (COMS, MAP-1EM 50X Model). Within the almost whole area of the crater bottom, the bright melted structure was observed as is shown in Figure 7, which was obtained with the above digital microscope.

The more detailed surface investigation was made with a laser microscope (Olympus, LS1200 Model). The average depth of the Pb craters, irradiated with the same condition as the above LiPb, is shown in Figure 8 as a function of the total number of accumulated laser shots. An almost proportionality between the depth and the total number of laser shot was observed at the left-bottom corner in the same figure, while a depart from the same proportionality started after the number of two hundreds. This fact reveals that the conditions for the laser absorption and the laser ablation of the irradiated material were changed around at this two hundreds. The reason of this change may be partial melting/re- melting of the crater bottom. In the case of Pb targets, we observed craters with similar flow-associated walls to the case of LiPb.

In the case of tungsten targets, the above proportionality continued until the 10^4 total number of laser shots (Figure 9). When we accumulated 10^5 laser shots in one place, we also observed a slight difference from the proportionality. At the bottom of Fig. 10, an average crater depth is plotted as a function of the distance along the vertical axis on the surface image of the central part of the same figure.

This was obtained after 10^4 laser shots in one place. In such experiments with tungsten targets, we could not observe such walls around the craters, formed by the melted material flow. We also used here the laser microscope. A different kind of diagnostic result with the same microscope is shown in Figure 11, which shows the 3-dimensional plot of a tungsten crater without any material flow around the crater. We observed a similar shape of crater (without the material flow) after the 10^5 laser shots in one place, as the above-mentioned depart from the proportionality was slight.

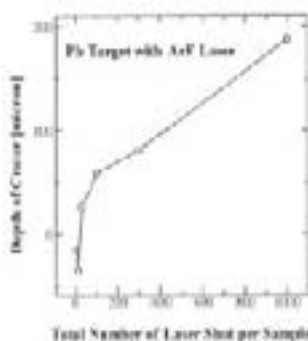


Fig. 8. Crater depth vs. laser shot number for Lead.

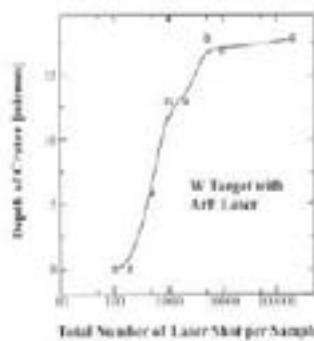


Fig. 9. Crater depth vs. shot number for Tungsten.

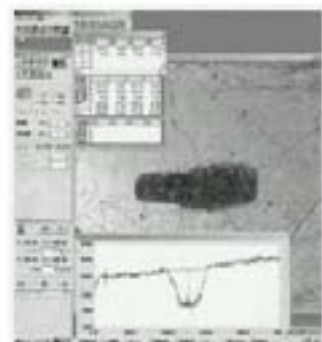


Fig. 10. 1D and 2D images of Tungsten, observed by a laser microscope.

An Al₂O₃ ceramic was also irradiated at the angle of 10° with respect to the normal to the target surface, with the laser repetition rate of $f = 50$ Hz and the average fluency of 15 J/cm². After the accumulated 10⁵ laser shots in one place, a crater was formed with a wall higher than the original surface before the laser irradiation (Fig. 12). Because the melting temperature of Al₂O₃ ceramic is very high (2,050°C), and because the wall material is supposed to be aluminum, such crater could be produced. Here the oxygen within the Al₂O₃ was supposed to be ablated and go far away from the original surface, although the aluminum was supposed to remain on the original surface. This was because the ablated oxygen under the gas condition is more mobile than the solid or liquid aluminum, after the chemical bindings were broken. It could escape from the crater more quickly than the aluminum. Melting temperature of aluminum is 660.4°C, which means that in time of accumulated 10⁵ laser shots, the temperature of crater bottom becomes higher than the melting temperature of the aluminum.

The C, SiC and SiC -Si were irradiated at the angle of 10° with respect to the normal to the target surface, with the laser repetition rate of $f = 10$ Hz and the average fluency of 15 J/cm². Under these experimental conditions we could not observe the thermal (melted) effects.

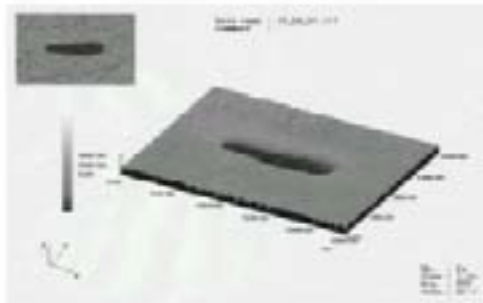


Fig. 11. Bird-eye-view of Tungsten crater.

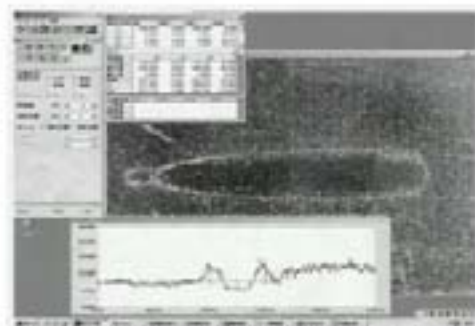


Fig. 12. 1D- and 2D- images of Al₂O₃ crater.

5. DEVELOPMENT OF NEW ION SOURCES FOR TARGET IRRADIATIONS

5.1. Cryogenic diode with compact cryogenic cooler

A new cryogenic diode with a compact cryogenic cooler was designed and operated very recently to produce pure, high efficient and high brightness beams for the target irradiation oriented for the purpose including the chamber wall ablation. The cross-sectional view of the diode and the preliminary temperature history vs. time after the start of operation shall be shown elsewhere after we shall get the clearance issued by the collaborating US Laboratories. Xe beams were produced with this cryogenic ion driver.

5.2. Production of medium-mass ion sources including C and Si

Room temperature diodes to produce carbon and silicon beams were newly proposed, and the initial experimental results were obtained. DLC (diamond like carbon) film and silicon wafer were possible to be used in our intense pulsed ion diodes. The micro-divergence angle of the Si ion beam on the anode surface was obtained in our first experimental demonstration.

6. SUMMARY

Simultaneous measurements of intense proton beam diode and ablation characteristics were performed successfully. Newly operated diode could produce intense Xe, C and Si beams

recently. The present results of the experimental investigations concerning the laser-created crater-shapes in different materials suggest that the main mechanism for the absorption of the ArF laser radiation is the photochemical absorption. In the case of the low melting temperature materials, and with the accumulation of the large number of laser shots in one place, the flow of melted materials appear around the crater, which is supposed to be the thermal effects. Our present results can also suggest that a small part of such short wavelength ArF laser is absorbed by the classical absorption mechanism.

ACKNOWLEDGEMENTS

The authors acknowledge the following people and foundations for their supports during this study. Many kinds of materials to be irradiated with the beams were endorsed by several groups in Japan and USA. This study was sponsored by (1) IAEA, (2) The Ministry of Education, Science, Culture, Sports and Technology in Japan, (3) ILE, Osaka University, (4) the Japan Society for Promotion of Science, and (5) TI Tech. This work was performed under the IAEA Coordinated Research Project on "Elements of Power Plant Design for Inertial Fusion Energy", RC-845-F1.30.08, Vienna, Austria, and the 2001-2003 US-Japan Collaboration Project in the field of Nuclear Fusion on "Wear and Tear of Reactor Wall Materials with High Flux Ion Beam and Pulsed X rays" between SNL and TI Tech. International collaboration project between Japan and Poland was supported by the Centennial Memorial Foundation of the Tokyo Institute of Technology and the EUREKA E 2841 ADVANCED PLD project, sponsored by State Committee for Scientific Research of Poland.

REFERENCES

- [1] KASUYA, K., KASAMATSU, A., RENK, T., OLSON, C. et al., J. Nuclear Materials 313–316 (2003), pp.235–238.
- [2] MROZ, W., PROKOPIUK, A., MAJOR, B., KASUYA, K. et al., Applied Surface Science 197–198 (2002), pp.371–375.
- [3] KASUYA, K., ARAYA, S., KAMIYA, T., Proceedings of 14th International Conference on High-Power Particle Beams and 5th International Conference on Dense Z-Pinches, June 23–28, 2002, Albuquerque, NM, USA, (2002), pp.425–428.
- [4] KASUYA, K., KAMIYA, T., MROZ, W., YAMANAKA, T., NAKAI, S., *ibid*, (2002), pp.433–436.
- [5] KASUYA, K., RENK, T., OLSON, C., NORIMATSU, T., NAGAI, T., YAMANAKA, T., NAKAI, S., *ibid*, (2002), pp.429–432.
- [6] KASUYA, K., RENK, T., OLSON, C., *ibid.*, (2002), pp.437–440.

Chamber dynamic response, laser driver-chamber interface and system integration for inertial fusion energy

M.S. Tillack, F. Najmabadi, A.R. Raffray

University of California San Diego, La Jolla, California, United States of America

Abstract. The University of California at San Diego maintained an active program of research on inertial fusion energy (IFE) technology for the duration of the IAEA Coordinated Research Program. Significant progress was made in all three areas of our collaboration.

Introduction

In the area of IFE Chamber Physics, we made progress in both modeling and experimental studies. The SPARTAN 2D gasdynamic code was developed, validated and used to study the dynamic response of dry-wall IFE chambers following target explosions. In addition to SPARTAN, substantial new modeling capabilities were added in the area of radiation hydrodynamics (Hyades, Helios) and atomic physics (Cretin, Hullac). A new laboratory was constructed, and experiments were performed on ablation plume dynamics, phase change physics and magnetic diversion of expanding plasma. New research programs were initiated in the related topics of EUV lithography and atomic processes in dense plasmas.

In the area of Final Optics, we continued to lead US efforts on the development of grazing-incidence metal mirrors for laser-IFE. We expanded our experimental capabilities through the addition of a KrF laser and associated diagnostics, and worked with vendors to develop several promising techniques for the manufacture of power plant optics. Scaled prototype testing has demonstrated the survival of these mirrors up to 18 J/cm^2 of laser fluence over 10^5 shots. These studies are now continuing under the auspices of the High Average Power Laser (HAPL) program.

In the area of IFE Design Studies, UCSD led a national conceptual design study entitled ARIES-IFE. This study focused on an assessment of IFE chambers and chamber interfaces for the three main chamber types: dry walls, wetted walls and liquid walls. The study was completed in November 2003, and a special issue of the journal *Fusion Science and Technology* was prepared.

Following is a summary of the technical progress in each of these areas.

Chamber Physics

Progress on chamber physics is summarized in the following five subtopics: (1) development of the SPARTAN gasdynamic code, (2) ablation plume dynamics, (3) magnetic diversion of ablation plumes, (4) experimental studies of laser propagation in chamber gases, and (5) homogeneous nucleation and growth of nanoclusters in ablation plumes.

1. SPARTAN. [A1-A2] Many physical phenomena with different time scales occur in the chamber following the target explosion. After the target-generated x rays and ion debris traverse the chamber, the chamber environment is in a non-equilibrium phase (e.g., non-

uniform pressure) and material is introduced in the chamber (e.g., ejecta from the wall as well as desorbed target constituents implanted in the wall). Afterward, the chamber environment evolves mainly in the hydrodynamics time scale. Understanding the evolution and dynamics of the chamber environment during this “long” timescale is essential in developing a rep-rated laser-fusion facility. We have developed the SPARTAN code to investigate chamber evolution. Strong shocks born out of the target blast are captured by a second order Godunov algorithm for compressible Navier-Stokes equations. Arbitrary chamber geometry is incorporated into a Cartesian grid and resolved by embedded boundary method. Simulations demonstrate the robustness of the numerical algorithm in treatment of highly nonlinear chamber dynamics with fast moving discontinuities. For this purpose, the effects of selected parameters (viscosity and heat conduction) on the chamber state prior to the insertion of the next target were evaluated.

2. Ablation plume dynamics. [A3-A4] The effect of ambient gas on the expansion dynamics of plasma generated by laser ablation of an aluminum target has been investigated using frequency doubled radiation from a Q-switched Nd:YAG laser. The diagnostic tools include fast photography of overall visible plume emission using a 2 ns gated intensified charged coupled device and space and time resolved emission spectroscopy using a 50 cm monochromator/spectrograph and photomultiplier tube. The expansion behavior of the plasma was studied with ambient air pressure ranging from 10^{-6} to 100 Torr. Free expansion, plume splitting and sharpening, hydrodynamic instability, and stagnation of the plume were observed at different pressure levels. Space and time resolved emission spectroscopic studies showed a twin peak distribution for Al and Al⁺ species at farther distances illustrating plume splitting at pressures higher than 100 mTorr. Combining imaging together with time resolved emission diagnostics, a triple structure of the plume was observed. The expansion of the plume front was compared with various expansion models and found to be generally in good agreement.

3. Magnetic diversion of ablation plumes. [A5-A6] The interaction between plasma clouds and a magnetic field is one of the most fundamental problems in plasma physics. The presence of magnetic field during the expansion of the plasma may lead to confinement, ion acceleration, enhanced emission intensity, instabilities, etc. The idea to use magnetic fields to confine or divert high-energy ions emanating from IFE target explosions has been considered from the early days of IFE power plant research. It has been postulated that a cloud of laser produced plasma is stopped by the magnetic field B in a distance $R \sim B^{-2/3}$. In this work, we explored the expansion dynamics of a laser-produced plasma into several magnetic configurations, including fields aligned along or transverse to the expansion direction, and a cusp with the axis aligned with the expansion direction. Plasma was produced using pulses from a Q-switched Nd:YAG laser supplying power density in the range of $\sim 10^9 - 10^{12}$ W cm⁻². Significant changes were observed in the plume dynamics, including enhanced emission, confinement of the plasma, etc. Observation of the temporal evolution of laser-created plasma expanding across a magnetic field clearly demonstrated magnetic confinement of the plume.

4. Laser propagation. [A7-A8] The energy absorption and laser propagation characteristics of air (at 1 atm) and argon (from 10 Torr to 1 atm) sparks have been investigated. To create the sparks, 532 nm pulses from a frequency doubled Q-switched Nd:YAG laser were used. We employed 2 ns gated fast photography for studying the time evolution of the kernel at early times. Optical emission spectroscopy was used to infer temperature and density of the sparks. Significant energy absorption by the plasma is observed just above the breakdown threshold. The energy absorption and propagation in the spark indicated that an argon plasma is more absorptive than air plasma. The absorption of the spark increases with laser energy, and at higher energies absorption saturation is observed. A spiky behavior is observed in the

transmitted temporal profiles of lasers at higher energies and this is explained as due to the formation of a self-regulating regime. Whereas significant energy absorption by the plasma was observed at high pressures (>100 Torr), there was negligible absorption when the pressure is lower than 50 Torr. The plasma kernel showed distinct behavior with respect to laser energy. At a laser energy well above the breakdown threshold, the spark moved only in the backward direction and the forward component was absent indicating the strong absorption of the laser by the spark front. A spiky behavior is observed in the transmitted temporal profiles of the laser at higher energies and at high pressures and can be due to the formation of a self-regulating regime.

5. *Condensation in ablation plumes.* [A9] Ablation plumes caused by short-pulse laser irradiation provide conditions which are well suited to the formation of nanoclusters. The high saturation ratios and presence of ionization lead to extraordinarily high nucleation rates and small critical radii. We have explored the homogeneous nucleation and heterogeneous growth of condensate from Si targets expanding into a low-pressure He ambient using a Nd:YAG laser with pulse length of 8 ns, wavelength of 532 nm and intensities in the range of 5×10^7 to 5×10^9 W/cm². Clusters in the range of 5–50 nm have been produced. In the highly dynamic, non-linear regime of short-pulse laser-matter interactions, plume evolution and condensation processes are strongly coupled and difficult to predict accurately from modeling alone. Both numerical predictions and experimental results were used to quantify the competing effects of ionization and supersaturation. The results suggest a dominant influence of ionization for nearly all intensities above the ablation threshold.

Final optics

The final optic in a laser-IFE power plant beamline experiences direct line-of-sight exposure to target emissions, including neutrons, x rays, high-energy ions and debris. It must withstand this environment reliably over many months of continuous operation, while simultaneously meeting stringent optical requirements. A grazing-incidence metal mirror has been considered as a potentially robust design option that can survive acceptably high laser fluence as well as the harsh environment of an inertial fusion reactor chamber. We explored the design options and responses of metal mirrors in a coordinated program of modeling, mirror fabrication and experiments. Our results indicate that grazing-incidence metal mirrors have the ability to survive the IFE environment while satisfying the requirements on beam quality necessary for successful target implosion.

Several fabrication techniques were explored in order to develop a mirror with acceptable optical quality as well as high laser-induced damage threshold. We created mirrors by bonding foils to substrates, thin film deposition, electroplating, diamond-turning, polishing, and various combinations of these. Test articles were exposed with a Lambda Physik Compex 201 excimer laser producing 248-nm light with a pulse length of approximately 25 ns.

We have shown that a grazing incidence metal mirror is a credible option for the final optic in a laser-driven IFE power plant [B1-B4]. Mirrors have been fabricated up to 10 cm in diameter using technologies that scale to a full-size power plant optic. Testing and analysis have demonstrated thermomechanical resistance to laser-induced damage up to 10^5 shots using 248-nm light from a short-pulse KrF laser.

Damage resistance is improved by controlling the microstructure, especially the grain size, and by avoiding high thermal stresses at the interface between the reflector and substrate. Thin films thicker than 2 microns appear to survive 10^5 shots at the design fluence (5 J/cm²) if

the substrate is highly polished, but these coatings are inherently fragile. Very thick films (achieved with electroplating or thick PVD coatings) combined with a post-processing step to provide optical quality appear to be the most robust design choice. End-of-life exposures of mirrors are still needed in order to fully demonstrate these concepts.

System integration

The ARIES-IFE study was a national US effort involving universities, national laboratories and industry. As opposed to previous IFE power plant studies, ARIES-IFE did not focus on developing a single design point. Rather, we performed detailed analysis of various subsystems parametrically to uncover key physics and technology uncertainties and to identify constraints imposed by each subsystem on the feasibility of IFE chamber concepts. The constraints from various subsystems were then combined in order to understand the trade-offs among subsystems, to develop operational windows for IFE chamber concepts, and to identify high-leverage R&D directions for IFE research. Several publications were written by UCSD authors [C1–C9], and a special issue of Fusion Science and Technology was prepared.

Many combinations of drivers (lasers, heavy ions, Z-pinch), targets (direct and indirect drive), and chamber concepts (dry-wall, thin-liquid protection, thick-liquid walls) can be envisioned for an IFE power plant. An IFE power plant cycle starts with the explosion of the target in the chamber. The X ray, ions and neutrons generated from target explosion traverse the chamber, interact with the chamber constituents and deposit their energy on the chamber wall. Clearly, the particle and energy loads on the wall will depend on the target yield and energy spectra as well as the chamber constituents.

The three classes of chamber concepts use different schemes to ensure survival of the first wall: gas protection for dry walls or liquid protection for the other two. In each case, the requirement for survival of the first wall leads to severe constraints on the chamber size and geometry, material choices, and maintenance of chamber protection scheme (e.g., replenishment of liquid protective layer). As a result of interaction of target particle and energy flux with the first wall, material is evaporated or ejected into the chamber. These materials evolve, cool, and are pumped out during the interval between driver shots. The chamber environment prior to the next shot will depend on the evolution of the chamber constituents during the time between shots. A cryogenic target must be injected and tracked in this chamber and the driver beams should be able to propagate and be focused in this pre-shot chamber environment.

In our study, we have followed the above approach: we started from the target, found the response of the chamber to the target explosion, evaluated the chamber condition prior to the next shot and studied whether targets can be successfully injected and ignited by the driver. This approach has allowed us to decouple the driver design from chamber performance to a large extent. Study of target fabrication, injection, and tracking can also be done independently of other variations as they depend mainly on the target design and not on the chamber or driver concept. A major difference between ARIES-IFE and previous US IFE power plant studies is the fact that detailed characterization of IFE target yield and spectrum is now available. This detailed information of the target yield and spectrum plays a crucial role in defining the operational windows for IFE systems. We also showed that for dry-wall and thin-liquid wall concepts, the blanket will experience a quasi-steady-state load comparable to that envisioned for magnetic fusion energy (MFE) power plants. As such, the first wall protection system can be decoupled to a large degree from the blanket and our research has focused on the wall protection scheme as the thermal power conversion system.

REFERENCES

A. Chamber Dynamics

- A.1. Z. DRAGOJLOVIC, F. NAJMABADI, "Simulation of IFE chamber dynamics response by a second order Godunov method with arbitrary geometry," *Proc. International Symposium on Inertial Fusion Science and Applications, IFSA-2003* (Monterey, CA, Sept. 2003).
- A.2. Z. DRAGOJLOVIC, F. NAJMABADI, M. DAY, "An Embedded Boundary Method for Viscous, Conducting Compressible Flow," Submitted for Publication in *J. Comp. Physics*, 2004.
- A.3. S.S. Harilal, C.V. Bindhu, M. S. Tillack, F. Najmabadi, A.C. Gaeris, "Internal structure and expansion dynamics of laser ablation plumes into ambient gases," *Journal of Applied Physics* **93**, 5 (March 1, 2003) 2380-2388.
- A.4. S.S. Harilal, C.V. Bindhu, M. S. Tillack, F. Najmabadi, A.C. Gaeris, "Plume splitting and sharpening in laser-produced aluminum plasma," *Journal of Physics D: Applied Physics* **35** (2002) 2935–2938.
- A.5. M.S. TILLACK, S.S. HARILAL, F. NAJMABADI, J. O'SHAY, "Magnetic Confinement of an Expanding Laser-Produced Plasma," *Inertial Fusion Science and Applications 2003*, Monterey CA, Sept. 2003, 319–322.
- A.6. S.S. HARILAL, M.S. TILLACK, B. O'SHAY, C.V. BINDHU, F. NAJMABADI, "Confinement and dynamics of laser-produced plasma expanding across a transverse magnetic field," *Phys Rev. E* **69** (2004).
- A.7. C.V. BINDHU, S.S. HARILAL, M.S. TILLACK, F. NAJMABADI A.C. GAERIS, "Laser propagation and energy absorption by an argon spark," *J. Applied Physics* **94** no. 12 (15 Dec. 2003).
- A.8. C.V. BINDHU, S.S. HARILAL, M.S. TILLACK, F. NAJMABADI A.C. GAERIS, "Energy Absorption and Propagation in Laser Created Sparks," *Applied Spectroscopy* **58**(6) (June 2004) 719–726.
- A.9. M.S. TILLACK, D. BLAIR, S.S. HARILAL, "The effect of ionization on cluster formation in laser ablation plumes," *Nanotechnology* **15**, issue 3, pages 390–403 (January 2004).

B. Final Optics

- B.1. M.S. Tillack, J. Pulsifer, K. Sequoia, "UV Laser-Induced Damage to Grazing Incidence Metal Mirrors," *Inertial Fusion Science and Applications 2003*, Monterey CA, Sept. 2003, 810–814.
- B.2. M.S. TILLACK, S.A. PAYNE, N.M. GHONIEM, M.R. ZAGHLOUL, J.F. LATKOWSKI, "Damage threats and response of final optics for laser-fusion power plants," *Inertial Fusion Science and Applications 2001*, Kyoto Japan, Sept. 2001, 717–721.
- B.3. M.R. ZAGHLOUL, M.S. TILLACK, T.K. MAU, "Sensitivity of Metal Mirrors to Laser-Induced Damage Under Long-Term Exposure at Shallow Angle of Incidence," *Proc. 19th IEEE/NPSS SOFE*, Atlantic City NJ, Oct. 2–5, 2001.

- B.4. T.K. MAU, M.S. TILLACK, M.R. ZAGHLOUL, “Modeling of Mirror Surface Damage Effects on Beam Propagation in a Laser-Driven IFE Power Plant,” Proc. 19th IEEE/NPSS SOFE, Atlantic City NJ, Oct. 2–5, 2001.

C. System Integration

- C.1. M.S. TILLACK, F. NAJMABADI, L.A. EL-GUEBALY, D. GOODIN, W.R. MEIER, R.R. PETERSON, D.A. PETTI, K.R. SCHULTZ, L.M. WAGANER, AND THE ARIES TEAM, “ARIES Inertial Fusion Chamber Assessment,” *Fusion Technology*, **39** 343–348, 2001.
- C.2. F. NAJMABADI, “Assessment of Chamber Concepts for Inertial Fusion Energy Power Plants — The ARIES-IFE Study,” *Proc. International Symposium on Inertial Fusion Science and Applications, IFSA-2001* (Kyoto, Japan, September 2001).
- C.3. A.R. RAFFRAY, S.I. ABDEL-KHALIK, D. HAYNES, F. NAJMABADI, J.P. SHARPE, “Thin liquid wall behavior under IFE cyclic operation,” *Fusion Science & Technology*, **44**, 106–110, 2003.
- C.4. A.R. RAFFRAY, D. HAYNES, F. NAJMABADI, “IFE chamber wall: Requirements, design options, and synergy with MFE plasma facing components,” *J. Nuclear Materials*, **313-316**, 23–31, 2003.
- C.5. F. NAJMABADI, A.R. RAFFRAY, AND THE ARIES-IFE TEAM: S.I. ABDEL-KHALIK, LESLIE BROMBERG, LAILA A. EL-GUEBALY, D. GOODIN, D. HAYNES, J. LATKOWSKI, W. MEIER, R. MOORE, S. NEFF, C.L. OLSON, J. PERKINS, D. PETTI, R. PETZOLDT, D.V. ROSE, W. M. SHARP, P. SHARPE, M.S. TILLACK, L. WAGANER, D.R. WELCH, M. YODA, S.S. YU, M. ZAGHLOUL, “Operational Windows for Dry-Wall and Wetted-Wall IFE Chambers,” *Fusion Sci. & Technology* **46** (2004) 401–416.
- C.6. A.R. RAFFRAY, S.I. ABDEL-KHALIK, D. HAYNES, F. NAJMABADI, P. SHARPE, M. YODA, M. ZAGHLOUL, AND THE ARIES TEAM, “Thermo-fluid dynamics and chamber aerosol behavior for the liquid wall under IFE Cyclic Operation,” *Fusion Science & Technology* **46** (2004) 438-450.
- C.7. A.R. RAFFRAY, L. EL-GUEBALY, G. FEDERICI, D. HAYNES, F. NAJMABADI, D. PETTI, AND THE ARIES TEAM, “Dry wall survival under IFE conditions,” *Fusion Science & Technology* **46** (2004) 417–437.
- C.8. A.R. RAFFRAY, W. MEIER, S. ABDEL-KHALIK, R. BONAZZA, P. CALDERONI, C. S. DEBONNEL, Z. DRAGOJLOVIC, L. EL-GUEBALY, D. HAYNES, J. LATKOWSKI, C. OLSON, P. F. PETERSON, S. REYES, P. SHARPE, M.S. TILLACK, M. ZAGHLOUL, “IFE Thick Liquid Wall Chamber Dynamics: Governing Mechanisms and Modeling & Experimental Capabilities,” to appear in *Fusion Science and Technology*.
- C.9. M.R. ZAGHLOUL, A.R. RAFFRAY, “IFE Liquid Wall Response to the Prompt X ray Energy Deposition: Investigation of Physical Processes and Assessment of Ablated Material, accepted for publication in *Fusion Science & Technology*.”

Vapor cleaning rate and condensation study for IFE liquid chambers

A. Ying

University of California, Los Angeles, California, United States of America

Abstract. The work presented here investigates the condensation of excited vapors generated from a molten salt composed of lithium fluoride and beryllium di-fluoride. The material, denominated flibe, is used in the design of Inertial Fusion Energy systems when the chamber protection scheme involves a liquid layer. The HYLIFE-II design is used as reference. The high repetition rates necessary to keep the IFE power plant economically competitive makes the issue of chamber clearing a key feasibility factor. The motivation behind this work stems from the need for an experimental assessment of the achievable condensation rates of flibe vapors under IFE relevant conditions. The experiments use a high-current electrical arc to generate the excited vapors from a pool of molten salt. The vapor expands inside a scaled chamber and condenses in contact with the walls, which are maintained at a controlled temperature. The experiments show that vapor clearing is characterized by an exponential decay with a time constant of 6.58 milliseconds in the density range between $5 \times 10^{17} \text{cm}^{-3}$ and $2 \times 10^{15} \text{cm}^{-3}$. The low limit of the range is determined by the impurities dissolved in the salt. Extending the result to the expected low limit of HYLIFE-II ($3 \times 10^{13} \text{cm}^{-3}$), the period for vapor clearing is 68 milliseconds, which is compatible with the required 6 Hz repetition rate.

Accomplishments

- Developed an innovative and inexpensive scheme to generate superheated prototypical liquid vapor in conditions relevant to inertial fusion energy liquid chamber design studies (IFE, Z-pinch)
- Demonstrated experimentally that vapor clearing rates are short enough to allow high repetition rates in IFE power plants with flibe liquid protection schemes

Introduction

The objective of this project was the experimental study of vapor condensation for the assessment of chamber clearing in Inertial Fusion Energy systems that include a liquid protection scheme. The HYLIFE-II chamber concept is considered as reference design, but the study is relevant to all the applications of liquid walls in IFE chambers. In the IFE chamber, super heated vapor is generated from the absorption of the energy released in the fusion pulse by the protective liquid. Vacuum conditions must be restored after each fusion pulse to efficiently couple the energy drivers with the target. Since economic assessment of energy generation forces us to consider repetition rates of few pulses per second, the study of the transient condensation of vapors becomes a key issue for the feasibility of liquid walls protection schemes in IFE systems. A facility is constructed to produce partially ionized superheated vapor by a high current, pulsed electrical discharge. The experiments are designed to scale the initial density of the generated vapor, the initial energy density and the surface area available for condensation in order to generate data that are relevant to HYLIFE-II chamber conditions.

In practice, clearing rates are evaluated from the measured pressure history inside the scaled chamber. The main objective of this work is then to measure the pressure decay, and especially the time needed for the pressure to drop from a prototypical initial peak to the low

pressure level required in the IFE chamber design. To further characterize the condensation process, other diagnostic tools are employed. In particular, emission spectroscopy is used to analyze the dynamics of recombination and composition of the gases and local gas thermodynamic properties such as vapor properties at the liquid/vapor interface. The composition of the gas after the discharge is investigated with mass spectroscopy. Scanning Electron Microscope analysis of material condensed on collecting plates is used to investigate the issues of in-flight volumetric condensation as well as the effect of the vapor velocity direction on the condensation rate.

Experimental work

The experiments were carried out at the Fusion Science and Technology laboratories at UCLA. The design and construction of a facility for the generation of IFE prototypical quantities of partially ionized flibe started in 1999, and characterization of the excited vapor source was completed in 2001. For the purpose of this work, the most important feature of the source is that the discharge period is contained in less than 300 μs . This effectively ensures time decoupling between generation of the excited vapors and the condensation process in the expansion chamber, which happens in periods on the order of a few tenths of a second. The source design is relevant to this research work also because the mechanism of vapor generation determines the initial state of the excited gas, which must be scaled correctly in order to ensure relevance for IFE application.

The design of the excited vapor source is based on a series of experiments at North Carolina State University. During the experiments at NCSU, certain plasma parameters were experimentally measured, and others were extrapolated with numerical models. During the first two years of operation the UCLA facility has proved to work in good agreement with NCSU published experiments, although some design changes have been applied. Therefore NCSU results have been used to characterize plasma parameters that were not measured during the experiments at UCLA.

The partially ionized vapor of the material under investigation is generated by an ablation controlled arc. The plasma generated in such devices is usually characterized by high density (10^{25} – 10^{26} / m^3) and low temperature (1–3 eV)]. In general terms, the passage of an electrical current through an ionized gas leads to plasma generation by resistive heating of the conducting media. The arc is generated by storing a large amount of energy in a group of capacitors, and quickly releasing it to produce a high-current discharge. A plasma column is formed in the confined volume between anode and cathode by a discharge precursor mechanism. At first this mechanism was simply the ionization of a background gas, and subsequently the vaporization of a thin copper wire. The electrical power is injected in the plasma column and is used to maintain the plasma at temperatures of few electronvolts for the period of the discharge, typically 100 μs . The injected power is transferred as radiative flux to the wall surrounding the plasma and used to ablate, dissociate and heat the wall surface material. The surface is composed of the material under investigation in the solid state. The vapor formed from ablation quickly builds up pressure in the volume of the source.

Constricting the discharge in the small volume inside the liner creates high pressure gradients between the source and the expansion chamber, typically in the hundreds of atmosphere range. Due to pressure buildup, the plasma is transported axially, which leads to both particle and convective energy loss. The material produced by ablation of the surface balances the axial mass loss in the plasma jet. Under these conditions, the hydrodynamic expansion dominates over the drift velocity imposed by the electric field and the effect of the interaction

of the plasma current with the self-generated magnetic field (pinch effect). A rapid bulk transport of plasma out of the source governs the loss mechanism inside the source and results in a high velocity plasma jet expanding into the chamber. The plasma jet undergoes abrupt expansion at the source exit, generating alternating expanding and compressing waves reflecting on the chamber walls, and localized shock waves. The complex hydrodynamic phenomena are characterized by a time scale on the order of the current discharge period.

The performance of the facility at maximum energy has been evaluated for the design of the source with a numerical model developed at NCSU. It is preferable to work at lower voltages and higher capacitance for safety reasons and to optimize the response of the discharging circuit. The values of the discharge period and maximum current peak are extrapolated from models of the plasma arc resistivity that have been validated by the experiments at lower energies.

The facility is composed of three main components: the electrical network responsible for the generation and control of the discharge, the vapor source (where the mechanism described before is actually taking place) and the expansion chamber where the excited vapors are injected. The source cathode is connected to the pulse forming network by a tri-axial transmission line that delivers the high intensity current from the negative side of the capacitor bank to the plasma, and collects the return current to the grounded side of the bank. The source is sealed to the expansion chamber, which is connected to the pump system and electrically grounded. The pulse forming network is composed of power supply, energy storing system, high current ignitron switch, tri-axial transmission line and other circuits for component protection and general electrical safety as shown in Figure 1. The capacitor bank is formed by four modules of three capacitors each that can be independently connected to the experiment, and charged up to 22 kV. All components are contained in a grounded stainless steel box. The metal enclosure serves the purpose of isolating the electromagnetic noise produced by the discharge to avoid interference with laboratory instruments and protecting the operators from flying debris in case of failure of one of the capacitors.



Figure 1. A major part of the facility is the electrical network system, which provides a pulsed energy source simulating the pellet explosion for rapid vapor generation.

Experimental study features a staged design implementation taking into account the need for characterization of superheated vapor source in comparison to other experiments using electro-thermal sources, the handling of toxic materials (beryllium component in flibe), and the need for the development of diagnostics.

Experimental results

LITHIUM FLUORIDE RESULTS

The last step in the staged implementation of the experiments before using the IFE prototypical material flibe ($2\text{LiF}\text{-BeF}_2$) involved its non-toxic component, lithium fluoride. The main goal of the LiF experiments was to reduce the amount of residual non-condensable gases (as were produced from Teflon experiments) to a value at which their effect on condensation rates could be considered negligible. In addition, it provides the condensation rate data for the non-volatile part of flibe vapor compositions. The material in its crystal form is used to fabricate optical instruments such as lenses and view ports because of its high transmittivity in the UV range. Although commercially available, the material is produced by crystal growth, and is therefore expensive. The source used for LiF experiment is the same as that of Teflon experiments¹. A new expansion chamber was built for LiF experiments. The main body is a stainless steel tube 50 cm long and with a 10 cm diameter, designed to maintain the desired 4 liters expansion volume. Five ports are welded to the main body. Three of them support standard 2.75 inches Del-Seal CF metal flanges for high vacuum applications, and two support mini CF flanges. The anode of the vapor source is connected to the metal expansion chamber. Because of this no instrument can be directly mounted on the chamber without proper insulation to avoid damages to the sensors electronics by the high current spike generated by the arc discharge. The insulation must also be compatible with the high temperature requirements of the chamber wall (up to 460 C). The difficulty of this set of experiments is that the LiF sleeve is not capable of containing the arc because of its inherent fragility. Because of this, any secondary material used to contain the sleeve is also ablated, and the products of the recombination of the generated vapors reflect this flaw. As a result, residual non-condensable gases are inevitable when the generation of the excited vapor is based on the ablation of solid crystal materials such as LiF or flibe. This was the main motivation for the changes in the generation mechanism that will be described when flibe condensation results are presented.



Figure 2. Expansion chamber for LiF experiments.

Despite the high amount of residual gases, the results show that condensation of LiF vapors is completed in periods of less than 20 ms (Figure 3), which is a preliminary result compatible with IFE repetition rate requirements. The ratio between the pressure peak and the residual value is constant, and equal to about 9. Mass spectroscopy of the residual gases has been performed in order to understand the source of the non-condensable impurities and characterize the condensation of LiF vapors.

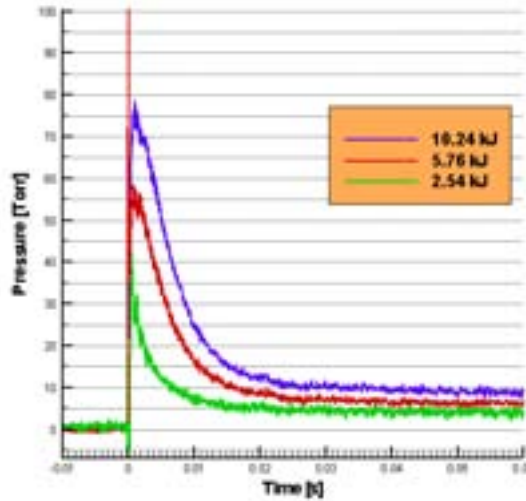


Figure 3. Pressure history of LiF experiments at different energies.

Figure 4 is the emission spectrum recorded during an experiment with LiF. The lines from the emission of the highly excited copper atoms due to the initial vaporization of the trigger wire are still present, as well as the weak fluorine lines. But thanks to the lower excitation potential of lithium respect to that of fluorine, there are 2 strong lines visible at 610.3 nm and 670.8 nm due to the emission of neutral lithium atoms (Li I).

FLIBE EXPERIMENTAL RESULTS

The results presented in the previous section obtained using one of the two components of the eutectic flibe were encouraging from the point of view of demonstrating that the molten salt condensation rate is compatible with IFE requirements. However, the experiments also indicated that the generation of traces of non-condensable gases is associated with the use of source material in the solid, crystal form. Because of this, a new approach was used for flibe and the resulting experiment that will be described here is the key original engineering contribution of this research work. The approach stems from two main ideas. First, in all fusion systems flibe is used in its liquid form. Thus, using liquid flibe as the source of excited vapor and measuring the condensation rates in an environment that is uniformly heated above the melting point of flibe (500°C) is a further step to ensure that the results are relevant to IFE applications. Second, the molten salt in its liquid state is an electrolyte, thus a weak conductor of electricity.

The liquid itself could be used as the trigger mechanism to initiate the discharge. A similar idea is used in the design of high current liquid metal switches where the cathode electrode is slightly dipped into the liquid. In the case of the flibe experiments, the electrode is first slightly dipped in the liquid pool, and then retracted by about 2–3 mm. The high viscosity and surface tension of the molten flibe is such that a meniscus is formed between the electrode and the pool surface. The contact of the electrode with the liquid pool is ensured by measuring the value of the resistance between the tungsten rod (disconnected from the capacitors) and the ground. The vaporization and ionization of the meniscus is the initiation mechanism of the discharge.

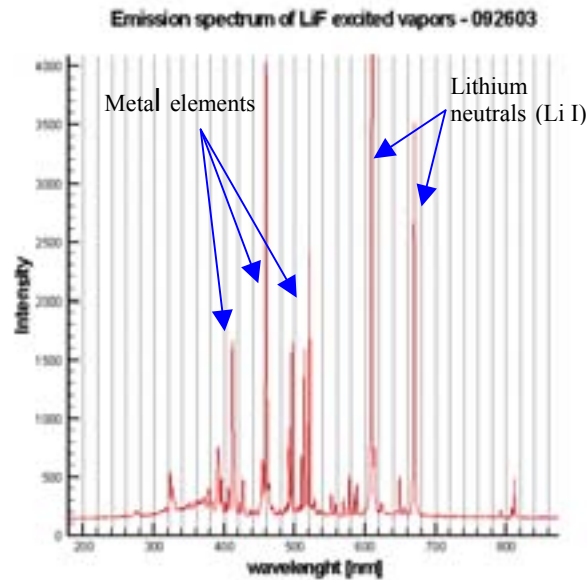


Figure 4. Emission spectrum of LiF superheated vapors.

A schematic of the experimental setup for flibe experiments is shown in Figure 5. The vacuum chamber is built around a standard 6-way cross with 0.07 m flanges which is electrically and thermally insulated by ceramic breaks. The upper port is used to insert the cathode, which is a 0.3 m tungsten rod that can slide along the vertical axis. The rod is connected to the negative side of a large bank of capacitors (Figure 1 as shown previously) through a high-current switch and a conditioning circuit. The lower port is used to insert the crucible that holds the liquid flibe. The crucible is a 0.0254 m diameter nickel rod that is welded to a stainless steel tube. To maintain high-purity conditions in the expansion chamber the heater is mounted inside a separately pumped volume. The assembly is connected to the return leg of the capacitor bank to collect the discharge current, thus the flibe pool and the crucible act as the discharge anode (maintained at ground potential). A high resonant frequency and low sensitivity to acceleration piezo-resistive absolute pressure sensor is mounted on one of the four remaining ports. A capacitive manometer with millisecond time resolution is mounted on the facing port before the valve that connects the chamber to the turbo-molecular pump. A residual gas analyzer is also connected before the valve. Although not exactly a point source, the vapor generated in the arc discharge can be assumed to expand initially along the radius of hemisphere with the center corresponding to the liquid flibe surface. Three experiments involving flibe have been performed for the purpose of this work, two at different energy and the chamber walls uniformly heated to 300°C and one with the chamber walls at 500°C.

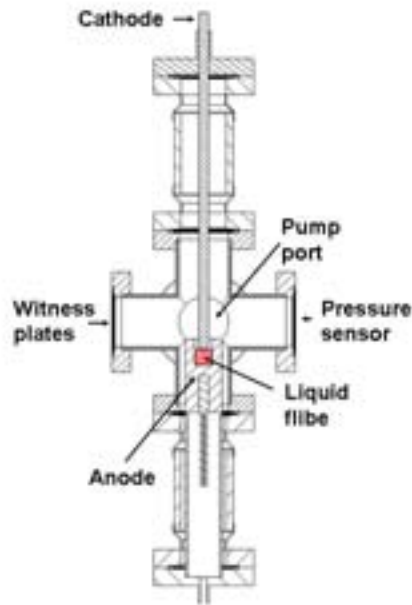


Figure 5. Scheme of the experimental setup for flibe.

The main objective of the experiments is to measure the pressure decay in the expansion chamber after a single discharge, and in particular the time needed for the pressure to drop from the initial peak to the equilibrium value. Pressure data measured by the high sampling frequency sensor during the experiments with the chamber at the uniform temperatures of 500°C and 300°C respectively are shown in Figure 6. The energy coupled in the discharge was the same for both experiments (2.56 kJ), thus the same amount of material is vaporized and the same initial pressure peak measured. The pressure decay can be fit very precisely with an exponential curve. The exponential decay is usually characterized by its time constant, which represents the period necessary for the pressure to fall from its peak value to about 36% of the same, or $1/e$ with the peak referenced to 1. The decay time constant at 300°C is 4.27 ms, while at 500°C is 6.58 ms. This shows that the condensation rates in the pressure range covered by the experiments is mostly a function of the system temperature. The latter value is the reference value for HIF systems, as the structures in contact with the liquid must be constantly maintained at a temperature above the melting point of flibe, which is 460°C.

To compare the experimental data with numerical simulations of chamber clearing processes for HYLIFE-II, the measured pressure can be translated in terms of particle density, assuming that the vapor is in equilibrium with the liquid and follows the ideal gas equation of state. The range covered by the experiments then corresponds to a peak of about $5 \times 10^{17} \text{ \#/cm}^3$, and an equilibrium value of about $2 \times 10^{15} \text{ \#/cm}^3$. The latter is measured with the low frequency sampling capacitive manometer. The low pressure range data are referred to the vertical axis on the right in milli Torr units. During one cycle of the HYLIFE-II power plant the density in the chamber varies from the initial density of $9 \times 10^{17} \text{ \#/cm}^3$ to $3 \times 10^{13} \text{ \#/cm}^3$, which is a conservative level considered acceptable for ion beams propagation. If the measured decay constant of 6.58 ms is considered to be valid in the whole range, the clearing period for HYLIFE-II is calculated as 68 ms, which is substantially lower than the 200 ms limit imposed by the 6 Hz repetition rate of the power plant. Thus the main conclusion of this work is that flibe vapor clearing for IFE chambers involving a liquid protection scheme is compatible with the high repetition rates dictated by the economic attractiveness of the power plant.

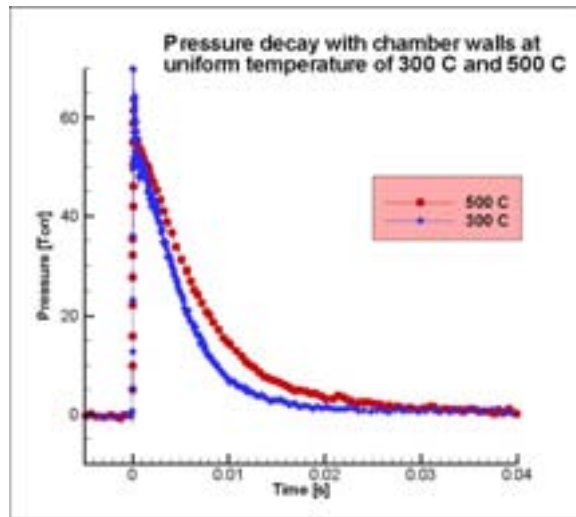


Figure 6. Pressure history of Flibe experiments with different environmental temperatures.

Mass spectroscopy of the residual gases after the condensation process shows that the condensation of LiF and BeF₂ is complete, and that the remaining gases are non-condensable species. Figure 7 is a typical scan of the residual gases for all experiments. About 56% of the total pressure is composed of hydrogen. Another 26% is due to the light hydrocarbon products of C and H atoms recombination (ethylene and ethane), and 12% due to recombination of carbon with oxygen to form CO₂ and CO. The only possible sources of impurities in the experiments are either the metal surfaces of the electrodes or the flibe itself. All metal surfaces are well conditioned before the experiment by the necessary high temperature. In order to verify that the flibe itself is the source of the impurities, we have measured the composition of the vapors in equilibrium with the liquid pool inside the crucible as the liquid temperature was increased linearly from 460°C to 700°C in about 10 minutes. The RGA results showed a large amount of impurities dissolved in the liquid, especially hydrogen. Those impurities are the source of the non-condensable gases measured in the experiments. The results show that impurity control and purification technology of the molten salt become crucial issues for applications that require recovery of vacuum conditions in the 10¹³ cm⁻³ range.

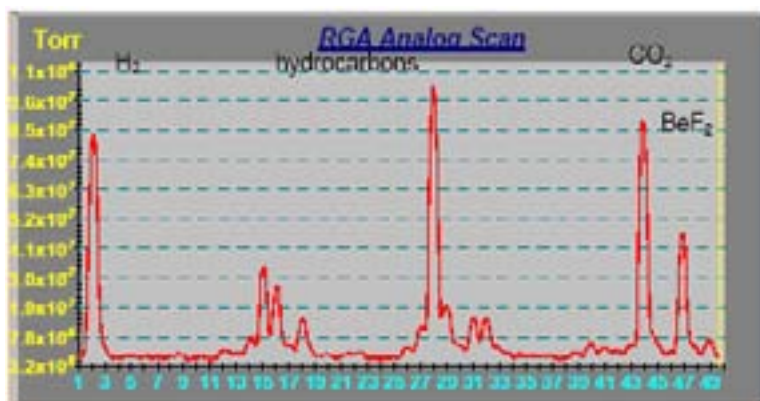


Figure 7. Measured composition of flibe vapors in equilibrium with a liquid surface.

BIBLIOGRAPHY

The research project has provided excellent educational benefits due to its rich science.

P. Calderoni, A. Ying, T. Sketchley, M.A. Abdou, Vapor Condensation Study for HIF Liquid Chambers, presented at 15th International Symposium on Heavy Ion Inertial Fusion, June, 2004, to be published in a Special Issue of Nuclear Instruments and Methods in Physics Research - Section A

L. Schmitz, P. Calderoni, A. Ying, and M.A. Abdou, A Novel Diagnostic for Time-Resolved Spectroscopic Argon and Lithium Density Measurements, 16th PSI, Portland, NH, May, 2004, to be published at Nuclear Fusion Material

X.Y. Luo, M. Ni, A. Ying, M.A. Abdou, A Variable-Density Projection Method for Free Surface Flow with Phase Change, presented at the 43rd AIAA Aerospace Sciences Meeting and Exhibit, Dec. 2004

P. Calderoni (Ph. D. March, 2004): On the study of vapor condensation for the assessment of Inertial Fusion Energy liquid chamber clearing

P. Calderoni, A. Ying, and M.A. Abdou, Experimental and numerical study of transient condensation of lithium fluoride excited vapors for IFE systems, presented at Symposium on Fusion Energy, San Diego, CA, 2003

Ying, M. Abdou, P. Calderoni, T. Sketchley, M. Ni, Ionized Flibe Vapor Condensation Rate in a Simulated Flibe-Liquid Chamber: an Experimental and Numerical Investigation, presented at Second IAEA Technical Meeting on Physics and Technology of IFE Targets and Chamber, San Diego, USA, 2002

P. Calderoni, A. Ying, T. Sketchley, and M.A. Abdou, 2001, "Description of a facility for vapor clearing rates studies of IFE reactors liquid chambers ", *Fusion Technology*, Vol. 39, N. 2, pp 711–715

Ying, P. Calderoni, T. Gianpaolo, T. Sketchley, and M. A. Abdou, Vapor Clearing Rate and Condensation Study for IFE Liquid Chambers, Progress Report for IAEA Research Agreement No. 11641, Vienna, 2nd RCM meeting, 2001

P. Calderoni, 2001, *An experimental facility to investigate flibe condensation and reactor chamber clearing rates in Inertial Fusion Reactors*, Master of Science Thesis, University of California, Los Angeles

Investigation of secondary processes by interaction of plasma streams with various materials

R.T. Khaydarov, G.R. Berdiyev, U. Kunishev, M. Khalmuratov, E. Tojikhonov

Scientific-Research Institute of Applied Physics at the National University of Uzbekistan,
Tashkent, Uzbekistan

Abstract. We investigated the charge and energy spectra of laser-produced W, Mo, V, Al plasma ions after their interaction with secondary targets (Mo, Al), located at the distance $2\div 10$ mm from the surface of the first target. It was found experimentally that the presence of the secondary target changes mass-charge and energy spectra of plasma ions and single charged ions of the secondary target was detected in a narrow low energy range ($E=100\text{--}300$ eV). The emission of ions from the secondary target depends on plasma parameters, material of secondary target and on the distance between primary and secondary targets.

INTRODUCTION

At present, experimental modeling of processes at the interaction of plasma with reactor chamber materials and the choice of materials for first wall of reactor chambers are one of main problems for the future design of reactors on the base of IFE scenarios [1–4]. The investigation of the influence of the plasma on physical and chemical characteristics of materials for the first wall is of great interest in order to predict the suitability of these materials and alloys to use in thermonuclear power engineering on the base of inertial confinement of plasma. There are many experimental and theoretical works about different kind of drivers (laser and heavy ion drivers) [3, 4], about target fabrication and testing [5, 6] and about chamber system [7, 8]. Chamber concepts using both solid and liquid walls have been proposed and the latter providing the possibility of armor replenishment prior to each shot.

In the IFE power plant, the target is first injected into the chamber. The driver (laser or heavy ion) beam is focused on the target, compressing it and initiating a fusion micro-explosion. Following each micro-explosion, the chamber wall is subjected to a large flux of photons, energetic particles and neutrons. Depending on the chamber wall loads, a background gas may be needed to attenuate the energy deposition on the chamber wall absorption and re-radiation over a longer time. The chamber has to be cleared in preparation for the injection of the next target with a typical repetition rate about 1–10 times per second [9].

In the present work we investigate the charge and energy spectra of ions formed at the interaction of laser-produced W, Mo, V, Al plasma with secondary targets (Mo, Al) located at 2–10 mm from the surface of first target.

EXPERIMENTAL SETUP

Experiments were carried out in a laser mass-spectrometer with mass resolution of $m/\Delta m \sim 100$ and time-of-flight distance $L=100$ cm, which was described in detail in Ref. [10]. The Neodymium glass laser, working in the frequency mode was used in experiments and the laser beam was directed perpendicular to the surface of the target. The duration of the laser impulse

is 15 ns and the power density of the laser radiation at the target surface is $q=5 \cdot 10^{10} \text{ W/cm}^2$. The peak power of laser radiation varied within 5 % and the experimental value are average over five impulses of a laser radiation. All experiments were carried out at the same inertial conditions (vacuum (10^{-6} Tor.), focusing condition of laser radiation, parameters of electrostatic mass-spectrometer, etc). The construction of the target chamber allows one to put 10 targets with diameter 10 mm and change the place of interaction of laser radiation with target. The main characteristics of plasma ions were measured in two regimes: free expansion of the plasma into vacuum and in the case of secondary target on the way of plasma expansion. The secondary target is a thin plate made of Al, Mo with a slot in the center with size 0.4×20 mm in order to lead-out the plasma to the time-of-flight energy-mass analyzer. Materials with different emission characteristics were chosen as secondary targets in order to see the changes of plasma characteristics after the interaction. The secondary targets are placed parallel to the first target and the distance between targets was varied over the range 2–10 mm. In experiments we used two kinds of Mo targets, Mo mono-crystal (mono) and Mo poly-crystal (poly).

EXPERIMENTAL RESULTS

The mass-charge and energy spectra of laser-produced W, Mo, V, Al plasma ions after their interaction with the surface of secondary targets Al and Mo have been obtained experimentally, depending on parameters of plasma, target materials and on the distances between targets. We detected the secondary ions formed at the interaction of the plasma with the secondary target. In order to the influence of the secondary target we also investigated the parameters of the plasma without the secondary targets.

Mass-charge spectra of W plasma ions, which are shown in Figs. 2 (a-c) at the presence of secondary Al target at the distance $d=2.5$ (b) mm and $d=5.0$ (c) mm from the first one and without the secondary target (a), show the influence to the secondary target to the formations of spectra of ions. In all cases we detected W ions with maximal charge $Z_{\text{max}}=6$ and the presence of the secondary target at $d=2.5$ mm increases the intensity of single charged W ions and decreases the intensity of ions with higher charges. In this case we see the small peak of Al^{+1} ions emitted from the secondary target. If we increase the distance between the targets the intensity of all W ions decreases and the Al ions is not detected.

From the obtained mass-charge spectra we got the energy distribution of plasma ions and next we give energy spectra of different kinds of plasma ions, depending on target nature and distance between the targets. Fig.2 shows the energy spectra of ions in W (a), V (b), Mo (mono) (c), Mo (poly) (d), Nb (e), and Al (f) without the presence of the secondary target. It is seen from this figure that, ions of W plasma have maximum charge ($Z_{\text{max}}=6$) and energy ($E_{\text{max}}=2600$ eV), while ions of Nb plasma have the maximum energy ($E_{\text{max}}=1600$ eV).

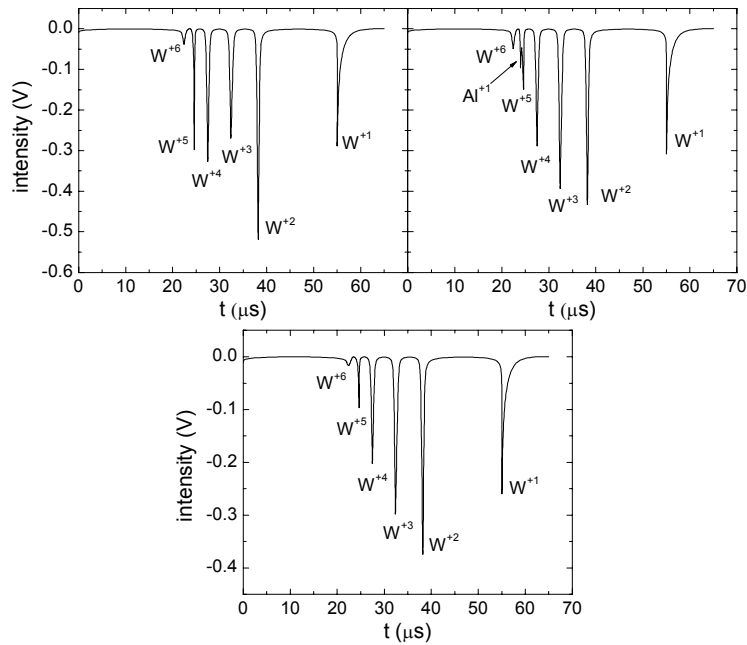


Figure 1. Mass-charge spectra of W plasma ions without (a) and with secondary targets at the distances $d=2.5$ mm (b) and $d=5$ mm (c).

The energy of the ions generated from the Mo mono-crystal is higher than the energy of ions of Mo poly-crystal, which indicates the influence of the target nature to the formation of the energy spectra of ions. Al and Mo plasma ions, which have been used as a secondary target, have maximal charge $Z_{\max}=4$ and 5, and maximal energy $E_{\max}=800$ eV and 2000 eV, respectively.

Figure 3 shows the energy spectra of W (a), V (b), Mo (mono) (c), Mo (poly) (d) and Nb (e) plasma ions at the presence of Al target at the distance $d=2.5$ mm. The maximal charge of ions in all case is equal to $Z_{\max}=5$, except for the W plasma ions, which have $Z_{\max}=6$, and the maximal energy varies between $E_{\max}=1500$ eV and $E_{\max}=2000$ eV.

It is noticeable that at the interaction of laser-produced plasma with the surface of Al at the distance $d=2-5$ mm, single charged ions of secondary target appear in mass-spectra in low energy ranges, comparatively to multiply charged ions of W plasma. The intensity of these ions depends on the distance between primary and secondary targets. As the distance increases ($d \leq 5$ mm) single charged ions of secondary target disappear. The presence of peaks of Al ions in the energy spectra shows the role of secondary processes at the interaction of multiply charged ions with the surface Al up to the final stages of inertial flight. When the W plasma interacts with the surface of Mo (mono) ions of the secondary target was not observed, which can be explained by the higher potential of ionization of Mo than Al. The maximal charge and energy of W ions in this case is the same when the plasma interacts with Al target.

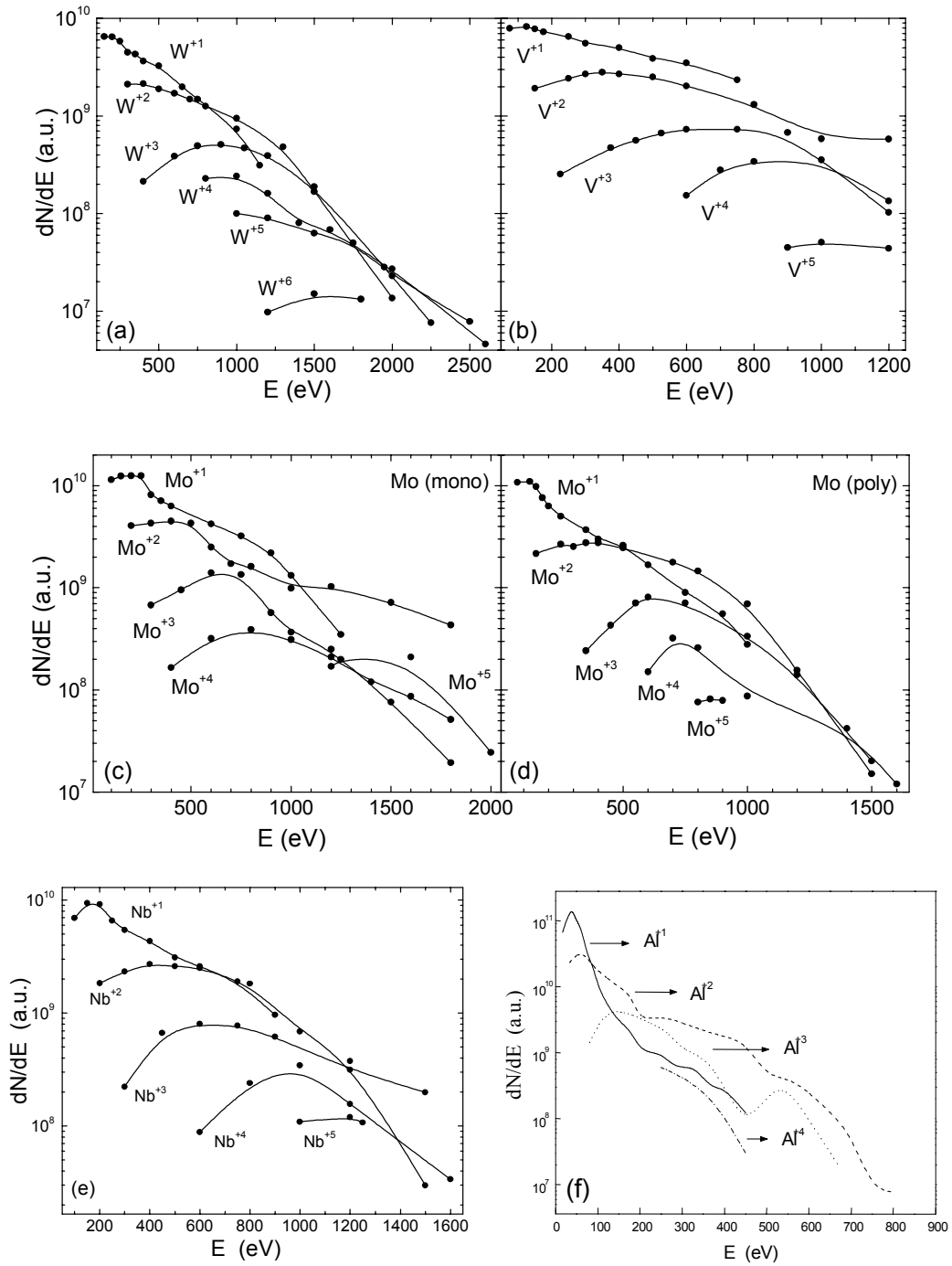


Figure 2. Energy spectra of *W* (a), *V* (b), *Mo* (mono) (c), *Mo* (poly) (d), *Nb* (e), and *Al* (f) plasma ions obtained at $q=5 \cdot 10^{10} \text{ W/cm}^2$ without the presence of the secondary target.

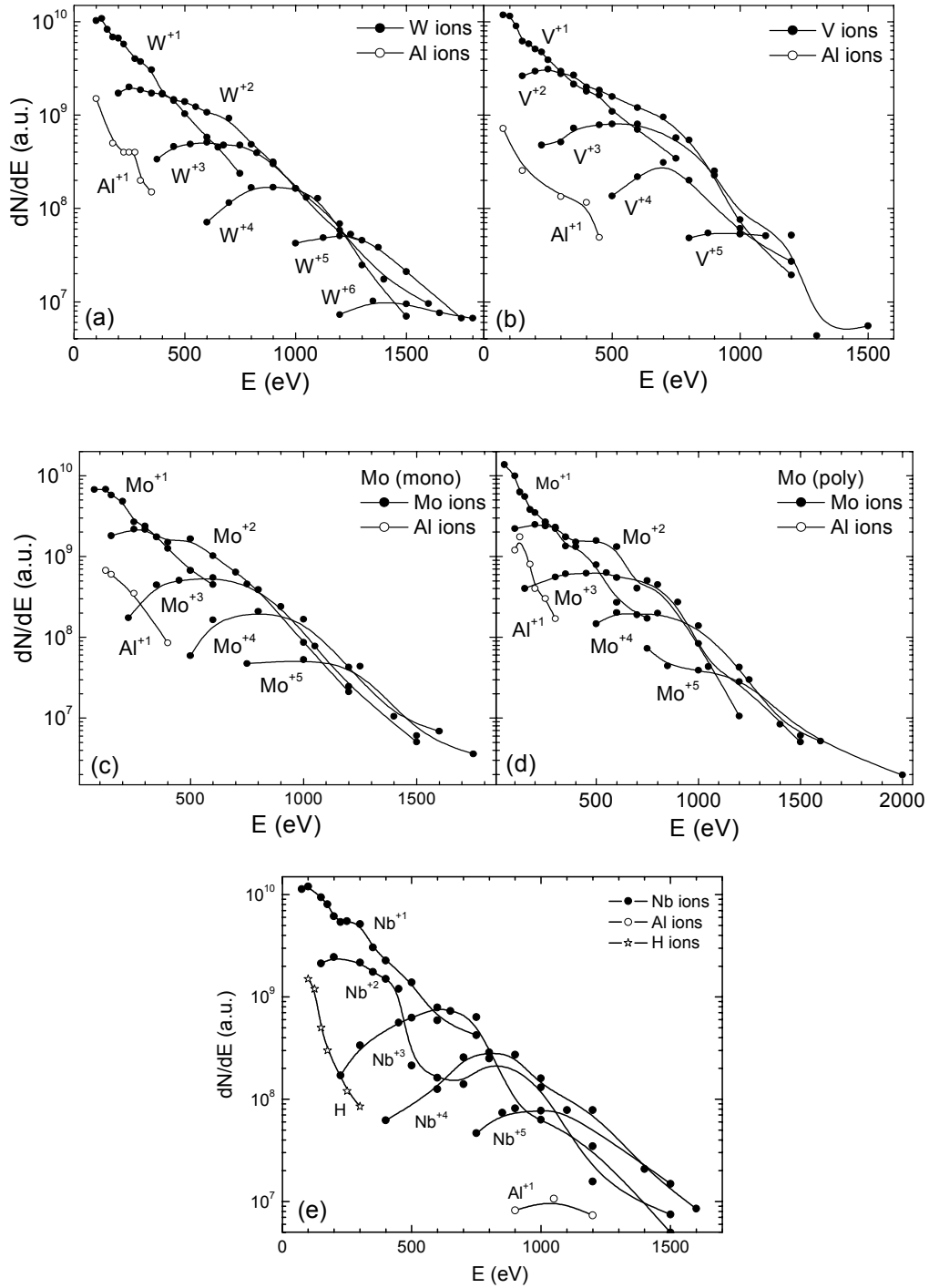


Figure 3. Energy spectra of W (a), V (b), Mo (mono) (c), Mo (poly) (d), and Nb (e) plasma ions at the presence of the secondary Al target at the distance $d=2.5$ mm.

Figure 4 shows the energy spectra of V and Al plasma ions in the presence of the secondary Mo (mono) target at $d=2.5$ mm. The maximal charge and energy of V ions decreases compared to the case of the secondary Al target (see Figure 3(b)) and equals $Z_{\max}=5$ and $E_{\max}=1050$ eV. We also see the decrease of the energy of Al ions and the change in the energy distribution compared to the free expansion of plasma (Figure 2 (f)).

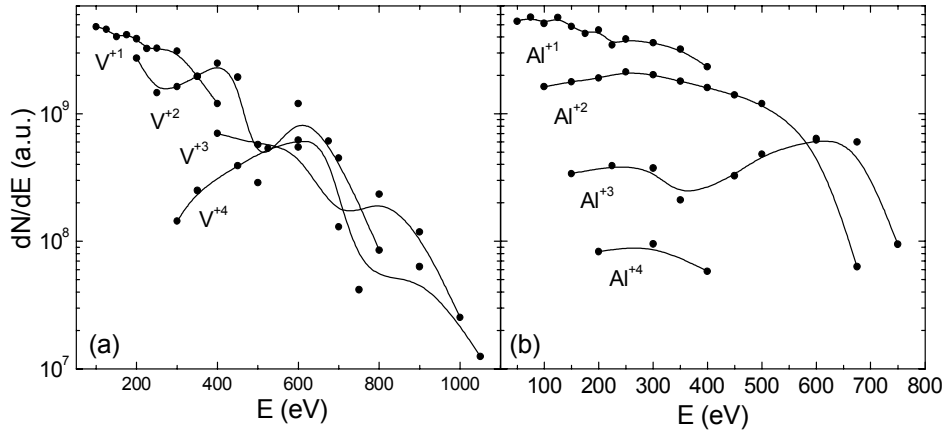


Figure 4. Energy spectra of V and Al plasma ions at the presence of the secondary Mo (mono) target at $d=2.5$ mm.

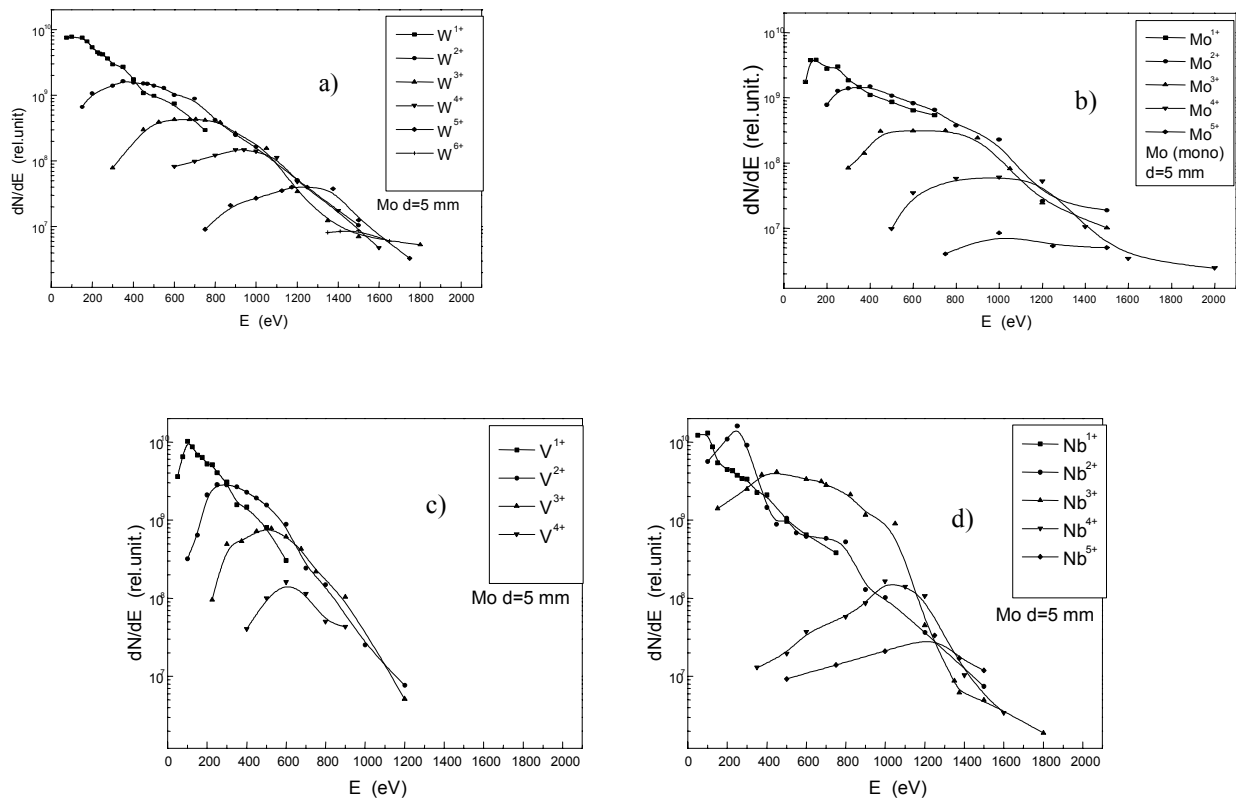


Figure 5. The energy spectra of W (a), Mo (mono) (b), V (c), and Nb (d) plasma ions with the secondary target Mo (mono) at $d=5.0$ mm.

Figure 5 shows the energy spectra of W (a), Mo (mono) (b), V (c), and Nb (d) plasma ions with the secondary target Mo (mono) at $d=2.5$ mm. The increase of the distance between two

targets decreases the energy and intensity of plasma ions and we did not observe ions emitted from the secondary target. These changes in the energy spectra of ions show the effect of the secondary target on the recombination processes when the plasma goes through the secondary target. The influence of solid-state barriers on the dynamics of laser plasma expansion was investigated in the work [7]. It was shown that solid-state barriers influence upon the nature of phosphorescence of plasma, changing the hydrodynamic parameters, such as density and temperature of electrons. Here effects connected with arising of shock waves play essential role. The structure of a shock wave front, expanding in the plasma has features connected with decelerating exchange of energy between ions and electrons and greater motions of electrons than ions that stipulates their higher thermal conductivity than one for ions.

Experimental results show that the presence of the secondary target (at the distance 2-10 mm from the target) changes not only the energy distribution of the ions but also the intensity of them. As an example we plotted in Fig. 6, the dependence of amount of W ions at the distances $d=5$ mm (a) and $d=10$ mm (b) from the surface of secondary target. It is seen from this figure that the increase of the distance leads to the decrease in ions' intensity for all charge of ions, which shows the increasing of recombinational loses on the multiply charged ions of plasma, mainly in far distances and with different thermal physical characteristics of the materials.

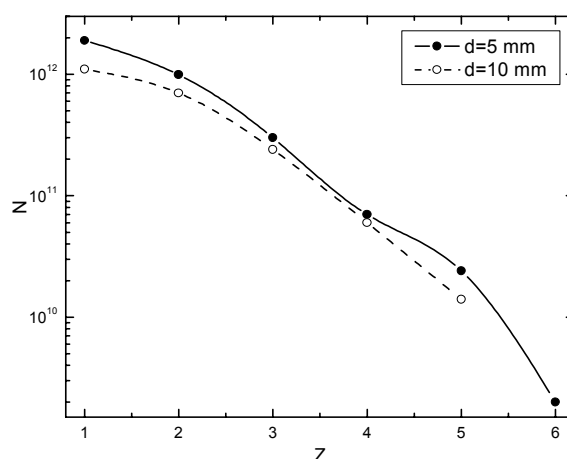


Figure 6. The intensity of W ions at the presence of the secondary target (Al) at the distances $d=5$ mm (a) and $d=10$ mm (b).

The experimental results and comparison with the theoretical calculation [7-11] show that, the presence of the secondary target on the way of the laser-produced plasma changes the kinematics of plasma expansion, which leads to the increase of the recombination processes and to increase of the plasma temperature at the inertial stage of plasma expansion. These changes have an influence to the dynamics of formation of mass-charge and energy spectra of multiply charged ions.

SUMMARY

The analyze of experimental results on interaction of laser-produced W, V, Mo, Nb plasmas with the surface of secondary Al and Mo targets depending on the distance between two targets show that: (i) the presence of the secondary target at a small distance from the first one leads to the increase of the single charged ions of the plasma and the intensity of ions with

higher charges decreases, and it also changes considerably the energy distribution of ions; (ii) in the case of secondary Al target single charged Al ions were observed in a narrow energy range, while for Mo (mono) secondary target we did not detect Mo ions; (iii) the increase of the distance between the first and second targets leads to the decrease of charge, energy, and intensity of ions in all cases of the plasma. Obtained experimental results show that at the presence secondary target on the way laser plasma expansion influence on the kinetics of expansion of plasma that leads to the reducing of recombination processes on the initial stages of plasma expansion. These influences upon the dynamics of the formation of the energy distribution of multiply charged ions, emitted from the plasma, enlarging the energy range of highly charged ions. The increasing of energy range of highly charged ions shows that the increasing of the temperature of electrons on the front of the shock wave reduces recombination losses in the initial stages of inertial expansion of plasma. On the other hand, the emission of single charged ions from the surface of secondary target under the action of laser-produced plasma, accompanied by the damage of the secondary target surface. We showed that, using different materials with determined emission characteristics with different d, it is possible to change kinematics and dynamics of expansion of the laser plasma and properties of surfaces of the secondary target. This is important for choice of materials of first wall of the future reactors chambers on the base of inertial fusion syntheses.

REFERENCES

- [1] Energy from inertial fusion. – Vienna: International Atomic Energy Agency. 1995.
- [2] HOFFMANN, D.H.H., et al. Handbook of Energy, Springer Verlag, Berlin.
- [3] KADAMA, R., et.al., Plasma Phys and Control Fusion 41(1999)A419-A425.
- [4] PERLADO, J.M., MALERBA L., DIAR DE LA RUBIA T., Fusion Technology, 34/3 (1998) 840.
- [5] SHARKOV, B.Yu., et.al., Nuclear Instruments and Methods in Physics Research. 1–5 (2001).
- [6] KORESHEVA, E., et.al., Fusion Science and Technology. Vol.43, 290–300,(2003).
- [7] WARREN, P., et.al., Fusion Science and Technology. Vol.43, 301–306,(2003).
- [8] PETERSON, P.F., et.al., Fusion Science and Technology. Vol.43, 378–3384,(2003).
- [9] ANDERSON, J.K., et.al., Fusion Science and Technology. Vol.43, 401–408,(2003).
- [10] RAFFRAY, A.R., HAYNES, D., NAJMABADI, F. Journal Nuclear Materials 23–31 (2003).
- [11] BEDILOV, M.R., KHAYDAROV, R.T., Kvantovaya elektronika,31,N4(2001) p.321–324.
- [12] BOYKO, V.A., BRUNETKIN B.A.,and etc. Kvantovaya elektronika, 12, N 11 (1985) 2340.
- [13] BEDILOV, M.R., KHAYDAROV, R.T. Plasma Phys. 26 (2000) p. 862.
- [14] WIENHOLD, P., PHILIPPS, V., Journal of Nuclear Matereroals 311–320 (2003).

TARGET PHYSICS

Investigation of the high-z laser produced plasma with the use of ion-diagnostics for optimization of the laser interaction with Hohlraumtype targets

J. Wolowski

Institute of Plasma Physics and Laser Microfusion, Warsaw, Poland

Scientific co-workers participating in this Research Project:

J. Badziak¹, F. P. Boody², S. Gammino³, H. Hora⁴, K. Jungwirth⁵, J. Krása⁵, L. Láška⁵, A.M. Mezzasalma⁶, P. Parys¹, M. Pfeifer⁵, K. Rohlena⁵, A. Szydłowski⁷, L. Torrisci^{3,6}, J. Ullschmied⁸, E. Woryna¹

¹ Institute of Plasma Physics and Laser Microfusion, Warsaw, Poland,

² Ion Light Technologies, Bad Abbach, Germany

³ INFN-Laboratori Nazionali del Sud, Catania, Italy

⁴ University of New South Wales, Sydney, Australia

⁵ Institute of Physics, ASCR, Prague, the Czech Republic

⁶ Messina University, Messina, Italy

⁷ Institute for Nuclear Studies, Otwock-Świerk by Warsaw, Poland

⁸ Institute of Plasma Physics ASCR, Czech Republic.

Abstract. In recent works some useful aspects of fast ion emission from plasma produced with the use of high power laser generating ultrashort pulses have been emphasised. In particular, the possibility of applying laser-produced intense high-energy ions in inertial fusion has been suggested. In this paper our recent studies on fast proton generation in the plasma produced by an intense 1-ps laser pulse, carried out at the Institute of Plasma Physics and Laser Microfusion (IPPLM), Warsaw are presented. The characteristics of ion fluxes emitted forward from various kinds of single- and double-layer targets were measured with the use of ion collectors and an electrostatic ion-energy analyser. The amplitudes of the hard X rays emitted from the plasma were measured with the use of semiconductor detectors. Our experiments showed that a double-layer system makes it possible to obtain higher energies and higher proton current densities than single-layer systems. The mechanisms of proton acceleration and the possibility of production of picosecond proton beams of ultrahigh current densities, useful for inertial fusion, are discussed in the paper.

1. GENERAL

Studies of high-Z plasma produced with high-power laser are directed towards the determination of physical processes in such a plasma (e.g., energy transformation and transport, x ray generation, ionization and recombination, ion acceleration, nonthermal phenomena and others) as well as towards important applications: optimisation of indirect laser fusion, x ray laser-plasma source and sources of multi-charged ions.

The ion emission from laser-produced plasmas is a well known phenomenon which has been studied since the early 1960s. For a long time the interest in studies of the ion emission has been stimulated by the importance of this phenomenon for laser-driven inertial confinement fusion. In more recent works, however, some useful aspects of ion emission from laser-produced plasma have been emphasised. The energy of an intense laser pulse interacting with a target is not completely transferred to the plasma in the collisional (thermal) processes. In particular, as a result of the long-wavelength laser-plasma interaction, the nonthermal and

nonlinear processes transfer a part of laser energy into hot electrons energy of fast ions ([1, 2, 3]). The efficiency of these depends on characteristics of laser pulse, target and irradiation geometry.

The main objective of this project was application of ion diagnostic methods to investigate the physical properties of high-Z plasma generated by laser beams similar to the plasma produced inside the Hohlraum target. In this project the characteristics of such plasma was investigated in dependence on laser pulse parameters (intensity, wavelengths, energy), irradiation geometry (focus position, target tilt angle) and target material. Combined measurements of high-Z laser-produced plasma using different diagnostic methods are better for quantitative analysis of the processes essential for optimal indirect implosion of thermonuclear capsule.

The investigations described here, were carried out at the IPPLM in Warsaw with use of the IPPLM CPA Nd:glass laser generating 1-ps or 0.5-ns pulses at $\lambda = 1.05 \mu\text{m}$ and at the PALS Research Centre in Prague with the use of the iodine PALS laser system with output energy up to 750 J at the fundamental wavelengths ($1.315 \mu\text{m}$) or up to 250 J at the 3rd harmonic ($0.438 \mu\text{m}$) in a 0.4 ns pulse. These studies were carried out by means of ion diagnostics (i.e. ion collectors, a cylindrical electrostatic ion energy analyser) and additionally with the use of X ray detectors and nuclear track detectors for fast ions.

The investigations performed at the IPPLM in Warsaw and at the PALS Research Centre in Prague were carried out within multilateral co-operation with the Institute of Physics and Institute of Plasma Physics ASCR in Prague and with scientists from several other institutes. In this Final Report we present most interesting results of our experimental studies and summarized conclusions related to the properties of the high-Z Hohlraum-like plasma.

2. INVESTIGATION OF THE ION EMISSION FROM HIGH-Z PLASMAS GENERATED BY THE HIGH ENERGY LASER PALS AT THE FUNDAMENTAL AND THE 3rd HARMONIC FREQUENCIES

Introduction

The interaction of a high-intensity laser beam with a target leads to the generation of plasma in which the absorbed energy is not completely transferred to the plasma in the collisional (thermal) processes. In particular, as a result of the long-wavelength laser-plasma interaction, the nonthermal coupling processes transfer a part of laser energy into the energy of hot electrons. The efficiency of the hot electron production decreases with the decreasing of the laser wavelength (e.g. [1]). There are also several nonlinear phenomena (e.g. filamentation and self-focusing of the high intensity laser beam, ponderomotive forces, (see e.g. [2]) weakly dependent on the laser wavelength, which can lead to the fast ion production in the case of the short-wavelength laser-plasma interaction. It is interesting to compare the characteristics of fast ions accelerated in plasmas produced by the intense long- and short-wavelength laser radiation in similar experimental conditions.

Until now most of the investigations of the ion emission from the plasma produced by high power lasers have been performed with the use of the long-wavelength lasers (e.g. [3, 4]). In this work the study of the parameters of ion stream produced by the iodine laser at PALS, is presented and results are compared as a function of the laser energy at two laser wavelengths: 438 nm and 1315 nm. These common investigations were performed at the PALS Research Centre in Prague (Czech Rep.).

Experimental set up

Investigations of heavy ion emission from laser-produced plasma were performed within a common experiment at the PALS research Laboratory of ASCR in Prague, with the use of iodine laser PALS (up to 1.2 kJ, 0.4 ns, 1315 nm for ω_0 and up to 0.25 kJ, 0.4 ns, 438 nm for $3\omega_0$) [5]. The laser beam was focused on the planar surface of the metal targets (Cu, Ag and Ta) placed in the vacuum chamber (10^{-6} torr). The minimum focus spot was about 70 μm .

In our experiments we used ion collectors (IC) and a cylindrical electrostatic ion energy analyzer (IEA) based on the time-of-flight method (TOF). The IC measures a charge-integrated time-resolved signal of ions, from which the energy-charge product and the total charge carried by ions, as well as the mean ion energy can be derived [6]. The IEA gives the possibility of identifying the ion species produced, i.e. of determining their mass-to-charge ratios, energies and abundance [6]. The set-up of the experiment is shown in Fig. 2.1.

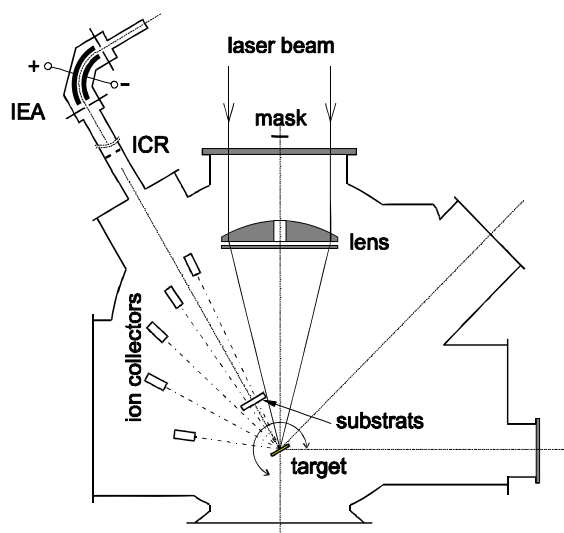


Figure 2.1. Experimental set-up.

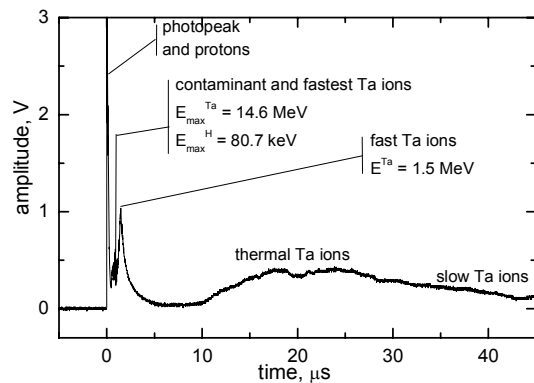


Figure 2.2. Typical IC signal ($3\omega_0$, $E_L \sim 200$ J).

Results and discussion

The results of the ion time-of-flight measurements with the use of IC demonstrate the existence of fast ions as well as thermal and slow ones emitted from the plasma produced by both a high-energy long-wavelength (1315 nm) laser pulse and a short-wavelength (438 nm) laser pulse (Fig. 2.2). Simultaneously, the ion spectra were measured by IEA. The ion charge, the average ion kinetic energy, the maximum ion current density and the maximum recorded charge state of ions were measured as a function of the laser pulse energy and focus position with respect to the target surface. The examples of the IEA spectra of ions recorded in the similar laser shots at 1315 nm and at 438 nm laser radiation wavelengths are given in Fig. 2.3. The shapes of the IEA spectra for both wavelengths are different. In particular, the stream of fast highly-charged ions was much more intense in the case of infrared radiation than at visible laser radiation. The IEA ion spectra enable the determination of the total number of ions, as well as the energy carried by them. The total number of ions, as well as the energy carried by them was determined from the set of the IEA ion spectra measured at fixed experimental conditions for different values of the IEA deflecting voltage. Fig. 2.4 shows the existence of highly charged ($z > 35$) high-energy Ta ions, which carried a significant part of the total energy of all the ions. But in the case of 1315 nm radiation this group is more

significant than for 438 nm light. It is believed that this effect corresponds to the different mechanisms of ion acceleration in the case of visible laser light.

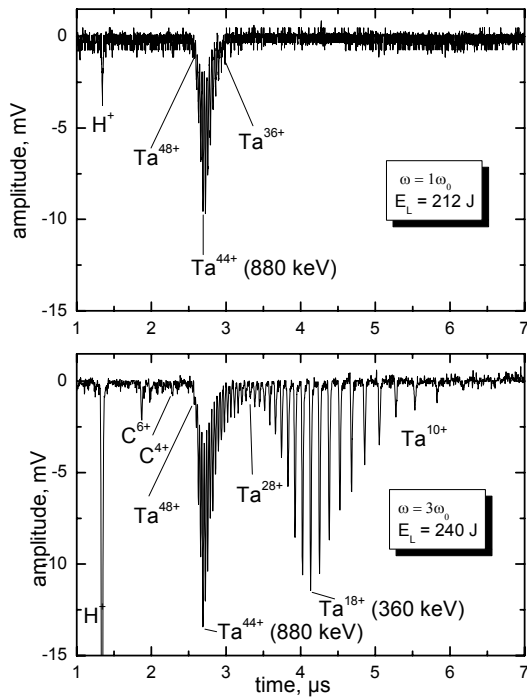


Fig. 2.3. IEA ion spectra recorded at the laser wavelengths of 1315 nm (top) and 438 nm (bottom).

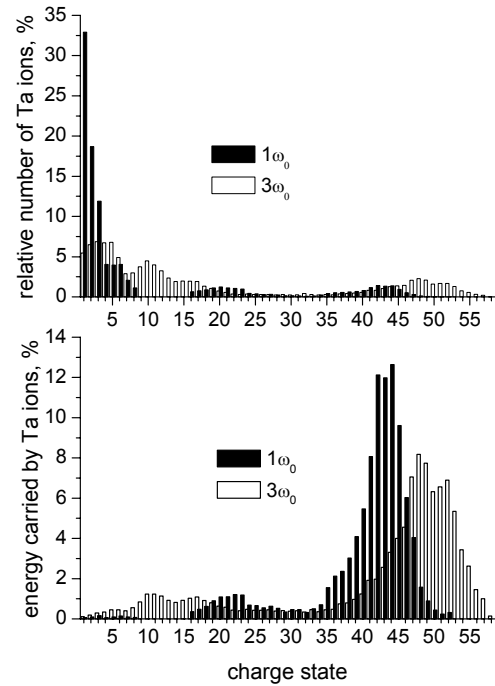


Fig. 2.4. Distrib. of Ta ion energy (top) and abundance (bottom) with charge ($E_L \sim 225 \pm 15$ J).

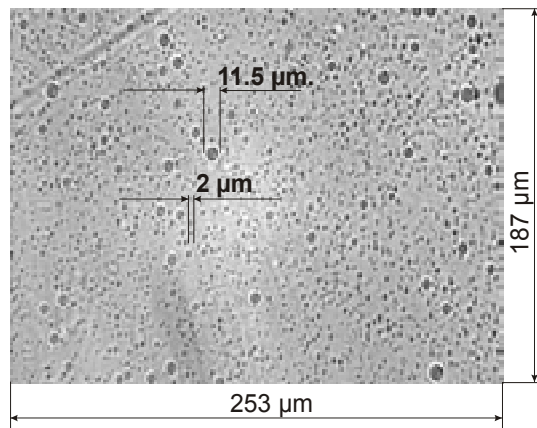


Fig. 2.5. Ion tracks (Ta-ions - 11.5 μm , H-ions - 2 μm) recorded on the PM-355 detector sample covered with a 4 μm Al-foil filter ($E_L \sim 80$ J).

The parameters of both x ray and ion emissions change clearly depending on the lens-target separation and these changes are well correlated with each other. The most radical changes in the emission are observed when the target is shifted into a close vicinity of the focal plane. The changes are manifested by an abrupt rise of hard x ray emission, lowering the amount of ions and narrowing the angle distribution.

The fast ions emitted from the laser-produced plasma were also measured with the use of solid-state nuclear track detectors of the PM-355 type [7]. Track densities above 10^7

tracks/cm² for Ta ions were observed on detectors placed 86.5 cm from the target. Large tracks induced by Ta ions that penetrated 4 μm Al foil thickness were observed (Figure 2.5). This confirms the fact that Ta ions of energies ≥ 20 MeV were emitted from the targets irradiated both with the use of short- and long wavelength high-energy laser beams.

The mechanisms of the fast ion generation with the use of the short wavelength laser radiation should be explained taking into consideration other phenomena than those in the case of the long wavelength laser radiation. In particular, the evident difference in the relation of the abundance of a fast ion group with the highest ion charge states to the abundance of the ion group with medium energies and charge states should be explained.

On the basis of the ion diagnostic investigations the existence of nonthermal and nonlinear accelerating processes was demonstrated for the plasma produced by high energy long-wavelength as well as short-wavelength laser pulses. It is believed that in the case of the short-wavelength laser-plasma interactions besides possible thermal ambipolar acceleration of ions, nonlinear force effects including ponderomotive and relativistic self-focusing may contribute to the appearance of high kinetic energy, highly charged ions.

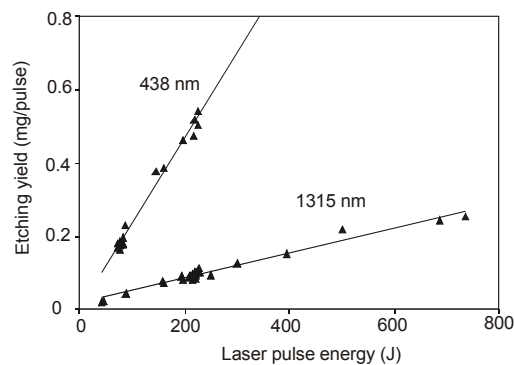


Figure 2.6. Ablation rate as a function of the laser pulse energy for the two used wavelengths.

The growth of the crater diameters on the target with the laser pulse energy was practically the same for both 438 nm as for 1315 nm, while the visible radiation produces deeper craters with respect to the infrared radiation. The tantalum ablation rate, shown in Fig. 2.6 was about 0.1 mg/pulse for the infrared radiation and about 0.5 mg/pulse for the visible radiation at laser pulse energy of ~200 J. These etchings correspond approximately to 3.3×10^{17} atoms/pulse and 1.7×10^{18} atoms/pulse at 438 nm and 1315 nm, respectively. At a shorter laser wavelength, the critical density surface is located closer to the target surface than for a longer laser wavelength. It results in stronger thermal and nonthermal (hot electrons, fast ions and hard X rays) interactions on the target surface at 438 nm laser wavelength than at 1315 nm laser wavelength.

Conclusions

Using the high-intensity long-wavelength as well as short-wavelength PALS laser pulses (1315 nm and 438 nm, respectively), the production of highly charged, high-energy ions have been demonstrated, using IC, IEA, and solid-state track detector measurements. For Ta ions

$z_{\max} = 57$ and $E_i > 20$ MeV. The ion collector signals recorded at higher laser pulse energies clearly show the existence of three separate ion groups: fast, thermal and slow. At high laser pulse energies, $E_L > 200$ J, fast ion current density attains $j_{\max} \sim 20$ mA/cm² at the distance of 1 m from the target.

Described here studies demonstrated the existence of a group of fast highly-charged ions produced not only by the intense infrared laser beams but also by intense laser radiation of shorter wavelength (visible light) focused on high-Z targets. An efficient production of highly charged high-energy ions, by an intense short-wavelength laser pulse suggests that the mechanisms of the fast ion generation with the use of such laser pulses should be clarified taking into account that the classical process of fast ion acceleration by hot electrons ([1–4]) escaping from plasma decreases with the decreasing wavelength. Thus, in the case of short-wavelength laser-plasma interactions other phenomena only weakly dependent on the laser wavelength e.g. ponderomotive forces and self-focusing of laser radiation ([1, 2]) may contribute to the acceleration of ions in the plasma.

REFERENCES

- [2.1] KRUER, W.L., Phys of Fluids 25 (1982) 2324.
- [2.2] HORA, H. et al., Optics Comm. 207 (2002) 333.
- [2.3] LASKA, L., et al., Rev. Sci. Instrum. 71 (2000) 927.
- [2.4] WOŁOWSKI, J., et al., Plasma Phys. Control. Fusion 44 (2002) 1277.
- [2.5] JUNGWIRTH, K., et al., Phys. Plasmas 8 (2001) 2495.
- [2.6] WORN, E., PARYS, P., WOŁOWSKI, J., MRÓZ, W., Laser and Particle Beams 14 (1999) 293.
- [2.7] SZYDŁOWSKI, A., et al., Czech J. Phys. 52 (2002) 299.

3. THE INFLUENCE OF PRE-PULSE PLASMA ON ION AND X RAY EMISSION FROM Ta PLASMA PRODUCED BY A HIGH ENERGY LASER

Introduction

The plasma produced with the use of a sub-nanosecond laser pulse (≤ 1 ns) at intensities of 10^{14} – 10^{16} W/cm² emits ions with a broad range of charge states and with energies from hundreds of eV to hundreds of MeV as well as x rays of energies from tens of eV to tens of keV depending on the irradiated target material and the parameters of the laser used [1–8]. A part of laser energy heating the target at high radiation intensities is converted into ion kinetic energy by a variety of nonlinear phenomena. The essential characteristics of the laser-generated ion streams and x rays depend, among other factors, on distribution of the electron density during interaction of the high-intensity laser radiation with the plasma produced by a leading edge of the laser pulse. This dependence can be investigated using low intensity laser prepulses to generate pre-plasmas with which the main laser pulse will interact. Experimental efforts in this field have concentrated on the influence of the pre-plasma produced by the prepulse on characteristics of the x rays emitted from laser-generated plasma [9–11]. Recently, a prepulse experiment has been proposed [12] for investigation of a relativistic self-focusing phenomenon accompanying the very high intensity laser-plasma interactions. In this paper we present the results of investigations of the properties of laser-produced ion streams and x rays performed in the presence of small prepulses with different durations.

Experimental arrangement

The experiment was performed with use of iodine laser system PALS at the PALS Research Centre in Prague (Czech Rep.) operating at a wavelength of 438 nm (3rd harmonics of fundamental frequency). The laser beam of energy up to 250 J in a 400-ps pulse was focused onto a Ta target perpendicularly to the target surface forming the laser spot with the minimum diameter equal $\sim 70 \mu\text{m}$. The measurements were performed with the use of fixed laser pulse energy $E_L = 140 \pm 10 \text{ J}$ corresponding to a power density of $\sim 9 \times 10^{15} \text{ W/cm}^2$. The main laser pulse was preceded by a prepulse having either 0.7% or 7% of the main-pulse energy corresponding to the prepulse energy $E_{p-L} \sim 1 \text{ J}$ or $\sim 10 \text{ J}$, respectively. The main pulse was delayed by $\Delta t_{p-L} = 0, 0.6, 1.2, 2.3 \text{ ns}$ or 4.6 ns with respect to the pre-pulse.

In our experiments we have also used ion collectors (ICs) and a cylindrical electrostatic ion energy analyzer (IEA) for measurements of the characteristics of laser-generated ions [13]. Angular distribution of ion emission was measured with the use of 5 ion collectors located at different angles with respect to the target normal: $0^\circ, 25^\circ, 28^\circ, 34,6^\circ$ and 45° . The IEA was located at the angle of 30° . The x ray measurements were performed with the use of photodiodes covered with different filters. For measurements of soft X ray component (energy ranges $0.8\text{--}1.5 \text{ keV}$ and $1.9\text{--}5.5 \text{ keV}$) the silicon photodiodes with an active layer of about $2 \mu\text{m}$ (at 20-V bias) and a dead layer of about $0.15 \mu\text{m}$ were used. For the measurement of the harder x ray component (energy range $7.6\text{--}23.4 \text{ keV}$) the photodiodes with the $380\text{-}\mu\text{m}$ thickness of the active-layer were used.

Results of measurements

The groups of fast, thermal and slow Ta ions were recorded by the ion collectors. The characteristics of three ion groups depend on the different mechanisms of ion acceleration. The characteristics of group of faster nonthermal Ta ions in the collector signal, if analysed by the IEA, is found to be composed of high charge state ions. The slowest ions were emitted from a cooler plasma produced by X rays generated in the hot laser-heated plasma.

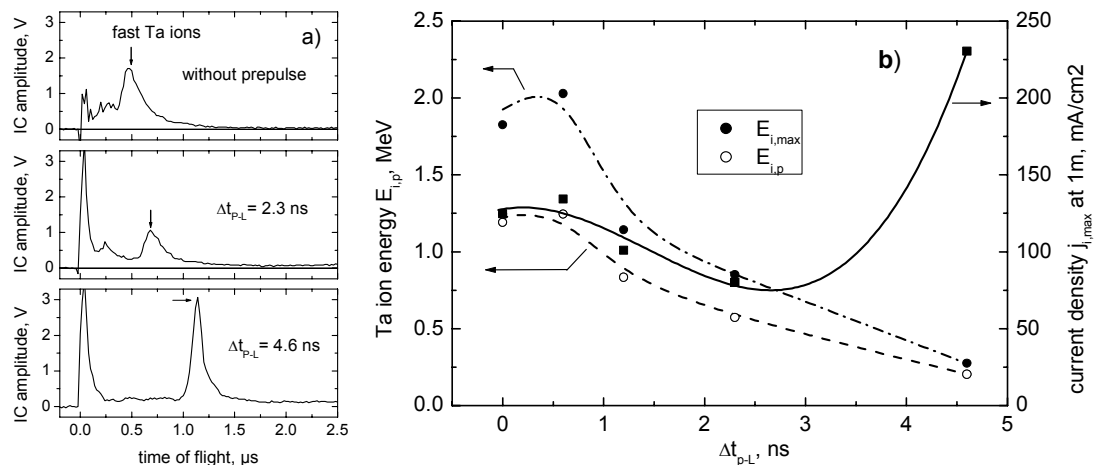


Figure 3.1. a) The typical ICs signals of the fast Ta ions recorded at 0° and at delay times $\Delta t_{p-L} = 0, 2.3$ and 4.6 ns . b) The current density as well as maximum and peak energies of the fast Ta ions in dependence on Δt_{p-L} . $E_{p-l} \sim 10 \text{ J}$ (7% energy of the main pulse).

A shape of a part of the IC signal corresponding to the fast Ta ions changes with the increase in Δt_{p-L} as shows Fig. 3.1a. In particular, the fast ion peak for $\Delta t_{p-L} = 4.6$ ns is evidently narrower in comparison with the wider fast ion signals for shorter Δt_{p-L} . However, the velocity (energy) of fast ions at $\Delta t_{p-L} = 4.6$ ns is considerably lower then in the case of shorter Δt_{p-L} . A maximum current density of the fast Ta ions (j_f) as well as maximum and peak energies of the fast Ta ions ($E_{i,max}$ and $E_{i,p}$, respectively) recorded by the ion collector located at an angle of 0° are presented in Fig. 3.1b for a prepulse energy of ~ 10 J (7% energy of the main pulse) in dependence on delay times (Δt_{p-L}). The peak ion energy corresponds to the maximum of the fast ion collector signal. This diagram shows that $E_{i,max}$ and $E_{i,p}$ attains a maximal values for $\Delta t_{p-L} < 1$ ns. $E_{i,max}$ and $E_{i,p}$ decrease for longer delay times while $j_{f,max}$ reach the highest value for 4.6 ns after attaining shallow minimum ~ 2.5 ns. Similar dependencies were observed also in the case of a prepulse energy of ~ 1 J (0.7% of main pulse energy).

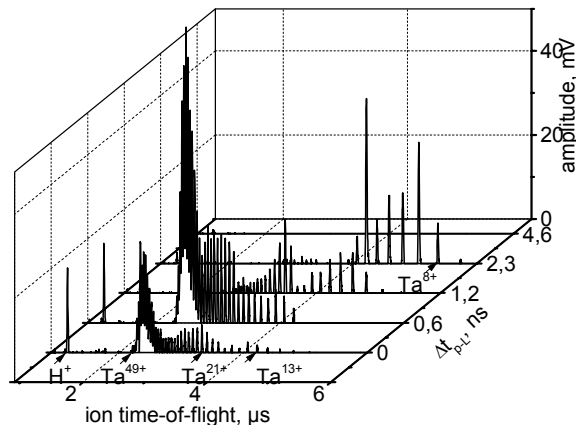


Figure 3.2. The spectra of fast Ta ions recorded at deflecting voltage of 30 kV and at the prepulse energy of ~ 10 J for different delay times between the pre-pulse and the main laser pulse.

The maximum current density of thermal Ta ions increases while the peak energy of these ions changes slightly with the increase in Δt_{p-L} . In the case of group of slow ions both the total current density and the peak ion energy decrease with increase in Δt_{p-L} . A large amount of slow ions recorded by the IC at 0° (which is proportional to the current density of slow ions) for $\Delta t_{p-L} = 0$ falls up to practically the undetectable amount for $\Delta t_{p-L} = 4.6$ ns.

Examples of ion spectra recorded at 30° using IEA with an applied deflecting potential of 30 kV are shown in Figure 3.2. for different time intervals between the 10-J prepulse and the main laser pulse (Δt_{p-L}). The relative abundance of different Ta ion species depends significantly on the Δt_{p-L} . The diagram shows that for a deflecting potential of 30 kV selecting the high energy ions ($E_i = 30z$ keV, where: z – ion charge state) the highest ion charge states ($z_{max} \sim 50+$) occur for $\Delta t_{p-L} = 0, 0.6$ and 1.2 ns. For $\Delta t_{p-L} = 2.3$ ns the maximum ion charge state was only $z_{max} \sim 25+$, while for $\Delta t_{p-L} = 4.6$ ns the highest ion charge state was $3+$. The IEA spectra and the dependence $z = f(\Delta t_{p-L})$ for the prepulse energy of $E_{p-L} \sim 1$ J, not presented here, are very similar to those for ~ 10 J.

The dependence of the amplitude of the hard- and soft x ray signals on Δt_{p-L} are shown in Figure 3.3. for $E_{p-L} \sim 10$ J. These dependences measured for $E_{p-L} \sim 1$ J are also very similar to those presented in Figure 3.3.

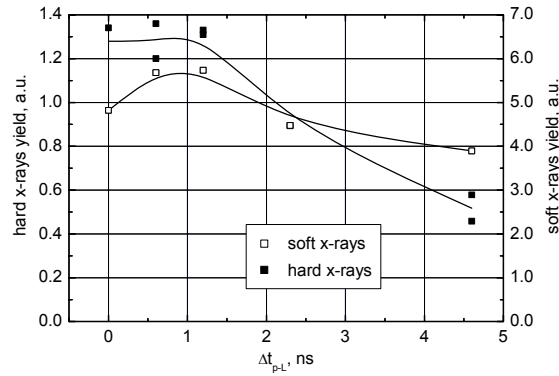


Figure 3.3. The dependence of the yield of the soft (0.7-1.5 keV) and hard (7.6-23.4 keV) x rays on the delay times Δt_{p-L} (prepulse energy $E_{p-L} \sim 10$ J).

Analysis of results and conclusions

It has been found that the laser pulse at the energy of ~ 140 J (laser power density of $\sim 9 \times 10^{15}$, wavelength of 438 nm, pulse duration of 400 ps) heating the plasma without a prepulse can produce high energy (up to several MeV) highly-charged Ta ions and hard x rays (recorded in the energy range of 7.6–23.4 keV) similarly as in our previous experiments [6, 7, 8, 14]. A small prepulse creating pre-plasma before the arrival the main pulse changes considerably the condition of laser-matter interaction, particularly, the efficiency of the fast ion acceleration. The results of performed investigations show that the characteristics of laser-generated ions and x rays are very similar for both the prepulse energies used $E_{p-L} \sim 10$ J and ~ 1 J (7% or 0.7% of the main-pulse energy, respectively).

The maximum and mean energy of the fast ions as well as the yields of both the hard and the soft x rays attain highest values for the delay times in a range of ~ 0 -1.2 ns and decrease for longer delay times. The ion current density also decreases at $\Delta t_{p-L} > 1$ ns but, after attaining a shallow minimum at delay times ~ 2.5 ns, reach highest values for $\Delta t_{p-L} = 4.6$ ns. It can be supposed that within the range of delay times from 0 to ~ 1 ns there exist optimum conditions maximising the fast ion energies as well as yields of soft and hard x rays at considerably high fast ion current density. However, to identify the physical phenomena occurring under these conditions measurements with much fine steps of Δt_{p-L} are necessary.

At longer delay times the prepulse plasma screens effectively the target surface and the main pulse interacts in fact with a plume of the expanding plasma producing the thermal ions as well as the fast and the slow ions of decreasing amount and energy with the increase in the delay time. But for $\Delta t_{p-L} \sim 4.6$ ns intense streams of fast ions ($j_{f,max} \sim 260$ mA/cm²) expanding close to the target normal with lower mean energy $E_{i,p} \sim 200$ keV but of weak energy spread (~ 40 keV) were observed both for $E_{p-L} \sim 10$ J and ~ 1 J. In this case surely other mechanisms of ion acceleration along the laser beam axis should be taken into consideration. For instance, parametric Brillouin and Raman back scatterings (BBS and RBS) [15] are more efficient at low electron concentrations and low density gradient even at laser power density lower than one the occurring at shorter Δt_{p-L} .

REFERENCES

- [3.1] HASEROTH, H., HORA, H., Laser and Particle Beams **14** (1996) 393.
- [3.2] BOODY, F.P., et al., Laser Part. Beams **14** (1996) 443.
- [3.3] LASKA, L., et al, Rev. Sci. Instrum. **69** (1998) 1072.
- [3.4] CLARK, E.L., et al, Phys. Rev. Lett. **85** (200) 1654.
- [3.5] BADZIAK, J., et al, Appl. Phys Letters **78** (2002) 1823.
- [3.6] WOLOWSKI, J., et al, Plasma Phys. Control. Fusion **44** (2002) 1277.
- [3.7] RYC, L., et al, Plasma Phys. Control. Fusion **45** (2003) 1079.
- [3.8] TORRISI, L., et al, Appl. Surf. Sci. **220** (2003) 1087.
- [3.9] KUHLKE, D., et al, Appl. Phys. Lett. **50** (1987) 1785.
- [3.10] TEUBNER, U., et al, Appl. Phys. B **54** (1992) 439-499.
- [3.11] ZHANG, P., et al, Phys. Rev. E **57** (1998) R3746-R3748.
- [3.12] HORA, H., et al, Opt. Commun. **207** (2002) 333.
- [3.13] WORYNA, E., et al, Laser Part. Beams **14** (1996) 293.
- [3.14] LÁSKA, L., et al, Plasma Phys. Control. Fusion, **45** (2003) 585.
- [3.15] KRUER, W.L., et al, Phys. Fluids **25** (1982) 2324.

4. COMPARISON OF FAST ION EMISSION FROM HIGH-Z PLASMA PRODUCED BY HIGH INTENSITY SHORT (1 ps) AND LONG (0.5 ns) PULSES

Introduction

Both from physical and practical points of view it is important to compare properties and mechanisms of the generation of ion fluxes emitted from plasmas produced by ultrashort and long laser pulses. It is especially interesting when a fast component of the ion fluxes is considered. Such a comparison was carried out at the IPPLM with the use of 1-ps and 0.5-ns laser pulses produced by the same CPA Nd:glass laser system [1, 2]. Excluding the pulse duration and intensity (up to 8×10^{16} W/cm² for 1-ps and up to 2×10^{14} W/cm² for 0.5-ns pulses) other parameters of the laser beam (energy, wavelengths and focal spot diameter) were roughly identical for both pulses. An on-axis parabolic mirror ($f = 27$ cm) with a hole in the mirror centre was used to focus the laser beam onto a flat massive Au target perpendicularly to the target surface.

Experimental arrangement

For measurements of backward-emitted (against the laser beam) ion fluxes, the linearly polarised laser beam of the ps CPA laser was focused by an on-axis $f/2.5$ parabolic mirror, with a hole in the centre, onto a massive Au target at an angle of 0° with respect to the target normal (Fig. 5). The maximum intensity of the focused laser beam ($d_f \approx 20\mu\text{m}$) was about 10^{17} W/cm². By removing the grating compressor from the optical path of the CPA system the laser delivered high-contrast 0.5-ns pulses of intensity up to 2×10^{14} W/cm² and of the wavelength, laser energy (up to 0.7J) and focal spot diameter close to those of the ps pulses. The measurements of the ion flux parameters were performed with the use of ion collectors (ICs) and an electrostatic ion-energy analyzer (IEA). The IEA and the ring ion collector (IC1) measured the backward-emitted ions passing through the hole in the parabolic mirror along the target normal and the laser beam axis. For a rough estimation of the angular distribution of ion emission two additional collectors, viewing the target at angles Θ of 26° and 34° with respect to the target normal, were applied.

To compare the ps-laser-driven ion fluxes with the ion fluxes produced by the long pulses of power and intensity comparable to those of the ps pulses, we used the PALS iodine laser system generating high-energy pulses of 0.4 ns duration [3]{51}. The 0.438- μm laser beam of energy about 140J was focused onto a massive Ta target perpendicularly to its surface producing the laser intensity $\sim 10^{16}$ W/cm². The IEA and 5 ion collectors located at different angles with respect to the target normal were used for measurements of ion flux characteristics (for details see e.g. [4].

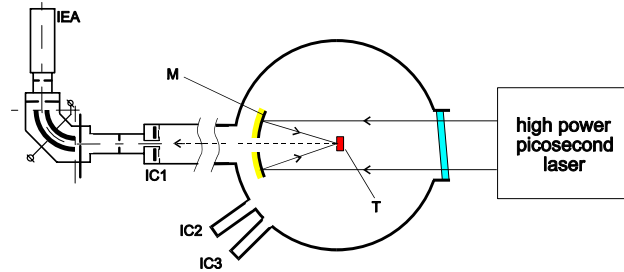


Figure 4.1. Scheme of the experimental arrangement. IEA – electrostatic ion-energy analyzer; IC1, IC2, IC3 – ion collectors; T – target; M – parabolic mirror.

Results

The typical ion collector signals illustrating temporal runs of the backward ion emission along the target normal are shown in Fig. 4.2 for the cases of 1-ps, 0.5-ns and 0.4-ns laser pulses.

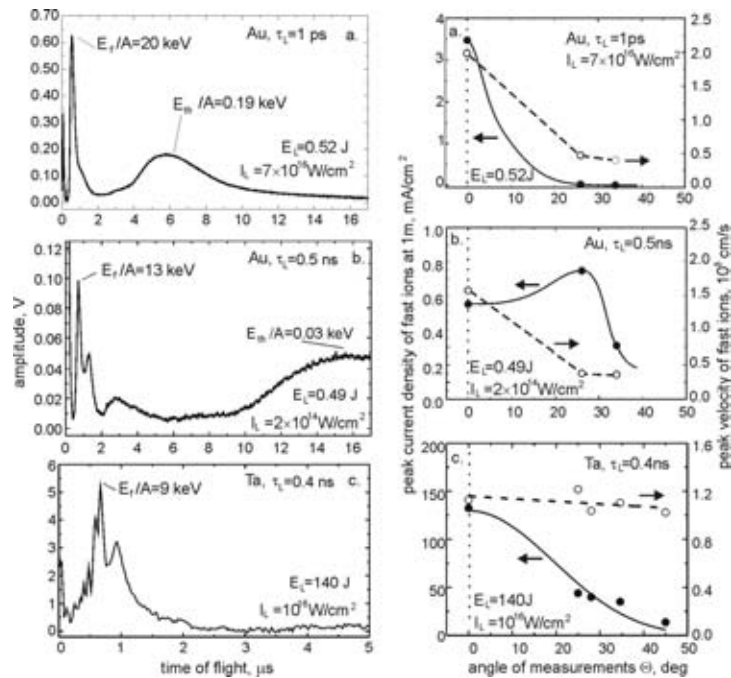


Figure 4.2 (right). IC1 collector signals from Au plasmas produced by 1-ps (a) and 0.5-ns (b) laser pulses of 1-ps laser. For comparison the IC signal from Ta plasma produced by PALS laser (c) is shown. The average ion energies per nucleon for the fast and thermal ion groups are indicated. A is the ion mass number.

Figure 4.3 (left). The rough angular distributions of peak current densities and peak velocities of fast ions driven by 1-ps (a) and 0.5-ns (b, c) laser pulses.

The rough angular distributions of fast ion emission are presented in Fig. 4.3. The above figures demonstrate principal differences in properties of fast ion fluxes emitted from plasmas produced by short and long laser pulses. In the long-pulse case several groups of fast ions (index f in Fig. 4.2) are generated and the angular divergence of the fast ion expansion is high. In the short-pulse case only a single fast ion group is generated and this group is well separated in time from the thermal ion group. The fast ions driven by the short pulse expand with small angular divergence and with a pronounced maximum along the target normal (at $\theta \geq 26^\circ$) only fast ions of the current density by more than 100 times less than that for $\theta = 0^\circ$ were recorded) as it could be expected for the quasi-planar geometry of ion acceleration.

Significant differences in properties of the fast ion fluxes produced by ps and subns laser pulses one can also observe when dependencies of the maximum and mean ion energies (measured along the target normal) on the laser intensity I_L are considered (Fig. 4.4). For the subnanosecond pulses the ion energies follow approximately the square-root dependence on the intensity, which is consistent with the hot electron temperature dependence on $I\lambda^2$ obtained by Gitomer et al. [5] by means of a compilation of data from various laboratories. However, for the ps pulses, the ion energies increase roughly linearly with the laser intensity.

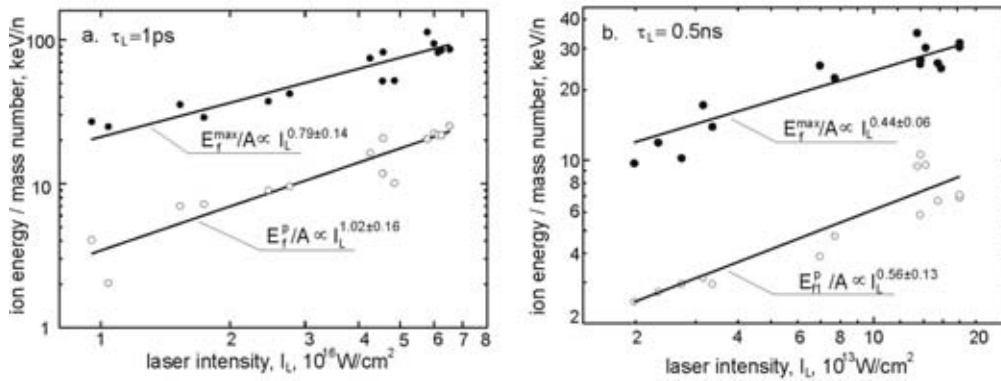


Figure 4.4. The maximum and the mean energies of fast ions, measured in the direction normal to Au target, as a function of laser intensity for 1-ps (a) and 0.5-ns (b) laser pulses.

Figure 4.5 presents the dependence of the ion current density at the source on the laser intensity, $j_s(I_L)$, for the backward ion emission driven by the ps pulse. The dependence was obtained with the use of equation $j_s \approx Q_i/\tau_{is}S_s$, assuming $\tau_{is} = \tau_L$, $S_s = S_f$ and $Q_i = Q_{IC1}$, where Q_{IC1} is the fast ion charge passing through the IC1 collector, seen within the angle of 3° from the source. Q_i is the total charge of fast ions measured in the far expansion zone (due to a possible recombination, $Q_i \leq Q_{is}$, where Q_{is} is the fast ion's charge flowing out of the ion source); τ_{is} is the duration of fast ion generation at the source, which is roughly equal to the laser pulse duration, $\tau_{is} \approx \tau_L$; S_s is the area of the fast ion source.

In general, $S_s \geq S_f$ (S_f is the laser focal spot area). As $Q_{IC1} < Q_i \leq Q_{is}$ (the ion beam divergence is expected to be higher than 3°), the calculated ion current densities actually represent the lower limits of their real values. It can be seen that j_s follows approximately the square-root dependence on I_L – predicted from equation [6]: $j_s \approx 74 (s z/A)^{1/2} \lambda^{-1} I^{1/2}$, [A/cm^2 , μm , W/cm^2] and numerical simulations – with $j_s \approx 10^{10} \text{A}/\text{cm}^2$ at $I_L \approx 10^{17} \text{W}/\text{cm}^2$. Unfortunately, for subns laser pulses, the dependence $j_s(I_L)$ could not be derived from our measurements, as the ion source area S_s could significantly exceed the focal spot area in this case. The upper limits for j_s , calculated for the low-energy 0.5-ns and the high-energy 0.4-ns laser pulses assuming that $S_s = S_f$, are $j_s \approx 2 \times 10^6 \text{A}/\text{cm}^2$ and $j_s \approx 2 \times 10^7 \text{A}/\text{cm}^2$ respectively.

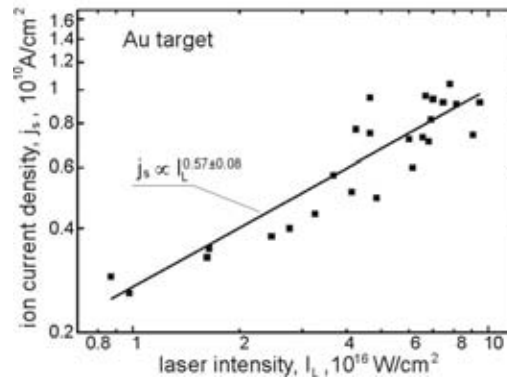


Figure 4.5. The fast ion current density at the source for the ions emitted backward within the angle of 3° as a function of 1-ps laser pulse intensity.

Conclusions

Both temporal and spatial characteristics of fast ion emission as well as physical mechanism leading to the ion acceleration are essentially different in plasmas produced by short and long laser pulses from a solid target. We have found that in the short-pulse case principally only a single group of fast ions with small angular divergence is generated in the direction normal to the target surface. Non-linear (ponderomotive) force from skin-layer interaction is the most probable mechanism of the ion acceleration in this case. Contrary to this, in the long-pulse case at least two groups of fast ions are generated from plasma and they are emitted in a relatively large solid angle. Ponderomotive and relativistic self-focusing seems to be responsible for the observed properties of the fast ion emission from long-pulse-produced plasma. Ion beams generated by short-pulse skin-layer interaction can be particularly promising for producing high fusion gain from D-D or D-T reaction as it has been demonstrated recently in a small-scale experiment by Norreys et al. [7].

REFERENCES

- [4.1] BADZIAK, J., et al., Opt. Commun. **134**, (1997) 495
- [4.2] BADZIAK, J., et al., Phys. Rev. Lett. **87**, (2001) 215001
- [4.3] LÁSKA, L., JUNGWIRTH, K., KRÁLIKOVÁ, B., et al., Plasma Phys. Control. Fusion **45**, 585 (2003).
- [4.4] WOŁOWSKI, J., BADZIAK, J., PARYS, P., et al., Czech. J. Phys. **54**, C385 (2004).
- [4.5] GITOMER, S.J., JONES, R.D., BEGAY, F., et al., Phys. Fluids **29**, 2679 (1986), and references
- [4.6] HORA, H., Czech. J. Phys. **53**, 199 (2003).
- [4.7] NORREYS, P., et al., Phys. Rev. Lett. **76**, 1832 (1996).

5. FAST ION GENERATION IN THE PLASMA PRODUCED BY A 1-ps HIGH INTENSITY LASER PULSE INTERACTING WITH THE FOIL TARGETS

Introduction

The rapid development of high-peak-power lasers generating short (≤ 1 ps) pulses (SPs), opened principally new possibilities of applications of ion beams emitted from laser-produced plasmas. Unlike large long-pulse (ns or subns) laser installations, a short-pulse laser (SP-laser) even of low energy (≤ 1 J) makes it possible to produce very high laser intensities and, as a result, to generate intense high-energy ion bursts of ions of subnano- or picosecond duration [1, 2] which are not achievable by other sources currently known. This feature creates a prospect of different unique applications of SP-laser-driven ion beams, in particular, in inertial confinement fusion (ICF). These applications require also extremely high ion current densities, in some cases surpassing 10^{10} A/cm² [2 – 4]. Such ion current densities are attainable with a target normal sheath acceleration (TNSA) mechanism [1, 5] using relativistic laser intensities and curved targets enabling ballistic focusing of a laser-driven ions [2, 5].

Just recently, we have proposed and demonstrated another method, which makes it possible to produce ion beams of very high current densities in a planar geometry at subrelativistic laser intensities and at a low energy (≤ 1 J) of the laser pulse [6, 7]. This method – referred to as the “skin-layer ponderomotive acceleration” (S-LPA) – uses ponderomotive forces induced at the skin-layer interaction of a short laser pulse with a self-created preplasma layer produced by a laser prepulse in front of solid target. In this paper, we examine the influence of target structure on the current densities and energies of fast protons produced by the S-LPA mechanism at laser intensities $\sim 10^{17}$ W/cm². Results of our measurements are compared to those obtained from the recent short-pulse experiments using the TNSA mechanism at relativistic laser intensities ($\sim 10^{20}$ W/cm²).

In the S-LPA method [6, 7], an essential role plays a thin preplasma layer (of the thickness L_{pre} at last several times smaller than the laser focal spot diameter d_f) produced by the laser prepulse in front of a solid target. The main short laser pulse interacts most intensely with the plasma in the skin layer near the surface of the critical electron density, n_{ec} , and the geometry of the interaction is almost planar ($L_{pre} \ll d_f$). The ponderomotive forces break the plasma near the critical surface and drive two thin plasma blocks towards vacuum and towards the plasma interior, respectively. The block area is approximately equal to the laser focal spot area: $S_{bl} \approx S_f$ and the block thickness $L_{bl} \approx S\lambda$, where $S = (1/|n|) \geq 1$ is the dielectric swelling factor. As the density of the plasma blocks is high even at moderate ion velocities $v_i \sim 10^7$ – 10^8 cm/s, the ion current densities $j_s = ze n_i v_i$ can be very high ($\sim 10^9$ – 10^{10} A/cm² or higher). The time duration of the ion current flowing out of the interaction region (which functions as the ion source) is approximately equal to the laser pulse duration. Due to almost planar acceleration geometry, the angular divergence of the ion beam is small.

For subrelativistic laser intensities: $I \ll I_{rel} \approx 4.1 \times 10^{18}/\lambda^2$ [W/cm², μm], the ion energies, E_i , and the ion current densities, j_s , of the plasma blocks can be estimated from the equations [6]:

$$E_i \approx 0.93 \times 10^{-16} s z I \lambda^2, \text{ [keV, W/cm}^2, \mu\text{m}] \quad (1)$$

$$j_s \approx 74 (s z/A)^{1/2} \lambda^{-1} I^{1/2}, \text{ [A/cm}^2, \mu\text{m, W/cm}^2] \quad (2)$$

where $s = S$ for the forward-accelerated ions or $s = S - 1$ for the backward-accelerated ions, and A is the atomic mass number. The swelling factor S essentially depends on the plasma density gradient and at very steep density gradients $S \approx 1$ [8]. As it can be seen from (1) and (2), at $S = 1$ only forward-

accelerated ion beam is produced and the forward-directed ponderomotive force becomes the usual light pressure. In such a case, for instance, a 1- μm laser pulse of intensity 10^{17} W/cm^2 produces ~ 10 -keV proton beam of the current density $j_s \approx 23 \text{ GA/cm}^2$. The optimum plasma density gradient results in a significant increase of both the proton energies and the proton current densities [8].

To estimate the fast ion current density at the source (in the close vicinity of the target surface) on the basis of measurements (e.g. the time-of-flight measurements) we can use the expression [6, 7]:

$$Q_i \approx \tau_{is} / S_s \quad (3)$$

where: Q_i – the total charge of fast ions measured in the far expansion zone; τ_{is} – the duration of fast ion generation at the source, which is roughly equal to the laser pulse duration, $\tau_{is} \approx \tau_L$ [2, 5]; S_s – the area of the fast ion source. In general, $S_s \geq S_f$ (S_f is the laser focal spot area), and, e.g., for the TNSA method S_s can be even tens times larger than S_f [9, 10]. However, as it was mentioned earlier, at the short-pulse subrelativistic S-LPA and $d_f \gg L_{pre} > \lambda$, the changes of S_s due to the plasma or hot electron's expansion during the acceleration process can be neglected, thus $S_s \approx S_f$

Experimental arrangement

The experiment was performed with the use of 1-ps, 1.05- μm subjoule laser pulse generated by a terawatt CPA Nd:glass laser [10]. To measure forward-emitted ion fluxes the f/1 aspheric lens asfocusing the 1-ps laser beam on a thin target normally to its surface (see Fig.1). The maximum laser intensity approached $2 \times 10^{17} \text{ W/cm}^2$ at 30 – 40% of laser energy concentrated in the focal spot of $d_f \approx 10 \mu\text{m}$. A specific feature of the 1-ps pulse was its temporal shape comprising the long-lasting ($>0.3\text{ns}$) low-intensity background and the short-lasting prepulse (a sequence of a few ps pulses covering the time period $\sim 10^{-10}\text{s}$) of the intensity $\sim 10^4$ times lower than the intensity of the main ps pulse [11]. As the intensity of the long-lasting background was at least 10^8 times lower than that of the main pulse [10, 11], no preplasma was produced on the surface. The short-lasting prepulse produced the preplasma of thickness $L_{pre} \leq 5 \mu\text{m}$ [11, 12]. This preplasma thickness was at least several times smaller than the laser focal spot diameter d_f , thus the condition for the quasi-planar skin-layer interaction of the laser beam with the preplasma was fairly well fulfilled (section 2). Both single-layer and double-layer targets were used in the experiment, in particular: (1) polystyrene targets of the thickness, L_T , of 1 μm (marked as PS1); (2) Al target of $L_T = 0.75\text{-}\mu\text{m}$ (marked as A10.75); (3) double-layer target with a 0.05- μm Au front layer (facing to the laser) and a 1- μm polystyrene back layer (marked as Au0.05/PS1); (4) double-layer target with a 1- μm polystyrene front layer and a 0.05- μm Au back layer (marked as PS1/Au0.05). The thickness of the target was selected in such a way that the condition: $L_T \leq \lambda$, L_h was fulfilled, where $L_h \approx 1 - 2 \mu\text{m}$ is the characteristic path length of the heat wave in the target generated by the leading edge of the laser pulse (including the prepulse), calculated from the classical heat transport formulas [15, 16].

The characteristics of fast ion fluxes emitted forward from thin foil targets were measured using the time-of-flight method. Three ion collectors and an electrostatic ion- energy analyser (IEA), located as shown in Figure 5.1, were used to record ions [11]. In particular the IEA and the ring ion collector (IC1) recorded ions emitted close to the target normal and the laser beam axis. The ion measurements were supplemented with the measurements of hard X rays in the range of 4 – 30 keV performed with the use of Si photodiode with proper filters.

Results and discussion

Figure 5.2 presents typical IC signals from Au0.05/PS1 and PS1/Au0.05 double-layer targets recorded in the direction normal to the target. We can see that for both the targets only a single fast proton group (identified by the IEA), well separated in time from other ion groups, is generated.

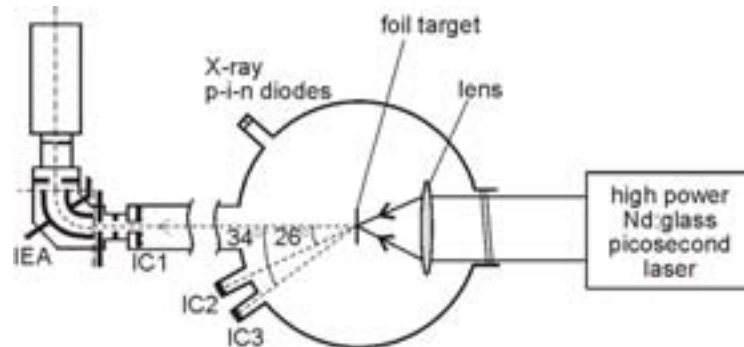


Figure 5.1. Scheme of the experimental arrangement. IEA – electrostatic ion-energy analyzer with windowless electron multiplier; IC1, IC2, and IC3 – ion collectors.

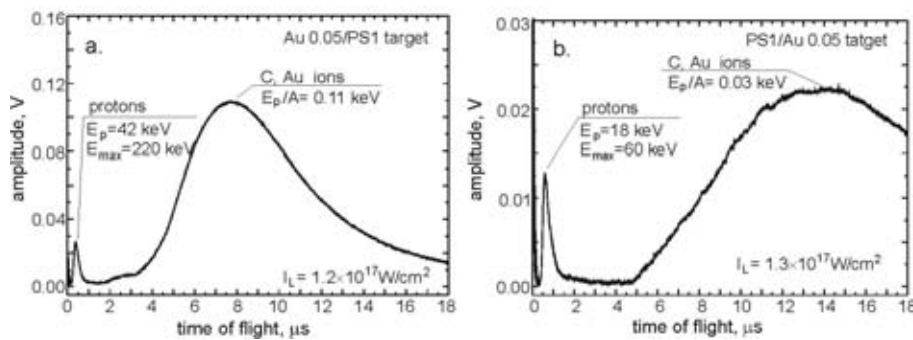


Figure 5.2. The ion collector signals from the double-layer targets irradiated by 1-ps laser pulse, recorded in the direction normal to the target.

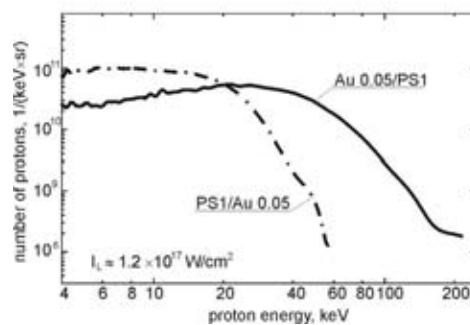


Figure 5.3. The energy distributions of protons emitted from the double-layer targets normally to the target. $I_L \approx 1.2 \times 10^{17} \text{ W/cm}^2$.

The fast proton beam was deduced to be highly collimated as no fast protons were recorded at 26° and 34° angles. A single fast proton group emitted with a small angular divergence was also observed for the other targets used in the experiment, in agreement with a simple physical picture of S-LPA sketched in sec. 5.1.

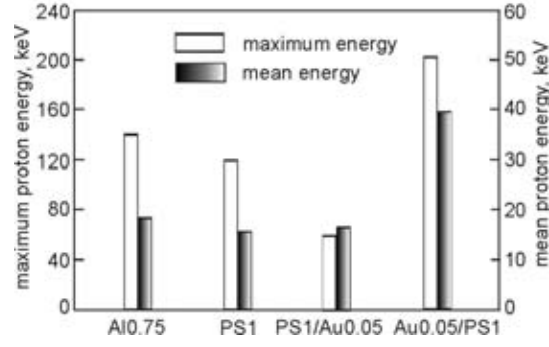


Figure 5.4. The maximum at the source and the mean energies of protons produced from various thin foil targets. $I_L = (1.2 \pm 0.2) \times 10^{17} \text{ W/cm}^2$.

Examples of energy distributions of protons emitted in the normal direction from Au0.05/PS1 and PS1/Au0.05 targets are presented in Fig. 5.3, and the mean and the maximum proton energies (averaged over many laser shots) for all the targets used are shown in the diagram in Figure 5.4. The highest proton energies are achieved for the double-layer target with the Au front layer. Both the mean and the maximum proton energies for this target are about 2 times higher than the ones for the PS1 target and 3 – 4 times higher than those for the PS1/Au0.05 target. The Au0.05/PS1 target also produced the highest hard X ray signal. In particular, this signal was ten times higher than the one from the PS1 target and about 4 times higher than that from the PS1/Au0.05 target.

A plausible explanation of the observed properties can be as follows. In the Au-H-C plasma mixture of the front part of the Au/PS target, the ratio of the density of fast electrons (driven directly by the ponderomotive force) to the density of protons, n_{ef}/n_p , is higher than in the case of the H-C plasma mixture of the PS target. In the case of the PS/Au target, the relatively cold and dense Au layer on the rear side of the target does not contribute to the fast electron balance in front of the target, but it rather acts as a damper for the protons propagating through the target. As a result, the proton energies from the PS1/Au0.05 target are significantly lower than the ones from the Au0.05/PS1 target and even lower than those from PS1 target. On the other hand, the high-Z back layer is a reason for a higher efficiency of hard X ray emission in relation to the low-Z PS target.

To estimate the fast proton current density at the source, j_s , we used the equation (3) and assumed: $\tau_{is} = \tau_L$, $S_s = S_f$ and $Q_i = Q_{IC1}$, where Q_{IC1} is the fast ion charge passing through the IC1 collector (Fig. 5.1) seen within the angle of 3° from the ion source. As $Q_{IC1} < Q_i$ (the ion beam divergence is expected to be higher than 3°), the calculated proton current densities actually represent the lower limit of their real values. The current densities of protons emitted within the 3° angle cone from the particular targets as well as the proton current densities recalculated to 1 steradian are shown in Table 1. The highest proton current densities ($> 1 \text{ GA/cm}^2$ within the 3° angle) are produced from the Au/PS target though the difference in relation to the case of the PS target is not so significant here as the difference between energies of protons for these targets. For comparison, the table also contains the proton current densities achieved in the experiments with short-pulse high-energy lasers (VULCAN in England and PETAWATT in USA), where the TNSA mechanism at relativistic laser intensities was expected to produce the fast proton beam [9, 10]. To calculate these current densities we used eq. (3) and the data related to the total charge of fast protons, the area of the proton source and the laser pulse duration (we assumed $\tau_{is} = \tau_L$) available from [9, 10]. It can

be seen that: (a) the proton current densities at the source produced within 3° angle by subrelativistic S-LPA are comparable to those generated within greater angles by TNSA at

Table 1. Parameters of ion beams produced in various experiments. (a) The current densities of protons emitted within 3° angle cone. $I_L = (1.2 \pm 0.2) \times 10^{17} \text{W/cm}^2$. (b) The current density of protons emitted within 20° angle cone – Ref. 10. (c) The current density of protons emitted within 40° angle cone – Ref. 9.

method	laser	target	proton current density at the source, GA/cm ²	proton current density at the source per steradian, GA/cm ² sr	mean proton energy, keV
S-LPA	0.5J/1ps 10^{17}W/cm^2	Al 0.75	0.3 (a)	100	18
		PS1	1 (a)	350	16
		PS1/Au0.05	0.9 (a)	320	17
		Au0.05/PS1	1.3 (a)	460	40
TNSA	50J/1ps $8 \times 10^{19} \text{W/cm}^2$ VULCAN	Al 100 μm	1.6 (b)	12	4×10^3
	500J/0.5ps $3 \times 10^{20} \text{W/cm}^2$ PETAWATT	CH 100 μm	8 (c)	16	6×10^3

relativistic laser intensities; (b) the proton current densities at the source, recalculated to 1 steradian, are significantly higher for S-LPA than for TNSA (it confirms, in particular, that the ion beams produced by S-LPA are highly collimated). This fairly surprising result can be understood, if we realize that in the S-LPA method a compact high-density ($n_i \approx n_{ec}/z$) plasma block is generated as opposed to the TNSA method, where a lower-density ($n_i \ll n_{ec}/z$) more extended plasma layer is accelerated.

One drawback of subrelativistic S-LPA is a relatively low energy of generated ions, limited to $\sim 1 \text{MeV/nucleon}$. This drawback could be overcome by an extension of the advantages of subrelativistic S-LPA – whose most important symptom is a quasi-planar acceleration of the high-density plasma block, to the relativistic intensity region. It seems to be feasible if the laser pulse and the target thickness is carefully optimised [19 – 21]. The relativistic regime of S-LPA has been demonstrated just recently with the use of 3D PIC simulations [20] (the authors called this regime the “laser piston”). The interaction of a 25-fs laser pulse of intensity 10^{23}W/cm^2 with a 1- μm solid-density plasma slab resulted in a quasi-planar generation of relativistic ($E_i \approx 3 \text{GeV}$) high-density ($n_i \approx 3n_{ec}$) proton block with the estimated proton current density $\approx 10^{13} \text{A/cm}^2$. Although such extreme ion block parameters are still a matter of the future, the production of high-density ion blocks with multi-MeV ion energies using relativistic S-LPA is fully realistic with the current laser technology.

Conclusions

The very high ion current density and ps duration of the fast ion pulse produced by S-LPA opens a prospect for new experiments in high energy-density physics and nuclear fusion. In particular, a block of DT plasma accelerated by a ps laser pulse towards the DT plasma interior seems to be ideal for generation of a laser fusion ignition front. The plasma block acts like a (space charge neutral) DT ion beam for which the ignition condition in solid density

(frozen) DT fuel of $>10^{10}$ A/cm² current density [22] for optimum ion energy (80 keV) can be easily achieved by ps laser pulses of $I < I_{\text{rel}}$. For example, a ps laser pulse of $I \sim 0.3 I_{\text{rel}}$ can produce an ~ 80 -keV DT ion flux with a current density of $j_s \sim 5.5 \times 10^{10}$ A/cm² at $\lambda = 1.05 \mu\text{m}$ or $j_s \sim 5 \times 10^{11}$ A/cm² at $\lambda = 0.35 \mu\text{m}$. We see that such extremely high ion current densities are attainable even at low energies (≤ 1 J) and subrelativistic laser pulse intensities, which can be easily generated at high repetition rate. In particular, it is possible to accomplish highly efficient DD or DT fusion in small-scale devices for, e.g., fast neutron production. Achievement of high fusion gain through use of an optimized DT ion beam from the ps skin layer interaction in large-scale experiments can also be imagined, but it needs to be confirmed by further detailed studies.

REFERENCES

- [5.1] HATCHETT, S.P., BROWN, C.G., COWAN T.E., et al., Phys. Plasmas **7**, 2076 (2000).
- [5.2] PATEL, P.K., MACKINNON, A.J., KEY, M.H., et al., Phys. Rev. Lett. **91**, 125004 (2003).
- [5.3] ROTH, M., COWAN, T.E., KEY, M.H., et al., Phys. Rev. Lett. **86**, 436 (2001).
- [5.4] MILEY, G.H., OSMAN, F., HORA, H., et al., Proc. SPIE 5449 (2004) paper 138.
- [5.5] WILKS, S.C., LANGDON, A.B., COWANT, E., et al., Phys. Plasmas **8**, 542 (2001).
- [5.6] BADZIAK, J., GŁOWACZ, S., JABŁOŃSKI, S., et al., Appl. Phys. Lett. **85** (October 2004).
- [5.7] BADZIAK, J., GŁOWACZ, S., JABŁOŃSKI, S., et al., Plasma Phys. Control. Fusion, in print.
- [5.8] GŁOWACZ, S., BADZIAK, J., JABŁOŃSKI, S., HORA, H., Czech. J. Phys. **54**, C460 (2004).
- [5.9] SNAVELY, R.A., KEY, M.H., HATCHETT, S.P., et al., Phys. Rev. Lett. **85**, 2945 (2000).
- [5.10] BORGHESI, M., MACKINNON, A.J., CAMPBELL, D.H., et al., Phys. Rev. Lett. **92**, 055003 (2004).
- [5.11] BADZIAK, J., CHIZHOV, S.A., KOZLOV, A.A., et al., Opt. Commun. **134**, 495 (1997).
- [5.12] BADZIAK, J., MAKOWSKI, J., PARYS, P., et al., J. Phys. D: Appl. Phys. **34**, 1885 (2001).
- [5.13] BADZIAK, J., HORA, H., WORYNA, E., et al., Phys. Lett. A **315**, 452 (2003).
- [5.14] CLARK, E.L., KRUSHELNICK, K., DAVIES, J.R., et al., Phys. Rev. Lett. **84**, 670 (2000).
- [5.15] ZEPF, M., CLARK, E.L., BEG, F.N., et al., Phys. Rev. Lett. **90**, 064801 (2003).
- [5.16] CARUSO, A., GRATTON, A., J. Plasma Phys. **11**, 839, (1969).
- [5.17] ROSEN, M.D., Proc. SPIE 1229, 160, (1991).
- [5.18] MACKINNON, A.J., BORGHESI, M., HATCHETT, S.P., et al., Phys. Rev. Lett. **86**, 1769 (2001).
- [5.19] MORA, P., Phys. Rev. Lett. **90**, 185002 (2003).
- [5.20] KALUZA, M., SCHREIBER, J., SANTALA, M.I.K., et al., Phys. Rev. Lett. **93**, 045003 (2004).
- [5.21] ESIRKEPOV, T., BORGHESI, M., BULANOV, S.V., et al., Phys. Rev. Lett. **92**, 175003 (2004).
- [5.22] SENTOKU, Y., COWAN, T.E., KEMP, A., et al. Phys. Plasmas **10**, 2009 (2003).
- [5.23] HORA, H., Atomkernenenergie-Kernntechnik **42**, 7 (1983).

Summary

- Using the high-intensity long-wavelength as well as short-wavelength PALS laser pulses (1315 nm and 438 nm, respectively), the production of highly charged, high-energy ions have been demonstrated, using IC, IEA, and solid-state track detector measurements. For Ta ions $z_{\text{max}} = 57$ and $E_i > 20$ MeV.
- The ion collector signals recorded at higher laser pulse energies clearly show the existence of three separate ion groups: fast, thermal and slow. At high laser pulse energies, $E_L > 200$ J, fast ion current density attains $j_{\text{max}} \sim 20$ mA/cm² at the distance of 1 m from the target.

- Described here studies demonstrated the existence of a group of fast highly-charged ions produced not only by the intense infrared laser beams but also by intense laser radiation of shorter wavelength (visible light) focused on high-Z targets. In this case other phenomena only weakly dependent on the laser wavelength e.g. ponderomotive forces and self-focusing of laser radiation may contribute to the acceleration of ions in the plasma.
- The parameters of both x ray and ion emissions change clearly depending on the lens-target separation (it means on a laser power density) and these changes are well correlated with each other.
- A small prepulse creating pre-plasma before the arrival the main pulse changes considerably the condition of laser-matter interaction, particularly, the efficiency of the fast ion acceleration. The results of performed investigations show that the characteristics of laser-generated ions and x rays are very similar for both the prepulse energies used $E_{p-L} \sim 10$ J and ~ 1 J (7% or 0.7% of the main-pulse energy, respectively).
- The maximum and mean energy of the fast ions as well as the yields of both the hard and the soft x rays attain highest values for the optimum delay times (in a range of ~ 0 -1.2 ns in our case).
- We have found that in the short-pulse case principally only a single group of fast ions with small angular divergence is generated in the direction normal to the target surface. Non-linear (ponderomotive) force from skin-layer interaction is the most probable mechanism of the ion acceleration in this case. Contrary to this, in the long-pulse case at least two groups of fast ions are generated from plasma and they are emitted in a relatively large solid angle. Ponderomotive and relativistic self-focusing seems to be responsible for the observed properties of the fast ion emission from long-pulse-produced plasma.
- We have shown that the S-LPA mechanism in the system with a double-layer target containing high-Z front layer and low-Z hydrogen-rich back layer produces a proton beam of higher proton energies and proton current densities than in the case of using a single-layer target. Independent of kind of the target, the beam is highly collimated and it consists only of a single fast proton group. In spite of low energy and subrelativistic intensity of the laser pulse, the proton current densities at the source produced by the S-LPA mechanism attain extremely high values (> 1 GA/cm²), which are comparable to those achieved with the TNSA mechanism at significantly higher energies and relativistic intensities of a laser pulse.
- It opens the prospect for tabletop experiments in high energy-density physics and nuclear fusion. In particular, it makes possible to accomplish highly efficient DD or DT fusion in small-scale devices for fast neutron production and other applications.
- The results of the experiments performed within the IAEA project No 11535 demonstrate the importance of nonthermal processes in Hohlraum-like plasmas even at relatively short-wavelength (438 nm) of laser radiation, the correlation of fast ion acceleration in such plasmas with a hard x ray emission and possible improvement of the fast ignition concept of the ICF based on a thermonuclear ignition with the use of energetic laser-generated proton (deuteron) beams.

PUBLICATIONS AND CONFERENCE PRESENTATIONS REPORTING WORKS DONE UNDER RESEARCH PROJECT No. 11535/RO

1. J. Wołowski, J. Badziak, P. Parys, E. Woryna, Investigation of the high-Z laser-produced plasma with the use of ion diagnostics for optimization of the laser interaction with the Hohlraum-type targets (preliminary studies), *report presented at the First RCM Meeting of the participants of CRP F1.30.08, Elements of Power Plant Design for IFE, 21 - 25 May 2001, IAEA Headquarters, Vienna, Austria* (included to the Final Report of this meeting).
2. J. Wołowski, J. Badziak, J. Krása, L. Láska, P. Parys, K. Rohlena and E. Woryna, Investigations of ion emission from plasma produced by high-power 1-ps laser pulse (short version of the manuscript), *Proc. of the 25th International Conference on Phenomena in Ionized Gases, July 17-22, 2001, Nagoya, Japan, ed. T. Goto, Vol. 1, pp. 11–12 (Invited lecture)*.
3. E. Woryna, J. Badziak, J. Makowski, P. Parys, A. B. Vankov, J. Wołowski, J. Krása, L. Láska, K. Rohlena, Influence of the laser focus position on characteristics of Au plasmas generated by sub-nanosecond and picosecond laser pulses, *Proc. of the PLASMA'2001 Conf., 19–21 Sept. 2001, Warsaw, Poland, <http://plasma2001.ifpilm.waw.pl>, paper No P4.13 (4 pages)*.
4. E. Woryna, J. Badziak, J. Makowski, P. Parys, A.B. Vankov, J. Wołowski, J. Krása, L. Láska, K. Rohlena, Dependence of parameters of laser-produced Au plasmas on the incident laser energy of sub-nanosecond and picosecond laser pulses, *Proc. of the PLASMA'2001 Conf., 19-21 Sept. 2001, Warsaw, Poland, <http://plasma2001.ifpilm.waw.pl>, paper No P4.14 (4 pages)*.
5. J. Wołowski, J. Badziak, F. P. Boody, H. Hora, V. Hnatowicz, K. Jungwirth, J. Krása, L. Láska, P. Parys, V. Perina, M. Pfeifer, K. Rohlena, L. Ryc, J. Ullschmied, and E. Woryna. Fast ion emission from the plasma produced by the PALS laser system. *Plasma Phys. Control. Fusion* **44** (2002) 1277–1283.
6. J. Badziak, E. Woryna, P. Parys, J. Wołowski, K. Yu. Platonov, and A. B. Vankov. Effect of foil target thickness on fast proton generation driven by ultrashort-pulse laser. *J. Appl. Phys.* **91** (8) (2002) 5504–5506.
7. J. Wołowski, J. Badziak, J. Krása, L. Láska, P. Parys, K. Rohlena, and E. Woryna. Investigations of ion emission from plasma produced by a high-power 1 ps laser pulse. *Plasma Sources Sci. Technol.* **11** (2002) A173–A177.
8. H. Hora, J. Badziak, F. P. Boody, R. Höpfl, K. Jungwirth, B. Králiková, J. Krása, L. Láska, P. Parys, V. Perina, M. Pfeifer, K. Rohlena, J. Skála, J. Ullschmied, J. Wołowski, and E. Woryna. Effects of ps and ns laser pulses for giant ion source. *Optics Comm.* **207** (2002) 333–338.
9. H. Hora, J. Badziak, G. Banstetter, F.P. Boody, R. Höpfl, K. Jungwirth, J.C. Kelly, B. Králiková, J. Krása, L. Láska, P. Parys, V. Peřina, M. Pfeifer, K. Rohlena, J. Skála, J. Ullschmied, J. Wołowski, E. Woryna, M. Ghoranneviss, A.H. Sari, M.R. Hantehzadeh, Plasma techniques with giant laser ion sources causing surface crystal modification in solid targets, *IAEA-ICTP Workshop on Plasma Diagnostics and Industrial Appl. of Plasmas, Trieste/ Italy, March (2002) 11–13*.
10. H. Hora, J. Badziak, F. P. Boody, R. Höpfl, K. Jungwirth, B. Králiková, J. Krása, L. Láska, P. Parys, V. Perina, M. Pfeifer, K. Rohlena, J. Skála, J. Ullschmied, J. Wołowski, and E. Woryna. Giant emission of laser driven ion source and picosecond interaction. In K. A. Tanaka, D. D. Meyerhofer, and J. Meyer ter Vehn, editors, *Inertial Fusion Sciences and Applications'2001*, The Data Science Library, pages 396-399, Paris, 2002. Elsevier.
11. L. Láska, K. Jungwirth, B. Králiková, J. Krása, M. Pfeifer, K. Rohlena, J. Skála, J. Ullschmied, J. Badziak, P. Parys, J. Wołowski, E. Woryna, S. Gammino, L. Torrissi, and

- F. P. Boody. Generation of Ta ions at high laser-power densities. *Czech. J. Phys.*, **52** (Suppl. D) (2002) 283–291.
12. A. Szydłowski, J. Badziak, P. Parys, J. Wołowski, E. Woryna, K. Jungwirth, B. Králiková, M. Pfeifer, J. Krása, L. Láska, K. Rohlena, J. Skála, J. Ullschmied, F. P. Boody, S. Gammino, and L. Torrissi. Solid state track detectors applied in measurements of ion streams produced by the high energy laser pulses. *Czech. J. Phys.* **52** (Suppl. D) (2002) 299–304.
 13. T. Pisarczyk, J. Badziak, A. Kasperczuk, P. Parys, J. Wołowski, E. Woryna, K. Jungwirth, B. Králiková, J. Krása, L. Láska, K. Masek, M. Pfeifer, K. Rohlena, J. Skála, J. Ullschmied, M. Kálal, and P. Pisarczyk. Fast and slow plasma components produced by the PALS facility - comparison of interferometric and ion diagnostic measurements. *Czech. J. Phys.* **52** (Suppl. D) (2002) 310–317.
 14. J. Badziak, S. Jabłoński, P. Parys, L. Ryc, J. Wołowski, E. Woryna, J. Krása, L. Láska, M. Pfeifer, and K. Rohlena. High-intensity interactions of 1-ps and 0.5 ns laser pulses with a high-Z target - a comparison. *Czech. J. Phys.* **52** (Suppl. D) (2002) 318–323.
 15. L. Torrissi, S. Gammino, L. Andó, A. M. Mezzasalma, L. Torrissi, J. Badziak, P. Parys, J. Wołowski, E. Woryna, K. Jungwirth, B. Králiková, J. Krása, L. Láska, M. Pfeifer, K. Rohlena, J. Skála, J. Ullschmied, and F. P. Boody. Study of the etching process and crater formation induced by intense laser pulses at PALS. *Czech. J. Phys.* **52** (Suppl. D) (2002) 329–334.
 16. H. Hora, F. Osman, R. Höpfl, J. Badziak, P. Parys, J. Wołowski, E. Woryna, F. Boody, K. Jungwirth, B. Králiková, J. Krása, L. Láska, M. Pfeifer, K. Rohlena, J. Skála, and J. Ullschmied. Skin depth theory explaining anomalous picosecond-terawatt laser plasma interaction. *Czech. J. Phys.* **52** (Suppl. D) (2002) 349–361.
 17. J. Krása, K. Jungwirth, B. Králiková, L. Láska, M. Pfeifer, K. Rohlena, J. Skála, J. Ullschmied, V. Hnatowicz, V. Peřina, P. Parys, J. Wołowski, E. Woryna, A. Szydłowski. Highly charged ions generated with intense laser beams, 11th Int. Conf. on Phys. of Highly Charged Ions, Caen (France), (2002) C4-3-5, p.190.
 18. J. Badziak, P. Parys, J. Wołowski, and E. Woryna. Investigation of ion emission from picosecond and nanosecond laser-produced plasmas by the time-of-flight method. *German-Polish Conference on Plasma Diagnostics for Fusion and Applications*, Greifswald, Germany, September 2002, CD-ROM: Paper 09
 19. J. Badziak, S. Jabłoński, P. Parys, J. Wołowski, and E. Woryna. Comparison of angular distributions of ion emission from picosecond and subnanosecond laser-produced plasmas. *German-Polish Conference on Plasma Diagnostics for Fusion and Applications*, Greifswald, Germany, September 2002.
 20. J. Wołowski, J. Badziak, F.P. Boody, S. Gammino, H. Hora, K. Jungwirth, J. Krása, L. Láska, P. Parys, M. Pfeifer, K. Rohlena, L. Torrissi, J. Ullschmied, and E. Woryna. Diagnostic of ions emitted from plasma produced by the PALS 3rd-harmonics beam (438 nm). *German-Polish Conference on Plasma Diagnostics for Fusion and Applications*, Greifswald, Germany, September 2002, CD-ROM: Paper B-02
 21. L. Ryc, J. Badziak, L. Juha, J. Krása, B. Králiková, P. Parys, M. Pfeifer, K. Rohlena, J. Skála, J. Ullschmied, and J. Wołowski. The use of semiconductor detectors for x ray detection in PALS plasma experiments. *German-Polish Conference on Plasma Diagnostics for Fusion and Applications*, Greifswald, Germany, September 2002, CD-ROM: Paper B-01.
 22. K. Rohlena, K. Jungwirth, J. Krása, E. Krausky, L. Láska, K. Masek, M. Pfeifer, J. Wołowski, J. Badziak, P. Parys, T. Pisarczyk, L. Ryc, E. Woryna, and J. Ullschmied. Diagnostics of PALS experiments. *German-Polish Conference on Plasma Diagnostics for Fusion and Applications*, Greifswald, Germany, Sept. 2002, CD-ROM: Paper 05.

23. J. Wołowski, J. Badziak, F.P. Boody, S. Gammino, H. Hora, K. Jungwirth, B. Králiková, J. Krása, L. Láska, P. Parys, M. Pfeifer, K. Rohlena, J. Skála, L. Torrissi, J. Ullschmied, and E. Woryna. Production of fast ions by the 3 μ m PALS laser beam. Proc. of the *XXVII European Conference on Laser Interaction with Matter (ECLIM 2002)*, Moscow, Russia, October 2002.
24. J. Badziak, H. Hora, S. Jabłoński, L. Láska, P. Parys, K. Rohlena, J. Wołowski, and E. Woryna. Comparison of properties of fast ion emission from plasmas produced by picosecond and subnanosecond laser pulses. Proc. of the *XXVII European Conference on Laser Interaction with Matter (ECLIM 2002)*, Moscow, Russia, Oct. 2002.
25. H. Hora, J. Badziak, F. Boody, R. Hopfl, K. Jungwirth, B. Králiková, J. Krása, L. Láska, M. Pfeifer, K. Rohlena, P. Parys, S. Skála, J. Ullschmied, J. Wołowski, and E. Woryna. Skin depth theory explaining anomalous picosecond-terawatt laser plasma interaction. *XXVII European Conference on Laser Interaction with Matter (ECLIM 2002)*, Moscow, Russia, October 2002.
26. H. Hora, J. Badziak, F. Boody, R. Hopfl, K. Jungwirth, B. Králiková, J. Krása, L. Láska, M. Pfeifer, K. Rohlena, P. Parys, S. Skála, J. Ullschmied, J. Wołowski, and E. Woryna. Skin depth theory explaining anomalous picosecond-terawatt laser plasma interaction. *Czech. J. Phys.* **52** (Suppl.D):349–361, 2002.
27. Z. Składanowski, J. Badziak and J. Wołowski. Review of studies of ion streams produced by high-intensity subnanosecond laser pulses. Proc. of the *XXVII European Conference on Laser Interaction with Matter (ECLIM 2002)*, Moscow, Russia, October 2002. Invited paper.
28. L. Láska, J. Badziak, F.P. Boody, S. Gammino, H. Hora, K. Jungwirth, J. Krása, P. Parys, M. Pfeifer, K. Rohlena, L. Torrissi, J. Ullschmied, J. Wołowski, E. Woryna, Multiply charged ions produced at laser power densities from 10¹⁰ W/cm² to 10¹⁷W/cm². Proc. of the 11th International Congress on Plasma Physics, Sydney, July 15–19, 2002. Invited review talk.
29. H. Hora, J. Badziak, F.P. Boody, R. Höpfl, K. Jungwirth, B. Králiková, J. Krása, L. Láska, P. Parys, V. Peřina, M. Pfeifer, K. Rohlena, J. Skála, J. Ullschmied, J. Wołowski, E. Woryna, Laser giant ion source and the prepulse effect at picosecond interaction for high gain Laser fusion, Proc. of the 11th International Congress on Plasma Physics, Sydney, July 15–19, P 46, p.85, 2002.
30. L. Láska, J. Badziak, F.P. Boody, S. Gammino, H. Hora, K. Jungwirth, J. Krása, P. Parys, M. Pfeifer, K. Rohlena, L. Torrissi, J. Ullschmied, J. Wołowski, E. Woryna, Generation of multiply charged ions at low and high laser-power densities, *Czechoslovak J. Phys.*, **52**(Suppl. D):283–291, 2002.
31. J. Wołowski, J. Badziak, F. P Boody, S. Gammino, H. Hora, K. Jungwirth, J. Krása, L. Láska, A.M. Mezzasalma, P. Parys, M. Pfeifer, K. Rohlena, A. Szydłowski, L. Torrissi, J. Ullschmied, E. Woryna, Comparison of Characteristics of Ions Emitted from Plasmas Produced by the PALS Laser System at 1315 nm and 438 nm Wavelengths, 30th EPS Conference On Controlled Fusion and Plasma Physics, St. Petersburg, Russia, July 7–11, 2003 (SPIE Conf. Proc. Vol.27A, P-4.146).
32. J. Badziak, S. Jabłoński, P. Parys, Z. Składanowski, J. Wołowski, H. Hora, L. Láska, K. Rohlena, Production of intense fast ion fluxes by skin-layer picosecond laser-plasma interaction, Third International Conference on Inertial Fusion Sciences and Applications, Monterey, USA, September 7–12, 2003.
33. H. Hora, F. Osman, J. Badziak, F.P. Boody, Yu. Cang, S. Gammino, Xian-Tu He, R. Höpfl, K. Jungwirth, B. Králiková, J. Krása, L. Láska, Hong Liu, G.H. Miley, P. Parys, Han-Sheng Peng, M. Pfeifer, K. Rohlena, J. Skála, Z. Składanowski, L. Torrissi, L. Ullschmied, J. Wołowski, Jie Zhang, Weiyang Zhang, Petawatt-picosecond laser pulse generation of nonlinear force driven blocks from skin layer interaction for fast ignitor,

Third International Conference on Inertial Fusion Sciences and Applications, Monterey, USA, September 7–12, 2003.

34. J. Badziak, H. Hora, E. Woryna, S. Jabłoński, L. Láska, P. Parys, K. Rohlena, and J. Wołowski, Experimental evidence of differences in properties of fast ion fluxes from short-pulse and long-pulse laser-plasma interactions, *Phys. Lett. A* **315** (2003) 452–457.
35. J. Wołowski, J. Badziak, F.P. Boody, S. Gammino, H. Hora, K. Jungwirth, J. Krása, L. Láska, P. Parys, M. Pfeifer, K. Rohlena, A. Szydłowski, L. Torrissi, J. Ullschmied and E. Woryna, Characteristics of ion emission from plasma produced by high-energy short-wavelength (438 nm) laser radiation, *Plasma Phys. Control. Fusion* **45** (2003) 1087–1093.
36. H. Hora, J. Badziak, F. P. Boody, R. Höpfl, K. Jungwirth, B. Králiková, J. Krása, L. Láska, P. Parys, V. Perina, M. Pfeifer, K. Rohlena, J. Skála, J. Ullschmied, J. Wołowski, and E. Woryna, Laser giant ion source and the prepulse effects for picosecond interaction for high gain laser fusion, In I. S. Falconer, R. L. Dewar, and J. Khachan, editors, *Proceedings of the 11th International Congress on Plasma Physics: ICPP'2002*, volume 669, pages 739–743, Sydney, Australia, July 2003, American Institute of Physics.
37. J. Badziak, S. Jabłoński, P. Parys, and J. Wołowski. Anomalous properties of plasma produced by the interaction of picosecond laser pulses with a high-Z target. *Czechoslovak J. Phys.*, 54(Suppl. C):C444–C451, 2004.
38. J. Badziak, P. Parys, J. Wołowski, and E. Woryna. Studies of ion fluxes emitted from picosecond and nanosecond laser-produced plasmas. *J. Tech. Phys.*, 45(1):3-20, 2004.
39. H. Hora, Cang Yu, Zhang Jie, F. Osman, J. Badziak, F. P. Boody, S. Gammino, R. Höpfl, K. Jungwirth, B. Králiková, J. Kraska, L. Láska, Liu Hong, G. H. Miley, P. Parys, Peng Hansheng, M. Pfeifer, K. Rohlena, J. Skála, Z. Składanowski, L. Torrissi, J. Ullschmied, J. Wołowski, and Zhang Weiyan. Generation of nonlinear force driven blocks from skin layer interaction of petawatt-picosecond laser pulses for ICF. *Plasma Science and Technology*, 6(1):2172–2178, February 2004.
40. L. Láska, K. Jungwirth, B. Králiková, J. Krása, E. Krouský, K. Masek, M. Pfeifer, K. Rohlena, J. Skála, J. Ullschmied, J. Badziak, P. Parys, L. Ryć, A. Szydłowski, J. Wołowski, E. Woryna, G. Ciavola, S. Gammino, L. Torrissi, and F. P. Boody. Review of laser ion sources developments in Prague and production of over 50+ ions at Prague Asterix Laser System (invited). *Rev. Sci. Instr.*, 75(5):1546–1550, 2004.
41. L. Láska, K. Jungwirth, B. Králiková, J. Krása, M. Pfeifer, K. Rohlena, J. Skála, J. Ullschmied, J. Badziak, P. Parys, J. Wołowski, E. Woryna, L. Torrissi, S. Gammino, and F. P. Boody. Charge-energy distribution of Ta ions from plasmas produced by 1 ω and 3 ω frequencies iodine laser. *Rev. Sci. Instr.*, 75(5):1588–1591, 2004.
42. L. Láska, K. Jungwirth, J. Krása, M. Pfeifer, K. Rohlena, J. Ullschmied, J. Badziak, P. Parys, J. Wołowski, F. P. Boody, S. Gammino, and L. Torrissi. Generation of extreme high laser intensities in plasma. *Czechoslovak J. Phys.*, 54(Suppl. C):C370–C377, 2004.
43. G. H. Miley, F. Osman, H. Hora, J. Badziak, K. Rohlena, K. Jungwirth, J. Wołowski, Y. Cang, X. He, J. Zhang, and P. Hammerling. Plasma block acceleration by ps-TW laser irradiation. In Claude R. Phipps, editor, *Proceedings of the SPIE High Power Laser Ablation*, pages 1–13, April 2004. Paper 138.
44. L. Torrissi, S. Gammino, A. M. Mezzasalma, A. M. Visco, J. Badziak, P. Parys, J. Wołowski, E. Woryna, J. Krása, L. Láska, M. Pfeifer, K. Rohlena, and F. P. Boody. Laser ablation of UHMWPE-polyethylene by 438 nm high energy pulsed laser. *Applied Surface Science*, 227:164–174, 2004.
45. J. Wołowski, J. Badziak, P. Parys, M. Rosiński, L. Ryć, K. Jungwirth, J. Krása, L. Láska, M. Pfeifer, K. Rohlena, J. Ullschmied, A. Mezzasalma, L. Torrissi, S. Gammino, H. Hora, and F. P. Boody. The influence of pre-pulse plasma on ion and x ray emission from Ta plasma produced by a high-energy laser pulse. *Czechoslovak J. Phys.*, 54 (Suppl. C):C385–C390, 2004.

Fast electrons for the fast ignitor scheme of inertial confinement fusion

I.B. Földes¹, J. Bohus², K. Gál¹, B. Hopp³, G. Kocsis¹, N.R. Kresz³, E. Rácz¹,
T. Suta⁴, T. Smausz³, S. Szatmári², Zs. Tóth³, G. Veres¹

¹ Dept. of Plasma Physics, Association EURATOM, KFKI-Research Inst. of Particle and Nuclear Physics of the Hungarian Academy of Sciences, Budapest, Hungary

² Dept. of Experimental Physics, University of Szeged, Szeged, Hungary

³ Dept. of Optics and Quantum Electronics, University of Szeged, Szeged, Hungary

⁴ Dept. of Experimental Physics, University of Debrecen Debrecen, Hungary

Abstract. This paper summarizes the work carried out within the frames of the Research Project No 11633/RBF (Hungary) as a part of the IAEA Coordinated Research Project F1.39.08 on “Elements of Power Plant Design for Inertial Fusion Energy”. Experiments were carried out with the ultrashort pulse KrF laser of the HILL laboratory to investigate nonlinear phenomena as high-harmonics generation. Also preliminary results are presented concerning isochoric heating, another phenomenon relevant in the physics of fast ignitors. The group also participated in the high-intensity experiments of the MPQ which aimed to generate fast electrons and protons for fusion applications, thus giving hints for the birth and propagation of the electron beam. As a byproduct in a laser laboratory, material damage studies for UV radiation concerning prospective chamber-wall materials were initiated, too.

1. INTRODUCTION

Short pulsed lasers opened new possibilities in controlled inertial confinement thermonuclear fusion researches. According to the scheme of fast ignitor it is not necessary to compress the fusion target as strong as necessary for the traditional hot spark ignition, but after a certain compression ignition is started by a fast, MeV electron beam. After the implosion of the capsule to high density a hole is bored by the high-intensity ultrashort laser pulse through the capsule corona composed of the ablated material, then the fuel is ignited by suprathermal electrons produced in the high-intensity laser plasma interactions propagating from the critical density to the high-density core. This scheme may reduce both the necessary driver energy and the symmetry requirements concerning the target itself and the target illumination. Although inertial confinement experiments, including laser fusion researches still need large facilities in the leading laboratories, fast ignitor physics opens a possibility even for small groups to participate directly by investigating physical phenomena concerning electron acceleration and transport. The reason is, that recently table-top laser facilities became capable to deliver TW intensities in short pulses. The obtainable high focused intensity allows for these modest systems to study new physical phenomena in this field.

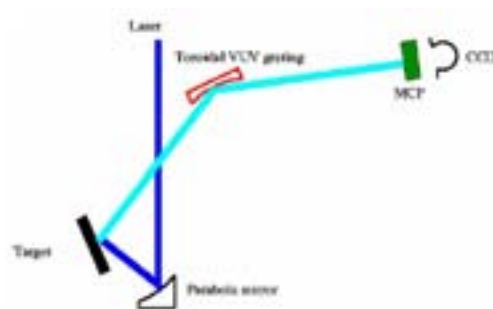


Figure 1. Experimental arrangement for high intensities.

The KrF laser system of the HILL laboratory in Szeged - where the joint researches of the Department of Plasma Physics of the KFKI Research Institute for Particle and Nuclear Physics and the Department of Experimental Physics of the Szeged University are carried out - serves as a basis for the experimental work in Hungary. The laser system delivers presently 15 mJ energy of 600 fs duration on the 248 nm wavelength. Lasers of short wavelengths are generally appropriate high X ray conversion and they generate less nonlinear phenomena than lasers of long wavelengths. The latter is why 0.25 μm lasers might be appropriate candidates for fast ignitor: longer wavelength lasers of intensities sufficient for hole boring may generate electrons with energies as high as 10 MeV, too hot for efficient ignition. Besides fast electron studies and investigations of nonlinear phenomena KrF lasers allow us to investigate UV resistance of possible chamber wall materials, thus damage threshold for 248 nm radiation of different materials can be investigated.

We can divide the activity of our group into two parts. The main emphasize was the upgrading of our laser system, and experiments in the HILL laboratory with the existing facility. Besides using our own facilities we are active in international collaboration with participating in experiments on large facilities in order to be able to investigate fast ignitor relative physics in a broader parameter range. Our group participated in the experiments with the ATLAS Ti-sapphire laser of the MPQ, Garching, the aim of which is to investigate generation of MeV electron in preformed plasmas, and their transport through the overdense plasma. Herewith we describe the following works performed within the present CRP from 2001 to 2004:

- Upgrading the KrF laser system in the University of Szeged and increasing the focused intensity up to $5 \cdot 10^{17} \text{ W/cm}^2$,
- laser plasma experiments on high harmonics generation as an interesting nonlinear phenomenon give insight to the intrinsic nature of surface rippling, thus being relevant even for the physics of fast ignition,
- preparation for spectroscopic studies of isochoric heating,
- damage threshold studies for possible wall materials,
- participation in the high intensity experiments in the MPQ, Garching on self-focusing and fast electron generation in a preformed plasma and on
- fast electron propagation in high-density matter.

2. LASER PLASMA EXPERIMENTS IN THE HILL LABORATORY

Upgrading laser plasma experiments

The KrF laser system [1] delivers a laser pulse of 600 fs duration with a maximum energy of 15 mJ on the wavelength of 248 nm. In our early experiments it was focused by a simple f/10 lens on the target which was aligned to 45° of incidence. The maximum intensity obtained this way was $5 \cdot 10^{15} \text{ W/cm}^2$. On the other hand the short wavelength, nearly diffraction limited beam and the short wavelength of the laser allows a very tight focusing, thus intensities up to 10^{19} W/cm^2 can be obtained [2] with such a pulse. This requires focusing with mirrors, thus an f/2 parabolic mirror (from Janos Technology Inc.) was chosen. With the arrangement shown in Fig. 1 an intensity of $5 \cdot 10^{17} \text{ W/cm}^2$ has been obtained even with the modest 15 mJ laser energy. The intensity on the target was $3.4 \cdot 10^{17} \text{ W/cm}^2$ for 45° angle of incidence.

An advantage of the KrF laser system is that the pulse is directly amplified, therefore no pulse compression is needed (not a CPA system). The final amplification in this laser system is carried out in a KrF amplifier after frequency doubling of the 496 nm dye laser pulse. This is the reason why there is no pedestal, the only possible source of prepulse can be the ASE of the KrF amplifier. Due to the long (10–20 ns) duration of the ASE and its bad focusability, the ASE intensity in the focus was lower than 10^7 W/cm². It means that the contrast of the beam for our system is better than 10^{10} ! This ASE intensity is low enough that it does not produce a preplasma. The arrangement is described in detail in [3]. Figure 1 also illustrates the main diagnostics prepared for the experiments. A holographic toroidal VUV grating images the target onto the surface of a phosphor-coated MCP detector. The detector here is a similar MCP. The visible light of the screen is then imaged onto a CCD detector.

High-harmonics experiments

Earlier experiments with lens-focusing up to 5×10^{15} W/cm² showed up to the 3rd harmonics with the following properties: The harmonics propagated in the direction of the specularly reflected light from the target. Both p- and s-polarized radiation generated harmonics and the harmonics conserved the polarization of the beam [4]. As this behaviour at these low intensities cannot be well explained by the theoretical models based on resonance absorption a theoretical model was developed with the participation of our group which is based on a single electron model. The model which takes into account the evanescent electric and magnetic field in the overdense plasma layer claims that the $\mathbf{v} \times \mathbf{B}$ force cannot be neglected in the overdense region even for nonrelativistic intensities, and it may be a source for high harmonics either for p- or for s-polarized radiation. If this mechanism is responsible for high harmonics, they will have a polarization similar to the incoming laser radiation [5]. The calculation method could be applied to an interesting other phenomenon, the intensity dependent anomalous transmittivity of thin (overdense) plasma layers, too [6].

The question arose however, what happens at higher intensities. High-intensity experiments with pulse-durations similar to ours, i.e. longer than ~ 150 fs showed harmonics generation for both laser polarization, too [7] but the harmonics propagated diffusely which was explained by the rippling of the critical surface. Experiments with the same, 248 nm wavelength of 1 ps duration showed harmonics only up to the 4th order for 10^{19} W/cm², and they also showed that rippling and thus diffuse harmonics propagation starts between 10^{16} and 10^{17} W/cm², well above the intensities of our previous experiments [4]. Those results were however obtained with not clean laser pulses, i.e. with strong prepulse. The question arose whether surface rippling is an effect which occurs in the preformed plasma, or it is an intrinsic effect. Also, it

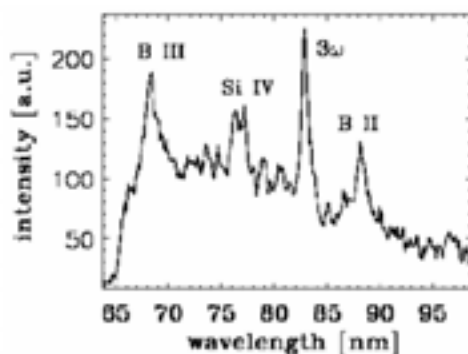


Figure 2. Spectrum from a B target.

is well-known that prepulses may strongly affect harmonics generation, thus we wanted to know the effect of the intense beam in case of an initially clean, steep surface. Experiments

were carried out with the 248 nm laser beam of pulse duration 700 fs on the target, with high contrast up to $3.4 \cdot 10^{17}$ W/cm² intensities. Harmonics up to the fourth order were observed on different targets [8]. Figure 2 illustrates the spectrum from B target showing strong 3W signal and boron spectral lines. The Si feature is coming from the glass under the evaporated B layer.

The appearing new even (4th) order harmonics (near threshold-behaviour) confirms again that it was generated on the steep density gradient and not in a preplasma with central symmetry. The harmonics show some features different from the low intensity case. It was confirmed that above 10^{16} W/cm² the amount of harmonics emitted diffusely, a significant amount of radiation could be detected well outside the original light cone. The polarization behaviour changes as well. At low intensities the harmonics keep the polarization of the laser. The higher the intensity, the more mixed is the polarization of the generated harmonics. For intensities above 10^{17} W/cm² the generated harmonics contain roughly equally p- and spolarized components, independently from the polarization of the incoming beam. These observations demonstrate the rippling of critical surface. The mechanism can be understood as a consequence of the unstable balance of light pressure and plasma expansion. 1D PIC simulations show that light pressure is in equilibrium with the expanding plasma, therefore the plasma gradient does not change significantly even if the pulse duration changes. Clearly this equilibrium is unstable and Rayleigh-Taylor-like instabilities may evolve, especially when the laser pulse duration is at least as long as several hundred fs. This finding has a relevance for the physics of fast ignitors. A fast igniting laser has a pulse duration of about 10 ps, therefore rippling of the critical surface will necessarily start which may strongly affect the generation and propagation of fast electrons.

Laser plasma spectroscopy

Clearly, in the case of fast ignition the heating of the target occurs isochorically. Soft X ray spectroscopy is the tool to investigate isochoric heating of matter. Numerical simulations with the MULTI hydrocode show that when using a KrF laser of our intensity at least $1\text{--}2 \cdot 10^{-4}$ g/cm² matter is heated isochorically up to some hundreds of eV. Even our highharmonics experiments show some features of high temperature in the depth of the target. The investigated target was 500nm thick B or C layer evaporated on the glass. Figure 2 showed the SiIV feature coming from the glass plate but SiV features were visible, too. These preliminary results refer to high temperatures of above 100 eV.

In order to carry out more precise spectroscopical investigations a von Hamos spectrometer has been developed. The PET crystal allows the investigation of the spectral lines between 1.45 and 2 keV, thus allowing the investigation of Al and Si K-shell radiation with a resolution up to $\Delta\lambda/\lambda=2000$. Most of the spectrometers in this wavelength range are based on films. Our spectrometer uses however phosphor-coated CMOS detectors which – according to our hope – may allow single-shot experiments even for our modest laser energy.

The detector was developed together with a group of the University of Debrecen and L. Hudson from the NIST. The first characterization experiments of the spectrometer are now in progress. Isochoric heating experiments are planned for the first half of 2005.

Damage threshold studies of possible wall materials

The HILL laboratory has both nanosecond and femtosecond lasers on the 248 nm wavelength. Possible fusion wall materials as W and glassy carbon (Sigradur) were investigated both with

600 fs and 20 ns pulses. In a collaboration with the Department of Optics and Quantum Electronics of the Szeged University experiments were carried out to determine the damage threshold in single-shot and multiple-shot (600) experiments. As a detection optical microscopy was used as a diagnostics for multiple-shot experiments (deep crater) and atomic force microscopy for the single-shot case (shallow crater).

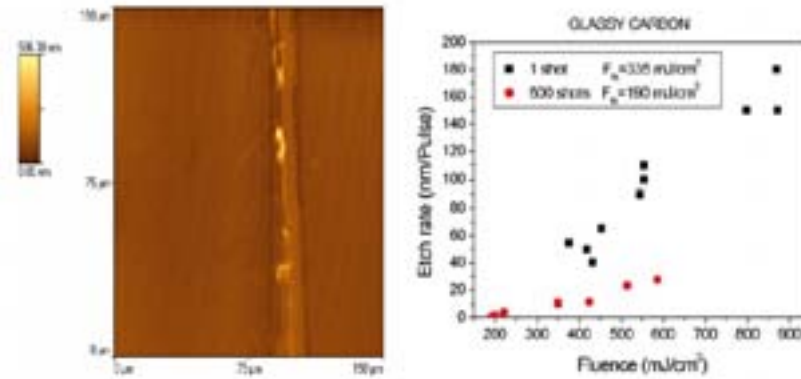


Figure 3. Atomic force microscope image of the etched glassy carbon after single shot of 350 mJ/cm² and crater depth (etch rate) as a function of laser fluence.

Figure 3 shows an image of the effect of UV laser light on Sigradur and the crater depth as a function of laser fluence for 20 ns laser pulse. The single-shot damage threshold is a factor of 2 higher than the multiple-shot value. The threshold does not depend significantly from the laser pulse duration. Tungsten however proved to be much more resistant. The measured multiple-shot threshold was $\sim 1.6 \pm 0.2$ J/cm² for W, nearly an order of magnitude higher than for glassy carbon. It is even higher than the known threshold value of 1 J/cm² for SiC. The data can well be explained on the basis of simple thermodynamical estimations.

3. COLLABORATION WITH THE MPQ, GARCHING, FRG: GENERATION AND PROPAGATION OF FAST ELECTRONS

We participated in the work of a group of the Max-Planck-Institut für Quantenoptik, Garching, Germany (participants: M. Kaluza, M.I.K. Santala, G. Tsakiris, K. Witte) to study the generation and propagation of MeV electrons. Experiments with a preformed plasma aimed to generate a high number of fast electrons, determining the temperature, whereas electron beam propagation in the bulk solid target was investigated, too.

Self-focusing and heating effect in a preplasma

In the case of fast ignition a laser beam having an intensity of 10^{18} – 10^{20} W/cm² is used first to bore through the ablative corona and push the surface of critical density (up to where the laser light can propagate) near to the high-density core of the pellet. Clearly, nonlinear effects as self-focusing play an important role here. Experiments were carried out in a preformed plasma of long scalelength using a Nd:glass laser delivering 15 J, 3 ns pulses on the 2ω , 0.53 μm wavelength. Hydrodynamic 1D simulations predict the creation of an underdense plasma of several 100 μm length which is followed by an overdense layer of several 10 μm thickness. The fast electrons are produced by a synchronized 1 J, 150fs pulse from the

ATLAS Ti-sapphire laser facility. They are generated after self-focusing of the laser beam which is originally (i.e. before self-focusing) of more than 10^{19} W/cm² intensity. An electron spectrometer was situated behind the target [9] which gave an effective temperature of 2 MeV behind 10 μ m plastic, which means that electrons well above 10 MeV were detected as well. From the preformed plasma the light scattered on the 2ω wavelength was detected with large magnification. A synchronized 150-fs probe beam converted to 395 nm back-lighted the target, providing interferometric images of the interaction region. The contribution of our group was the investigation with an X ray pinhole camera using 50 μ m pinholes with Al or Be filters. The angle of observation was 12 relative to the target plane. Together with the X ray-sensitive CCD detector this diagnostics was sensitive in the 1–25 keV range.

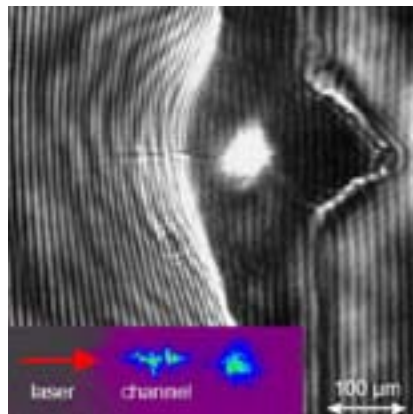


Figure 4. Interferometric image of the self-focused filament and scattered light (insert) on the 2ω wavelength.

Figure 4 shows the interferometric image and the scattered light from the self-focused filament. The interferometric snap shot of the preformed plasma was approximately coincidental with the arrival of the CPA pulse, which was 1.9 ns after the onset of the 3 ns prepulse in this shot. The electron densities were between 8×10^{19} and 8×10^{20} cm⁻³ with a scale length of 110 μ m on the laser axis. Both the interferogram and the side-scattered image show a self-focused filament extending to more than 100 μ m in length evincing whole-beam relativistic self-focusing.

Figure 5 illustrates an X ray pinhole image obtained with a 2- μ m thick Al filter, i.e. most of the detected radiation is above 1 keV with a fraction around 100 eV. The emission from the preplasma can clearly be distinguished at the target surface. The red cone is the image of the ultra-intense laser pulse propagating in the preformed plasma (note that it is longer than the total scale in Fig. 4). The conical structure corresponds to the focusing angle of the 150 fs pulse. The strong emission is clearly a consequence of heating and ionizing effect of the ultrashort pulse; no signs of a self-focused filament can be seen within this cone.

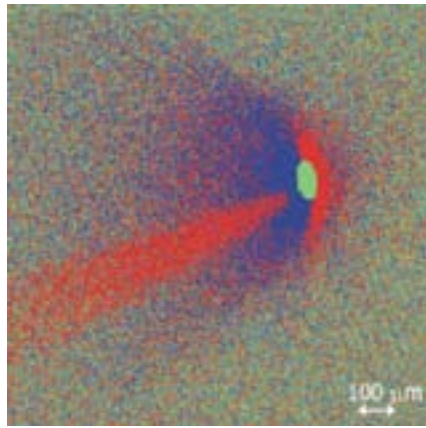


Figure 5. X ray pinhole photograph of the short laser pulse in the preformed plasma.

The reason why it is not seen within the x ray spectral range of the pinhole camera is most likely because in this plasma the optical thickness is low. The observation of whole beam focusing in the x ray spectral range in the experiments in Osaka [10] may be attributed to the higher density of the preformed plasma reaching critical density near the initial surface of the target. The arrangement used in the present experiment has however the advantage of generating high energy electrons with modest lasers. The increase of on-axis intensity due to self-focusing and the heating of the preformed plasma is clearly demonstrated by the visible and pinhole-images [11].

Target rear side diagnostics shows low divergence of the fast electrons in dense matter

Experiments were carried out with the high-intensity beam of the ATLAS laser system focused directly on solid targets, i.e. without a prepulse. One purpose of the MPQ group was to generate and optimize the proton beam from the rear side of the target [12]. The other aspect – and this was the purpose of our participation here – was the investigation of the electron beam propagation inside the solid target material. In this case the x ray pinhole camera viewed the rear side of the target for the radiation above 1 keV photon energy.

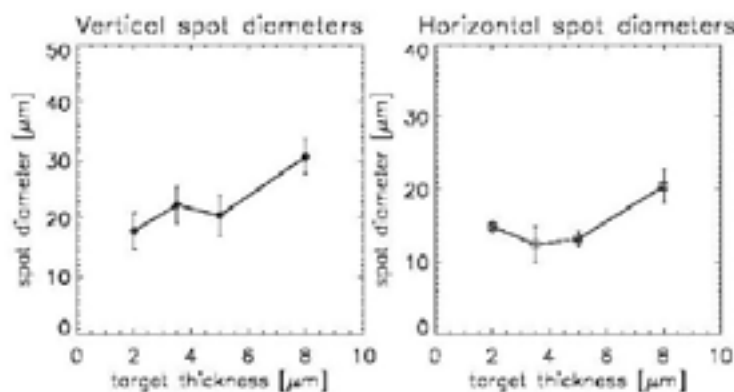


Figure 6. Rear spot size from x ray pinhole photography.

Figure 6 shows the measured rear spot size for different target thicknesses. Note that due to the not perpendicular angle of incidence the vertical spot size differed from the horizontal one. The results show that the spot size does not increase significantly with increasing target thickness, therefore it was concluded that the divergence angle of the MeV electron beam was less than 12° in agreement with previous results obtained with different laboratories for different laser parameters. We used another method for comparison with the pinhole photography, namely the X ray diffraction on a razor blade.

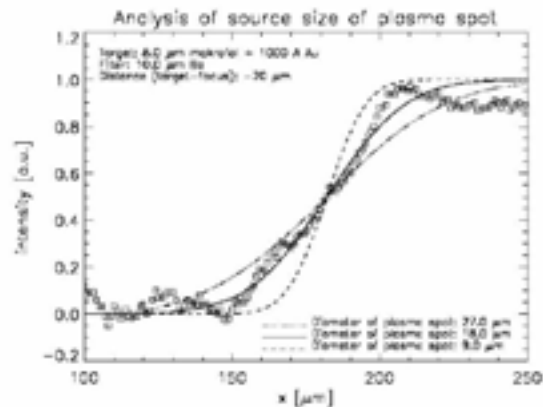


Figure 7. X ray diffraction on a razor blade.

Figure 7 shows the result of X ray diffraction for the case of $8 \mu\text{m}$ plastic using $10 \mu\text{m}$ Be X ray filter. Fitting of the diffraction data shows a best value of $18 \mu\text{m}$, in good agreement with the pinhole data. Summarizing these results we can see that both X ray diffraction and pinhole photography show a well-collimated propagation of the MeV electron beam, which strongly affect the intense proton beam generation on the rear side of the target.

REFERENCES

- [1] SZATMÁRI, S., *Appl. Phys. B*, 58, 211 (1994).
- [2] SZATMÁRI, S., et al., *Appl. Phys. B*, 63, 463 (1996).
- [3] FÖLDES, I.B., GÁL, K., KOCSIS, G., RÁCZ, E., SZATMÁRI, S., VERES, G., *Proc. SPIE*, 5228, 473–479, 2003.
- [4] FÖLDES, I.B., et al., *Laser Physics*, 10, 264 (2000).
- [5] GÁL, K. and VARRÓ, S., *Opt. Commun.*, 198, 419 (2001)
- [6] VARRÓ, S., GÁL, K., FÖLDES, I.B., *Laser Phys. Lett.*, 1, 111–114 (2004).
- [7] NORREYS, P., et al., *Phys. Rev. Lett.* 76, 1832 (1996).
- [8] FÖLDES, I.B., KOCSIS, G., RÁCZ, E., SZATMÁRI, S., VERES, G., *Laser and Particle Beams*, 21, 517–521 (2003).
- [9] GAHN, C., et al., *Rev. Sci. Instrum.*, 71, 1642 (2000).
- [10] TANAKA, K.A., et al., *Phys. Plasmas*, 7, 2014 (2000).
- [11] KALUZA, M., FÖLDES, I.B., RÁCZ, E., SANTALA, M.I.K., TSAKIRIS, G.D., WITTE, K.-J., *IEEE Trans. on Plasma Science*, in press (2005).
- [12] KALUZA, M. et al., *Phys. Rev. Lett.*, 93, 045003 (2004).

Thermal smoothing of laser imprint using low-intensity prepulse or low-density porous matter

M. Káral¹, N.N. Demchenko³, S.Yu. Gus'kov³, A.I. Gromov³, A. Kasperczuk⁴, V.N. Kondrashov⁶, E. Krouský², J. Limpouch^{1,2}, K. Mašek², M. Pfeifer², P. Pisarczyk⁷, T. Pisarczyk⁴, K. Rohlena², V.B. Rozanov³, J. Ullschmied⁵

¹ Czech Technical University in Prague, FNSPE, Prague, Czech Republic

² Institute of Physics, AS CR, Prague, Czech Republic

³ P. N. Lebedev Physical Institute of RAS, Moscow, Russian Federation

⁴ Institute of Plasma Physics and Laser Microfusion, Warsaw, Poland

⁵ Institute of Plasma Physics, AS CR, Prague, Czech Republic

⁶ Troitsk Institute of Innovation and Thermonuclear Research, Troitsk, Russian Federation

⁷ Warsaw University of Technology, ICS, Warsaw, Poland

Abstract. An overview of earlier studies of laser imprint treatment employing a low-intensity prepulse of the iodine laser PERUN is complemented by recently performed much more sophisticated prepulse experiments (so far only preliminary) using the powerful PALS laser facility. Subsequently, much closer attention is paid to the alternative approach to laser imprint treatment – application of layers from a low-density porous matter. Interaction of PALS beam with low-density foam targets and acceleration of Al foils by the pressure of heated porous matter have been investigated, both experimentally and theoretically. The experimental results are in a good agreement with our two-dimensional hydrodynamic calculations that do not take fine structure of foam material into account. The only exception is the case of the thinner PVA foam where the code predicts much higher rear side velocities due to heating and expansion of the foil material. It indicates that heat flux is overestimated to a certain extent in the simulation code. Consequently, heat conductivity value should be revised in the case when the foam homogenization is not complete during the heat wave propagation. A simplified analytical model has been presented that does not include heating and expansion of the foil on the target rear side. The derived rear side velocities agree well with the experiment and it is another indication that foil is accelerated without significant expansion.

Introduction

A very smooth ablation pressure profile (typically up to a few percent) is required in the direct-drive laser fusion experiments to suppress the onset and a subsequent growth of *Rayleigh-Taylor* and *Richtmyer-Meshkov* instabilities, which might disrupt the target compression. As it is generally very difficult to meet the required uniformity level in the ablation pressure by an improvement of the illumination scheme as such (mainly due to the interference structures formed as a result of the multi-beam target illumination), other smoothing mechanisms have been proposed, which are based on a modification of the laser-target interaction process. There are two approaches under consideration how to deal with this problem. One of them employs the method of *preliminary irradiation of the target* by a comparably low intensity laser pulse (*prepulse*). Another approach is based on the application of *low-density porous matter* (e.g. foams) as the absorber of laser radiation of IFE targets. The foam would also very likely play the role of protective coating preventing the frozen DT fuel from melting on its way to the interaction region of the IFE target chamber due to friction with the residual atmosphere created mainly as a result of the wall/coolant evaporation caused by previous microexplosion.

In our initial proposal submitted almost three years ago (where many valid details for our current proposal can be found) we intended to study mainly the *prepulse* method on the newly

acquired high power iodine laser facility PALS (Prague Asterix Laser System). We already had some preliminary experience in this field from experiments performed on much smaller (approx. 20 times) iodine laser facility PERUN which could be put to a good use. Results of these numerical and experimental studies are presented on Figs 1 and 2. More detailed description can be found elsewhere [1–2]. Continuation in this line of research on PALS, however, required e.g. several (at least 4) mirrors of large diameter which were rather expensive to buy.

DOUBLE-PULSE EXPERIMENTS PERFORMED ON PALS

Purchasing of 4 quartz mirrors (500 mm in diameter) with dielectric coating for separations of the first, second and third harmonics (total price of US \$ 70 000) together with other pieces of equipment during the last summer eventually allowed for steps to be taken in realization of our initial plans with *double-pulse* (i.e. *prepulse and the main pulse*) *plasmas* using PALS laser facility.

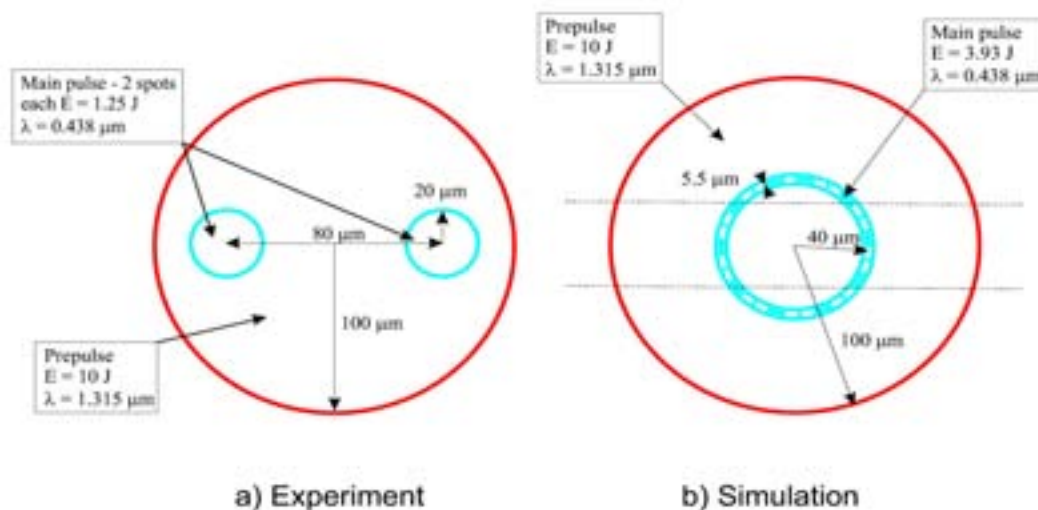


Figure 1. Target illumination (focal plane) scheme in the experiment (a) and in the simulation (b) with the outline of the slab (dashed horizontal line) used for the shadowgraph reconstruction.

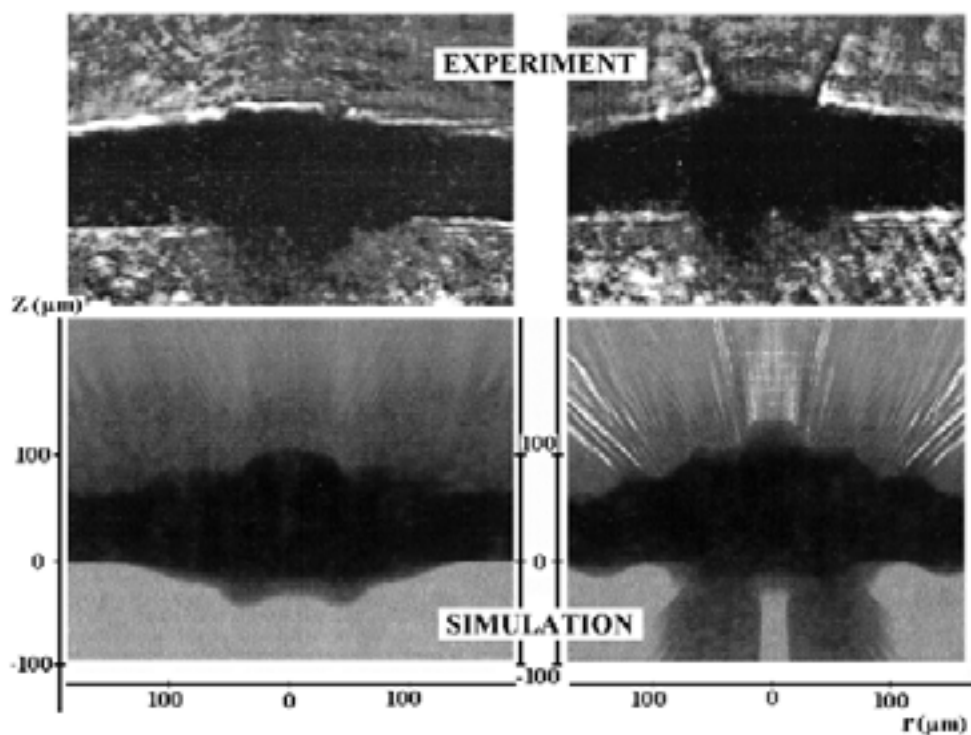


Figure 2. The experimental and synthetic side-on view shadowgraphs taken with the probe beam shifted 0.3 ns after the main pulse. The delay of the main pulse with respect to the background pulse (prepulse) is 0.5 ns (left) and 0 ns (right). The laser beams are incident downwards along Z axis, original foil position $z = 0-7 \mu\text{m}$, focal plane center $r = 0$.

Recent studies of thermal smoothing, when the target was illuminated by double-pulse, have used only the technique of *optical probing* to investigate behaviour of the *front* and *rear* side of the target in the dependence on delay time of the main pulse. *Submitted project was intended to bring more detailed information on denser region close to the ablation front, which is more important from viewpoint of uniformity of the plasma, using the X ray backlighter.* Parameters of the laser and the plasma would be now comparable to those generated by the world largest laser facilities.

Our *work plan* for the last project year therefore consisted of both *experimental* as well as *theoretical* investigations of the *energy transfer mechanisms* and *energy distribution smoothing processes* in *double-pulse plasmas*.

First series of preliminary experiments already took place in the year 2004. Targets for these experiments were stripes of aluminium 500 μm wide and up to 10 μm thick. For formation of double-pulse the focusing optics was set to 3ω radiation while the preceding first harmonic was focused by an auxiliary lens to create a preplasma of the proper size. The main 3ω pulse was spatially modulated by a wedge inserted into the beam to generate a well-defined non-uniformity on the background of the preformed plasma. Time delay of the spatially modulated 3ω beam with respect to the first harmonic was adjustable in the range from zero to several nanoseconds. An auxiliary beam of PALS was exploited for setting up an auxiliary X ray source for backlighting and/or as a diagnostic beam converted to the third harmonic. Details of these preliminary experiments are illustrated in Figures 3–5.

Thermal Smoothing by Double Laser Pulse

Pre-plasma produced by a defocused infrared beam
(focal spot diameter 0.3 mm)

Two hot spots generated by focused blue beams delayed
by 0.5 ns.
Distance of the spots 0.2 mm.

Plasma expansion is studied by two
X-ray pinhole CCD cameras.

X-ray backlighting provides
shadowgrams of the dense plasma
regions.

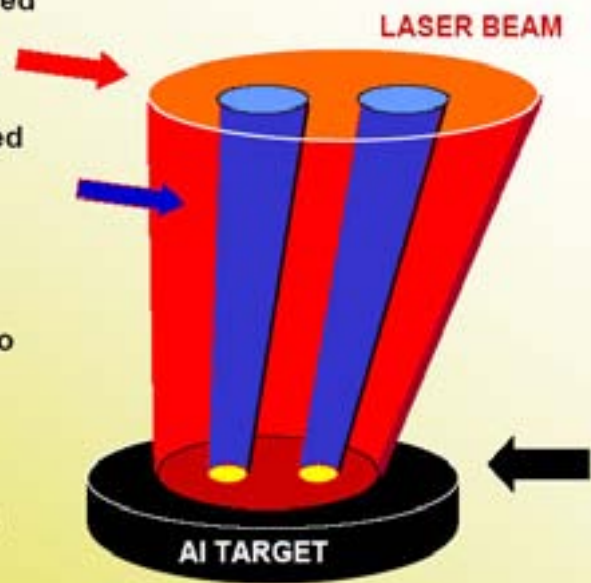


Figure 3. Concept of the double-pulse technique used in laser imprint smoothing. Three laser beams are hitting the target: the wide prepulse (red - 1ω) is followed by two simultaneous beams (blue - 3ω) delayed to generate inhomogeneity (hot spots). Plasma expansion is studied by two X ray pinhole CCD cameras using X ray backlighting.

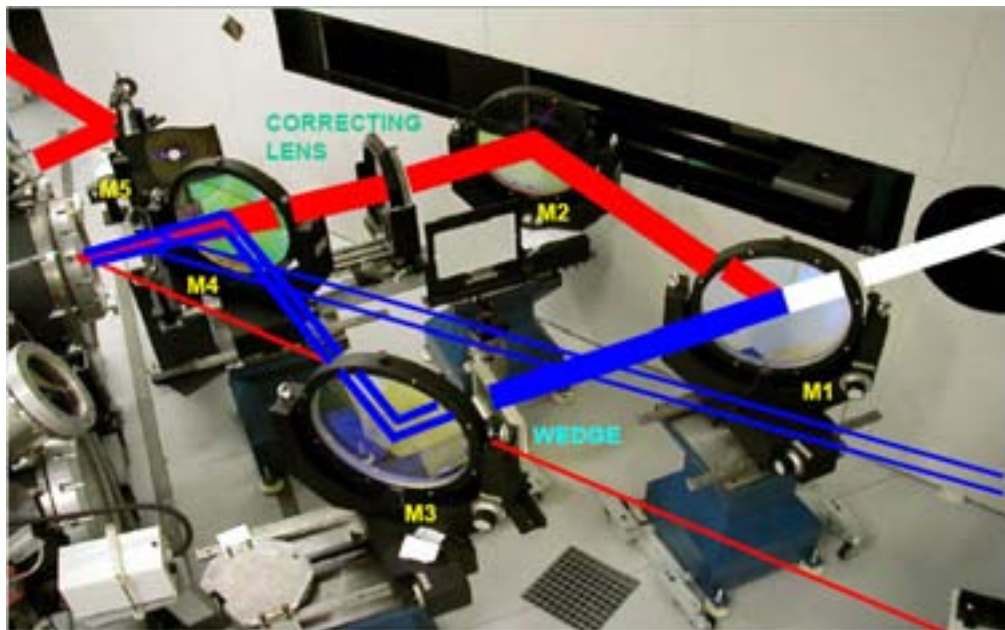


Figure 4. Laser beam trajectories before entering the target chamber for the double pulse arrangement (red - 1ω , blue - 3ω).

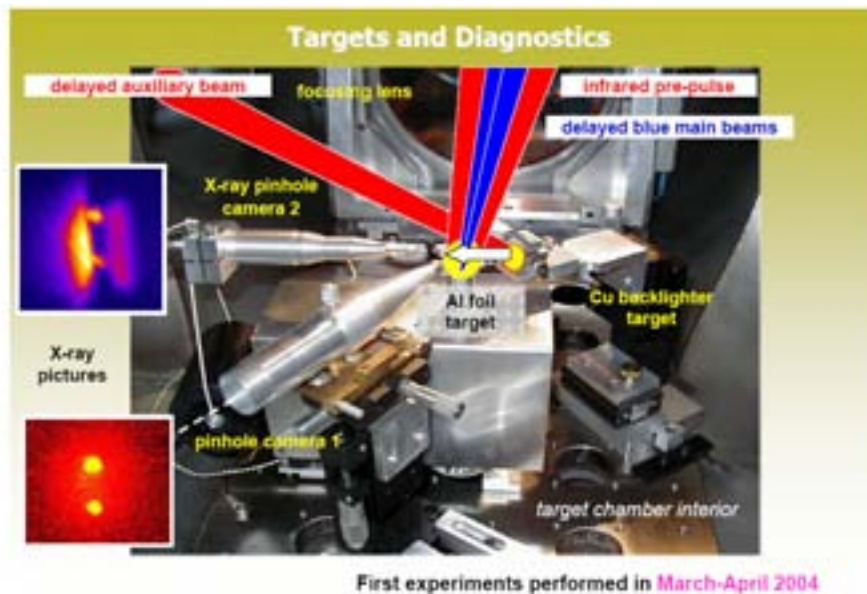


Figure 5. Laser beam trajectories inside of the target chamber for the double pulse arrangement (red – 1ω , blue - 3ω) together with the Al foil target, Cu backlighter target and two X ray pinhole cameras.

EXPERIMENTS WITH POROUS MATTER TARGETS PERFORMED ON PALS

While gradually purchasing necessary components from various resources to allow for the double-pulse experiments to take place, for the time being we also concentrated our close attention to the second approach adopted in *laser imprint* treatment - i.e. *porous matter* targets. Enlarging our research team by some additional experts already active in this field we became sufficiently competent and capable of completely covering this complicated subject. Detailed results of our activities in this field covering the *experimental*, *numerical* and *analytical* studies were already published as well as presented at various conferences [3–14].

The main goal of this part of our work was to study *energy transport* through the low-density porous matter and to demonstrate a *sufficient efficiency* of *thin foil acceleration* together with *substantial smoothing effect* of the low-density foam absorber.

Here, we use targets without thin high-Z layer at the laser-irradiated side that is usually applied for laser energy conversion to X rays preheating the foam. The basic smoothing mechanism is electron thermal conduction and thus laser imprint smoothing can be achieved even without X ray preheat, which may additionally lead to deleterious vaporization of the foil. This study succeeds to our previous work [3] and the distinctive feature of these experiments is the interaction of *subnanosecond* laser pulses with foams containing *large pores* when laser pulse is shorter than the time needed for full homogenization of the foam matter.

The laser provided 400 ps (FWHM) pulse with the energy up to 600 J at the basic harmonics ($\lambda_1 = 1.32 \mu\text{m}$). Laser was incident normally on the target; the laser spot radius in the best focus was $R_L \approx 40 \mu\text{m}$. Here, the target surface was placed approximately 200 μm in front of the best focus and thus the laser spot radius on the target surface was $R_L \approx 150 \mu\text{m}$. Laser irradiances were varied from $I \approx 10^{14} \text{ W/cm}^2$ up to $I \approx 10^{15} \text{ W/cm}^2$. No method of optical

smoothing was used, and thus one can assume that the laser beam focus was not quite uniform and contained small-scale intensity inhomogeneities.

Several types of foam target were used. Most experiments were done with polystyrene foam of density in range $8 - 10 \text{ mg/cm}^3$ and of typical pore diameter $D_p \approx 50 - 70 \text{ }\mu\text{m}$. Other polystyrene foams of density $\rho \approx 30 \text{ mg/cm}^3$, and of pore diameter $D_p \approx 10 \text{ }\mu\text{m}$, and also of $\rho \approx 20 \text{ mg/cm}^3$, and $D_p \approx 5 \text{ }\mu\text{m}$, as well as polyvinylalcohol (PVA) foam of density $\rho \approx 5 \text{ mg/cm}^3$, and of typical pore diameter $D_p \approx 5 \text{ }\mu\text{m}$ were used, too. Foam thicknesses varied from $100 \text{ }\mu\text{m}$ to $500 \text{ }\mu\text{m}$. A $2 \text{ }\mu\text{m}$ or $0.8 \text{ }\mu\text{m}$ thick aluminum foil was placed at the foam rear side in the majority of foam targets.

The diagnostic system included optical and X ray methods. Slit image of plasma X ray emission was recorded by KENTECH low magnification X ray streak camera placed in a side view. The temporal resolution was either 30 or 70 ps and spatial resolution of $50 \text{ }\mu\text{m}$ was in the direction normal to the target surface (target depth). The recording channel included $17 \text{ }\mu\text{m}$ of mylar and 40 nm of Aluminum; the transmission was negligible for photons of energy $< 1.1 \text{ keV}$, while the transmission was approximately 20 % for 1.7 keV photons.

Optical diagnostics employing interferometry and shadowgraphy were carried out by means of 3-frame interferometric system with automated image processing technique. Each of three recording channels was equipped with a CCD camera of the Pulnix TM-1300 type, with a matrix of 1300×1030 pixels. The diagnostic system used a probing beam at the third harmonics with similar, but slightly shorter pulse duration than that of the main beam. Interferogram processing included parasitic noise filtering, comparison of object and reference interferograms, and a subsequent reconstruction of radial electron density distributions.

The target self-emission was imaged with eleven-fold magnification on the x ray streak camera entrance slit through $50 \text{ }\mu\text{m}$ wide slit providing spatial resolution along the target depth. A comparison of X ray streak records taken for laser-foam and laser-foil interaction is presented in Fig. 6 for normal incidence of laser beam on the targets. Bright images were obtained for the aluminum foils. The most emitting region of the laser-irradiated foil, hot dense plasma behind the critical surface, moves at first inwards due to ablative acceleration of the foil and then after the end of the laser pulse it moves outwards to the vacuum due to the plasma thermal expansion.

On the other hand, the amount of X ray emission was rather low for the foam targets as foams contained exclusively light elements. Usable records (weak, but significantly above x ray streak sensitivity limit) were obtained for the foams with the largest pore diameter ($50 - 70 \text{ }\mu\text{m}$) only. From the record in Fig. 6a), the upper estimate of the laser penetration depth is the thickness of about $120 \text{ }\mu\text{m}$ of the immediately heated layer. Thus, the laser penetration is not more than two pore layers into this overdense foam (electron density in the fully ionized homogenized foam is approximately 4 times critical). Later, some signs of foam material expansion into vacuum are seen. However, the basic process in this period is heat wave propagation into the foam. The blurred boundary of the emitting region complicates heat wave speed determination from the streak images. However, the inward propagation velocity of the X ray emitting plasma region is found to be approximately $\sim 1.4 \times 10^7 \text{ cm/s}$ from the slope of the advancement of the rear edge of the heated x ray emitting region denoted by full line in Fig. 6a). Though the X ray signal lasts for nearly 3 ns, the X ray emitting zone covers only about two thirds of the foam thickness and no emission near the Al foil at the target rear

side is detected. This is a strong indication that the foil at the rear side of 400 μm thick foam is not heated to high temperatures by hydrothermal wave. Consequently, the foil at the target rear side is supposed to be accelerated as a whole without significant expansion. In this acceleration mode, the foil velocity can be measured by optical probing.

Foam expansion at the target front side and the target rear-side motion was monitored by a sequence of 3 interferometric pictures, in the first picture the target rear side is displayed via shadowgraphy. Typical experimental sequence of pictures taken in one laser shot is presented in Fig. 7. While the foam expansion against the incident laser beam is partly obscured by the plasma evaporated from the target holder – see lower right part of all pictures and the right central part in Fig. 7a), a clear picture of the target rear side motion is obtained. The rear side target boundary is sharp in interferograms Figs. 7b), 7c) with no signs of low-density plasma behind the target. At the beginning of the foil acceleration, the rear side shape resembles spherical wave propagating from the laser absorption region. Later, the curvature centre of the accelerated part of the foil is moved in the direction to the target rear surface. The shape of the accelerated foil is smooth without any detectable small-scale structures, and thus a certain level of thermal smoothing inside the foam is indicated. Quantitative measurement of the uniformity of the accelerated part of the foil is, however, beyond the scope of the present experiment, and it will be addressed in the next experiment using optical streak measurement of the shock wave arrival to the target rear side.

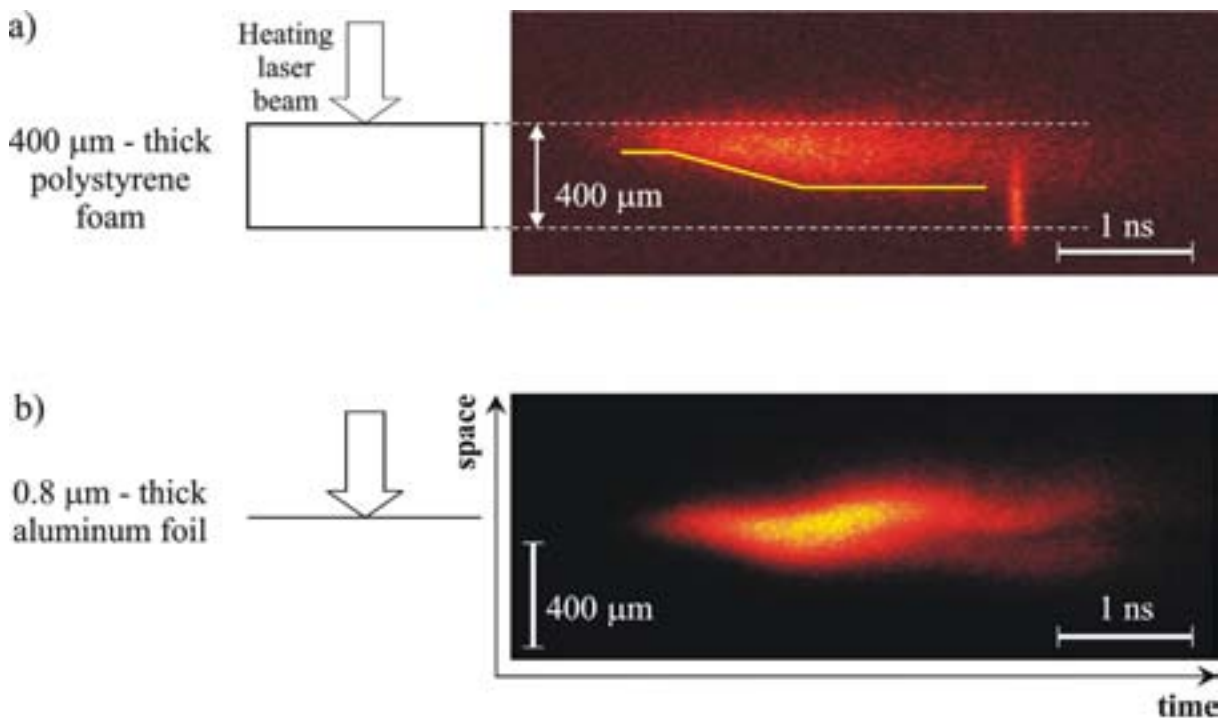


Figure 6. Laser interaction with targets recorded by X ray streak camera. a) Polystyrene foam of density $\rho \approx 9 \text{ mg/cm}^3$ and typical pore diameter $D_p \approx 50 - 70 \mu\text{m}$, 400 μm thick and 2 μm thick Al foil placed at its rear side. Laser energy, intensity, pulse length, wavelength and beam radius 92 J, $3.1 \times 10^{14} \text{ W/cm}^2$, 400 ps, 1.32 μm , 150 μm . Solid line denotes the rear boundary of x ray emitting region. b) Al foil 0.8 μm thick. Laser energy, intensity, wavelength and beam radius 118 J, $4.0 \times 10^{14} \text{ W/cm}^2$, 1.32 μm , 150 μm .

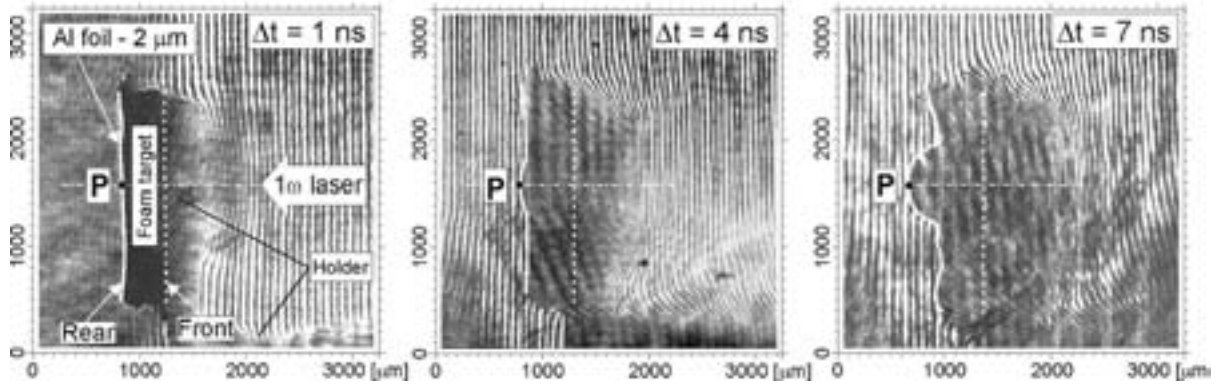


Figure 7. Shot #25030 recorded by the 3-frame interferometric system in time instants 1, 4 and 7 ns after the main laser pulse maximum. Laser energy, intensity, wavelength, and beam radius were 173 J, $6.2 \times 10^{14} \text{ W/cm}^2$, $1.32 \mu\text{m}$, and $150 \mu\text{m}$, respectively. Polystyrene foam with $\rho \approx 9 \text{ mg/cm}^3$ and $D_p \approx 50 - 70 \mu\text{m}$ was $400 \mu\text{m}$ thick and $2 \mu\text{m}$ thick Al foil was placed at its rear side. Parasitic effect of the target holder is denoted in the first frame.

The position of the point P (rear side opposite to the laser beam centre) is measured with the precision of $5 - 10 \mu\text{m}$. The speed of the accelerated Al foil can be determined from the difference in point P positions in different frames. The speed of accelerated foil grows with the laser energy. Moreover, the time t_f when the hydrothermal wave reaches the foil may be estimated from the graph plotted on the basis of these data. When $100 \mu\text{m}$ thick PVA foam is used, foil acceleration during the laser pulse is inferred. For $400 \mu\text{m}$ thick polystyrene foams, the shock wave reaches the foil only 2–4 ns after the laser pulse, and the delay decreases with laser energy.

NUMERICAL STUDIES OF LASER INTERACTION WITH POROUS MATTER TARGETS

Simulations were performed by two-dimensional Lagrangian hydrodynamics code ATLANTHE including an advanced treatment of laser propagation and absorption. The code is based on one fluid two temperature model of plasma with the Spitzer's heat conductivities for electrons and ions. It includes laser refraction, inverse bremsstrahlung absorption in a strong electromagnetic field (absorption coefficient dependent on radiation intensity), resonance absorption, fast electron generation and fast electron transport in approximation of frictional force due to the ionization losses. Explicit difference scheme and triangular Lagrangian mesh was used for the fluid equations. Heat transport is solved via implicit differencing. Radiative transport is considered in a simple three-temperature (3T) approximation.

Due to excessive computational complexity, we disregard detailed structure of the foam in the global two-dimensional simulations presented here. Though the fast homogenization stage, when plasma expanding from the foam solid elements fills the empty space inside foam pores, lasts approximately 50–100 ps, i.e. much less than laser pulse, omission of the foam structure is not correct here as the second homogenization stage leading to uniform medium is much longer (up to several ns) than laser pulse. However, foam structure was taken into account in our previous simulations of the early stage of laser-foam interactions.

The simulations are performed in cylindrical geometry. Gaussian laser beam is assumed to be incident normally on homogeneous laser of the foam material of density equal to the foam average density, thin Al layer is assumed on the target rear side. Since the average foam

density significantly exceeds the critical density, critical surface is located in the plasma flow into vacuum where plasma is fully homogenized during the fast homogenization stage. Thus, laser absorption and refraction is treated correctly in our simulations with the exception of the leading edge of the pulse. The energy transfer from the absorption region into the foam interior is due to the hydrothermal wave. The negligible role of radiative transport, revealed in our code, is due to absence of high-Z conversion layer and due to low Z number of the foam material. The influence of the foam fine structure on the hydrothermal wave velocity was studied in detail earlier via one- and two-dimensional hydrodynamic simulations. The resulting pressures do not essentially differ in comparison with a homogeneous medium (difference of 10-50 % depending on the pore size). Nevertheless, substitution of the foam by low-density homogeneous medium in simulations may lead to a certain underestimation of the time t_f needed for the hydrothermal wave propagation through the foam.

The simulation results for parameters of Fig. 7 are plotted in Fig. 8. The calculated laser absorption was approximately 50 %. Plasma radius in the figures essentially exceeds the laser beam radius on the target due to fast lateral heat transport in the low-density porous matter. A smooth shape of the accelerated foil is observed with the width considerably larger than the laser beam diameter. The fast electrons do not preheat unevaporated Al layer significantly for the laser flux density of Fig. 7. On the other hand, our simulation for laser beam radius of 40 μm and laser intensity 10^{16} W/cm^2 shows an exploding Al layer near the beam axis. The maximum temperature of thermal electrons does not differ from the case of 150 μm laser beam radius due to the lateral heat transport in the foam plasma. Therefore the explosion was caused by hot electrons and not by a thermal heat wave.

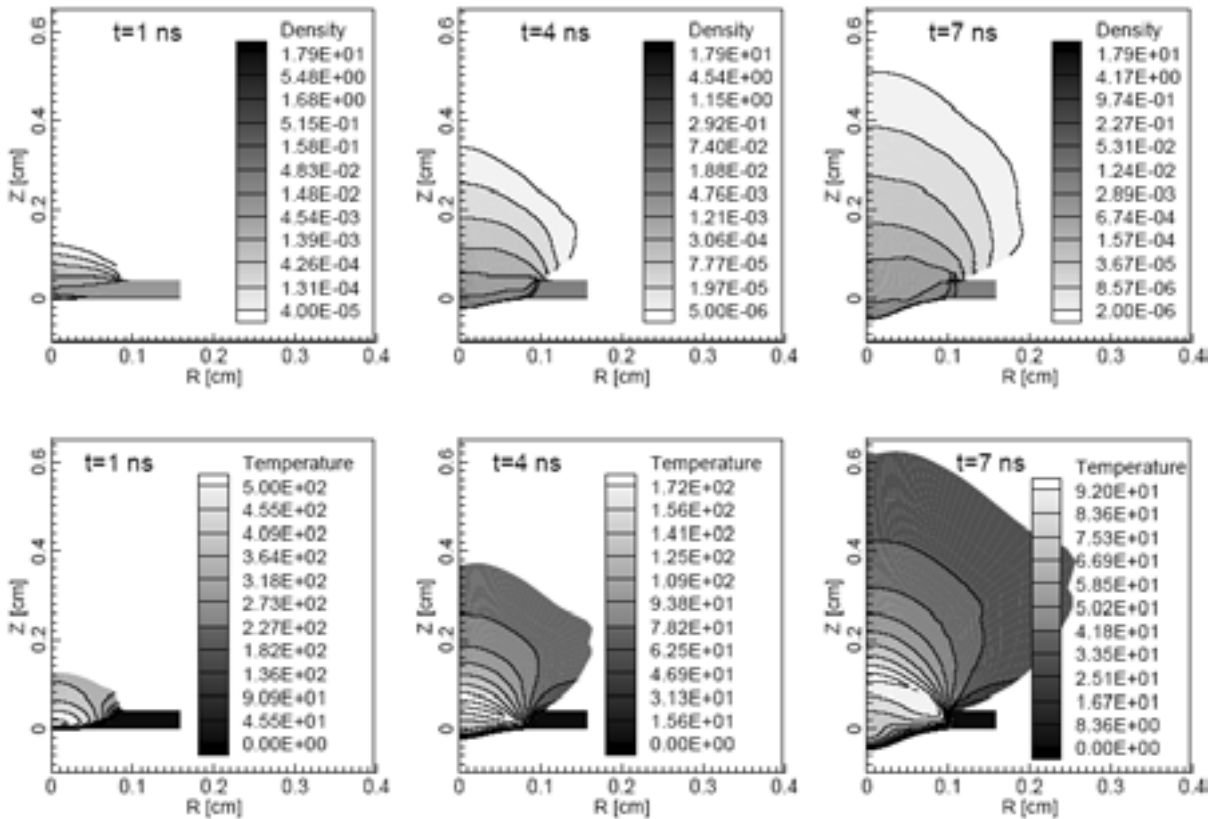


Figure 8. Density (in g/cm^3) and electron temperature (in eV) profiles at times 1, 4 and 7 ns after laser pulse maximum calculated numerically for conditions of Figure 7.

ANALYTICAL THEORY AND RESULT COMPARISON

The wave of hydrodynamic perturbations in a foam matter is accompanied by gradual destruction of foam solid elements and their subsequent homogenization. Such a process of energy transfer can be described by the so-called hydrothermal wave propagating in a homogeneous medium of average foam density with the front velocity close to the sound speed. As the low-density porous matter is heated to high temperatures by the hydrothermal wave, the temperature distribution behind the wave front is smoothed efficiently by electron heat conductivity.

The analytical model does not take into account electron heat conductivity, radiative transport, generation and transport of fast electrons, and heating and expansion of the foil, attached to the foam rear side. The hydrothermal wave is treated simply as a spherical wave propagating from instant point release of energy into medium with negligible initial pressure. The velocity of hydrothermal wave front and the pressure behind the front may be expressed via absorbed laser energy E_{ab} and foam average density ρ_f , as follows

$$V_{ht} \cong 0.4 \times \left[\frac{3 \left(\frac{5}{3} \right)^2 (\gamma-1) E_{ab}}{\pi \rho_f} \right]^{1/5} \times t^{-3/5} \quad (1)$$

$$P_{ht} \cong 0.16 \times \left[\frac{3 \left(\frac{5}{3} \right)^3 \rho_f^{3/2} E_{ab}}{\pi (\gamma-1)^{3/2}} \right]^{2/5} \times t^{-6/5}, \quad (2)$$

where t is the time from the laser pulse maximum and ideal gas equation of state is assumed with the adiabatic constant γ , which is usually set here to $\gamma=5/3$.

Let us estimate the hydrothermal wave velocity and pressure behind the wave front in the experiments with polystyrene foam with density $\rho_f \approx (8-10) \text{ mg/cm}^3$ at the time instant of 1 ns which is slightly less than the time of the wave front arrival onto the rear side of the foam layer. Here, the approximate value 50 % of laser absorption efficiency is taken from our numerical simulations. Then, according to the formulae (1) and (2), the hydrothermal wave speed is $V_{ht} = 1.3 \times 10^7 \text{ cm/s}$ and its pressure is $P_{ht} = 2.5 \text{ Mbar}$ for the laser energy $E_L = 92 \text{ J}$. The respective values for the higher laser pulse energies are $V_{ht} = 1.5 \times 10^7 \text{ cm/s}$ and $P_{ht} = 3.3 \text{ Mbar}$ for the laser energy $E_L = 173 \text{ J}$, and $V_{ht} = 1.6 \times 10^7 \text{ cm/s}$, $P_{ht} = 3.7 \text{ Mbar}$ for the laser energy $E_L = 238 \text{ J}$.

The hydrothermal shock wave front reaches the centre of the foam-foil boundary approximately at the time t_f

$$t_f \approx \frac{\Delta_f^{5/2}}{\left[\frac{3 \left(\frac{5}{3} \right)^2 (\gamma-1) E_{ab}}{\pi \rho_f} \right]^{1/2}}, \quad (3)$$

where Δ_f is the foam layer thickness.

For the polystyrene foam layer of density $\rho_f \approx (8-10) \text{ mg/cm}^3$ and of thickness $\Delta_f = 400 \text{ }\mu\text{m}$, the times of the wave breakthrough, calculated via formula (3), are $t_f = 1.5 \text{ ns}$, 1.2 ns and 1.03 ns for laser energies $E_L = 92 \text{ J}$, 173 J and 238 J , respectively. These values are in a good agreement with numerical simulations, performed for a homogenous low-density medium. However, the experimental data are by about 2 ns greater. According to our opinion, such a fact is caused by the direct influence of initial structure of foam on the target dynamics. Namely, the delay of energy transfer wave in comparison with theoretical calculations made for uniform plasma is due to the foam homogenization phenomenon. During the homogenization period, the absorbed laser energy is partly contained in the energy of oscillatory colliding plasma flows and in the shock waves propagating out of the laser-heated exploding solid elements of the foam. Anomalously slow propagation of hydrothermal wave in foam was also predicted previously when laser was directly incident on the foam. When laser energy is converted to X rays in high-Z material, the speed of hydrothermal wave is increased due to foam homogenization by X ray preheat.

After the first collisions of the heated and expanding foam elements, the microscopic regions of dense matter have a size significantly larger than the solid particles of the foam matter in its initial state. When the ion-ion free path λ_i is much less than both the initial foam particle size b_0 and the distance D_p between them, the foam dynamics can be approximated by an isothermal expansion of plane solid foam elements, followed by an adiabatic compression of the colliding flows. Then, the average size b of the high-density regions in the heated foam is expressed, as follows

$$b = \frac{D_p}{(\beta+1)^{3/2}} \quad , \quad (4)$$

where the coefficient $\beta = 3 \times (\gamma-1)/2$. Thus, the size of the microscopic particles increases during this stage considerably and the dense plasma occupies a substantial part of the distance between the solid elements of the initial foam, explicitly its size is $b = D_p/2.8$ for $\gamma=5/3$.

The final stage of homogenization process, leading to a uniform medium with the average density of porous matter ρ_f , is controlled by the speed of viscous processes. The widening of the dense regions occurs due to the hydrothermal dissipation at the front of shock waves between the high- and low-density regions. The speed of the front widening is approximately equal to the length of ion-ion free path λ_i divided by the time t_s needed for the shock wave propagation to the next dense region. The time t_s is given by the relation $t_s \sim (D_p - b)/V_s$, where V_s is the velocity of the shock wave propagation. Therefore the duration t_h of the final stage of the homogenization is expressed, as follows

$$t_h = \frac{\left(\frac{D_p - b}{\lambda_i} \right)^2}{V_s} \approx 10^{-9} \times \frac{D_p^2 \rho_f}{T^{3/2}} \quad . \quad (5)$$

The numerical value in the second expression of the formula (5) has been derived for $\gamma=5/3$, and time expressed in seconds, length in micrometers, temperature in keV, and density in g/cm^3 . According to the equation (5), the duration t_h of final homogenization stage is approximately $2-3 \text{ ns}$ in the conditions of our PALS experiments, where the foam density is $\rho \approx (8-10) \text{ mg/cm}^3$, and the plasma temperature is estimated $T \sim 1 \text{ keV}$. This value is consistent

with the difference of the experimental breakthrough of energy transfer wave from the theoretical calculations using the approximation of uniform matter.

In the time instant t_f , when the hydrothermal wave front reaches the foam-foil boundary, the pressure of the heated foam matter starts to act on the aluminium foil. The initial value of the pressure accelerating the foil is then

$$P_0 = P_{ht} \left(t=t_f \right) \approx \frac{(\gamma-1) E_{ab}}{\pi \left(\Delta_f + R_L \right)^2 \Delta_f} . \quad (6)$$

The kinetic energy acquired by the aluminum foil is small compared to the laser energy absorbed in the foam layer in the conditions of our PALS experiments. Then, the motion of the aluminum Al-foil may be described in the approximation of adiabatic decline of the acting pressure due to the foam layer expansion and due to the transverse energy transfer inside the foam. The resulting aluminum foil velocity V_s is expressed, as follows

$$V_s = V_{\max} \times \left\{ 1 - \left[1 + \frac{c_0}{\Delta_f} \cdot (t - t_f) \right]^{-1} \right\} . \quad (7)$$

Here $c_0 = (\gamma P_0 / \rho_f)^{1/2}$ is the adiabatic sound velocity, corresponding to the pressure P_0 given by equation (6) and

$$V_{\max} = \frac{c_0 \rho_f \cdot \Delta_f}{\gamma \rho_s \cdot \Delta_s} \quad (8)$$

is the maximum foil velocity reached in the limit of $t \rightarrow \infty$. Here ρ_s denotes the solid foil density and Δ_s is the foil thickness.

The hydrodynamic efficiency η is the ratio of the foil kinetic energy to the absorbed laser energy, given by the expression

$$\eta = \frac{(\gamma-1) \rho_f \cdot \Delta_f}{2\gamma \rho_s \cdot \Delta_s} . \quad (9)$$

Using equations (7) and (9) and assuming 50% laser absorption, the maximum aluminum foil velocities are calculated $V_{\max} = 4.8 \times 10^6$ cm/s, $V_{\max} = 6.7 \times 10^6$ cm/s and $V_{\max} = 8.2 \times 10^6$ cm/s for laser energies $E_L = 92$ J, 173 J, and 238 J, respectively. The calculated hydrodynamic efficiency is $\eta \approx 0.12$.

In the Table 1, the foil velocities measured in the experiment, calculated in our simulations and via our analytical model are compared. A good agreement in the accelerated foil velocities is found for 400 μm thick polystyrene foams. Even if one takes into account that arrival of hydrothermal wave onto the target rear edge is earlier in the simulations than in experiment by about 2 ns, the accord of our simulations with experiment is still preserved. The average rear edge velocities in simulations in the interval 2–5 ns after laser pulse maximum are smaller than average velocities in the interval 4–7 ns by 4–10% only. For the 100 μm thick PVA foam, foil is heated up to 800 eV in the simulation and its expansion leads to an excessive velocity of the rear boundary. In this case, some foil expansion is also detected in interferograms at later times. However, the velocity of the plasma-vacuum

boundary is still in agreement with the analytical model that omits foil expansion. Thus, foil temperature is overestimated in our simulations probably due to an excessive value of the heat flux in the simulation model.

Table 1. (CH)_n is 400 μm thick polystyrene foam with 2 μm Al foil and PVA is 100 μm thick PVA foam of density 5 mg/cm³ with 0.8 μm Al foil. Experimental and simulation velocities are represented by their average values in the interval 4–7 ns after the laser maximum.

Laser energy	Target	v _{exp} (cm/s)	v _{simul} (cm/s)	V _{max} (cm/s)
92 J	(CH) _n	6.0×10 ⁶	4.9×10 ⁶	4.8×10 ⁶
173 J	(CH) _n	8.0×10 ⁶	8.2×10 ⁶	6.7×10 ⁶
238 J	(CH) _n	-----	1.1×10 ⁷	8.2×10 ⁶
238 J	PVA	1.4×10 ⁷	3.5×10 ⁷	1.32×10 ⁷

CONCLUSIONS FOR LASER INTERACTIONS WITH POROUS MATTER TARGETS

Interactions of laser beam of iodine laser PALS with low-density foam targets and acceleration of Al foils by the pressure of heated porous matter have been investigated, both experimentally and theoretically. The speed of the heat wave inside polystyrene foam has been estimated ~ 1.4×10⁷ cm/s from X ray streak measurements. The X ray streak records show no signal near the rear side of the 400 μm thick foam, and the optical interferometry does not observe any sign of low-density plasma behind the accelerated foil, too. This is a strong indication that the foil attached at the rear side of target is accelerated as a whole without significant expansion.

The position of the foil rear side opposite to the laser beam center is measured versus time and the foil velocity and the beginning of the foil motion is derived. Hydrodynamic efficiency up to 12-14 % was calculated from the experimental data. The shape of the accelerated part of the foil is smooth with any signature of small-scale non-uniformities that are present inside the laser beam.

The experimental results are in a good agreement with our two-dimensional hydrodynamic calculations that do not take fine structure of foam material into account. The only exception is the case of the thinner PVA foam where the code predicts much higher rear side velocities due to heating and expansion of the foil material. It indicates that heat flux is overestimated to a certain extent in the simulation code. Consequently, heat conductivity value should be revised in the case when the foam homogenization is not complete during the heat wave propagation. A simplified analytical model has been presented that does not include heating and expansion of the foil on the target rear side. The derived rear side velocities agree well with the experiment and it is another indication that foil is accelerated without significant expansion.

A delay is found in the energy transfer wave propagation in the foam in our experiments in comparison with our theoretical calculations performed in the approximation of low-density homogenous matter. This effect is important for understanding the physics of laser-produced plasma in foam matter. The delay is explained here by the phenomenon of non-equilibrium foam homogenization. During the homogenization period, the fraction of absorbed laser

energy is contained in the energy of oscillatory colliding plasma flows and it does not contribute significantly to hydrothermal wave propagation.

**SELECTED PUBLICATIONS ON DOUBLE PULSE PLASMA
BY MEMBERS OF THE IAEA CRP**

1. A. B. Iskakov, V. F. Tishkin, I. G. Lebo, J. Limpouch, K. Masek, K. Rohlena, *Two-dimensional model of thermal smoothing of laser imprint in a double-pulse plasma*, Physical Review E **61** (2000) 842-847
2. E. Krousky, O. Renner, K. Masek., M. Pfeifer, O. Pacheroova, B. Kralikova, J. Skala, K. Rohlena: *Experimental evidence of thermal smoothing in double-pulse produced plasma*, Laser and Particle Beams **18** (2000) 87-91

**SELECTED PUBLICATIONS ON POROUS MATTER TARGETS
BY MEMBERS OF THE IAEA CRP**

3. M. Kalal, J. Limpouch, E. Krousky, K. Masek, K. Rohlena, P. Straka, J. Ullschmied, A. Kasperczuk, T. Pisarczyk, S. Yu. Gus'kov, A. I. Gromov, V. B. Rozanov, V. N. Kondrashov; *Thermal smoothing by laser-produced plasma of porous matter*, Fusion Science and Technology **43**: (2003) 275-281
4. J. Limpouch, N. N. Demchenko, S. Yu. Gus'kov, V. B. Rozanov, A. Kasperczuk, T. Pisarczyk, M. Kalal, V. N. Kondrashov, E. Krousky, K. Masek, P. Pisarczyk; *Iodine Laser Interactions with Porous Matter*, Book of Proceedings (TuPo2.27), IFSA 2003, September 7 – 12, Monterey, USA
5. J. Limpouch, N. N. Demchenko, S. Yu. Gus'kov, M. Kalal, A. Kasperczuk, V. N. Kondrashov, E. Krousky, K. Masek, P. Pisarczyk, T. Pisarczyk, and V. B. Rozanov, *Laser interactions with plastic foam—metallic foil layered targets*, Plasma Phys. Control. Fusion **46** (2004) 1831-1841
6. M. Kalal, J. Limpouch, E. Krousky, K. Masek, K. Rohlena, J. Skala, P. Straka, A. Kasperczuk, T. Pisarczyk, J. Ullschmied, S. Yu. Gus'kov, V. N. Kondrashov; *Laser Imprint Problem and its Treatment by Double Pulse Plasma and Foam Layers*, Second Research Co-ordination Meeting on *Elements of Power Plant Design for Inertial Fusion Energy*, 4 – 7 November 2003, IAEA HQ, Vienna, Austria
7. J. Limpouch, S. Guskov, A. I. Gromov, M. Kalal, A. Kasperczuk, V. N. Kondrashov, E. Krousky, B. Kralikova, K. Masek, T. Pisarczyk, M. Pfeifer, K. Rohlena, V. Rozanov, J. Skala, J. Ullschmied; *Thin foil acceleration by the pressure of laser-produced plasma of porous matter*, ECLIM-2002 Proceedings, SPIE; vol. 5228 (2003)
8. M. Kalal, *Laser Imprint Problem and its Treatment by Double Pulse Plasma and Foam Layers*, Invited Talk, Institute of Plasma Physics and Laser Microfusion, Warsaw, Poland, 24.2.2004:

9. M. Kalal, *PALS, Laser Imprint and Foam Targets*, Invited Talk, Lawrence Livermore National Laboratory, USA, 27.6.2002
10. J. Limpouch, N. N. Demchenko, S. Yu. Gus'kov, M. Kalal, A. Kasperczuk, V. N. Kondrashov, E. Krousky, K. Masek, P. Pisarczyk, T. Pisarczyk, V. B. Rozanov *PALS Laser Interactions with Foam Targets*, Poster, 31 EPS, London, United Kingdom, June 28 – July 2, 2004
11. M. Kalal, J. Limpouch, N. N. Demchenko, S. Yu. Gus'kov, A. I. Gromov, A. Kasperczuk, V. N. Kondrashov, E. Krousky, K. Masek, M. Pfeifer, P. Pisarczyk, T. Pisarczyk, K. Rohlena, V. B. Rozanov, J. Sinor, and J. Ullschmied, *Interactions of Subnanosecond Laser Pulses with Low-Density Plastic Foams*, Oral, Third IAEA Technical Meeting (IAEA-TM) on *Physics and Technology of Inertial Fusion Energy Targets and Chambers*, Daejon, Republic of Korea, October 11 -13, 2004
12. M. Kalal, N. N. Demchenko, S. Yu. Gus'kov, A. I. Gromov, A. Kasperczuk, V. N. Kondrashov, E. Krousky, J. Limpouch, K. Masek, M. Pfeifer, P. Pisarczyk, T. Pisarczyk, K. Rohlena, V. B. Rozanov, and J. Ullschmied, *Thermal Smoothing of Laser Imprint in Double-Pulse Plasma*, Oral, IAEA Research Coordination Meeting (IAEA-RCM) for the Coordination Research Project on *Elements of power plant design for inertial fusion energy*, Daejon, Republic of Korea, October 14 – 15, 2004
13. M. Kalal, S. Yu. Gus'kov, A. Kasperczuk, V. N. Kondrashov, E. Krousky, J. Limpouch, K. Masek, T. Pisarczyk, K. Rohlena, J. Skala, and J. Ullschmied, *Prague Asterix Laser System (PALS) activities in laser fusion oriented research*, Invited Talk, Asia – Pacific Laser Symposium (APLS 2004), Yongpyong, Republic of Korea, March 1 – 6, 2004
14. M. Kalal, S. Yu. Gus'kov, A. Kasperczuk, V. N. Kondrashov, E. Krousky, J. Limpouch, K. Masek, T. Pisarczyk, K. Rohlena, J. Skala, and J. Ullschmied, *Foam Target and Double-Target studies at Prague Asterix Laser System (PALS)*, Invited Talk, GSI, Darmstadt, Germany, June 6, 2004

SELECTED PUBLICATIONS ON DOUBLE TARGETS AND CRATERS BY MEMBERS OF THE IAEA CRP

1. T. Pisarczyk, S. Borodziuk, A. Kasperczuk, S. Gus'kov, I.Ya. Doskach, V. Rozanov, J. Ullschmied, K. Jungwirth, B. Kralikova, E. Krousky, K. Masek, M. Pfeifer, K. Rohlena, J. Skala, M. Kalal, J. Limpouch, P. Pisarczyk; ***Experimental and Theoretical Investigations of Craters Formation in Solids in PALS Experiments***, CD of Proceedings, PLASMA 2003, September 9–12, Warsaw, Poland
2. T. Pisarczyk, S. Borodziuk, A. Kasperczuk, K. Jungwirth, B. Kralikova, E. Krousky, K. Masek, M. Pfeifer, K. Rohlena, J. Skala, J. Ullschmied, M. Kalal, J. Limpouch, P. Pisarczyk; ***Application of the Laser Simulation Method of Crater Creation in the Laser-Al Solid Target Experiment on the PALS Facility***, French–Polish Seminar on Plasma 2003, Bordeaux, France
3. T. Pisarczyk, S. Gus'kov, I. Ya. Doskach, A. Kasperczuk, S. Borodziuk, M. Kalal, E. Krousky, J. Limpouch, K. Masek, P. Pisarczyk, K. Rohlena, V. Rozanov, J. Ullschmied; ***Experimental and Theoretical Investigations of Craters Formation in Solid Targets***

Under the Action of Powerful Laser Pulse, CCPPA 2003 - First Cairo Conference on Plasma Physics and Applications, 11-15 October 2003, Cairo, Egypt.

4. S. Borodziuk, A. Kasperczuk, T. Pisarczyk, K. Rohlena, J. Ullschmied, M. Kalal, J. Limpouch, P. Pisarczyk; ***Application of laser simulation method for the analysis of crater formation experiment on PALS laser***. Czechoslovak Journal of Physics Vol. 53 (2003), 799-810, ISSN 0011-4626
5. I. Ya. Doskach, T. Pisarczyk, S. Gus'kov, K. Jungwirth, M. Kalal, A. Kasperczuk, B. Kralikova, E. Krousky, J. Limpouch, K. Masek, M. Pfeifer, K. Rohlena, V. Rozanov, J. Skala, J. Ullschmied; ***Laser-produced post-pulse crater formation in solids observed in PALS facility interaction experiment***, ECLIM 2002 - 27th European Conference on Laser Interaction with Matter, SPIE Vol. 5228 (2003), Eds: O. N. Krokhin, S. Yu. Gus'kov, Yu. A. Merkul'ev, 121-130, ISBN 0-8194-5101-0
6. S. Borodziuk, A. Kasperczuk, T. Pisarczyk, S. Gus'kov, J. Ullschmied, B. Kralikova, K. Rohlena, J. Skala, M. Kalal, P. Pisarczyk; ***Investigation of plasma ablation and crater formation processes in the PALS laser facility*** (accepted for publication in *Optica Applicata*)
7. S. Yu. Gus'kov, T. Pisarczyk, I. Ya. Doskach, A. Kasperczuk, M. Kalal, S. Borodziuk, K. Jungwirth, B. Kralikova, E. Krousky, J. Limpouch, K. Masek, M. Pfeifer, P. Pisarczyk, K. Rohlena, J. Skala, J. Ullschmied; ***Laser – Produced Post - Pulse Craters in Solids*** (submitted to *Quantum Electronics*)
8. T. Pisarczyk, S. Borodziuk, A. Kasperczuk, K. Jungwirth, B. Kralikova, E. Krousky, K. Masek, M. Pfeifer, K. Rohlena, J. Skala, J. Ullschmied, M. Kalal, J. Limpouch, P. Pisarczyk; ***Application of the Laser Simulation Method of Crater Creation in the Laser-Al Solid Target Experiment on the PALS Facility***, Journal of High Temperature Material Processes 7 (2003) 319-326
9. S. Borodziuk, Ya. Doskach, S. Gus'kov, K. Jungwirth, M. Kalal, A. Kasperczuk, B. Kralikova, E. Krousky, J. Limpouch, K. Masek, M. Pfeifer, P. Pisarczyk, T. Pisarczyk, K. Rohlena, V. Rozanov, J. Skala, J. Ullschmied; ***Experimental and theoretical investigations of craters formation in aluminum target on PALS experiment***, Nukleonika 49 (2004) 7–14
10. S. Borodziuk, A. Kasperczuk, T. Pisarczyk, N. N. Demhchenko, S. Yu. Gus'kov, V. B. Rozanov, M. Kalal, J. Limpouch, J. Ullschmied, K. Rohlena, J. Skala, V. N. Kondrashov, P. Pisarczyk, ***Application of the 3-frame interferometry and the crater replica method for investigation of laser accelerated macroparticles interacting with massive targets in the Prague Asterix Laser System (PALS) experiment***, Optica Applicata, Vol. XXXIV, No. 3 (2004) 385-403

Laser driven ablative surface instability in IFE

N. Rudraiah

National Research Institute for Applied Mathematics (NRIAM),
Jayanagar, Bangalore, India,

Abstract. The paper proposes to investigate the following surface instabilities at the ablative surface of IFE target: Rayleigh – Taylor Instability (RTI), Kelvin- Helmholtz Instability (KHI), Richtmyer – Meshkov Instability (RMI). We were able to investigate only RTI because of considering four mechanisms to reduce the growth rate of RTI at the ablative surface of IFE target.

DESCRIPTION OF RESEARCH CARRIED OUT

The depletion of fossil fuel and atmospheric vagaries have tremendously strained the provision of an uninterrupted energy supply required for the overall development of a country. A solution for this is to find new unconventional sources of energy that are affordable, practical and that provide an uninterrupted supply of energy that does not have as adverse an impact on the environment as does fossil fuel. International Atomic Energy Agency (IAEA) has realized (see Hogan and Bertel 1995) that of the many unconventional methods of power generation, one of the effective, efficient and everlasting sources is direct drive inertial fusion heading towards high-gain laser Inertial Fusion Energy (IFE). To achieve efficient extraction of IFE, it is essential not only one must produce a small hot spot within the imploding target from which thermonuclear burn can ignite but also control surface instabilities at the ablative surface of the IFE target. Recent simulations of a high-gain implosion with a mitigated requirement for pellet and irradiation uniformity include the following three types of surface instabilities:

- 1) Rayleigh-Taylor Instability (RTI) due to heavy plasma accelerated by lighter plasma
- 2) Kelvin Helmholtz Instability (KHI) due to shear produced at the interface between two plasmas
- 3) Richtmyer – Meshkov Instability (RMI) due to shock wave driven by the main pulse.

For efficient extraction of IFE there is a need to reduce the growth rate of these surface instabilities. At present only mitigation of the RTI in IFE target has been extensively investigated using the following mechanisms:

- (a) Gradual variation of density gradient to stabilize RTI under the assumption of inviscid, heterogeneous fluid without surface tension. Heterogeneity leads to equations with variable coefficients.
- (b) Non-viscous compressible fluid without surface tension where the compressibility makes the analysis very cumbersome.
- (c) Ablative surface with foam. The foam is deformable and may melt away at that high laser radiation.

To avoid the complications involved in the above mechanisms, and to provide a more efficient and economically viable system we have proposed in this CRP Research Project the following mechanisms.

- Case 1 The use of nanostructured porous lining at the ablative surface of the target.
- Case 2 The use of external constraint of magnetic field at the ablative surface of IFE target filled with an electrically conducting plasma.
- Case 3 The external constraint of magnetic field at the ablative surface lined with nanostructured porous lining of IFE filled with finitely conducting plasma.
- Case 4 The use of external constraint of electric field and variation of the electrical conductivity of plasma with temperature in a finite thickness layer of poorly conducting viscous plasma.
- Case 5 The effect of electric field, variation of conductivity with temperature and nanostructured porous lining in a finite thickness layer of poorly conducting plasma.
- Case 6 Replacing hallow shell with heterogeneous fluid saturated porous shell

The main objective of considering the above mechanisms (cases 1 to 6) in this project is to reduce the growth rate of RTI at the ablative surface considerably compared to the existing mechanisms (a) to (c) given above. In the cases (1) to (3) we use surface conditions in addition to boundary conditions to derive the dispersion relation for the growth rating using the usual normal mode technique. However in case 4 we use only boundary conditions together with a moment technique combined with Galerkin technique to derive the dispersion relation for the growth rate of RTI. From this general dispersion relation we derive particular cases relevant to effective reduction of the growth rate of ablative surface of IFE target.

RESULTS OBTAINED

The significant results obtained on the reduction of the growth rate of RTI at the ablative surface of IFE target using nanostructured smart porous lining at the ablative surface together with the external constraints of magnetic or electric fields are listed below:

- 1) Our Original and significant contribution pertains to the derivation of analytical expression for the dispersion relation as given by eq (2) which incorporates the constraints of
 - a) nano structured porous lining with incompressible viscous fluid in the presence of surface tension.
 - b) the effect of magnetic field in a conducting plasma of finite electrical conductivity.
 - c) the effect of electric field in a poorly conducting plasma of infinitesimal electrical conductivity.

These constraints reduce the growth rate of RTI significantly. This dispersion relation involves all the relevant physical parameters required for a suitable design of IFE target.

- 2) We have also derived an analytical expression for the growth rate considering laser radiation effect. This is done by solving the energy equations for shell and porous regions. The growth rate obtained, incorporating the laser radiation effect, will also involve all the relevant physical parameters required for the design of efficient IFE target.

The above works on RTI have been done during the last three years (2001-2004). In the last year of the project i.e. 2003-2004, we have just started investigating the Kelvin-Helmholtz instabilities at the ablative surface. The preliminary work with nano structure porous lining has been completed and obtained an analytical expression for the dispersion relation as in the case of RTI. This work was presented at the third and final CRP meeting held at KAIST Daejeon, South Korea during October 11 – 15, 2004.

CONCLUSIONS DRAWN

In IFE, it is known (see Manheimer et al 1982) that a continuous inward acceleration of spherical shells, by ablation pressure, alters the outer surface. The spherically symmetric calculations of the behaviour of laser direct driven fusion targets have demonstrated major advantages of employing ablatively imploded spherical shells for obtaining optimum performance. The use of solid pellets in the form of shells as opposed to the solid sphere has been shown to reduce significantly the peak laser power required to drive successfully a target of fixed mass. To overcome the major inconvenience due to the location of segregation of the inner skin of shells, hallow shells have been employed (see Boequet Blondeau et al 1990). The main purpose of using hallow shell has been to reduce the peak laser power requirement from the laser which decreases as the ratio A of shell radius r to the thickness Δr . That is

$$A = r / \Delta r$$

However, the hallow shell targets are shown to be hydrodynamically unstable in the ablation region where the pressure and density are of opposing signs (see McCrery and Morse 1976, Rudraiah et al 2003 b). It is observed that the continuous inward acceleration of a shell by the ablation pressure applied to outside surface causes surface instabilities of the type RTI, KHI and RMI at the ablative surface mainly due to the opposing nature of the pressure and density gradients. These surface instabilities caused by direct drive produce asymmetry in the pellet reducing the efficiency of IFE. For efficient extraction of IFE it is essential to propose mechanisms to mitigate the growth rate of surface instabilities of the type mentioned above. At present the control of the growth rate of RTI in IFE (in which heavy fluid is supported by a lighter fluid that is the lighter fluid accelerating the denser fluid is similar to the classical RTI but complicated with finite density scale lengths) is mainly due to the following mechanisms:

1. Gradual variation of density which stabilises the surface under the assumption of an incompressible inviscid heterogeneous fluid without surface tension (see Mikaelian 1992)
2. The inviscid compressible fluid without surface tension also plays a role in ablative stabilisation (see Takabe et al 1985, Kilkenney et al 1994, Betti et al 1995, Lindl 1995, Bychkov et al 1994).
3. The IFE –relevant ablation layers with foam have been considered (see Sethian et al 1999, Batani et al 200) to reduce the RTI growth rate.

In order to over come the complications involved in these mechanisms we have proposed in this CRP project the following mechanisms to mitigate the growth rate of RTI with the objective of proposing more efficient, economically viable and simple way of reducing the growth rate than the existing mechanisms given above at the ablative surface of IFE target which would literally give us the energy equivalent of oceans of oil. This is based on the fact that sea water contains about 40g of deuterium (D) and 0.1g of lithium per tonne, every barrel of sea water contains the energy equivalent of about 30 barrels of oil in D-fuel and about one-fifth of a barrel of oil in D-T fuel. A volume of sea water equal to the top meter of the Earth's ocean would yield enough fuel to supports D-T fusion reactors for thousand of years of electricity production at today's rate of usage.

Case 1: Nano structured Porous Lining at the ablative surface.

To replace the hallow shell we propose the use of nano structured porous lining at the ablative surface of IFE target with surface tension at the interface between the fluid saturated porous lining and the thin shell filled with viscous incompressible fluid. In other words, the hallow shell partly containing nanostructured fluid saturated porous layer abetting the ablative

surface and the remaining part filled with viscous incompressible fluid with or without the presence of laser radiation.

The DT fluid in nanostructure porous layer is assumed to be heavy lying on the top of lighter fluid in the remaining part of the shell. We deal only with linear two-dimensional RTI by considering infinitesimally small disturbance superposed on the basic state which is quiescent. We derived the general basic equations using ensemble averages involving a bilinear parameter X_p in such a way that $X_p = 0$ gives equations for the fluid shell and $X_p = 1$ for porous lining. Such general equations are useful in numerical computation of non-linear problem because we can get the results for both fluid shell and porous lining simultaneously. To study the RTI based on physical consideration we use stokes and lubrication approximations following Rudraiah et al (1997). To solve the resulting equations involving surface tension we use the following boundary and surface conditions.

- 1) The no slip boundary condition at the rigid surface.
- 2) The slip condition at the interface between fluid shell and porous layer
- 3) The dynamic condition involving surface tension and normal stress. This surface condition is expressed in terms of the bond number B which is assumed to be very small.
- 4) The Kinematic condition at the interface.

For inviscid compressible fluid in the absence of surface tension Takabe et al (1985) have obtained an analytical expression for the growth rate, n , of the form

$$n = 0.9\sqrt{lg} - \beta \ell \mathcal{G}_a \quad (1)$$

where $\beta = 3$ or 4 , l the wave number and \mathcal{G}_a transverse velocity at the interface.

For the first time in the IFE literature we have obtained, for viscous incompressible DT-fluid in the presence of surface tension and a nanostructured porous lining at the ablative surface, the analytical expression for the growth rate of the form,

$$n = \frac{1}{3} \ell^2 \left(\delta - \frac{\ell^2}{B} \right) - \beta \ell \mathcal{G}_a \quad (2)$$

which is analogous to one derived by Takabe et al (1985) given by (1). In (2) ℓ is the wave number, B the bond number based on the surface tension, $\delta = 1$ in the absence of laser radiation and $\delta = \theta_{p1} - \theta_{f1}$ in the presence of laser radiation, θ_p and θ_f are the temperatures

in the porous lining and fluid shell, respectively, $\beta = \frac{3\alpha\sigma}{4 + \alpha\sigma}$ and $\mathcal{G}_a = \frac{(4 + \alpha\sigma)}{12(1 + \alpha\sigma)} \ell (\delta - \ell^2) \alpha$

is the slip parameter at the interface and $\sigma = \frac{h}{\sqrt{k}}$ is the porous parameter, k is the permeability of porous lining. Experiments of Beavers and Joseph (1967) reveals $\alpha = 0.1$, experiments of Rajasekhar (1974) and Ranganna (1982) reveal $\alpha = -0.1$ and 4.0 and the experiments of Vortmeyer et al reveal $\alpha = 12$. In these experiments they have used foam metal for which $k = (1.1 \text{ to } 2.7) 10^{-5}$ and for aloxite material $k = (1.0 \text{ to } 2.48) 10^{-6}$ and $\epsilon = 0.016$ to 0.027 .

Takabe et al (1985) have shown using (1) the reduction of growth rate compared to the classical growth rate as 45%, where as in our case using (2) there is a reduction of growth rate 78.57% compared to the classical growth rate in the presence of surface tension for $\alpha = 0.1$ and $\sigma = 4$. This reduction of growth rate is very considerable and useful in the effective design of IFE target.

Setting $n=0$ in (2), we get

$$\ell_{ct} = \sqrt{B},$$

the cutoff wave number above which RTI is stabilized. Similarly, the maximum wave number, ℓ_m , is obtained from (2) in the form

$$\ell_m = \sqrt{\frac{B}{2}}$$

and the corresponding maximum growth rate, n_m , is obtained from (2) as

$$n_m = \frac{B(4 + \alpha\sigma)}{48(1 + \alpha\sigma)}$$

The maximum growth rate n_{mb} , in the absence of porous lining, is

$$n_{mb} = \frac{B}{\sqrt{2}}$$

which we call the classical growth rate.

Therefore

$$\frac{n_m}{n_{bm}} = \frac{(4 + \alpha\sigma)}{4(1 + \alpha\sigma)} \quad (3)$$

From this one can easily calculate the reduction of maximum for the growth rate n_m compared to the classical growth rate n_{bm} for the specific values of α and σ as given in the following Table 1.

Table 1. The ratio $G_m = n_m/n_{bm}$, of maximum growth rate

α	σ	G_m
0.1	4	78.57%
0.1	20	60%
4.0	20	26%

This analytical expression for the ratio of growth rate is original and significant which provides a suitable mechanism for reduction of growth rate in the design of IFE target.

Case 2: External constraint of magnetic field. In a finitely electrically conducting plasma (MHD)

We have studied the RTI due to direct laser drive accelerating the ablative surface of a thin electrically conducting incompressible plasma shell in an IFE target in the presence of a transverse magnetic field using linear stability analysis with the object of reducing the growth rate of RTI.

Following the analysis of case 1, explained above, we obtained the dispersion relation analogous to (2) with

$$\beta = \frac{M^3 - 3(M - \tanh M)}{3(M - \tanh M)}, \quad g_a = \frac{(M - \tanh M)}{M^3} \ell \left(\delta - \ell^2 / B \right)$$

where $M = \mu_h h H_0 \sqrt{\frac{\sigma}{\mu}}$ is the Hartmann number, μ_h the magnetic permeability, μ the

viscosity, σ the electrical conductivity, h the width of the shell and H_0 is the applied transverse magnetic field and δ has the same definition as in the case 1. Following the analysis of case 1, we obtain

$$\frac{n_m}{n_{bm}} = \frac{3}{M^3}(M - \tanh M) \quad (4)$$

This analytical relation has the same advantages as explained in case 1. Choosing a suitable values of M, we can reduce the growth rate compared to the classical growth rate n_{bm} . For example this ratio for different values of M are tabulated in Table 2.

Table 2. $\frac{n_m}{n_{bm}}$ for different values of M

M	$\frac{n_m}{n_{bm}}$
10^{-2}	0.99996
10^{-1}	0.99602
10^0	0.71522
10^1	0.00003

From this we conclude that choosing a suitable strength of transverse magnetic field (i.c.M) it is possible to reduce the growth rate considerably. This was published in the Journal of Laser and Particle Beam in References 3.

Case 3: In Case 3 with magnetic field together with nanostructured porous lining Rudraiah (2004) has shown

$$\beta = \frac{(M^3 - 3(M - thM) + \alpha\sigma(M^2 - 3)thM + 6\alpha\sigma(chM - 1)(MchM))}{3\left(M - thM + \alpha\sigma thM + \frac{2\alpha\sigma(1 - chM)}{MchM}\right)}$$

$$\text{and } v_a = \left(\frac{M - thM + \alpha\sigma thM + \frac{2\alpha\sigma(1 - chM)}{MchM}}{M^3\left(1 + \alpha\sigma \frac{thM}{M}\right)} \right) l \left(\delta - \frac{l^2}{B} \right)$$

These results for the ratio of maximum growth rate namely $G_m = \frac{n_m}{n_{bm}}$, are computed and represented in Table 3.

Table 3.

Authors	β	G
Rudraiah (2003) Case 1	0.75	0.79 ($\alpha = 0.1, \sigma = 4$) (79%)
Rudraiah et al (2004) Case 2	0.00004 0.003999981 0.398176	0.99996 (for M = 0.01) 0.99602 (for M = 0.1) 0.71522 (for M = 1.0) 0.02700 (for M = 10) 0.00030 (for M = 100)
Rudraiah et al (2004) Case 3	--	0.81 (for $\Delta = 0.1$) 81%

Case 4: External constraint of Electric field in a poorly electrically conducting plasma (EHD, electrohydrodynamics).

We have studied the linear RTI of direct laser driven accelerated ablative surface of a thin poorly electrically conducting incompressible plasma shell in an IFE target in the presence of a transverse electric field where electrically conductivity σ ($\ll 1$) increases with temperature with the objective of reducing the RTI growth rate at the ablative surface. As in the previous cases of 1 and 2 we have obtained

$$\frac{n_m}{n_{bm}} = (1 - \Delta)^2 \quad (5)$$

where $\Delta = \frac{\epsilon_0 v^2}{2h^2 \delta}$, ϵ_0 is the dielectric constant, V the applied potential due to electrodes,

h and δ have the same meaning as in the cases of 1 and 2 given above. The positive or negative sign in (5) depends on whether the applied electric potential is in the direction (+ve sign) or opposing (-ve sign) gravity. Suitably choosing Δ it is possible to reduce the growth rate considerably. The results are obtained for different values of Δ and are tabulated in the following Table 4.

Table 5. Ratio $G_m = \frac{n_m}{n_{bm}}$ for different values of $\Delta \leq 1$

Δ	G_m	%
10^{-2}	0.98	98%
10^{-1}	0.81	81%
10^0	0.00	

The results are published in the proceedings of Advances in Fluid Mechanics (2004) published by Tata McGraw Hill, New Delhi.

Case 5: In Case 5, the combined effects of the external constraint of electric field and nanostructured porous lining on growth rate is obtained, following the procedures of cases (3) to (4), in the form

$$n = n_b - \frac{\alpha\sigma}{4(1 + \alpha\sigma)} \ell^2 \left(1 - \ell^2/B\right) \pm \frac{(4 + \alpha\sigma)}{12(1 + \alpha\sigma)} \ell^2 \Delta \quad (6)$$

The results for the ratio of maximum growth rate are computed and represented in table 5 by considering negative sign in (6).

Table 6. $G_m = \frac{n_m}{n_{bm}}$ in the presence of nanostructured porous lining

α	σ	Δ	G_m	%
0.1	4.0	0.1	0.64	64%
4.0	4.0	0.1	0.24	24%
4.0	8.0	0.1	0.22	22%
4.0	20.0	0.1	0.21	21%

This Table reveals that the suitable values of α, σ and Δ reduce the growth rate of RTI considerably.

Case 6: Hollow shell replaced by Porous Shell

In this case we propose the use of porous shell instead of hollow shell to reduce the growth rate of RTI at the ablation surface of IFE target. Physically the reduction of growth rate by porous shell is attributed to the resistance offered by the solid portion of a porous medium. We show that the permeability of the porous region scaled with the Reynolds number decreases considerably the growth rate of RTI compared to that of a hollow shell resulting in an increase in the efficiency of the fusion reaction and the results are published in (2003 b), in the International Journal given in reference 2.

We consider a densely packed heterogeneous fluid saturated shell in the presence of surface tension. In this densely packed porous shell the basic momentum equation is governed by Darcy equation.

$$\rho \frac{\partial \vec{q}}{\partial t} = -\nabla p - \frac{\mu}{k} \vec{q} - \rho \vec{g} + \sum T_s \nabla_1^2 z_1 \delta(z - z_s) \quad (7)$$

$$\nabla \cdot \vec{q} = 0, \quad \frac{\partial \rho}{\partial t} + (\vec{q} \cdot \nabla) \rho = 0 \quad (8)$$

Eliminating the pressure p from (7) using (8) and using normal mode solution of the form $f(s, y, z, t) = f(z) e^{i(\ell x + m y) + n t}$

We get the stability equation

$$D(\rho D w) + \frac{\mu}{nk} D^2 w - \alpha^2 \left(\rho + \frac{\mu}{nk} \right) w + \frac{\alpha^2}{n^2} g(D\rho) w - \frac{\alpha^4}{n^2} \sum T_s \delta(z - z_s) w = 0 \quad (9)$$

where w is the z components of Darcy Velocity \vec{q} , μ the viscosity, k the permeability ρ the density of fluid, n the growth rate and $\alpha^2 = \ell^2 + m^2$, ℓ and m are the wave numbers and T_s is the surface tension.

Instead of following the procedure explained in cases 1 to 5 explained above we follow the moment method to derive the dispersion relation using Galerkin technique where we use the trial function $w = e^{-\alpha |z|}$. We multiply (9) by W^m (m=0 moment method and m=1 energy method) and integrate with respect to z and use the boundary conditions and the above trial function with m=0 to get the dispersion relation

$$n^2 = n_b^2 - \alpha g \mathcal{G}_a \quad (10)$$

The details are omitted and are given in our research paper reference 2 given in the end. To know the validity of the results we obtain the results for non-porous shell from (10) in the limit of $k \rightarrow \infty$ and we found agreement with those of Mikaelean (1986) for non-porous media. Several particular cases like large blow off thickness i.e. $h \rightarrow \infty$, long wave length perturbation, large shell thickness $\delta h \rightarrow \infty$, short wave length perturbation ($\alpha \gg \beta$), absence of shell region ($\delta h \rightarrow 0$), finite shell thickness i.e δh finite instead of $\delta h \rightarrow 0$ or $\delta h \rightarrow \infty$ are obtained. The dispersion relation (10) is computed numerically for different values of $\beta \delta h$, modified Reynolds number R and Bond number B and we found that the porous layer, surface tension or combined both the porous layer and surface tension reduce the growth rate considerably. Finally we conclude that a porous shell is more efficient then the hollow shell in the efficient extraction of IFE.

In the case of laser radiation the energy equation for thin film takes the form

$$v_a \frac{\partial T_f}{\partial y} = \kappa_f \frac{\partial^2 T_f}{\partial y^2} + I_0 \Omega e^{-\Omega y} \quad (11)$$

and for porous lining takes the form

$$0 = \kappa_f \frac{\partial^2 T_p}{\partial y^2} \pm I_0 \Omega e^{-\Omega y} \quad (12)$$

where T is the temperature, suffixes f and p on T denote, respectively, the T for fluid in the shell and in the porous lining, I_0 is the initial intensity of laser radiation, Ω is the absorption frequency and the wave length is $0.53\mu\text{m}$. For computational purpose, we have chosen laser radiations of 2×10^{13} , 10^{14} and 5×10^{14} watts cm^{-2} and the frequency of the order 2×10^{13} . These energy equations have been solved using the following two sets of boundary conditions:

- Set 1. Isothermal boundary conditions at both the boundaries
 Set 2. Lower boundary isothermal and upper boundary – radiation.

The results are obtained and published in the papers enclosed at the end of this summary.

CITATION OF PERIODICALS REPORTING WORK DONE UNDER THIS CONTRACT

(i)

- 1) Effect of Porous Lining on Reducing The Growth Rate of RTI in the IFE Target By N. Rudraiah, Fusion Science and Technology, Vol 43, May 2003, Pages 307 – 311.
- 2) Laser Driven Ablative Surface Instability In IFE By Prof. N. Rudraiah, P. Sridharan and Tare Desai, Int. J. of Applied Mechanics and Engineering, Vol 8, No.4 pages 665 – 676, 2003.
- 3) Effect of a Magnetic field on the growth rate of the RIT of a laser accelerated thin ablative surface By N. Rudraiah, B. S. Krishnamurthy, A. S. Jalaja and Tara Desai, Laser and Particle Beams, Vol 22, Pages 29-33, 2004.
- 4) Electrohydrodynamic Rayleigh – Taylor Instability In A Finite Thickness Layer of Poorly Conducting of Viscous Fluid By N. Rudraiah, I. S. Shivakumara and Krishna B, Chavaraddi Procs. Int. Symposium on Advances in Fluid Mech. Tata McGraw Hill, 2004
- 5) Effects of Magnetic Field, Laser Radiation and Nano structure Porous Lining At the Ablative surface of IFE Target By N. Rudraiah presented at the second RCM meeting of IAEA held at Vienna, Austria, during November 4 – 7, 2003, (submitted for publication)
- 6) Kelvin – Helmholtz Instability of A viscous thin film past a nanostructure porous lining By N. Rudraiah, presented at CRP third and final meeting held in KAIST, Dajeon, South Korea (submitted for publication).

(ii) Other relevant literature references

- 1) Use of Hollow Shell IFE Target To Generate IFE By Boequet Blondeau, R, Pitruault, L, Badeau J. B. and Dumount R., Ponter Generation Technology, Richard Knox Ed, Pages 141–146, 1990
- 2) Steady State Planar Ablative Flow By Mancheiner W.M., Colombant D. G. and Gardner J.H., Phys. Of Fluids, Vol. 25, No. 9 pages 1644–1650, 1982
- 3) “Approximate Treatment of Density Gradients In RTI By Mikaelian K. O. Phys. Rev. Vol. A33 No. 2 pp 1216–1222, 1986

- 4) RTI in stratified Fluids By Mikaelian, K.O. Phys. Rev. Vol. A 26, No. 4, Pages 2140 – 2158, 1982
- 5) Coupled parallel Flows in a channel and Bounding Porous Medium of Finite Thickness By N. Rudraiah, ASME J. of LFluid Eng, Vol. 107, pages 321– 28, 1985
- 6) The effect of oblique Magnetic Field on the Surface Instability of A finite Conducting LFluid Layer By N. Rudraiah, B. S. Krishnamurthy, R. D. Mathad, Acta Mech. Vol. 119, page 165, 1996
- 7) The RTI of a viscous Fluid Layer with viscosity Stratification, By N. Rudraiah, R.D. Mathad and H. Betigeri, Current Sci, Vol. 72, No. 6, Page 391, 1997
- 8) Self Consistant growth rate of the RTI in an Ablative accelerating plasma By H. Takabe, K.K. Mima, L. Montierth and R. L. Morse, Phys. Fluids Vol 28, No. 12, Page 3676, 1985
- 9) Laser Driven IFE; Present and Prospective By S. Nakai and K. Mima Rep. Prog. Phys. Vol. 67, pages 321-349, 2004.

AN EXPLANATION OF ANY SIGNIFICANT DEPARTURE FROM THE LEVEL OF ACTIVITY FORESEEN BY THE CONTRACT

We proposed to investigate the following surface instabilities at the ablative surface of IFE target:

- 1) Rayleigh – Taylor Instability
- 2) Kelvin- Helmholtz Instability
- 3) Richtmayer – Meshkov Instability

We were able to investigate only RTI because of considering four mechanisms to reduce the growth rate of RTI at the ablative surface of IFE target. We have just initiated KHI concerning only the mechanism of porous lining. We have to still investigate KHI for other Mechanisms we have to still investigate MRI. If, IAEA extend our CRP for further period of three years, we can complete investigating the remaining problems.

TARGET TECHNOLOGY

Extension of free-standing target technology on IFE requirements

E.R. Koresheva, I.V. Aleksandrova, G.D. Baranov, S.V. Bazdenkov, V.I. Chtcherbakov, E.L. Koshelev, B.V. Kuteev, A.I. Nikitenko, S.M. Tolokonnikov, I.E. Osipov, I.D. Timofeev, T.P. Timasheva, L.S. Yaguzinskiy

Lebedev Physical Institute of RAS, Moscow, Russian Federation

Abstract. Inertial fusion energy (IFE) research indicates that the energy generation by means of cryogenic target compression requires that targets must be injected to the target chamber center at a rate of about several Hz. That means that the operation with free-standing targets is one of general IFE requirements.

INTRODUCTION

Technologies based on using the free-standing targets (i.e. FST-technologies) in each step of cryogenic target fabrication are the research area that has been intensively explored at the Lebedev Physical Institute of Russian Academy of Sciences (LPI) since 1989. A prototypical target system has been created at LPI, which operates with 5-to-25 free standing targets at one time [1]. The transport process is target injection between fundamental system elements: shell container – layering channel – test chamber. The targets move downward along the layering channel in a rapid succession - one after another, which results in a repeatable target injection into the test chamber (Fig.1). During the target movement inside the layering channel, the fuel freezing goes due to the heat removal through the contact area between the shell and the cold wall of the channel, while layer symmetrization goes due to target random rotation. Depending on the layering channel geometry, the target residence time inside it may vary in the range of 1÷15 sec.

Using the created system we have demonstrated, on a reduced scale, the main steps of IFE targets supply: D₂-fuel filling, cryogenic layering and injecting the millimeter size targets into the test chamber with a rep-rate of 0.1 Hz [2,3].

In this report, we address the study being done for an issue of the FST-technologies extension on IFE requirements related to the activity under the IAEA Research Contract #11536/RBF over the period of 2000-2004.

The scientific scope of the project #11536/RBF are as follows:

1st year activity: Theory, simulation program and numerical experiments for modeling the FST for reactor-scaled targets production.

2nd year activity: Further development of the design of the existing layering module and equipment, focusing on the layering module/injector assembly.

3rd year activity: Development of a full-scaled scenario for repeatable IFE target fabrication and injection based on the FST technologies.

4th year activity: Development of the optical system for fast threshold characterization based on holographic method of image recognition.

The main results obtained under the implementation of the Contract #11536/RBF have been reported at a number of IAEA Meetings and other international conferences [2-18] and published in 7 papers [5,6,19-23]. The results are presented as follows.

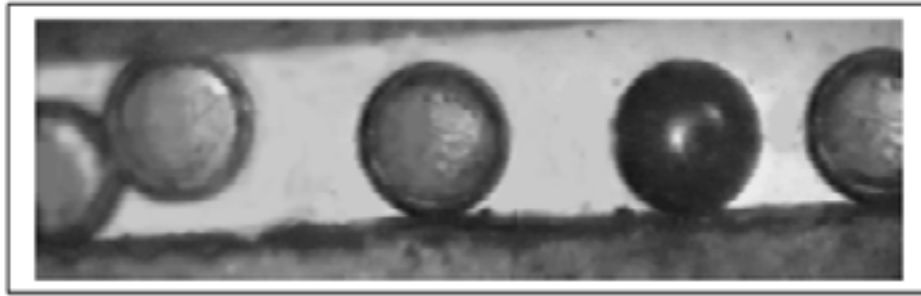


Figure 1. Cryogenic targets injection from the layering module into the test chamber with the rate of 0,1 Hz. CH shells of 1 mm-diam. with 90 μ m-thick H₂ solid layer.

FST TECHNOLOGIES FOR IFE TARGETS PRODUCTION

The FST layering simulation code was first developed for millimeter size targets [20]. It is based on solving the Stephen's problem for moving boundaries between the fuel phases (gas, liquid and solid) and for nonlinear boundary condition onto the outer shell surface. Then the code was adaptable and scalable for numerical experiments with reactor targets. As a result of these activities, it has been well documented (theoretically and experimentally) that the FST layering method forms thick solid cryogenic layers (up to 100 μ m) inside moving polymer shells (1.8 mm-diam.) for the time less than 15 s.

Theoretically we considered two configurations of a classical high gain target: CHGT-1 (4 mm diam. and 45 μ m-thick CH shell with 200 μ m-thick fuel layer) and CHGT-2 (5.5–6 mm diam. and 300–500 μ m-thick CH shell with fuel layer of 200–300 μ m-thick). The estimated work area to form CHGT1 is the following [14, 19]: the fill pressure is about 423atm (for D₂) and 427 atm (for DT); gas fill time by diffusion is about 14 hours for D₂ (16 hours for DT- mixture); the layering time does not exceed 15 s for initial fuel temperature before layering equal to 26 K (Fig.2; χ is the relative contact area between the target and the channel wall). This allows to apply the existing layering module with a spiral channel, which provides the target residence time in the channel in the range of 4–15 s. In the estimations the Young's modulus of CH shell is 3.83×10^9 Pa, D₂-permeability factor is 6×10^{-15} mol/m³ Pa. This allows carrying out first experiments on reactor target formation by FST using the existed layering module.

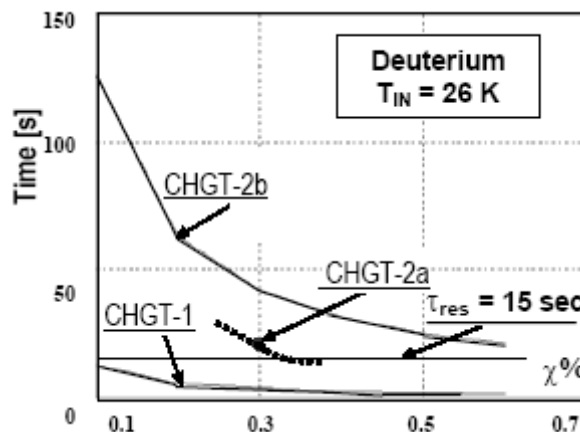


Figure 2. The layering time vs. the parameter χ .



Figure 3. In the R&B cell layer symmetrization and freezing take place in the same small area.

The CHGT2 is noted for its thick polystyrene shell with a low thermal conductivity, which results in a considerably long layering time: between 66 and 127 s, which depends on the shell thickness (Fig.2). That means that the existing layering module should be modified. In this regard we created and tested a miniature device, so-called rotating and bouncing cell (R&B cell), which is mounted at the bottom of the layering module, directly in the optical test chamber (Fig.3; [22,23]). A vibrating membrane is an integral part of the cell. The couple "membrane & target" is driven by an input signal generated due to inverse piezo-electric effect. The R&B cell operates at cryogenic temperatures, which are controlled within the rates of 0.1-60 K/min. If we hold fixed temperature, it is controlled in to ± 0.01 K. Modulation of the input signal impresses information on the carrier frequency and amplitude. This allows placing the target in such a trajectory, which has the modes similar to those of the FST-layering channel. The advantages of the R&B cell application for fuel layering are that the time of target residence is unlimited and the device dimensions are rather small (Table 1). At the moment our experiments have shown that the R&B cell application allows fabricating uniform small-grained D_2 layer on the inner surface of CH shell (Fig.4).

For reactor-scaled targets, there is one more important issue – fuel core survival. The critical point is to withstand the environmental effects: excess heat and mechanical load arising during target delivery. Our investigations have shown that the properties of fuel material, its microstructure and composition have a dominant effect on the cryogenic layer quality and substantially determine the fuel layer response to the environment.

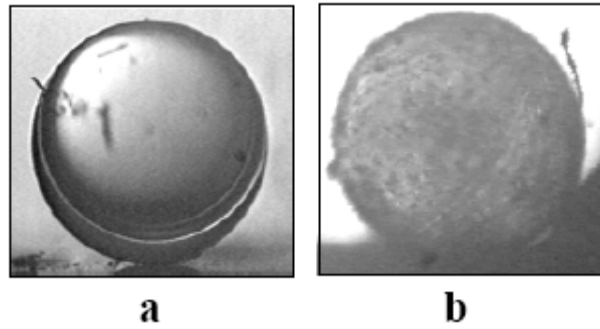


Figure 4. Cryogenic D₂-layering using the R&B cell (a) before layering, 20K;(b) after layering, 5.8K; 1.2 mm-diam. CH shell filled with D₂ up to 300 atm at 300 K. Piezocrystal: 10 kHz, 75V; Layer thickness: ~ 47 μm; Formation time: < 60 sec.

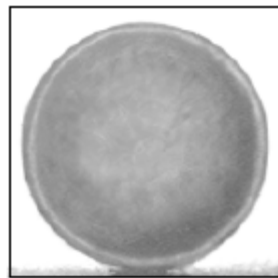


Figure 5. Solid cryogenic layer in a glassy state CH shell: 2R=1.5 mm Coating: 200Å Pt/Pd 50-μm solid cryolayer from 97%D₂+3%Ne.

Table 1. Comparative characteristics of the FST-layering devices

Symmetrization & Freezing	Dimension, mm ³	Residence time limitation
Layering channel	1500x25	< 1-to-15 s
R&B cell	5x25	Unlimited

For example, introduction of minor dopes (HD) to hydrogen (H₂) allows forming the cryogenic layer with glassy or super dispersed structure, which has extremely smooth surface finish [21]. These experiments were carried out with more than 30 targets. It is of particular importance that obtained glassy layer is highly stable and remains transparent upon target heating at least within one heating cycle from 5 K to triple point and higher. This layer property has large prospects for future IFE application, because it enables the target to be injected into the reactor chamber at very low temperatures, when risk of both mechanical and thermal damage is minimal. Currently, we can form glassy layers with different doping agents and study their influence on the layer quality (Fig.5) [16,23].

Modeling results have shown [15] that surface finish spoiling of crystalline fuel layer goes quicker than that of finely dispersed layer, which follows from anisotropy in the sound wave propagation through a crystal. Thus, the problem of finely dispersed and amorphous layers technology is very important in the scope of fuel core survival during the delivery process.

Further developments are designed to keep the study in the area of super dispersed structures formation.

IFE TARGET CHARACTERIZATION

The goal of ICF target characterization is to provide reliable information in a definite time. From this viewpoint, the following two stages of producing the targets are of special interest: (1) layering technique development, which requires to obtain the most complete information on the object (i.e. 3D reconstruction of target is necessary); (2) fueling of a commercial power plant, which requires 500, 000 fusion targets each day or six fusion targets each second.

In the first case it is required to enhance information about the target configuration, whereas in the second – to shorten the characterization time (fast quality control).

For precise and accurate characterization of individual target (microshell or cryogenic target) a prototype of the tomograph has been created at LPI (Fig.6) including the system of a target scanning and image recording, the tomographic test chamber and the special developed software “*Target Studio*” for target 3D reconstruction using a set of its backlit images obtained in visual light [12,13,24]. The spatial resolution of the optical system is 1 μm for 490 nm wavelengths; the accuracy of target angular positioning is ± 1.5 -to- 2.5 minutes. The prototype operation was demonstrated in a number of controlled experiments with polystyrene microshells for a projection set ranging from 60-to-100 backlit images. The prototype has the following distinguished features: (a) operation with both free-standing and pre-mounted targets; (b) scanning of a target both at room and cryogenic (4.2-to-77 K) temperatures.

Methods for fast target characterization is also under way at LPI, namely: time minimization of all the processing stages, threshold characterization, fast characterization of a target batch, moving target characterization with simultaneous control of its quality, velocity and trajectory [17]. One of the approaches to solve the enumerated issues is the application of the optical scheme based on Fourier holography (correlator with frequency plane).

Let us consider the optical scheme based on Fourier holography (Fig.7). The identification signal in the scheme is proportional to the image correlation of the testing target and the etalon target. The signal enhancing corresponds to the case of a better conformity between the testing and etalon targets. A combination of simple electrical threshold circuit and execution unit provides easy targets selection. Obviously, the execution unit and photo detector only determine the operational time of the system, which can be as small as $\sim 1 \mu\text{s}$ or less.

A simulation model was developed in the form of complete computer program *HOLOGRAM*. The shadow target images considered as amplitude transparencies enter the model input. Fast two-dimensional Fourier transformation in this program employs the library FFTW [25].

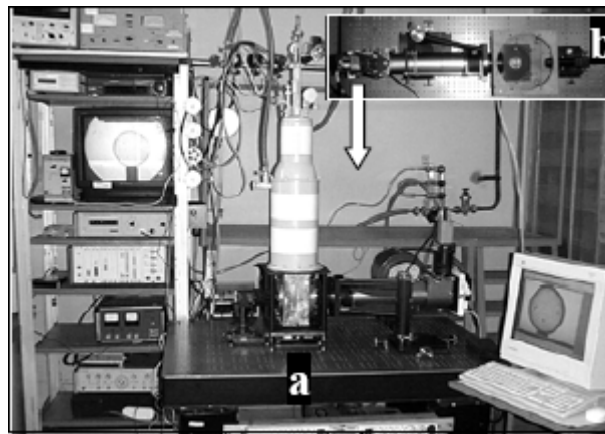


Figure 6. A 100-projections tomograph for free-standing targets characterization: views from the side (a) and top (b).

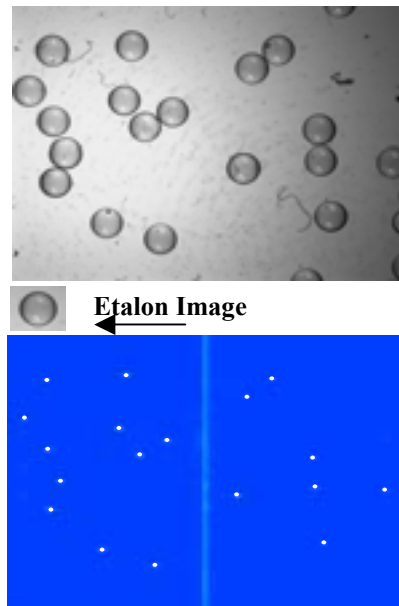


Figure 8. Holographic recognition of a target batch. The correlation peaks position corresponds to shell positions in the upper photograph.

The time-lapse t measured between the signals maxima from two detectors determines uniquely the target velocity $V = S_{in}/t$. We assume that the target moves uniformly. If it is not the case and the target accelerates, then the corresponding scheme becomes more complicated (it includes three or more detectors) and the calculation formula changes. It is not principal and we do not consider such situations for clarity. One can see that in the considered scheme the target velocity can be determined at the instant when the target passes position II. Assume that the distance between positions I and II is 3 cm. Then it will take 10^{-4} sec for target to cover this distance. Such time lapse can be easily measured with high accuracy. For example, at the TDC frequency of 10^9 Hz the accuracy equals to 10^{-3} %.

Figure 12 shows the possible electronic scheme for controlling the flying target trajectory. Presently, it is difficult to estimate the possible accuracy of determining the target trajectory, because it noticeably depends on a particular realization of mechanical, optical, and electronic components, and the algorithms of data processing. We may only assert that at the parameters given above it seems possible to determine the target position in the plane perpendicular to its trajectory with an accuracy of $\pm 2 \mu\text{m}$. The corresponding angular shift of target trajectory is approximately $\pm 2 \cdot 10^{-4}$ radian. We have considered determination of target trajectory in one plane only. It is obvious that for determination of trajectory in space we need two schemes shown in Fig.7 oriented in perpendicular directions.

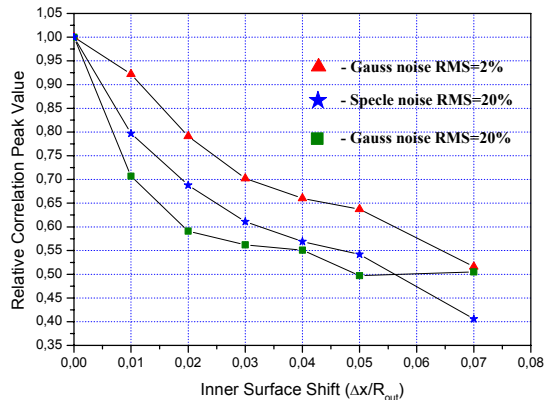


Fig. 9. Relative amplitude of correlation peak versus the shift of inner surface of cryogenic target.

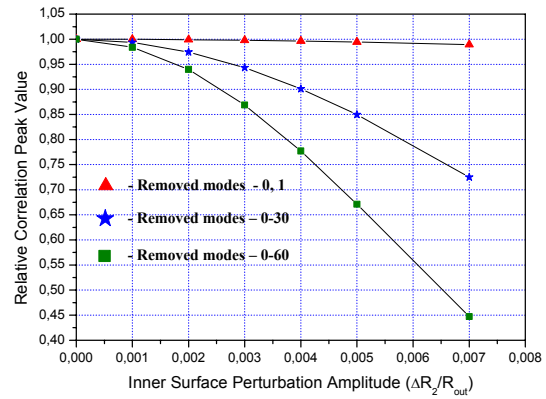


Fig. 10. The amplitude of correlation peak versus the amplitude of inner surface perturbations of cryogenic target at 3 different regimes of spatial-frequency filtering.

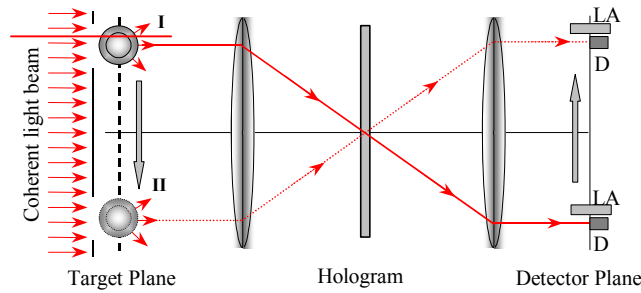


Fig. 11. Optical scheme for controlling target quality, velocity and trajectory. Positions II and I are control points along the target trajectory; D is photodiode; LA is line array. The arrows show the direction of target and correlation peak motion.

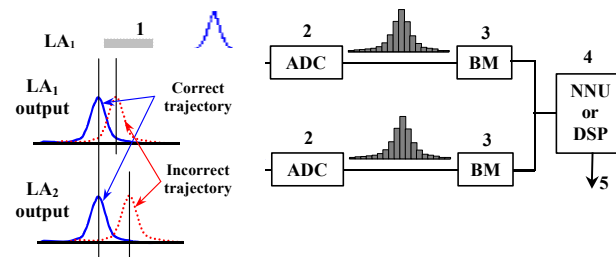


Figure 12. Schematic diagram of electronic unit for analyzing the target trajectory. LA_1 and LA_2 are line CCD arrays; 1- amplifier; 2- analogue to digital converter; 3- buffer memory; 4- processor; 5- output signal. On the left it is shown how the vector of target velocity can be determined.

Therefore, computer experiments have shown that application of the Fourier holography approach allows achieving the following results: (1) recognition of the target shape perturbations in both low- and high- harmonics, (2) quality control of both a single target and a target batch, (3) simultaneous control of the flying target quality, velocity and trajectory. Thus, the Fourier holography scheme looks promising for fast control of IFE targets. Its application will be topical especially in the cases where the time is of critical factor, i.e., at the final characterization stage of the FST facility yield.

IFE TARGET DELIVERY AND ELEMENTS ASSEMBLY

A number of target delivery issues have been considered under the Contract implementation, namely: target acceleration and injection, target protection from overloads and overheat, protecting sabot composition and geometry optimization, sabot and target assembly, etc.

As of today, it is of common knowledge that assembly of the target with a sabot shall precede the target acceleration and injection [26, 27]. The sabot allows (a) to transmit effectively an acceleration impulse to the target, and (b) to protect the target from damage during the acceleration process. One of the sabot design options is shown schematically in Figure 13.

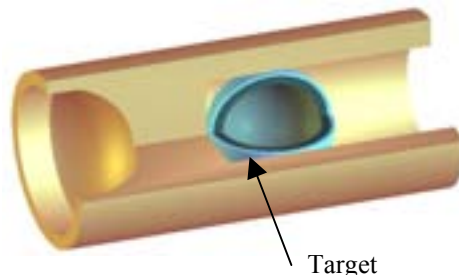


Figure 13. Protective sabot with a target on a support.

An important characteristic of the sabot design is the shape of a target support. Our study has shown that a proper choice of the support shape makes it possible to significantly increase the upper limit of the allowable overloads and to minimize the injector overall dimensions as well.

Based on the discrete-continuous physical model of shell stress, a simulation code SPHERA was developed that allowed to define the stress and deformation arising in the target material during the acceleration process. The allowable overloads were calculated for classical high gain target (CHGT) of two types: CHGT1 and CHGT2. The mechanical properties of target material used in these calculations are shown in Table 2.

Table 2. Mechanical properties of the target materials [28]

Material	E	ν	σ	σ^*
Polystyrene	200	0.25	1.49	1.146
D ₂ at 4.2 K	47.3	0.3	0.054	0.023

Notations: E is Young's Modulus, kg/mm²; ν is Poisson's coefficient, σ is tensile strength of material, kg/mm²; $\sigma^*=\sigma/3$ is the allowable stress of material

A shape analysis of the target support inside a sabot in terms of the target overload during its acceleration has been performed for three sufficiently different cases: (1) flat bottom, (2) semi-spherical bottom with $R \geq R_0$ (R and R_0 are the nest and the target radius, respectively), and (3) flat bottom with a conical hole in its center. The calculations showed that the value of allowable overloads is defined by (a) the value of cryogenic fuel tensile strength, and (b) the value of clearance $\Delta R=R-R_0$. Some important conclusions followed from the calculations (Table 3) are the following:

1. The semi-spherical nest takes its advantage only at a very small clearance ($\leq 5 \mu\text{m}$).
2. At clearance more than 20 μm stresses arising in the target material are close to those of the flat bottom.
3. It was found that the center hole allows target to withstand greater overloads as compared to the flat bottom.

Table 3. Allowable overloads for different shape of a target support (calculations for CHGT1 at 5K)

Clearance $\Delta R=(R-R_0)$, μm	a/g
∞ (flat bottom)	382
10	835
5	1779
0 ($R=R_0$)	19136

Thus, the shape of the target nest in the capsule play an important role for target injection without mechanical damage and allows to reduce significantly the injector overall dimensions. Technologically, the flat bottom with center hole has much promise than the semi-spherical one.

Shields (or covers) for application to protect injected target from a head wind of a residual gas have been considered in [27, 29]. We proposed a new design of a protective cover made from solid xenon, hydrogen or deuterium. We have analyzed the cover and the target interaction with the reactor chamber environment using the Direct Simulation Monte Carlo (DSMC) approach as well as using results of numerical studies of gas flows interaction with bodies [6, 30].

The following parameters were used in our estimations: injection speed is 250 m/s, residual gas is Xe at 0.5 Torr pressure, reactor chamber radius is 5 m, a cylindrical cover from solid Xe with a mass of 87 mg, the target mass is 5 mg. Just this cover design we consider in our

target survival program. In our drag force estimations two cases were considered: solitary and joint flight of target and cover. Correction for the solitary case (effect of wake) is about 30%. The estimations showed that, due to the drag force action, the distance between the target and the cover rises from the initial 1 mm at the moment of injection up to 15 mm at the center of reactor chamber. Thus, the drag force provides necessary separation of the cover and target inside the reaction chamber.

Protective cover forms a wake region with reduced flow velocity and temperature and effectively reduces the gas heat flow by a factor of 4-to-5, which is in a good agreement with calculations reported by Valmianski et al. [29].

Thus, the concept of protecting the direct drive target by a cover moving ahead can be considered as a possible way of solving the target delivery problem. Note, that the problem of fuel core survival is the more difficult the higher the target temperature at the moment of injection. Estimations showed that radiation heat flow from the chamber wall is an order of magnitude higher than the gas heat transfer. Therefore, target injection at 5 K is more preferable than at 17 K.

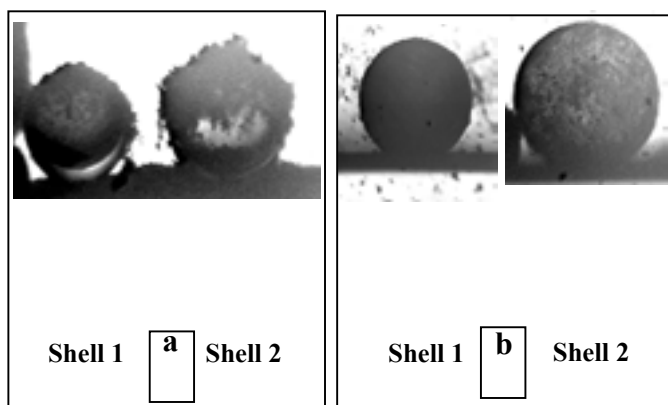


Fig.14. Deposition of the outer protective cryogenic layer onto the target using the R&B cell ($T=14.6\text{ K}$) (a) CH shells inside the R&B cell prior to the experiment. Shell 1 ($2R=1.2\text{ mm}$) has a palladium coating of 150 \AA thick; Shell 2: $2R=1.4\text{ mm}$; (b) An opaque protective cryogenic layer covers each shell after the R&B cell operation in the mode of target bouncing.

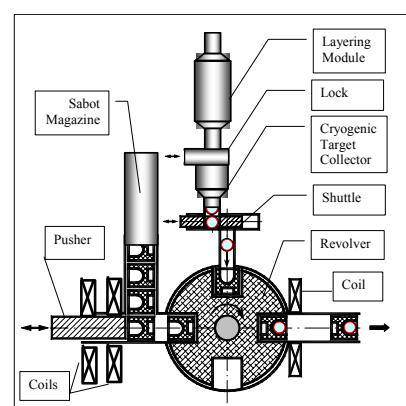


Fig.15. Facility for target and sabot assembly and acceleration.

Deposition of the outer ablating layer was also under consideration in the Project. The ablating layer can be used for (a) protecting target during its flight inside reactor chamber and (b) controlling the target flight trajectory. Using the R&B cell, we first demonstrated a process of deposition of the dispersed layer from solid oxygen onto the outer surface of the polystyrene shells (Fig.14) [15, 16]. Allowing for the obtained results (opaque protective layer), we propose the following physical layout of the target formation: fuel filling, fuel layer formation, target characterization, and if the target is within the specifications, deposition of the outer ablating layer.

The problem of the layering module/injector assembly has been considered in the Contract #11536 as well. In this scope, the design of the facility for continuous cryogenic target fabrication, target & sabot repeatable assembly and acceleration using the coil gun followed by sabot deceleration and target rep-rated injection has been proposed (Fig.15) [6, 22]. Small

changes of the design allow the repeatable assembling the elements of an indirect-drive target at cryogenic temperatures.

Theoretical and experimental study has been carried out, which first confirm the possibility of the ferromagnetic sabot acceleration in a single coil at cryogenic temperatures (Fig.16). Further analysis has shown that application of magneto dielectric instead of ferromagnetic makes it possible to reduce the sabot weight in 3-to-4 times with retention of its magneto active properties, which allows to accelerate effectively the sabot both in a coil and gas gun as well as in the hybrid injector. A physical model of acceleration of the magneto dielectric sabot in the electromagnetic field of solenoid has been created and relevant mathematical software *COIL* has been developed, which allowed optimization of sabot composition and geometry.

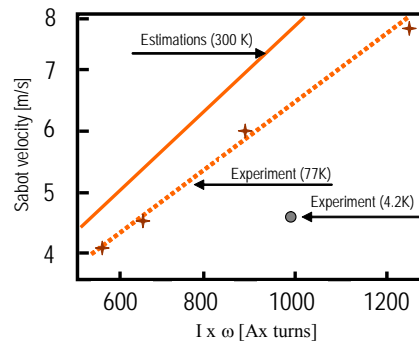


Figure 16. Ferromagnetic sabot acceleration in a single coil.

As a result of our study, we have proposed a full-scaled scenario for repeatable IFE target fabrication, injection and fast characterization basing on the FST technologies including the following steps:

1. Shells batch permeation filling with gaseous fuel and minor dope
2. Pre-cooling stage: mixing, achievement of optimum temperature before layering
3. Stage of the FST-layering (layer symmetrization and freezing-out)
4. Stage of creation of external ablative cryolayer using the R&B cell
5. Delivery of the finished targets into the target collector due to action of gravity
6. Continuous injection of the targets from the collector into the unit of their assembly with protective sabots (rep-rate of 1-to-10 Hz)
7. Target& sabot assembly followed by their acceleration in a coil gun
8. Sabot deceleration (electro-magnetically) followed by target injection into the test chamber
9. Fast control of the parameters of the flying target with the aim to study the fuel core survivability.

FUTURE APPLICATION OF THE RESULTS OBTAINED

Over the last 5 years, significant progress has been made in the technologies development based on operation with moving free-standing targets, which refers to as FST technologies. Currently, the FST-facility created at the Lebedev Physical Institute (LPI) allows to fabricate rapidly a fuel layer inside moving free-standing shells with the following characteristics: polystyrene shell diameter of 0.8-to-1.8 mm, D_2 -fuel layer thickness of 10-to-100 μm , layering time of 1-to-15 sec, production rate of 0.1 Hz.

Characterization of target parameters is an integral stage of its fabrication and delivery. Therefore, a 100-projections visual-light tomography for precise characterization of the shells and cryogenic targets with an accuracy of 1 μm has been created and tested at LPI. We plan to use this facility for further development in the area of ICF/IFE target technology. The development of methods for fast target characterization is also under way at LPI, namely: time minimization of all the processing stages, threshold characterization, fast characterization of a target batch, moving target characterization with simultaneous control of its quality, velocity and trajectory.

The objective of the IAEA Research Contract #11536/RBF was to address the issue of the FST-technologies extension on IFE requirements. The main results of the Contract, which have been obtained at the period of December 2000 – September 2004, are the following:

1. It has been shown theoretically that the existing FST-layering module can be used for first experiments on IFE targets production with the classical high gain target (CHGT) of 4 mm-diam, 45 μm wall thickness, and 200 μm fuel layer thickness.
2. We emphasize a certain potential benefits that can bring the rotating and bouncing (R&B) cell as a new device for the advanced FST-layering experiments with the CHGT-2 targets (5.5÷6 mm-diam, 300-500 μm wall thickness, 200-300 μm fuel layer thickness). Our experiments have shown that the R&B cell is also useful for the ablative cryogenic layer formation onto a target outer surface which can protect the IFE target during the injection process from the destruction due to overheat.
3. It has been shown experimentally that the minor doping application allows creating the fuel layer in glassy (super dispersed) state and reducing the sensitivity of the layer to heat loads. We emphasize a particular convenience of the minor doping technique to DT-fuel with low tritium content ($\leq 20\%$).
4. Our computer experiments have shown that the Fourier holography scheme is promising for fast control of IFE targets. Actuating unit and photo-detector only determine the operation rate of such a system (several μsec). In particular, this approach will allow to achieve the following results: (a) recognition of the target shape perturbations in both low- and high- harmonics, (b) quality control of both a single target and a target batch, and (c) simultaneous control of the flying target quality, velocity and trajectory.
5. A simple integration of the FST-layering module and a target injector into a unified facility has been proposed. The facility is capable of continuous fabrication of IFE targets and their repeatable assembly with protecting sabots followed by the sabot-&-target electro-magnetic acceleration at cryogenic temperatures.
6. It has been found experimentally that ferromagnetic sabot keeps its magnetic properties at cryogenic temperature (77 K and 4.2 K results).
7. Computer experiments have shown that sabot from magneto-insulator material can be accelerated in coil gun more effectively than sabot from pure ferromagnetic. In additional, application of magneto-insulator makes it possible to reduce the sabot weight in 3-to-4 times with retention of its magneto active properties, which allows to use such a sabot both in a coil and gas guns as well as in the hybrid injector.

Based on the prospects realized in the Research Contract #11536/RBF and on the IFE requirements a full-scaled scenario has been developed for repeatable fabrication of the reactor-scaled targets, their injection and fast characterization using the FST technologies.

The next and overwhelmingly important step is the experimental realization of the optimistic results achieved.

As a first step, we propose to build up a small-scaled experimental facility consisting of the following elements (see Fig.17): (a) layering module, (b) diagnostic chamber, and (c) module for fast characterization of the parameters of the injected target. The facility in such a configuration will be capable of:

- forming solid layer of fuel on the inner surface of a reactor-scaled polymer shells
- target acceleration due to gravity and its injection into the diagnostic chamber
- fast control of target in-flight parameters, namely: non-uniformity and roughness, velocity and trajectory.

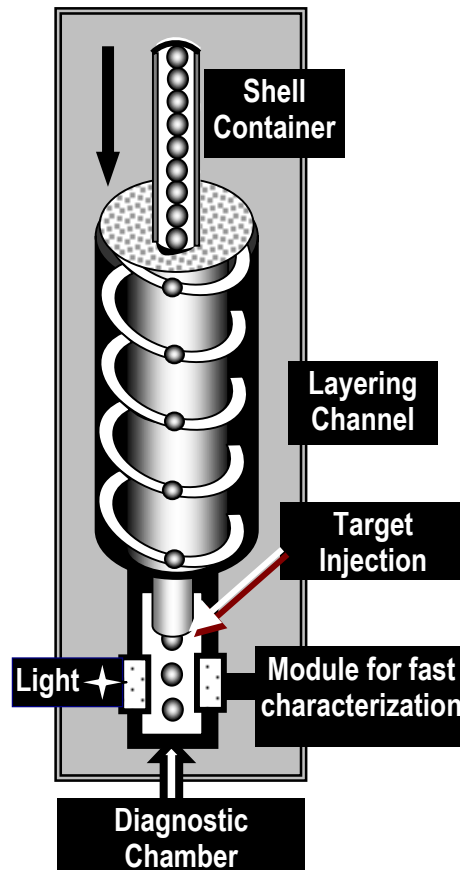


Figure 17. Experimental facility.

The facility will be built up using the previous created at LPI, highly specialized, FST technologies and corresponding FST system. This work includes the following 3 stages:

Stage 1. Modernization of the existed FST system to produce FST-layering inside reactor - scaled targets.

At stage 1, the elements of the FST system (fill facility, layering module, R&B cell etc.) will be updated for operation with the reactor-scaled targets. Target characterization will be carried out using a 100-projection visual-light tomograph existing at LPI.

Stage 2. Development of the module for target fast characterization.

For parameter characterization of the injected target we plan to use the on-line characterization system based on the Fourier holography approach. At stage 2 the hard- and soft-ware of the characterization system will be developed and tested.

Stage 3. Elements integration into a unified facility; demonstration of the facility operation.

At stage 3, a special diagnostic chamber will be constructed and connected to the prototype for the demonstration of its operation. The cryogenic target will be injected (under action of gravity) into the chamber from the layering module. The in-flight parameters of the target moving inside the diagnostic chamber will be controlled.

As a result of the implementation of the IAEA Research Contract #11536, we can outline the most promising options for further research and development activity in the area of IFE target technology, namely:

I. FST-layering approach to IFE targets production

- R&B cell for fuel layering inside free-standing reactor-scaled target
- Formation of a solid fuel layer in a “glassy” state using minor doping. Special emphasis: fuel with low tritium content ($\leq 20\%$).
- Target precise characterization using a 100-projections tomograph

II. Fast characterization of target parameters

- Threshold characterization and low-projection tomography
- Fourier holography approach application for (a) fast characterization of a target batch (quality control), and (b) target in-flight parameters control (quality, velocity and trajectory)

III. Elements assembly and transport at cryogenic temperature (single-step and repeatable modes)

- Assembly of the elements of indirect drive targets (laser and heavy ion fusion)
- Target assembly with protecting sabot
- Target-&-sabot electro-magnetic acceleration
- Creating a small-scaled experimental facility and additional theoretical works will make it possible to proof-of-principle studies of the options outlined.

REFERENCES

- [1] ALEKSANDROVA, I.V. KORESHEVA, E.R. OSIPOV, I.E., et al. Current Results in the Area of Cryogenic Fuel Layering Obtained at Realization of the ISTC Project #512. In.: Inertial Fusion Science and Applications'99 (ELSEVIER), p.897, 2000; Free-standing target system for ICF. Fusion Technology **38**, N^o2, p.166, 2000.
- [2] KORESHEVA, E.R., Extention of free-standing target technologies on IFE requirements: Results of the 1-st year of the IAEA Research Contract #11536/RBF. 1st IAEA RCM of CRP on Elements of IFE Power Plant Design for Inertial Fusion, 21–25 May 2001, Vienna, Austria.
- [3] ALEKSANDROVA, I.V., KORESHEVA, E.R., KROKHIN, O.N., OSIPOV, I.E., Status of the Lebedev Physical Institute in ICF- and IFE-cryogenics. 1st International conference on Inertial Fusion Science and Applications (IFSA2001), 9–14 September 2001, Kyoto, Japan.
- [4] KORESHEVA, E.R., OSIPOV, I.E., TIMASHEVA, T.P., YAGUZINSKIY, L.S., The issue of homogeneous solid H₂-layers formation inside free-standing microshells. Ibid.

- in: Inertial Fusion Science and Application 2001 (eds. K.A.Tanaka et al.), ELSEVIER, p.767, 2002.
- [5] KORESHEVA, E.R., OSIPOV, I.E., BARANOV, G.D., TIMOFEEV, I.D., KAPRALOV, V.G., KUTEEV, B.V., A device for cryotarget rep-rate delivery in IFE target chamber. Ibid. in: Inertial Fusion Science and Application 2001 (eds. K.A.Tanaka et al.), ELSEVIER, p.810, 2002.
 - [6] OSIPOV, I.E., et al, Demonstrated performance of free-standing target system. Ibid.
 - [7] ALEKSANDROVA, I.V., BAZDENKOV, S.V., CHTCHERBAKOV, V. I., KORESHEVA, E.R., OSIPOV, I.E., Rep-rate cryogenic solid layering inside free-standing target system. Ibid.
 - [8] KORESHEVA, E.R., ALEKSANDROVA, I.V., OSIPOV, I.E., et al, Progress in the extension of free-standing target technologies on IFE requirements. 2nd IAEA TM on Physics and Technology of Inertial Fusion Energy Targets and Chambers, 17–19 June 2002, San-Diego, USA; XXVII European Conference on Laser Interaction with Matter, 7–11 October 2002, Moscow, Russia.
 - [9] BARANOV, G.D., VASILIEV, R.P., KORESHEVA, E.R., et al, Design of a special carrier for IFE target acceleration inside the coil-&-gas gun. Ibid.
 - [10] YAGUZINSKIY, L.S., KORESHEVA, E.R., OSIPOV, I.E., et al, A mechanism of formation of glass solid layer of hydrogen inside a microshell. XXVII European Conference on Laser Interaction with Matter, 7-11 October 2002, Moscow, Russia.
 - [11] KORESHEVA, E.R., OSIPOV, I.E., ISHEINOV, O.V., et al, Formation of a thermo stable glassy fuel layer using the minor dope technique. 3rd International conference on Inertial Fusion Science and Applications (IFSA2003), 7–12 September 2003, Monterey, USA.
 - [12] BARANOV, G.D., OSIPOV, I.E., TIMOFEEV, I.D., et al, Multi-functional target-positioning devices for rapid tomographic data acquisition. Ibid.
 - [13] ALEKSANDROVA, I.V., BAZDENKOV, S.V., CHTCHERBAKOV, V.I., et al, Reconstruction algorithms for tomographic multiaspect shadowgraphing for application to ICF / IFE targets characterization. Ibid.
 - [14] CHTCHERBAKOV, V.I., BAZDENKOV, S.V., ALEKSANDROVA, I.V., Progress in the development of an integrated FST-layering code for the optimization of fuel ice formation in moving ICF/IFE capsules. Ibid.
 - [15] KORESHEVA, E.R., Development of a full-scaled scenario for repeatable IFE target fabrication and injection. 3rd IAEA RCM of CRP on Elements of IFE Power Plant Design for Inertial Fusion, 4–7 November 2003, Vienna, Austria.
 - [16] KORESHEVA, E.R., ALEKSANDROVA, I.V., OSIPOV, I.E., et al, FST technologies for IFE targets fabrication, characterization and delivery 3rd IAEA TM on Physics and Technology of Inertial Fusion Energy Targets and Chambers, 11–13 October 2004, Daejon, Republic of Korea.
 - [17] KORESHEVA, E.R., NIKITENKO, A.I., ALEKSANDROVA, I.V., et al, Possible approaches to rapid control of IFE target quality. Ibid.
 - [18] KORESHEVA, E.R., Extension of free-standing target technologies on IFE requirements- main results obtained over the period December 2000-October 2004. 4th IAEA RCM of CRP on Elements of IFE Power Plant Design for Inertial Fusion, 14 October 2004, Daejon, Republic of Korea.
 - [19] ALEKSANDROVA, I.V., BAZDENKOV, S.V., CHTCHERBAKOV, V.I., KORESHEVA, E.R., OSIPOV, I.E., Extension of free-standing target technologies on IFE requirements. in: Inertial Fusion Science and Application 2001 (eds. K.A.Tanaka et al.), ELSEVIER, p.762, 2002.

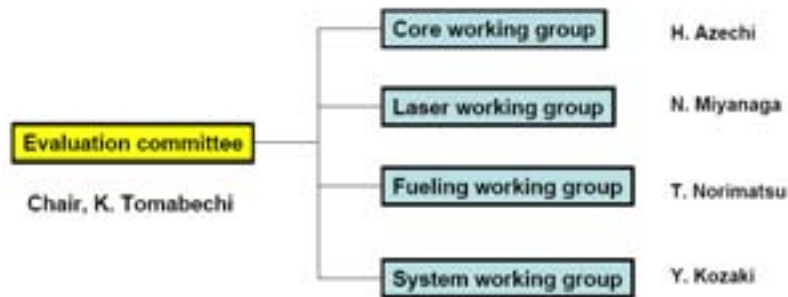
- [20] ALEKSANDROVA, I.V., BAZDENKOV, S.V., CHTCHERBAKOV, V.I., Rapid fuel layering inside moving free-standing ICF targets: physical model and simulation code development. *Laser and Particle Beams*, **20**,13, 2002.
- [21] KORESHEVA, E.R., OSIPOV, I.E., TIMASHEVA, T.P., YAGUZINSKIY, L.S., A new method of fabrication of the transparent solid hydrogen layer inside a microshell: the application to inertial confinement fusion. *J.Phys.D: Appl.Phys.* **35**, p.825, 2002.
- [22] KORESHEVA, E.R., ALEKSANDROVA, I.V., OSIPOV, I.E. et al, Progress in the extension of free-standing target technologies on IFE requirements. *Fusion Sci.&Tech.* **43**, N3 p.290, 2003.
- [23] ALEKSANDROVA, I.V., BAZDENKOV, S.V., CHTCHERBAKOV, V.I., et al, An efficient method of fuel ice formation in moving free-standing ICF/IFE targets. *J.Appl.Phys.D:* **37**, p.1163, 2004.
- [24] OSIPOV, I.E., ALEKSANDROVA, I.V., BARANOV, G.D., et al, A 100-projections microtomograph for cryogenic targets characterization. 3rd International Conference on Inertial Fusion Sciences and Application (IFSA2003), 7–12 September 2003, Monterey, USA.
- [25] FFTW, User manual, <http://www.fftw.org/>
- [26] GOODIN, D.T., et al, Developing the Basis for Target Injection and Tracking in Inertial Fusion Energy Power Plant. *Fusion Engineering & Design* **60**, p.27, 2002.
- [27] FRANK, T.G., et al, Power Plant Design for Inertial Confinement Fusion: Implications for Pellets. *J.Vac.Sci.Technol.* **20** N4, p.1381, 1982.
- [28] MALKOV, M.P., DANILOV, I.B., ZELDOVICH, A.G., FRADKOV, A.B., Handbook on cryogenics. *Energia*, Moscow, (1973) p.256 (in Russian).
- [29] VALMIANSKI, E.I., et al, Wake shield target protection. *Fusion Sci.&Tech.* **43**, N3 p.334, 2003.
- [30] KUTEEV, B.V., Interaction of Cover and Target with Xenon Gas in the IFE-Reaction Chamber. Nov. Research Report NIFS-718, National Institute for Fusion Science, Japan, 2001.

Next steps for target technology and power plant design

T. Norimatsu

Institute of Laser Engineering, Osaka University, Osaka, Japan

Abstract. Current activity at ILE Osaka on fabrication of fast ignition targets toward laser fusion reactor will be discussed. The issue includes fabrication of low density foam shell to form a solid fuel layer, machining of the foam shell to assemble a reentrant cone, fabrication of the cone as a laser focusing device and fuel loading in the future mass production process. We are going to present a new idea for the fuel loading, which would enable us to fill the fuel accurately in short time without any feedback control system. Tritium inventory in the target factory will be reduced to be $<1/10$ of that by conventional diffusion fill.



Roadmap committee of IFE Forum made proposal for laser fusion research:

•**Chair**

A. Tomabuchi (Cent. Res. Inst. for Electric Power Industry), Co-chair Y. Kozaki,

•**Reactor system**

–Y. Ueda (Osaka Univ.), M. Nishikawa (Osaka Univ.) , A. Koyama (Kyoto Univ.), K. Okano (Cent. Res. Inst. for Electric Power Industry), T. Konishi (JAERI), A. Sagara (NIFS), T. Muroga (NIFS)

• **Laser**

–T. Jitsuno, N. Miyanaga, M. Yamanaka, H. Nakano (Kinki Univ.), K. Ueda (Univ. Electro Com.), Y. Owadano (Electro-technical Laboratory Tsukuba), H. Kan (Hamamatsu Photonics), H. Kubomura (NEC)

•**Plasma**

–H. Azechi, K. Mima, K. Murakami, K. Tsubakimoto, Y. Nakao (Kyushu Univ.), Y. Ogawa (Univ. Tokyo),

•**Fueling**

–T. Norimatsu, T. Endo (Nagoya Univ.), T. Tanaka (Univ. Tokyo)



Figure 1. Laser Fusion Experimental Reactor, LFER.

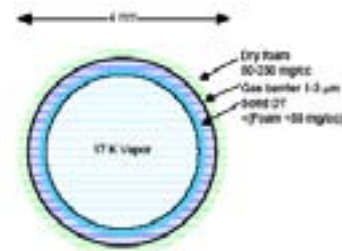
After activity of Roadmap Committee, ILE and IFE forum started a conceptual design committee of FI power plant form March 2004. The committee consists of 14 ILE staffs, 30 researchers of universities and institutes, and 6 researchers of private company.

Table 1. Basic specification of FI power plant

- Output electric power of plant: 1200 MWe (1100~1300 MW margin)
- Output electric power of a module: 300 MWe (the plant consists of 4 modules)
- Laser energy: 1.2 MJ
- Fusion gain: 167 (temporal)
- Fusion yield: 200 MJ
- Rep. rate of a module: 4 Hz
- Fusion power of a module: 800 MWth
- Blanket gain: 1.13
- Thermal output of a module: 904 MWth
- Total thermal output of plant: 3616 MWth
- Conversion efficiency: 42% (LiPb temperature 400~480°C)
- Gross electric power: 1519 MWe
- Laser efficiency: ~8% (compression), ~5%(ignition)
- Laser rep. rate: 16 Hz
- Power for laser operation: 240 MW ($1.2 \text{ MJ} \times 16 \text{ Hz} / 0.08$)
- Net electric power: 1203 MWe ($1519 \text{ MWe} - 240 \text{ MWe}(\text{laser}) - 76 \text{ MWe}(\text{utilities})$)
- Plant efficiency: 3.3% ($1203 \text{ MWe} / 3616 \text{ MWth}$)

•Assignments from system WG to core and laser WGs

- Target design, Gain, including uniformity of irradiation, influence of reactor environment.
- Specification for shell uniformity, out of roundness
- Specification for compression laser (2ω , 3ω , uniformity, beam number)
- Specification for ignition laser (rise time($\sim 2\text{ps}$?), pulse width (1~10ps?)) (FI case)
- Beam stirring
- Debris species, spectrum



•Assignments from core WG to system WG

- Propagation of ignition laser in chamber
- Beam shutter (Protection of final optics)
- Chamber clearance,

This seems most critical path toward reactor with wet wall. Beam stirring by PC SBS is attractive but we need target with homogenously reflecting surface and trade off is necessary between the system efficiency

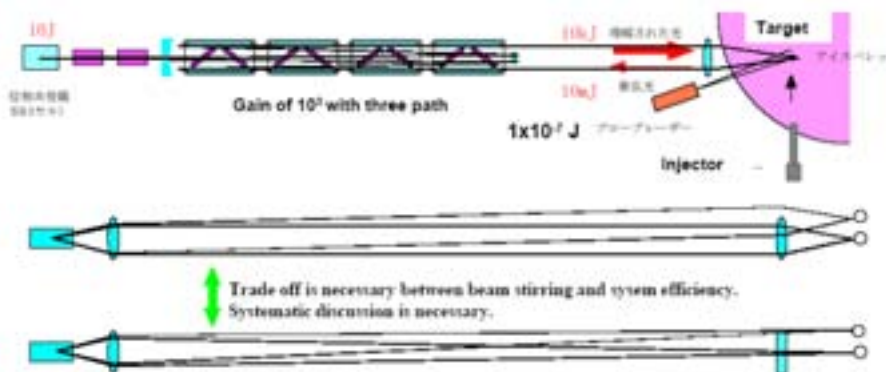


Figure 2. Beam stirring.

- Assignments for system WG
 - Feasibility of cooled laser system
 - Layout of final optics, space for maintenance
 - Protection of final optics, Influence of neutron damage on optical coatings
 - Neutron streaming through laser path
- Assignments for fueling WG
 - Endurance of solid fuel for acceleration, damage during delivery to the firing position
 - Quality of solid layer, characterization
 - Mass production, on-line-characterization
 - Tritium boundary, recovering
 - Tracking

Next step would be integration of elemental research of fueling (non-nuclear) and laser irradiation. In addition, more systematic evaluation and selection is necessary to concentrate our performance.

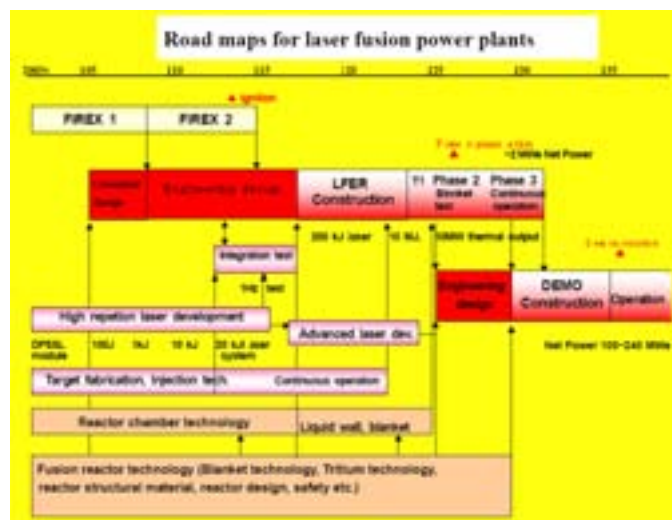


Figure 3. Road maps for laser fusion power plants.

IFE SYSTEM DEVELOPMENTS

IFE research at LLNL

W.R. Meier

Lawrence Livermore National Laboratory,
Livermore, California, United States of America

Abstract. The U.S. has been active in investigating and developing a wide variety of approaches to inertial fusion energy (IFE), including direct-drive, indirect-drive and fast-ignition target; heavy ion accelerators, lasers and z-pinch drivers; dry-wall, wetted-wall and thick-liquid-wall chambers; and target fabrication and injection technologies. Significant progress has been made in all of these areas since the last Technical Committee Meeting on IFE in 2002. Fusion research priorities in the U.S. have also changed since 2002, and some areas of IFE research are being impacted. A brief review of research activities at LLNL will be given and prospects for future work will be discussed.

INTRODUCTION

Lawrence Livermore National Laboratory (LLNL) is conducting research and development on many aspects of IFE including the National Ignition Facility, laser IFE, heavy ion fusion, z-pinch IFE and fast ignition. The scope of these activities is briefly reviewed here.

NATIONAL IGNITION FACILITY (NIF)

The NIF is currently being constructed at LLNL. It is expected to be complete in 2008 with ignition experiments in 2010. The U.S. National Nuclear Security Administration (NNSA) funds NIF for the primary purpose of stockpile stewardship. NIF will prove the scientific feasibility of ignition and energy gain in the laboratory, a key milestone for IFE. An overview of the project and early experiments with the first beam bundle is given in Ref. 1.

LASER IFE

LLNL's work on laser-driven IFE is conducted as part of the High Average Power Laser (HAPL) program. Key components of our research include the diode pumped solid-state laser (DPSSL) called Mercury, direct-drive target physics, x ray damage testing of optics and first wall materials and systems modeling. Mercury is described in Ref. 2 and x ray damage testing using the XAPPER facility is documented in Ref. 3. More information, including target physics work, can be found on the HAPL web site [4].

HEAVY ION FUSION (HIF)

LLNL is part the HIF Virtual National Laboratory (VNL) that coordinates U.S. research in this area. Recently the focus of the program has shifted from fusion energy to high energy density physics (HEDP). The technologies need to achieve well-focused beams for HEDP, however, are also important for future drivers for HIF. The recent International Symposium on Heavy Ion Inertial Fusion provides a good update on the field, including LLNL's activities [5]. Logan's paper provides an overview of HIF VNL's research [6].

Z-PINCH IFE

The Z-pinch IFE program is managed by Sandia National Laboratory and includes participants at many national labs, universities and private companies. LLNL's contributions have been in the areas of thick liquid wall chamber analyses, power plant safety and environmental assessments, and systems modeling. Olson's paper at the recent American Nuclear Society Technology of Fusion Energy (TOFE) meeting provides a good overview of the Z-IFE program [7].

FAST IGNITION

LLNL scientists are also conducting research on various aspects of fast ignition, including energy deposition and transport modeling, target physics, and fundamental experiments with short pulse lasers. The first demonstration of ballistic proton focusing was made with the LLNL JanUSP laser [8]. This approach is an alternative to electron energy deposition in fast ignition targets [9]. Plans are underway to eventually convert one of the NIF beam bundles to short pulse capability, which will provide a world-class fast ignition experimental capability at LLNL.

REFERENCES

- [1] WUEST, C.R., "The National Ignition Facility: Laser Performance and First Experiments," presented at the 16th Technology of Fusion Energy Conference (Madison, WI, Sept. 14–16, 2004), <http://fti.neep.wisc.edu/tofeprogram/oral/PL-II-3.pdf>, to be published in Fusion Science and Technology.
- [2] BIBEAU, C., et al., "Diode Pumped Solid-State Laser Driver for IFE," presented at the 16th TOFE Conference (Madison, WI, Sept. 14–16, 2004) <http://fti.neep.wisc.edu/tofeprogram/oral/O-I-2.3.pdf>, to be published in Fusion Science and Technology.
- [3] LATKOWSKI, J., et al., "Pulsed X ray Exposures and Modeling for Tungsten as an IFE First Wall Material," presented at the 16th TOFE Conference (Madison, WI, Sept. 14–16, 2004), to be published in Fusion Science and Technology.
- [4] High Average Power Laser Program, <http://aries.ucsd.edu/HAPL/>
- [5] 15th International Symposium on Heavy Ion Inertial Fusion (Princeton, NJ, June 7–11, 2004), <http://nonneutral.pppl.gov/HIF04/program.php>
- [6] LOGAN, B.G., "Overview of U.S. Heavy Ion Fusion Progress and Plans," presented at the 15th International Symposium on Heavy Ion Inertial Fusion (Princeton, NJ, June 7–11, 2004), <http://nonneutral.pppl.gov/HIF04/Presentations/Logan.ppt>
- [7] OLSON, C.L., AND Z-IFE TEAM, "Development Path for Z-IFE," presented at the 16th TOFE Conference (Madison, WI, Sept. 14–16, 2004), <http://fti.neep.wisc.edu/tofeprogram/oral/O-II-6.1.pdf>, to be published in Fusion Science and Technology.
- [8] PATEL, P., et al, Phys Rev Letters, **91**, 125004 (2003).
- [9] KEY, M., et al., "Studies of Electron Transport and Isochoric Heating and Their Applicability to Fast Ignition," Proc. Inertial Fusion Sciences and Applications (IFSA) 2003, ISBN 0-89448-686-1, p. 353 (2004).

Design study and technology assessment on inertial fusion energy power plant design

S. Nakai

ILE, Osaka University, Osaka, Japan

Kochi National College of Technology, Nankoku-City, Kochi, Japan

Abstract. This article describes the Japanese activities on IFE power plant development in the framework of the “IAEA-CRP on Elements of Power Plant Design for Inertial Fusion Energy”. The remarkable and steady progress in the development of the Inertial Fusion Energy (IFE) is due to the accumulated results of the efforts of many groups through out the world with the open discussion and exchange of information on the relevant science and technology.

1. INTRODUCTION

The recent results of the direct drive-central ignition experiments give us confidence in achieving fusion ignition, burning and energy gain using a multi-beam mega joule laser with full implementation of beam smoothing techniques, the effectiveness of which has been already experimentally proved. Fast ignition research is also progressing, which could give us a higher energy gain with lower laser energy. The science and technology of laser fusion power plants are beginning to attract wider attention, as forming the road map to achieve commercial power plants for cleaner, safer and abundant fusion energy.

The remarkable and steady progress in the development of the Inertial Fusion Energy (IFE) is due to the accumulated results of the efforts of many groups through out the world with the open discussion and exchange of information on the relevant science and technology. The role and contribution of IAEA on promotion of the IFE development have been effective, and will be important in the future toward the harnessing the fusion energy.

2. FUSION GAIN SCALING AND ITS CREDIBILITY

Figure 1 shows the fusion energy gain scaling with incident laser energy. The gain scaling curve for indirect and direct drive with central ignition, and fast ignition gain curve with different fuel densities are those reported from LLNL. The gain curve from ILE is shown for the fast ignition with $\rho=300\text{g/cc}$. Several point designs from different groups are also plotted on the same figure. The validity of the simulation code has generally been verified by the comparisons of the results with the experimental data. For this purpose, not only the integrated implosion but also the specified physics, which is one of the elementary processes of the implosion, are investigated with an adequately modeled experimental condition and compared with the numerical simulation. There are many data bases which have been accumulated over many years by many laboratories throughout the world relating to the elementary processes such as laser matter interaction, energy transport by radiation, thermal and non thermal particles, ablation and hydrodynamics, and the instabilities related to the implosion process. The experimental results relating to the integrated implosion and fusion reaction have also been compared with the numerical simulation results, which were reinforced by the individual verification for the each elementary process.

It should be noticed that fusion ignition and burning front propagation through compressed fuel has not yet been demonstrated experimentally. This is really the final goal of the physics research on inertial fusion.

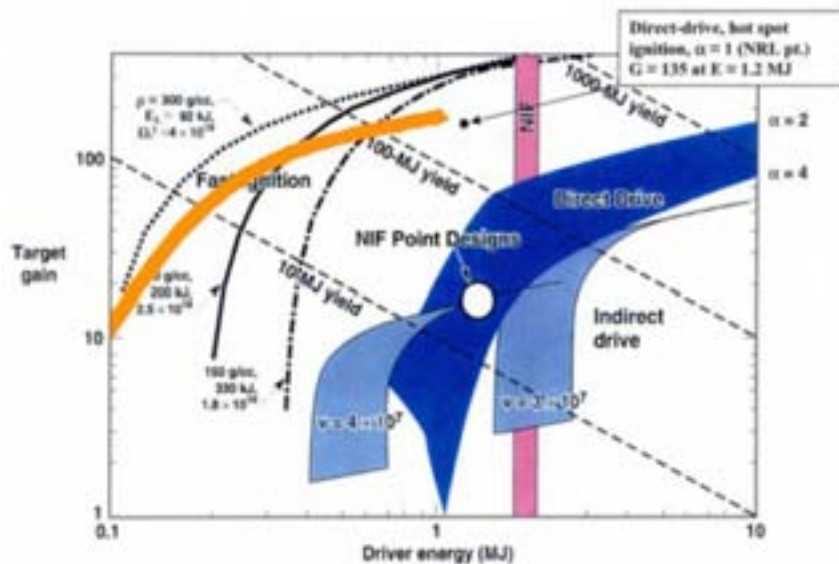


Figure 1. Target gain (fusion energy gain) as a function of the driver energy for central spark ignition with direct and indirect implosion and for fast ignition (Based on the LLNL chart).

It should be noted that the completion of NIF in about 2008 would demonstrate the fusion ignition and burning, and energy gain. It is highly expected that the uniform irradiation configuration of NIF 192 beams will be able to achieve the fusion ignition and burning, and energy gain. If the fast ignition works well, we can achieve a higher gain of 100~300 with less than 1 MJ laser energy.

3. IFE POWER PLANT DEVELOPMENT

IFE power plant systems

An inertial fusion energy (IFE) power plant consists of four major, separate but interconnected sub-systems (elements of a power plant) as shown in figure 2, the functions of which are as follows:

- (a) The driver, usually either a laser or particle accelerator, converts electrical power into short pulses of light or particles and delivers them to the fuel pellet in the proper spatial and temporal form to cause implosion, ignition and thermonuclear burn, i. e. fusion.
- (b) In the pellet factory, fuel pellets are manufactured, filled with DT fuel, and sent to the reactor, then injected into the reaction chamber.
- (c) In the reaction chamber, the injected fuel pellet (target) is tracked, i.e. their position, flight direction and velocity are precisely measured. Driver beams are directed to the target to implode it and to produce thermonuclear energy with a repetition rate of a few times a second. The thermonuclear emissions are captured in a surrounding structure called a blanket and their energy is converted into thermal energy (heat). Tritium is also produced in the blanket.
- (d) In the remainder of the plant, two major processes for material and energy are performed.

Tritium and some other target materials are extracted from the re-circulating blanket fluid material and from the reaction chamber exhaust gases. Then these extracted materials are

recycled to the target factory. The thermal energy in the blanket fluid is converted into electricity, a portion of which is conditioned and re-circulated to power the driver.

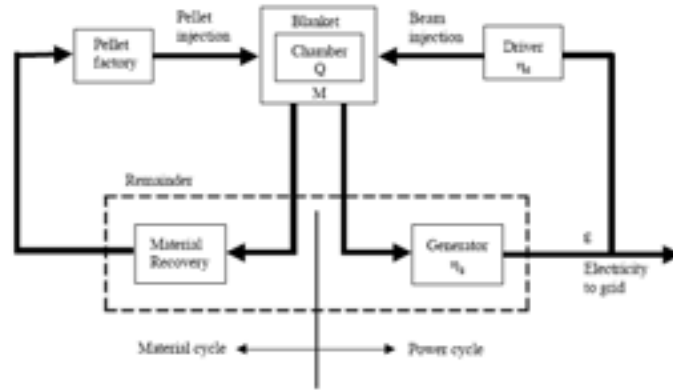


Figure2. IFE power plant system.

Corresponding to the major processes two cycles are formed in a power plant as shown in Figure 2: the target material cycle and the power cycle. In the material cycle, tritium fuel is manufactured from Li in the blanket. The tritium and other target materials are extracted, conditioned and returned to the target factory for use in the new target fabrication. In the power cycle, the basic condition of the power balance is shown as

$$\eta_d Q M \eta_g \varepsilon = 1$$

The recirculation power fraction ε should be less than 25% for economic reasons. If the recirculation power fraction is too large, then the cost of electricity sold rises rapidly because much of the plant equipment is used simply to generate electricity for the driver itself. The blanket gain M is about 1.05-1.25 depending on the design of the blanket material and structure. The efficiency of the turbine generator η_g ranges from 30~40%. Therefore, the product $\eta_d Q$ should be

$$\eta_d Q \geq 10$$

This product determines the minimum target gain necessary for any given driver efficiency. The estimated target gain is shown in figure 1. The typical values are $Q \approx 30$ for the indirect drive, $Q \approx 100$ for the laser direct drive, and $Q \approx 200$ for fast ignition. Corresponding to each gain value, the necessary condition for driver efficiency is given for an indirect drive with heavy ion beam accelerator (HIB) to be 30~40%, for a direct drive with laser to be 10% and for fast ignition, if it works well, 5%. The higher driver efficiency η_d , with a higher target gain Q at smaller driver energy, provides the condition for smaller recirculation power fraction ε and a lower driver cost, which gives us a competitive cost of electricity (COE).

An IFE power plant must be safe and must have minimum impact on the environment. Ensuring these features requires that all the system components of the plant and materials used must be examined carefully for their potential negative impacts. The economic, safety, and environmental (ESE) aspects should be examined in the technical design of each specific type of power plant. It should be noted that these aspects could be evaluated reasonably quantitatively with the recent developments in physics and technology related to the elements of IFE power plants.

Driver development

The specifications of the laser driver for a commercial power plant are (1) total energy (MJ /pulse), (2) intensity ($10^{14} \sim 10^{15} \text{ W / cm}^2$ on target), (3) pulse shape (tailored in 20~40 ns pulse), (4) wavelength (0.5~0.3 μm), (5) spatial uniformity of irradiation (<1% rms), (6) efficiency (>10% for direct implosion, >5% for fast ignition), (7) repetitive operation (~10Hz), (8) cost (capital and operating costs, including life and maintainability), and (9) reliability or availability [1].

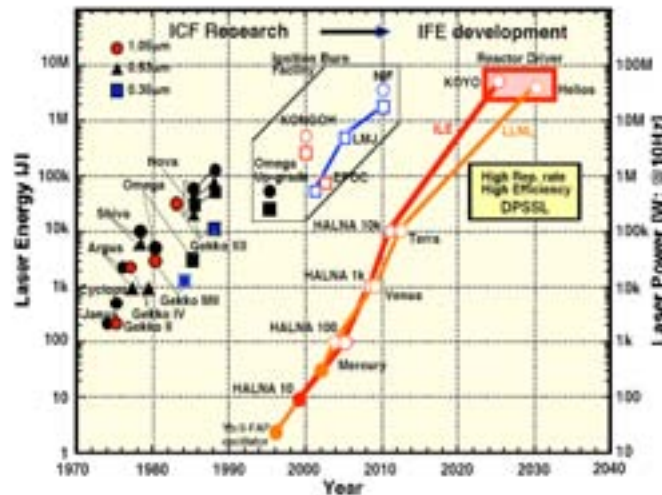


Figure 3. Glass laser system for implosion experiments and DPSSL development for power plants in the world.

In the above specifications, items (1) to (5) are those required for the research phase to demonstrate ignition and fusion gain. Items (6) to (9) are those required for a driver for a laser fusion power plant. Advanced solid-state laser [2] has demonstrated a breakthrough of diode laser pumping and has given us feasible prospect for the power plant driver [3, [4]. Figure 3 shows the progress of flash lamp pumped glass lasers on the left hand side which are basically single shot lasers and the expected development of Diode Pumped Solid State Laser (DPSSL) on the right hand side.

For better and more practical drivers of DPSSL for laser fusion power plants in commercial use, there are two major key issues. The first is high power laser diodes for pumping and the other is solid-state laser material. The laser diodes has progressed and achieved the required specification for pumping. A cost reduction in the diode laser of 10~100 times less than the present level is required and this is expected to be possible with the increase of demand for application of LD and/or DPSSL in industry and science as shown in figure 4 along with increased laser fusion power plant development [5].

As for the laser material, Very promising laser materials are under development in the technical field of optical ceramics. Ceramic YAG laser has already shown better performance than the single crystal YAG laser [6]. Yttria ceramic (Y_2O_3) has been made to optical quality and the properties as a laser material have been tested [6]. Fused silica is also a candidate for a large size solid-state laser material [7]. The unique properties of the high power LD pumping such as (a) spectrum optimization being matched to the laser material, (b) high intensity pumping with optimized pulse duration, (c) polarization control of the pumping light, and (d) areal distribution control of the pumping light, could lead to new optical materials for use as

the laser host material. The progress of DPSSL technology, which is that of LD, laser host material and also the optical technology, is now opening many new fields in industrial technology with optical and laser processes [8].

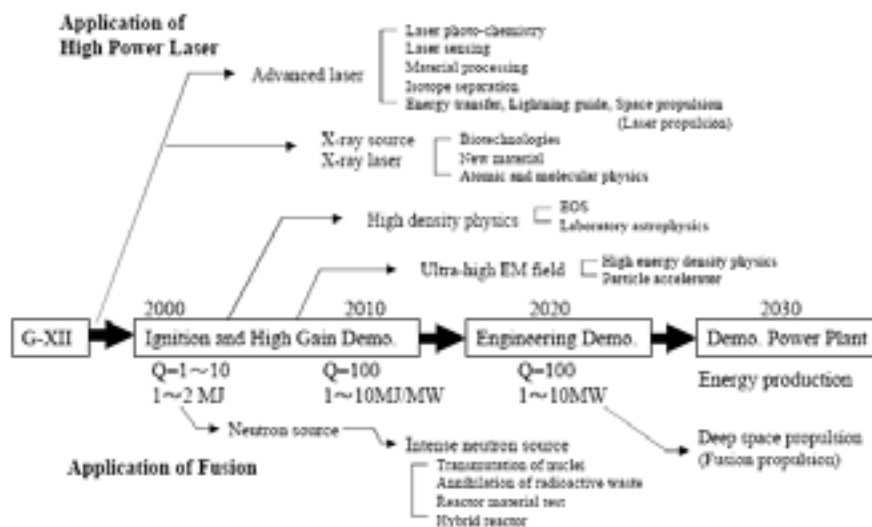


Figure 4. Application of high-power and spin-offs of IFE development.

4. ROAD MAP FOR IFE WITH DPSSL

The IFE Forum (University and Industry joint organization for supporting IFE activity in Japan) initiated a committee “The Committee on Road Map for Laser Fusion Energy” chaired

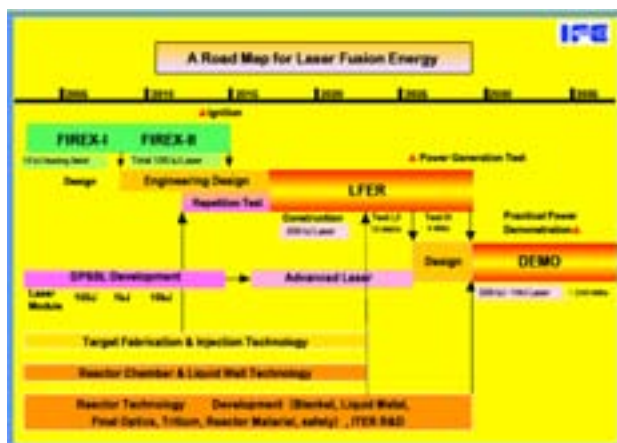


Figure 5. A road map for laser fusion energy.

by K. Tomabechi in 2002 to investigate technical key issues toward IFE power plant based on DPSSL and Fast Ignition. The report of the committee was published in 2004 and part of that was reported at the annual meeting of US Fusion Power Associates which was held in Washington DC, October 2003. The overall road map is shown in Figure 5. FIREX-I (Fast Ignition Realization Experiment) project has started in 2003 to demonstrate the heating of compressed fuel up to ignition temperature. FIREX-II is considered for demonstrating ignition and energy gain.

Following the FIREX project, LFER and DEMO will be investigated along with the developments of the elements of power plant with the estimated time span as shown in Figure 5. The milestones and objectives of the major facilities are shown in table I together with the rough estimation of project cost. To improve the accuracy of technology assessment and the reliability of road map, the conceptual design study has been started under the support of IFE Forum for a reactor with fast ignition. The comparative studies of KOYO-Fast (fast ignition) will reveal the features of the different concepts. The preliminary comparison is shown in Table II.

Table I. Major facilities and milestones for fusion power plants

Facility	FIREX	LFER	DEMO	Commercial plants
Milestones	Fast ignition physics establishment and ignition demonstration	Demonstration of integrated reactor technologies and net electric power	Demonstration of practical power generation	-
Objectives	Phase I (FIREX-I): Heating to ignition temperature (~20 keV) Phase II (FIREX-II): Ignition and burning	Phase I: high rep-rate burning Phase II: Solid wall with test blanket, and liquid wall chamber Phase III: Net power generation, long time operation	- Demonstration of a reactor module for practical power plants - Credibility and economics demonstration	- Economically, environmentally attractive plants - Competitive COE - Modular plants for scale up, flexible construction
Laser	~100 kJ (multiple 10 - heating 10)	200 kJ (~ 1 Hz)	0.5-1 MJ (~ 3 Hz)	0.5-1 MJ (10-30 Hz)
Fusion pulse energy/power output	~1 MJ (1 shot / hour)	10 MJ 10 MWh/ 4 MWe Net output 25MWe	100-200 MJ 300-600 MWh 100-240 MWe	100-200 MJ 3 Hrs (3-10 reactors) 600-1200 MWe
Construction cost	300-400 M\$	~1000 M\$	~2300 M\$	~2700 M\$ / 1GWe

Table II. From KOYO to KOYO-Fast

<ul style="list-style-type: none"> • KOYO design (Central hot spark ignition) <ul style="list-style-type: none"> • laser energy 4 MJ • Fusion yield 400-600 MJ • Reactor module ~ 600 MWe • Laser cost ~4000 M\$ (assumption of LD unit cost 5cent/W) • Large output modular plant ~2400MWe (for competitive COE)
<ul style="list-style-type: none"> • KOYO -Fast design (Fast ignition) <ul style="list-style-type: none"> • laser energy 500kJ-1 MJ • Fusion yield 100-200 MJ • Reactor module 100-240 MWe • Laser cost 500-1000 M\$ (LD unit cost 5 cent/W) • Small output modular plants 600-1200MWe • (for a variety of future energy needs)

5. SUMMARY

It is expected that fusion ignition and energy gain by laser implosion will be demonstrated around 2010 ~ 2015 using the MJ lasers which are under construction in USA and in France. The basic physics of implosion have been well understood, and the credibility of the numerical simulation of implosion has been increased by reinforcement from physical understanding. The progress in the achievements of the imploded plasma parameters was remarkable, that is 10 keV high temperature compression [9], and high-density compression of 1000 time over the initial density [10, 11, 12]. The recent achievement of the

demonstration of the formation of the hot spark surrounded by cold fuel with 1% rms uniform irradiation by Omega 60-beam at LLE of Rochester University [13] shows the feasibility of the ignition and gain by direct drive implosion with 194 beams at NIF, together with implementation of the established techniques for uniformity improvement.

On the other hand, the fast ignition concept has been experimentally demonstrated [14] to be feasible for heating the compressed core efficiently. This new concept has become technically possible with the invention of new laser technology such as chirped pulse amplification and compression for generation of ultra short pulse [15]. If the fast ignition concept works well in large scale for the compressed fuel for the reactor, it is very attractive in the design of laser fusion power plants because of the higher pellet gain with the smaller driver energy. A challenging project, FIREX: fast ignition realization experiment [16], has been kicked off aiming to demonstrate ignition and burning through the concept of fast ignition at ILE, Osaka University.

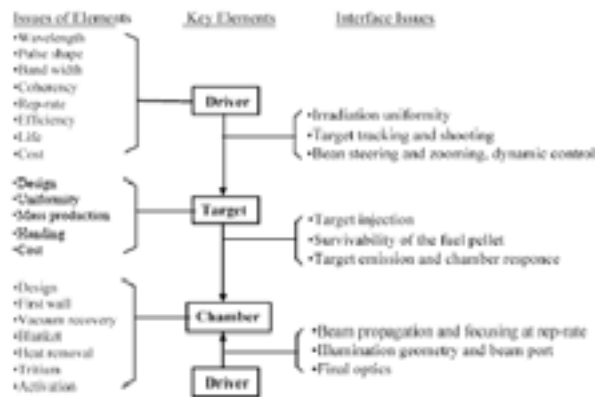
As for power plant development, many conceptual design studies have revealed the technical issues of the key elements that comprise a power plant such as “driver”, “chamber”, and “target factory”. The most critical element is the driver for a power plant which requires replate operation in the order of 10 Hz with a pulse energy of order MJ in a few tens ns with high efficiency over 10%. This is really a big jump in the development of laser technology. On the way towards the development of the power plant driver, we can expect many fields of laser application to open up new industrial technology, scientific methodology, and explore the physical parameter regions of new phenomena as shown in Figure 4.

It should also be noted that the technology related to the key elements of the IFE power plant span wide fields of science and technology. As shown in Table III, the issues regarding the key elements require engineering and physical knowledge.

It is an important feature of an IFE power plant that its key elements: driver, target factory, and chamber, are separated from each other and softly coupled to make a system. The relation between the three key elements is shown in Table III. Only the laser beam and the transport line of tiny fuel pellets connect the three areas of the driver, chamber, and target factory. Even with the physical separability, there are important interface issues when all of the elements work together as a system as shown in Table III.

The features of the IFE power plant such as wide range of physics and technology, the separability of the key elements, and the soft coupling at the interface are the reason that a coordinated and collaborative program is required and effective for the steady development of an IFE power plant.

Table III. Elements of IFE power plant and interface issues



The IAEA has been promoting IFE activity and maintaining international collaboration. Following the review work on IFE power plants by 80 experts from all over the world in 1991~95 (Hogan 1995), the “IAEA Coordinated Research Project on the elements of IFE power plant” has been initiated for the period 2001~2005. During this project, state of the art of IFE power plant technology has been investigated in detail so that a clear road map toward the future of IFE can be formulated. International collaboration is desirable and can be expected because of its already proven effectiveness in the development of IFE and also because of the commonality of goals between nations world wide, and their shared goal of objective of cleaner, safer and abundant energy for all human beings.

REFERENCES

- [1] HOGAN, W.J., et al, Energy from Inertial Fusion, IAEA, Vienna (1995).
- [2] KRUPKE, W.F., Fusion Technol. **15** (1989) 377.
- [3] NAITO, K., et al, Jpn. J. Appl. Phys. **31** (1992) 259.
- [4] ORTH, C.D., et al, Nucl. Fusion **44** (1996) 75.
- [5] NAKAI, S., AAPPs Bull. **10** (2000) 2.
- [6] LU, J., et al, Inertial Fusion Science and Application 2001, (TANAKA, K.A., MEYERHOFER, D.D., MEYER-TER-VEHN, J., Ed.), Paris: Elsevier (2002) 576–579.
- [7] FUJIMOTO, Y., NAKATSUKA, M., Inertial Fusion Science and Application 2001, (TANAKA, K.A., MEYERHOFER, D.D., and MEYER-TER-VEHN, J., Ed.), Paris: Elsevier (2002) 524–527.
- [8] KRUPKE, W.F., Proc. SPIE **3889** (2000) 21.
- [9] YAMANAKA, C., NAKAI, S., Nature **319** (1986) 757.
- [10] NAKAI, S., et al, Bull. Am. Phys. Soc. **34** (1989) 2040.
- [11] NAKAI, S. et al, 13th IAEA Fusion Energy Conf. (Washington DC, USA, 1–6 October 1990), IAEA-CN-53/B-I-3 (1990).
- [12] AZECHI, H., et al, Laser and Particle Beams **9** (1991) 193.
- [13] McCrory, R.L., et al, 19th IAEA Fusion Energy Conf., (Lyon France 14–19 October 2002, IAEA-CN-94/IF-1 (2002).
- [14] KODAMA, R., et al, Nature **418** (2002) 993.
- [15] STRICKLAND, D., MOROU, G., Opt. Commun. **56** (1985) 219.
- [16] MIMA, K., et al, 19th Fusion Energy Conf. (Lyon, France, 14–19 October 2002), IAEA-CN-94/IF3 (2002).

Elements of power plant design for inertial fusion energy at DENIM

G. Velarde¹, O. Cabellos¹, M.J. Caturla^{4,5}, R. Florido³, J.M. Gil³, P.T. León¹, R. Mancini⁶, J. Marian⁵, P. Martel³, J.M. Martínez-Val¹, E. Mínguez¹, F. Mota¹, F. Ogando^{1,2}, J. M. Perlado¹, M. Piera^{1,2}, R. Rodríguez³, J.G. Rubiano³, M. Salvador¹, J. Sanz^{1,2}, P. Sauvan^{1,2}, M. Velarde¹, P. Velarde¹

¹ Instituto de Fusión Nuclear - DENIM, Universidad Politécnica de Madrid, Spain

² Departamento de Ingeniería Energética, Univ. Nac. Educación a Distancia, Spain

³ Departamento de Física, Universidad de Las Palmas de Gran Canaria, Spain

⁴ Departamento. Física Aplicada, Universidad de Alicante, Alicante, Spain

⁵ Lawrence Livermore National Laboratory, United States of America

⁶ University of Nevada, Reno, United States of America

Abstract. This paper describes the activities at the Instituto de Fusión Nuclear – DENIM – related to inertial fusion energy target design and fluid dynamic simulations, inertial fusion features in degenerate plasmas, atomic physics, activation of materials: safety and environmental issues, radiation damage of fusion materials, tritium atmospheric diffusion and environmental pathways to human chain.

1. TARGET DESIGN AND FLUID DYNAMIC SIMULATIONS

A new target design for ICF has been proposed and simulated, in search for a new and simpler way to achieve ignition using fast ignition [1]. The new proposed design contains the main ideas of fast ignition, while using a single energy drive that produces both fuel compression and ultra-fast energy deposition on it. The deposition of energy is produced by the impact of a hypervelocity jet onto the compressed core, converting therefore kinetic energy into thermal energy that produces a hot spot. That hypervelocity jet is produced simultaneously to the fuel compression, by the ablationally driven collapse of a conically shaped system, which absorbs energy from the same energy source that produces the fuel compression. The design includes a spherical conventional target for fast ignition (that is, not a full sphere) coupled to one or two cones pointing inwards in such a way that, under the proper design, produce hypervelocity jets arriving at the center of the system in the very precise moment of highest compression and temperature of the nuclear fuel. Between fuel and the conical system, there are conical shapes facing outwards, with the mission of preventing interaction between the two mentioned zones of the target.

This design has been simulated using the ARWEN code [2] reaching to acceptable results [1]. The simulations have performed so far using one material for the whole system, showing in spite of that an appreciable temperature rise in the collision zone of the fuel core. In order to predict the propagation of the burning wave, conditions have to be established and proved to be reachable by the system in the simulations. The ARWEN code is being adapted to perform multimaterial calculations, which will show a better performance of the system. Other designs have been proposed [3] based on the idea of fast ignition by impact of high-speed matter, being the designs still in a stage of simulation and optimization of the designs.

The system has been simulated as inside of a hohlraum with an equivalent radiation temperature of 300eV, thus using indirect radiation. During the first instants, an ablation

process starts, producing along the whole contour shock waves travelling inwards. These shock waves produce two different effects in both fuel shell and conical regions. On the spherical shell, and thanks to the guiding effect of the outward-facing cones, matter is compressed in a uniform way, as was first shown in [4]. At the same time, the shock waves on the conical region produce a jet that grows in time on speed and mass.

Under a precise design that implies selecting angles and thickness, it was shown in [1] that an appropriate synchronisation could be achieved leading to a collision of the compressed fuel during the first stages of expansion while its core is in the most compressed state. The collision produce a hot spot in the lowest part of the compressed fuel.

2. INERTIAL FUSION FEATURES IN DEGENERATE PLASMAS

Very high plasma densities can be obtained at the end of the implosion phase in Inertial Fusion targets, particularly in the so-called fast-ignition scheme, where a central hot spark is not sought at all. By properly tailoring the fuel compression stage, degenerate states can be reached. In that case, most of the relevant energy transfers mechanisms involving electrons are affected. For instance, bremsstrahlung emission is highly suppressed [5]. In fact, a low ignition-temperature regime appears at very high plasma densities, due to radiation leakage reduction [6]. Stopping power and ion-electron coulomb collisions are also changed in this case, which are important mechanisms to trigger ignition by the incoming fast jet and to launch the fusion wave from the igniting region into the colder, degenerate plasma. All these points are reviewed in a recent paper [7]. Although degenerate states would not be easy to obtain by target implosion, they present a very interesting upper limit that deserves more attention in order to complete the understanding on the different domains for Inertial Confinement Fusion. A programme F.I.N.E. (fast ignition nodal energy) has been developed. In the programme, the equations defined are valid for the degenerate and classical region, taking into account the possibility that the plasmas pass from a degenerate state to a classical state during the heating process. The results of the programme are only valid to study the possibility of ignition of plasmas in the fast ignition concept, not the burn up phase of the target. Ions have been the choice for ignitor heating until ignition conditions are reached. The optimisation of the compression phase in fast ignition inertial fusion, to obtain low temperature and high-density plasmas, can lead to a degenerate plasma. The equations that governs these plasmas are different that the classical ones. The decrease in Bremsstrahlung emission permits the decrease in ignition temperature, for high-density plasmas. This assumption has been demonstrated. The high energy needed to obtain this high density degenerate plasmas decrease the gain as compared to the results obtained in more moderated densities.

3. ATOMIC PHYSICS

Optical properties of plasmas are a powerful tool for plasma diagnosis. As it is known, optical properties depend strongly on the level populations into the plasma, both for plasmas at LTE and NLTE conditions. Up to now the model proposed by us, ANALOP code [8], was only able to model optically thin plasmas, i.e. assuming that the self-absorption is negligible. For optically thick plasmas the rate equations and the radiation transfer equation are coupled and they should be resolved in a simultaneous way, since under these conditions the self-absorption of the radiation in the plasma influences considerably in the level populations.

Recently, we have proposed two different models in order to provide level populations for this kind of plasmas. The first one is based on the solution of the radiation transfer equation (LTNEP code) and the second one is based on the escape factor formalism (M3R-EF code).

In the LTNEP model, a 1D plasma divided into N cells is considered, having each cell different density and temperature. The profiles of density and temperature are provided by hydrodynamics calculations as input of the model. Then, the atomic kinetics and the radiation transfer equation are solved self-consistently for the whole plasma. The rates equations are solved in the Collisional-Radiative Steady State (CRSS) model and the atomic processes included are the following: spontaneous emission, resonant emission and stimulated emission, photoionization and radiative recombination, collisional excitation and deexcitation, collisional ionization and 3-body recombination and dielectronic recombination.

The other model, M3R-EF code, introduces the reabsorption of the radiation through the escape factor formalism. The escape factor θ denotes the mean probability that a photon emitted anywhere in the source travels directly to the surface of the source in any direction and escapes. In this work we have assumed a uniform distribution of emitting atoms and isotropic emission and a slab geometry [9]. The rate equations are also solved in the CRSS model including the same atomic processes but the resonant emission and photoionization.

In both codes, the atomic data required for the calculations are provided as an input file and the Stark profile is calculated by the Code Pim Pam Poum [10]. Then, the source function is obtained from the calculated line opacity and the bound-free opacity is provided by hydrogenic formulas. Finally, the specific intensity is determined solving the transfer equation with the known source function.

With these two models we have studied uniform aluminium plasmas, which length of 100 μm , for a fixed electronic density (10^{23} cm^{-3}) and several temperatures (from 200 to 500 eV). It has been seen that for these plasmas the self-absorption must be included because it introduces relevant changes in the level populations. For example, for the Lyman series we obtain that the ratio of the level populations calculated assuming optically thick and thin plasma, P_{thick} / P_{thin} , is equal to 10 for the ground states and 10^2 for the excited states while for the Helium series is equal to 1 and 10, respectively. Taking into account the results of the ratios of populations shown before and according with the relations between the populations and the source function we obtain that source function for optically thick plasmas is ten times greater than for the optically thin ones. We have also verified that the escape factor formalism is a good alternative to those methods based on the resolution of the rate equations coupled to the radiation transport equation for uniform plasmas since LTNEP and M3R-EF codes provide similar results.

4. ACTIVATION OF MATERIALS: SAFETY AND ENVIRONMENTAL ISSUES

In the field of computational modelling for S&E analysis our main contribution refers to the computational system ACAB [11] that is able to compute the inventory evolution as well as a number of related inventory response functions useful for safety and waste management assessments. The ACAB system has been used by Lawrence Livermore National Laboratory (LLNL) for the activation calculation of the National Ignition Facility (NIF) design [12] as well as for most of the activation calculations, S&E studies of the HYLIFE-II and Sombrero IFE power plants with a severe experimental testing at RTNS-II of University Berkeley [13]. Pulsed activation regimes can be modelled (key in inertial confinement fusion devices

test/experimental facilities and power plants), and uncertainties are computed on activation calculations due to cross section uncertainties. In establishing an updated methodology for IFE safety analysis, we have also introduced time heat transfer and thermal-hydraulics calculations to obtain better estimates of radionuclide release fractions. Off-site doses and health effects are dealt with by using MACSS2 and developing an appropriate methodology to generate dose conversion factor (DCF) for a number of significant radionuclides unable to be dealt with the current MACSS2 system. We performed LOCA and LOFA analyses for the HYLIFE-II design. It was demonstrated the inherent radiological safety of HYLIFE-II design relative to the use of Flibe. Assuming typical weather conditions, total off-site doses would result below the 10-mSv limit. The dominant dose comes from the tritium in HTO form. In the Sombrero design, a severe accident consisting of a total LOFA with simultaneous LOVA was analysed. Key safety issues are the tritium retention in the C/C composite, and the oxidation of graphite with air that should be prevented. The activation products from the Xe gas in the chamber are the most contributing source to the final dose leading to 47 mSv. We also analysed the radiological consequences and the chemical toxicity effects of accidental releases associated to the use of Hg, Pb, and Be, as IFE materials under HYLIFE-II framework scenario. For those three materials, the chemical safety requirements dominate strongly over radiological considerations. Also, the role of clearance as waste management option for HYLIFE-II was explored. For the confinement building, which dominates the total volume of the waste stream, all the material could be released from regulatory control for unconditional re-use after about one year of cooling following plant-shutdown. We also explored liquid wall options for tritium-lean fast ignition IFE power plants. Many single, binary, and ternary molten-salts were evaluated for their S&E characteristics, as well as for the required pumping power. In analysing the impact of cross section uncertainties on the contact dose rate from the activated concrete-gunitite outer shell of the NIF reaction chamber, it is shown that current cross sections allows a reasonable confidence in the results. Regarding IFE, uncertainties in the prediction of the neutron induced long-lived activity in all the natural elements shown that for the HYLIFE vessel a significant error is estimated in the activation of several elements, while the estimated errors in the Sombrero case are much less important.

5. RADIATION DAMAGE OF FUSION MATERIALS

Ferritic-Martensitic Steels (in their more advanced type using experimentally testing Oxide Dispersion Strength, ODS, technique), Composites namely based in SiC, and Vanadium alloys are those materials presently under discussion as structural materials, together with C, Be, W, as first wall materials and some ceramics (silica, alumina) as optics and insulators elements. A systematic experimental program is partially pursued in different countries to assess their performance under the specific conditions they will be working on. It is very certain that a large and new irradiation facility is critically needed, and International Fusion Materials Irradiation Facility (IFMIF) will cover such role. In the present time also Multiscale Modelling (MM) is getting a large role in obtaining predictive characteristic and defining the needed experiments. A common methodology work appears for fusion programs but also for other nuclear systems such as fission (advanced Fission Reactors/Generation IV and Accelerator Driven Systems for Transmutation) with coincidences in some of the analysed materials. Key value has the validation of MM against specific experiments step by step at the microscopic and macroscopic levels and real understanding of damage processes, and effects of alloying and impurities elements. Microscopic parameters (using Molecular Dynamics, MD, DENIM models), which identify the effect of irradiation through new defects formation and diffusion, are being generated for some specific metallic materials (Fe, binary alloys FeCr, FeCu, V...) and their diffusion conducted by MonteCarlo [14]. Next step is being their

interaction with dislocations (Dislocation Dynamics) and study of nucleation in the presence of He. That effect of He in FeCr alloys is certainly critical. We also derive macroscopic magnitudes using small-scale MM models in short simulation times by using MD defect-dislocation studies under stress [15]. We modelled pulse radiation damage, and we progress in the microscopic validation of Multiscale Modelling with experiments using pure and ultra-high pure Fe (effect of impurities) through a National Simulation-Experimental Program using ion irradiation [14]. Our work is also being concentrated in two IFE key materials (SiO₂/optics, SiC/low activation advance material). A MD *tight binding* scheme has been fully developed for β -SiC to understand the microscopic phenomena of the native defects and its diffusion at different temperatures. We reach an extraordinary good agreement among our calculated defects energetic and those results obtained using sophisticated and expensive method such as *ab-initio* at 2000K. We observe that β -SiC crystal remains perfect with its typical cubic structure at that temperature, and we have shown that the carbon atoms do not diffuse into the crystal. Self-interstitial silicon atom prefers the relation with atoms of the same specie due to the effect that the repulsive force of the silicon atoms is larger than the repulsive forces of the carbon atoms [16]. MD is also being used to study the defects produced in fused silica by energetic atoms, neutron and gamma irradiation. We determine the structure factor, the bond angle distribution, co-ordination and ring statistics, and we conclude very good agreement with measurement of generation of fused silica glass [17], (see *FIG. 4*). Threshold displacement energies have been computed as a function of the direction of movement of PKA, and cascades of 5 keV are being actually extended to 10 keV. Two modelling-experimental programs have been started with CIEMAT for Silica analysis, which will be extended in the future to Alumina as first wall and ceramics insulators.

6. TRITIUM ATMOSPHERIC DIFFUSION AND ENVIRONMENTAL PATHWAYS TO HUMAN CHAIN

A large and completely new work has been performed in the analysis of consequences of tritium release according with expected source emission from IFE Conceptual Reactors and others nuclear systems [18]. Key aspect here is to consider all chemical forms of tritium (HT and HTO) and their conversion to Organically Bound Tritium (OBT) with soil processes and consequences of re-emission to atmosphere. We report several important conclusions for the primary and, namely, secondary phases of tritium transport in the environment with final consideration of different time-dependent phases in dosimetry. Our new approach allows a more realistic simulation, and significant more restrictive limit in tritium handling as classically assumed in conceptual systems. This methodology has been successfully used in the work performed for establishing Vandellós site for ITER (Contract under EFDA). The whole study of secondary phase drives to the conclusion that the behaviour of the tritium should be simulated using two well-differentiated studies: deterministic and probabilistic. Deterministic calculations are based on a fixed meteorological data given "a priori", where the speed and directionality of the wind, class of atmospheric stability and rain intensity, as well as the boundary conditions of the means that surround to the atmospheric discharge (soil type, humidity of the air, temperature and solar intensity) are given. The probabilistic study is based on measured real meteorological analysis every hour, and the probability that individuals can present dose for internal irradiation of the tritium is considered. Our conclusion is that these probabilistic studies provide the real dynamics of the processes, which are different from deterministic case. The effect of formation of OBT is concluded of key importance.

ACKNOWLEDGEMENTS

Work performed under the Spanish National Programme on Thermonuclear Fusion Projects FTN2001-3886-C02-01 and FTN2001-3886-C02-02, the European Union keep-in-touch Program on IFE, and EFDA Tasks in Multiscale Modeling for Fusion (2003, 2004). A large collaboration exists on IFE activities with Lawrence Livermore National Laboratory and University of Berkeley (USA), SCK-CEN Mol (Belgium), Edf and CEA (France), University of Cagliari (Italy). This work has also performed under collaboration with CIEMAT in CSN/UNESA VENUS-II (2000-2003), and REVE Spanish Project (2004-2007).

REFERENCES

- [1] VELARDE, P., OGANDO, F., ELIEZER, S., SAULE, M., Proc 3rd IFSA (2004) 88.
- [2] OGANDO, F., VELARDE, P., JQSRT 71 (2001).
- [3] MURAKAMI, M., HIF 2004 conference, paper MI14 (2004).
- [4] KODAMA R., et al, Nature **412** (2001) 798.
- [5] ELIEZER, S., LEÓN, P.T., MARTÍNEZ-VAL, J.M., FISHER, D., Laser and Particle Beams, **21**, 599 (2003).
- [6] LEÓN, P.T., ELIEZER, S., MARTÍNEZ-VAL, J.M., PIERA, M., Physics Letters A, **289**, 135 (2001).
- [7] LEÓN, P.T., ELIEZER, S., MARTÍNEZ-VAL, J.M., PIERA, M., submitted to Laser and Particle Beams (2004).
- [8] MÍNGUEZ, E., GIL, J.M., MARTEL, P., RUBIANO, J.G., RODRÍGUEZ, R., DORESTE, L. (1998). Nucl. Instr. and Meth. in Phys. Res. A **415**, 539-542.
- [9] MANCINI, R., JOYCE, R.F. & HOOPER Jr., C.F. (1987). J. Phys. B: At. Mol. Phys. **20**, 2975–2987.
- [10] CALISTI, A., KHELFAOUI, F., STAMM R, TALIN, B., LEE, R.W. (1990). Phys. Rev. **42**, 5433–54440.
- [11] SANZ, J., ACAB, Activation Code for Fusion Applications: User's Manual V5.0., Univ. Nacional Edu. Distancia (UNED). Inst. Fusión Nuclear DENIM 490, Feb. 2000; Lawrence Livermore National Laboratory, UCRL-MA-143238, Feb. 2000.
- [12] SANZ, J., et al, Fusion Science and Technology, **43** (2003) 473-477.
- [13] LATKOWSKI, J.F., REYES, S., CADWALLADER, L. C., SHARPE, J. P., MARSHALL, T. D., MERRILL, B. J., MOORE, R. L., PETTI, D. A., Falquina, R., Rodriguez, A., Sanz, J., Cabellos, O., Fusion Science and Technology, **44** (2003) 34–40.
- [14] PERLADO, J.M., et al, Assessment of structural and silica materials under irradiation in inertial fusion reactors: comparison of multiscale modeling and microscopy, IFSA 2003, Elsevier Pub (2004).
- [15] MARIAN, J., WIRTH, B, ODETTE, B., SCHAUBLIN, R., PERLADO, J.M., J., Nucl. Mater. **323** (2003) 181–191.
- [16] SALVADOR, M., PERLADO, J.M., MATTONI, A., BERNARDINI, F., COLOMBO, J. Nucl. Mat. **329-333** (2004) 1219–1222.
- [17] MOTA, F., CATURLA, M.J., PERLADO, J.M., DOMÍNGUEZ, E., KUBOTA, A., Nucl. Mat. **329-333** (2004) 1190–1193
- [18] VELARDE, M., PERLADO, J.M., SEDANO, L., The role of organically bound tritium after ingestion in normal and accidental scenarios caused by releases from inertial fusion reactors, IFSA 2003, Elsevier Pub (2004)

LIST OF PARTICIPANTS

- Foldes, I. KFKI - Research Institute for
Particle and Nuclear Physics,
P.O. Box 49, H-1525 Budapest, Hungary
foldes@rmki.kfki.hu
- Hoffmann, D. GSI - Darmstadt,
Planckstr. 10, D-6429 Darmstadt, Germany
d.hoffmann@gsi.de
- Kalal, M. Faculty of Nuclear Sciences and
Physical Engineering,
Czech Technical University in Prague,
Brehova 7, 115 19 Prague, Czech Republic
kalal@fjfi.cvut.cz
- Kasuya, K. Department of Energy Sciences,
Tokyo Institute of Technology,
4259 Nagatsuta, Midori-ku, Yokohama,
Kanagawa, G3-35, 226-8502, Japan
kkasuya@es.titech.ac.jp
- Khaydarov, R. Institute of Applied Physics, National
University of Uzbekistan,
700206, Yunis-Obod, 14-39-26, Tashkent,
Uzbekistan
rkhaydarov@nuuz.nusci.net;
ragab@iaph.tkt.uz
- Kong, H.J. Dept. Physics, KAIST,
Gusong-dong, Yusong-gu, Daejeon,
305-701, Republic of Korea
hjkong@kaist.ac.kr
- Koresheva, E.R. P.N.Lebedev Physical Institute,
53, Leninskiy Prospect, 119991 Moscow,
Russian Federation
koresh@sci.lebedev.ru
- Louzeiro Malaquias, A. International Atomic Energy Agency,
Wagramer Strasse 5
A-1400 Vienna, Austria
A.Malaquias@iaea.org
- Mank, G. International Atomic Energy Agency,
Wagramer Strasse 5,
P.O. Box 100, A-1400 Vienna, Austria
g.mank@iaea.org

Miklaszewski, R. International Atomic Energy Agency,
Wagramer Strasse 5
A-1400 Vienna, Austria

Nakai, S. Koichi National College of Technology,
Monobe, Nankoku-City, Koichi, 783-8505,
Japan
pnakai@jm.kochi-ct.ac.jp

Norimatsu, T. Institute of Laser Engineering,
Osaka University,
2-6 Yamada-oka, Suita, Osaka 565-0871,
Japan
norimats@ile.osaka-u.ac.jp

Perlado, J.M. DENIM UPM Escuela Tecnica Superior
Ingenieros Industriales,
Jose Guterrez Abascal, 2 Madrid 28006,
Spain
mperlado@din.upm.es

Rudraiah, N. National Research Institute for Applied
Mathematics (NIRAM), 492/G,
7th Cross, 7th Block (West) Jayanagar,
Bangalore – 560070, India
rudraiahn@hotmail.com

Schneider, U. International Atomic Energy Agency,
Wagramer Strasse 5
A-1400 Vienna, Austria

Sharkov, B.Y. ITEP - B Cheremunshkinshaya 25,
117218 Moscow, Russian Federation
Boris.Sharkov@itep.ru

Tillack, M.S. University of California San Diego,
La Jolla CA, USA
mtillack@ucsd.edu

Wolowski, J. Head of Laser-Produced Plasma,
Department, Institute of Plasma Physics
and Laser Microfusion,
Hery St. 23, 00-908 Warsaw, P.O. Box 49,
Poland
wolowski@ifpilm.waw.pl

Ying, A. UCLA, Engineering IV,
Room 44-114,
Los Angeles, CA 90095-1597, USA
Ying@fusion.ucla.edu